JOSU OLMOS AMONDARAIN | Cost-optimal Integration of Innovative Powertrain Technologies into Rail Vehicles

Mondragon Unibertsitatea

DOCTORAL THESIS

COST-OPTIMAL INTEGRATION OF INNOVATIVE POWERTRAIN TECHNOLOGIES INTO RAIL VEHICLES

JOSU OLMOS AMONDARAIN | Arrasate-Mondragón, 2022

Cost-optimal Integration of Innovative Powertrain Technologies into Rail Vehicles

Ph.D. Thesis Dissertation

Doctoral Program in Applied Engineering

Mondragon Goi Eskola Politeknikoa

Electronics and Computing Department

Presented by

Josu Olmos Amondarain

Supervised by:

Dr. Iosu Aizpuru Larrañaga (MU)

Dr. Andoni Saez de Ibarra Martinez de Contrasta (Ikerlan)

Hernani, May 2022

This Ph.D. Thesis received funding from the BIKAINTEK 2018 program (grant number 20-AF-W2-2018-00010), and it was carried out in a collaboration framework between IKERLAN Technology Research Centre and CAF Power & Automation.

Esker Onak

Bueno, ba hemen gaude, hiru urte t'erdi ondoren. Oso ondo ezagutzen nauen pertsona batek esan zidan orain dela gutxi ez naizela hitz askoko pertsona bat, eta tira, ez det kontrakoa argudiatuko. Dena den, hiru urte askorako ematen dute, eta ez zen legezkoa izango bide honetan lagundu duten pertsona guztiei eskerrak ez ematea. Goazen ba.

Burura iristen zaizkidan ideia guztiak modu batean ordenatu behar direnez, hasieratik hasiko naiz. Lehenik eta behin, eskerrak eman behar dizkiet tesi hau egiteko pertsona egokia nintzela, nigan konfiantza osoa jarri, eta proposamena luzatu zidaten Igor, Haizea eta Joni. Kontuan izanda proposamena Ikerlanen apenas aste batzuk neramala jaso nuela, aurrera jarraitzeko erabakia ez zen erraza izan. Baina honetan, dudarik gabe, areako giro onak lagundu zuen, beraz 2018-ko Ikerlan Galarreta osatzen zenuten guztiei eskerrak eman nahi dizkizuet, zeharka izan bazen ere, erabaki hau hartzen laguntzeagatik. Y mención especial a Victor, que fue mi primer supervisor en Ikerlan, y claramente una figura a la que seguir en el momento de tomar la decisión.

Behin tesia hasita, eskerrak eman behar dizkiodan lehen pertsona Iñigo Gandi da. Tesiko lehen hilabete zail haietan bere esfortzua ezinbestekoa izan zen tesia aireratu ahal izateko. Eta noski, handik aurrera ere bere laguntza oso garrantzitsua izan zen hegaldiak bide egokia jarraitzeko eta okertzen ez hasteko. Hegaldi erditik aurrera, eta lurreratze honetara arte, Andonik hartu zuen lan hau, eta beraz toki inportante bat dauka esker onen lista honetan. Dokumentu honetan ikusiko dituzuen eduki guztietan parte hartu du berak ere, eta bere laguntza ezinbestekoa izan da urte hauetan zehar. Gainera, memoria guztia zuzentzeko lana hartu behar izan du, pff tienes el cielo ganado. Iosuri ere eskerrak eman behar dizkiot tesi zuzendari lanarengatik, bere laguntza beharrezkoa izan baita gure mila dudei irtenbidea emateko, eta bere aholkuak beti izan direlako lagungarri.

Arearekin jarrituz, puntu honetan doktoregai guztiak aipatu behar ditut, bai tesia hasterakoan beraien esperientziarekin lagundu zidatenak (Mattin, David, Iñigo, Amaia eta Jon Ander), zein ordutik piszinara botatzen joan direnak (Nerea, Olatz, Eneko, Markel eta Xabi, espero det zuei ere nire esperientziak lagundu izana). Hasieran bageneukan elkartasuna, baina argi dago elkartasun hau indartzen joan garela urte hauetan zehar (ejem esa taza es muy top), eta horrek pilo bat laguntzen du tesiaren egunerokotasunean. Zue-

tako batzuentzat ere esker berezia daukat. Jon Ander, zurekin izandako diskusio/gogoetek tesiaren norabidea definitzen joan ziren, zu gabe tesi hau ez zen berdina izango. Mattin eta David, batez ere tesiko lehen hilabeteetan asko lagundu zenidatelako (David, jo, pon un David en tu vida, que te resuelve todo). Eta azkenik, baina ez inportantzia gutxiagorekin, Nerea eta Olatz, niretzako kriston lujazoa izan da bide honetan zehar jada lehendik lagunak ziren, ez bat, baizik eta bi pertsona ondoan izatea. Argi izan hiru urte t'erdi hauek ez zirela berdina izango zu biok gabe, konfiantza oso handia eman dit beti ikustea hor zeundetela behar nuen edozertarako (eta ez soilik arlo profesionalerekin zerikusia zuenarako). Beraz, esker mila, benetan, eta animo gelditzen zaizuenarekin. Ez da erraza izango, baina azkenean, espero baino lehenago, maldaren amaierara iritsiko zarete.

Lehen esan det Galarreta 2018 ezinbestekoa izan zela tesia egiteko erabakia hartzerako orduan, baina horrek ez du esan nahi gainontzeko urteetan zehar arean egon zaretenok ez zaretenik garrantzitsuak izan. Oso beharrezkoak izan zarete lan hau aurrera eramateko, beraz esker onak ere 2018-2022 artean Ikerlan Galarreta osatu dezuten guztioi, modu batean edo bestean guztiek lagundu dezute tesi hau aurrera eramaten.

Eta bueno, lanetik kanpo ere pertsona askotaz oroitzen naiz. Lo primero, la familia, no solo porque la familia sea la familia, sino además porque tengo la suerte de haber nacido en esta familia. Y sin vosotros, pues no sería como soy ahora, y seguramente no estaría donde estoy. A los aitas, Asier, la amona, tíos, tías, primas, primos... de todos me acuerdo. Y recuerdo especial para el aitona y la abuela, que estaban aquí cuando empecé este camino hace tres años, y que aunque no vayan a estar al final, espero que estén orgullosos del trabajo que ha hecho su nieto.

Eta hurrengoa zu zara Eider, jo, eske zer egingo nuke zu gabe. Argi izan tesia amaitzera iristearen kulpa handi bat zurea dela. Badakizu zarela ese pilar super importante en mi vida. Que no se caiga nunca, eta bizitza ospatzen jarrai dezagula, izan edozein auzoko tabernetan, kontzertutan edo munduko beste puntan. Compta amb mi amiga, que incendiaremos el mundo otra vez. Eta animo zure tesi bukaerarekin ere.

Kuadrilako lagunei ere, beti hor daudelako, eta bizitza askoz aspergarriagoa izango zelako beraiek gabe. Eta a ver, que sino con quién voy a hablar yo de ese capitulo de los Simpsons o de esa etapa del giro. Y que además se os quiere. Eta kuadrilakoak ez diren, baina niretzako ere oso lagunak diren guzti horiei, mila esker nire bizitzaren parte izateagatik, tesi honen zatitxo bat ere zuena sentitu dezakezue.

Eta orokorrean, jada ixten joateko, hiru urte t'erdi hauetan nire bizitzan parte hartu dezuten guztioi, mila esker, ezin naiz guztietaz akordatu. Eta jo, tesia nahiko luzea da ya esker onetan beste 10 orri gehitzeko...

Bihotz bihotzez, mila esker guztioi,

Josu

Abstract

Title: Cost-optimal Integration of Innovative Powertrain Technologies into Rail Vehicles.

Railway is an essential transportation mode in nowadays society, both for passengers and goods. Considering that the relation between the carried passenger activity and the derived pollutant emissions is lower than in road transport, railway becomes an essential stakeholder in the path towards transport decarbonization. During the last decades, a significant effort to electrify railway lines has been carried out globally. However, due to its high cost, electrification is not always cost-efficient. Consequently, 65% of rail tracks are not electrified yet, and diesel still accounts for 53% of the global railway sector energy use. This demonstrates the importance of searching for cleaner alternatives also in the railway sector.

Recent techno-economic developments have pushed the use of greener technologies such as batteries and fuel cells in various transport applications, including railway vehicles. Due to their technical limitations, hybrid architectures such as the diesel-battery or the fuel cell-battery become the most promising options, or even the only feasible ones, in many cases. This hybridization involves additional complexity compared to traditional architectures. In essence, the main challenge consists of obtaining a cost-efficient solution compared to conventional vehicles, which will also enable a cleaner transportation.

With the aim of obtaining that cost-efficient solution, this Ph.D. Thesis focuses on the design of the powertrain of railway vehicles. Important features to be considered during the powertrain design include the selection of the technologies to be integrated into the powertrain, the size of the powertrain elements, and the energy management strategy. Traditionally, these features are defined *ad-hoc* for a specific context (i.e., for a particular driving cycle or economic framework), but this is a time-consuming process, and the replicability of the conclusions is limited. Therefore, evaluating the impact that the different features of the specific context have on the optimal powertrain design can help simplify the efforts of the design approach.

In order to overcome all these challenges, this Ph.D. Thesis proposes and implements *a holistic design methodology to achieve a cost-optimal integration of fuel cell and battery*

systems in railway vehicles.

The holistic design methodology is based on a complete analysis of the Life Cycle Cost, which is composed of several steps. Firstly, the cost of integrating different powertrain sizes, battery technologies and energy management strategies is compared. Secondly, the obtained conclusions are evaluated in different frameworks, including multiple railway routes and economic contexts. For the development of this analysis, a power flow-based simulation model is set. This model is based on the Itiner tool previously developed by CAF I+D, and it is fed with the data provided by CAF Power & Automation. This will allow using realistic vehicle and route data to develop the mentioned Life Cycle Cost analysis. Moreover, within the development of this analysis, this Ph.D. Thesis also proposes several innovative energy management strategies and a novel chemistry-dependent battery lifetime estimation model.

Once the holistic design methodology is explained in detail, the methodology and the whole Life Cycle Cost analysis are implemented in two case studies. Each of the case studies of this Ph.D. Thesis is based on one of the railway vehicle topologies mentioned above: (1) the diesel-battery hybrid topology, and (2) the fuel cell-battery hybrid topology. The development of the two case studies will provide valuable conclusions for the design of railway vehicle powertrains that integrate battery and fuel cell systems. These conclusions are claimed to be especially helpful for railway manufacturers to make decisions regarding the powertrain design of hybrid diesel-battery or fuel-cell battery vehicles.

Key words: railway, battery, fuel cell, hydrogen, energy management, life cycle cost analysis, optimization, battery ageing, sizing.

Laburpena

Titulua: Teknologia berritzaileen integrazio optimoa trenbideetako ibilgailuen potentzia-trenean.

Trenbidea funtsezko garraio mota da gaur egungo gizartean, bai pertsonen mugimendurako zein merkataritzarako. Errepideko garraioarekin konparatuz, trenbideek eragiten duten kutsadura bidaiari bakoitzeko baxuagoa da. Beraz, trenbidea funtsezko elementua bihurtzen da garraioaren dekarbonizazio bidean. Azken hamarkadetan trenbideak elektrifikatzeko ahalegin garrantzitsua egin da mundu mailan. Hala ere, bere kostu altuaren ondorioz, elektrifikazioa ez da beti errentagarria. Ondorioz, gaur egun trenbideen %65-a ez dago elektrifikatuta oraindik, eta sektorearen oinarrizko energia erabileraren %53-a dieselaren bidez egiten da. Honek erakusten du trenbidearen sektorean ere alternatiba garbiagoak bilatu behar direla.

Azken urteetako garapen tekno-ekonomikoen eraginez, hainbat garraio aplikazioetan (trenbide ibilgailuetan ere) bateriak eta erregai pilak bezalako teknologia garbien integrazioa bultzatu da. Teknologia hauen muga teknikoak direla eta, diesel-bateria edo erregai pila-bateria bezalako arkitektura hibridoak aukerarik egokienak, edo aukera bakarrak, dira kasu askotan. Hibridazioak konplexutasun gehigarria eragiten du arkitektura tradizionalen aldean. Funtsean, erronka nagusiena aukera tradizionalekin konparatuz irtenbide errentagarri bat lortzea da, zeinak garraio garbiago baten bidea irekitzea ahalbidetuko luke.

Irtenbide eraginkor hori lortzeko helburuarekin, Tesi Doktoral hau trenbide ibilgailuen potentzia-trenaren diseinuan zentratzen da. Diseinu honetan kontuan hartu beharreko aspektu garrantzitsuak honakoak dira: potentzia-trenean integratuko diren teknologien hautaketa, potentzia-treneko elementuen tamaina, eta energia kudeaketarako estrategia. Tradizionalki, ezaugarri hauek *ad-hoc* definitzen dira testuinguru jakin baterako (hau da, ibilibide edo tesituinguru ekonomiko jakin baterako), baina hau prozesu oso luzea da, eta lortzen diren ondorioen erreplikagarritasuna mugatua da. Hori dela eta, testuinguru espezifikoaren ezaugarriek potentzia trenaren diseinuan duten inpaktua ebaluatzeak diseinu prozesuan jarri beharreko esfortzua gutxitzen lagundu dezake.

Abstract

Erronka guzti hauek gainditzeko, Tesi Doktoral honek *tren ibilgailuetan erregai pila eta bateria sistemen integrazio errentagarria lortzeko diseinu metodo holistiko* bat proposatu eta inplementatzen du.

Diseinu holistikoaren metodologia "Life Cycle Cost" edo bizitza-ziklo kostuaren analisi integral batean oinarritzen da, zeina urrats desberdinez osatzen den. Lehenik, potentzia-trenaren elementuen tamaina desberdinek, bateria teknologia desberdinek, eta energia kudeaketa estrategia desberdinek duten kostua alderatzen da. Ondoren, lortutako ondorioak hainbat kontextuetan ebaluatzen dira, besteak beste, hainbat ibilbide edo testuinguru ekonomikoetan. Analisi hau garatzeko, potentzia fluxuetan oinarritutako simulazio eredu bat ezarri da. Eredu hau CAF I+D enpresak lehendik garatutako Itiner simulazio tresnan oinarritzen da, eta CAF Power & Automation enpresak emandako datuekin elikatu da. Honek bizitza-ziklo kostuaren analisia garatzerako orduan ibilgailu eta ibilbide errealistak erabiltzea ahalbidetu du. Gainera, aipatutako analisiaren garapenan, Tesi Doktoral honek energia kudeaketarako hainbat estrategia proposatzen ditu, eta baita baterien bizitza estimatzeko modelo berritzaile bat ere, zeina hainbat kimiketarako parametrizatu den.

Behin diseinu holistikoaren metodologia xehetasunez azalduta, metodologia eta bizitza-ziklo kostuaren analisi osoa ikerketa-kasu bietan aplikatzen da. Tesi Doktoral honen ikerketa-kasu bakoitza lehen aiptautako trenbide ibilgailu topologia batean oinarritzen da: (1) diesel-bateria arkitektura hibridoa, eta (2) erregai pila-bateria arkitektura hibridoa. Bi ikerketa-kasuen garapenak bateria eta erregai pilak integratzen dituzten trenbide ibilgailuen diseinurako ondorio baliagarriak emango ditu. Ondorio hauek lagungarriak izan daitezke trenbide ibilgailuen fabrikatzaileentzat, bereziki diesel-bateria edo erregai pila-bateria ibilgailuen diseinurako erabakiak hartzerako orduan.

Hitz gakoak: trenbideak, bateria, erregai pila, hidrogenoa, energia kudeaketa, bizitza-ziklo analisia, optimizazioa, bateria zahartzea, dimentsionamendua.

Resumen

Título: Integración óptima de tecnologías innovadoras en el tren de tracción de vehículos ferroviarios.

El ferrocarril es un modo de transporte esencial en la sociedad actual, tanto para pasajeros como para mercancías. Teniendo en cuenta que la relación entre el flujo de pasajeros/mercancías y las emisiones contaminantes derivadas es menor que en el transporte por carretera, el sector feerroviario se convierte en un actor importante en el camino hacia la descarbonización del transporte. Durante las últimas décadas, se ha llevado a cabo un importante esfuerzo para electrificar las lineas ferroviarias a nivel mundial. Sin embargo, debido a su elevado coste, la electrificación no siempre es rentable. En consecuencia, el 65% de las vías ferroviarias a nivel mundial aún no están electrificadas, y el diésel sigue representando el 53% del uso energético del sector ferroviario. Esto demuestra la importancia de buscar alternativas más limpias también en este sector.

Los recientes avances tecno-economicos han impulsado el uso de tecnologías más limpias, como las baterías y las pilas de combustible, en una amplia variedad de aplicaciones de transporte, incluidos también los vehículos ferroviarios. Debido a sus limitaciones técnicas, las arquitecturas híbridas, como la batería-diesel o la pila de combustible-batería, se convierten en las opciones más prometedoras, o incluso las únicas viables, en muchos casos. Esta hibridación implica una complejidad adicional en comparación con las arquitecturas tradicionales. Esencialmente, el principal reto consiste en obtener una solución rentable en comparación con los vehículos convencionales, lo que permitirá también un transporte más limpio.

Con el objetivo de obtener esa solución rentable, esta Tesis Doctoral se centra en el diseño del tren de tracción de los vehículos ferroviarios. Entre las características importantes que deben tenerse en cuenta durante el diseño del tren de tracción, se encuentran la selección de las tecnologías que se integrarán en él, el tamaño de los elementos que se integrarán, y la estrategia de gestión energética. Tradicionalemente, estas características se definen *ad-hoc* para un contexto específico (es decir, para un ciclo de conducción o un marco económico concreto), pero se trata de un proceso que require de mucho tiempo, y además, la posibilidad de reproducir las conclusiones es limitada. Por lo tanto, evaluar el

impacto que tienen las diferentes características del contexto específico en el diseño óptimo del tren de tracción puede ayudar a simplificar los esfuerzos del proceso de diseño.

Con el objetivo de superar todos estos retos, esta Tesis Doctoral propone e implementa *una metodología de diseño holístico para lograr una integración óptima de sistemas basados en pilas de combustible y baterías en vehículos ferroviarios.*

La metodología de diseño holístico se basa en un análisis completo del "Life Cycle Cost" o coste del ciclo de vida, el cual consta de varios pasos. En primer lugar, se compara el coste de integrar diferentes tamaños de los elementos del tren de tracción, diferentes tecnologías de baterías, y diferentes estrategias de gestión energética. En segundo lugar, las conclusiones obtenidas se evalúan en diferentes marcos, incluyendo múltiples rutas ferroviarias y contextos económicos. Para el desarrollo de este análisis, se establece un modelo de simulación basado en flujos de potencia. Este modelo se basa en la herramienta Itiner desarrollada previamente por CAF I+D, y se alimenta con los datos proporcionados por CAF Power & Automation. Esto permitirá utilizar datos de vehículos y rutas realistas para desarrollar el mencionado análisis del coste de ciclo de vida. Además, dentro del desarrollo de este análisis, esta Tesis Doctoral propone también varias estrategias innovadoras de gestión energética, y un novedoso modelo de estimación de vida útil de baterías, el cual se ha parametrizado para diferentes químicas.

Una vez explicada en detalle la metodología de diseño holístico, dicha metodología y todo el análsisis del coste del ciclo de vida se implementan en dos casos de estudio. Cada uno de estos casos se basa en una de las topologías de vehículos ferroviarios previamente mencionadas: (1) la topología híbrida diesel-batería, y (2) la topología híbrida pila de combustible-batería. El desarrollo de los dos casos de estudio proporcionará valiosas conclusiones para el diseño del tren de tracción de vehículos ferroviarios que integran sistemas de baterías y pilas de combustible. Estas conclusiones podrán ser especialmente útiles para que los fabricantes ferroviarios tomen decisiones sobre el diseño del tren de tracción de vehículos híbridos diesel-batería o pila de combustible-batería.

Palabras clave: ferrocarril, batería, pila de combustible, hidrógeno, gestión energética, análisis del coste del ciclo de vida, optimización, degradación de batería, dimensionamiento.

Contents

General Introduction

Transport accounts nowadays for nearly 25% of the global CO_2 emissions, which unveils the necessity of deploying initiatives to promote its decarbonization. Among the different transportation modes, railway mobility becomes an essential stakeholder in this path due to its intrinsic characteristics, especially the capacity of carrying a large number of passengers or goods with low energy consumption.

However, not all railway solutions are efficient in terms of pollutant emissions, as this mainly depends on the primary energy source used to power the vehicle. Railway vehicles powered by catenary systems are the most efficient alternative. However, the electrification of railway lines is not always cost-efficient, especially in low-traffic networks. Consequently, even if a great effort has been accomplished in last decades to electrify railway lines, 65% of the global rail tracks are not electrified yet. Considering that diesel-based vehicles are the primary option in these lines, switching to cleaner alternatives is necessary.

Recent techno-economic developments in power generation and energy storage technologies have encouraged searching for low-polluting alternatives for different transport sectors, including rail vehicles. On the one hand, battery-based energy storage systems have become the flagship of transport electrification thanks to their broad integration in electric vehicles. The development of technologies with higher specific energy (e.g., lithium-ion batteries) and the high reduction of acquisition costs (nearly 70%) have driven this integration in recent years. However, it is still necessary to overcome some challenges. The selection of an appropriate battery chemistry, the prevention of safety risks, or the management of temperature and degradation issues are critical challenges for the broader adoption of battery-based vehicles.

On the other hand, hydrogen-related technologies are recently gaining interest in various sectors, including mobility applications. A shift to a hydrogen-based economy can provide zero-emission power generation. Indeed, hydrogen can be obtained from renewable sources via electrolysis and then be used as a primary source to generate electricity via fuel cell systems. Therefore, integrating this technology in rail vehicles enables the attainment of zero-emission solutions. However, issues related to the fuel cell system cost, hydrogen supply, safety risks or degradation management need to be solved.

Due to the technical limitations of pure battery-based or fuel cell-based rail topologies, the development of hybrid architectures such as the hybrid diesel-battery or the hybrid hydrogen-battery becomes unavoidable. This hybridization involves additional complexity compared to traditional architectures. The main challenge consists of obtaining a cost-efficient solution compared to conventional vehicles, which is essential especially for the competitiveness of railway manufacturers. In order to obtain that cost-efficient solution, special attention must be given to the design of the powertrain. The design approach should consider in an integrated manner the selection of the technologies to be integrated in the powertrain, the size of the powertrain elements, and the control strategy for managing the power fluxes between the different sources.

Different technologies can be combined to derive the mentioned hybrid powertrains, including diesel generators, fuel cells or batteries. The selection of these technologies is a crucial design step, as their characteristics influence the optimal powertrain operation. For instance, the dynamic behaviour of a diesel generator differs from that of a fuel cell, which inevitably influences the powertrain operation. Moreover, different battery chemistries can be integrated into the vehicle, which differ in characteristics such as specific energy, energy density, acquisition cost or even the sensitivity to degradation factors.

The control strategy or Energy Management Strategy (EMS) becomes essential to reduce the operation costs of hybrid vehicles. On the one hand, the way the sources are managed directly affects the consumption of the different sources (i.e., diesel, hydrogen or electricity consumption), which contribute to a high proportion of the operation costs. Thus, obtaining an efficient powertrain operation is one of the main challenges of the EMS. On the other hand, the designed control strategy should ensure a low degradation of the power sources, since operation costs are increased as more replacements are required for these devices. Therefore, identifying the factors that affect their degradation and adequately foreseeing the replacements becomes essential. Accurate lifetime estimation algorithms are required for this approach.

As it can be inferred, the design of the control strategy is also constrained by the characteristics of the powertrain elements. The size of the different power sources limits the maximum power they can provide, affecting the range in which they operate efficiently. Accordingly, the degradation of the power sources can also be affected by their size, especially batteries that degrade at high power peaks or deep discharge cycles.

Consequently, a design methodology that considers in an integrated manner the definition of the powertrain elements (including technology and size) and the EMS needs to be developed if a cost-effective solution is aimed. Traditionally, optimal designs are solved *ad-hoc* for specific contexts, i.e. for a particular drive cycle or economic framework. However, developing these approaches is a time consuming process, and the replicability of the obtained solution is limited. Therefore, evaluating the impact of different features of the specific context (e.g., drive cycle characteristics or parameters of the economic model) in the optimal powertrain design can help simplify the efforts of the design approach.

Previous paragraphs have reviewed the main challenges related to the design and control of innovative powertrains. In short, the relevance of the technology and size of the power sources, the control strategy, the drive cycle and the economic framework have been highlighted. To face the identified challenges, this Ph.D. Thesis proposes the following objective:

Develop a holistic design methodology for the cost-effective definition of powertrain elements and control strategy in innovative railway vehicles.

Besides the main objective, other secondary objectives are defined for the successful development of this Ph.D. Thesis:

- To **propose, develop and evaluate different EMSs** in order to identify appropriate strategies for railway vehicles.
- To build accurate and straightforward **lifetime estimation models for** innovative powertrain technologies such as **batteries and fuel cells**.
- To implement and validate the proposed methodology in multiple **case studies involving hybrid diesel-battery and hybrid fuel cell-battery** rail topologies.

To cover these objectives, the Ph.D. Thesis is structured in different chapters and sections. In the following lines, the document organisation is detailed. Besides, Figure 1 helps understand the defined structure.

In the first chapter, the state of the art related to the main aspects covered by this Ph.D. Thesis is reviewed. In a first step, the innovative powertrain technologies that can potentially replace or supplement conventional diesel-based traction systems are analysed. Then, an evaluation of the possible topologies derived from the integration of these technologies in rail vehicles is carried out. This evaluation will help define the architectures to be analysed in this research work. In addition, a review of the literature related to control strategies and powertrain design approaches is developed. Thanks to this review, the main lacks and possible improvements over the current state of the art will be highlighted, which will serve as the basis for the definition of the contributions proposed by this Ph.D. Thesis.

In the second chapter, the holistic design methodology proposed as the main contribution of this Ph.D. Thesis is presented. The methodology is based on an integral life cycle cost analysis, which is composed of different steps. Additionally, in this chapter also all the models and methods required for the development of the life cycle cost analysis are detailed. Firstly, the methodology to calculate the life cycle cost of any case being analysed is presented. This calculation requires of a vehicle simulation model, an economic model and degradation models for fuel cell and battery systems. Indeed, the battery degradation model is presented as one of the novel contributions of this Ph.D. Thesis. Secondly,

the methodologies for the life cycle cost optimization are presented, which are based on exhaustive search-based and genetic algorithms-based approaches.

The first case study of this Ph.D. Thesis is presented in the third chapter. This case study is focused on the diesel-battery hybrid topology. First, the methodology proposed in the second chapter is particularized to the specific case study. For this approach, the specifications of the simulated vehicle, all the cases of the sensitivity analysis (including the energy management strategies, battery chemistries, parameters of the economic model and driving cycles) and the details of the life cycle cost optimization approaches are given. Then, the results obtained when deploying the holistic design methodology are presented. A comprehensive discussion of these results is also developed, which is divided according to the steps of the holistic design methodology: sensitivity analysis to the powertrain design, sensitivity analysis to the economic parameters, and sensitivity analysis to the driving cycle.

In the fourth chapter, the second case study of this Ph.D. Thesis is presented. This second case study is focused on the hybrid fuel cell-battery topology. As in the previous chapter, the first part of this chapter is focused on particularizing the holistic design methodology to the specific topology proposed in this case study. The specifications of the simulated vehicle, all the cases of the sensitivity analysis (including the energy management strategies, battery chemistries, parameters of the economic model and driving cycles) and the details of the life cycle cost optimization approaches are presented. Then, the results obtained when deploying the holistic design methodology are presented. As in the first case study, a comprehensive discussion of these results is also developed, which is divided according to the steps of the holistic design methodology.

Finally, in the fifth chapter the general conclusions and the main contributions of this Ph.D. Thesis are reviewed. In addition, in this chapter also some possible future lines related to the main topic of this Ph.D. Thesis are proposed.

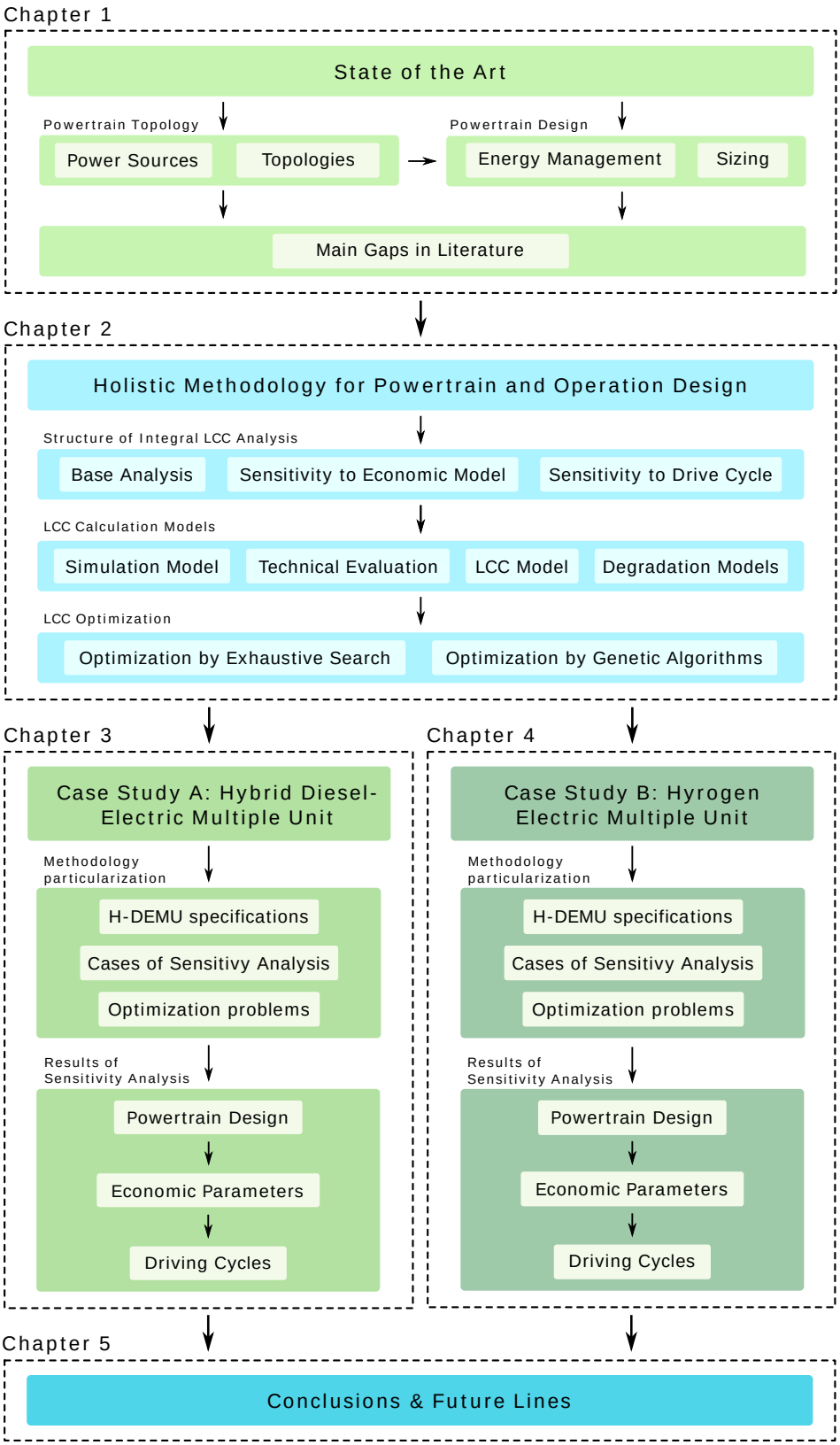

Figure 1: Document structure.

1

State of the Art

Summary

In this first chapter a review of the State of the Art related to the design and control of innovative powertrain technologies is developed. The analysis considers the potential power sources to be integrated in the powertrain, the derived innovative powertrain topologies, the control strategies, and the powertrain sizing approaches. The main gaps identified in the literature are highlighted, which serve as a baseline to define the research activities and main contributions of this Ph.D. Thesis.

1.1 Introduction

The increase of greenhouse gas and CO_2 emissions is one of the major concerns of nowadays society, as they are directly linked to climate change and its impacts [1]. Even if the importance of this issue has been pointed out from the general public for several years, a slight but steady increase in the emissions has ocurred in the last decades, only paused for very short periods during the 2009 crisis and the Covid-19 pandemic [2, 3]. As highlighted in Figure 1.1, transport is a major source of this pollution, accounting for nearly the 25% of the global CO_2 emissions.

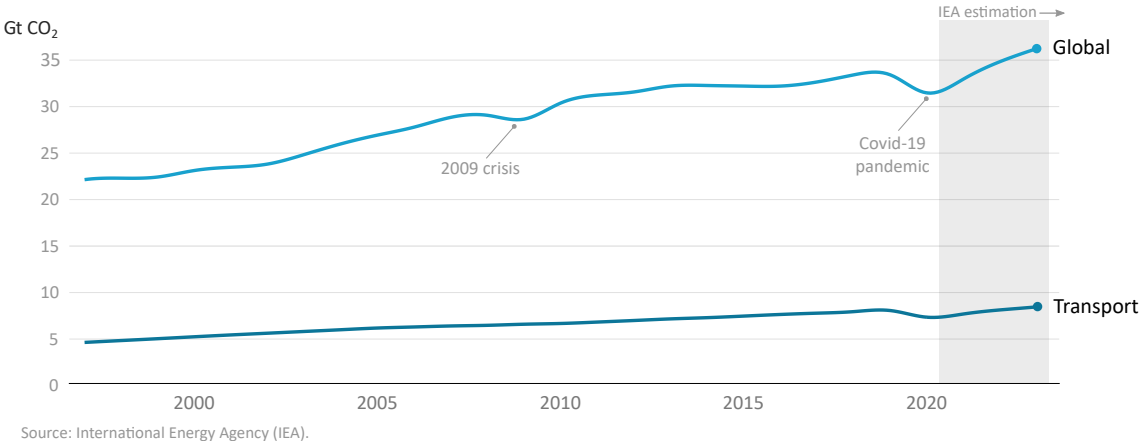

Figure 1.1: Global and transportation-related CO_2 emissions, adapted from [2, 3].

Therefore, it is not a surprise that many of the efforts to mitigate the effect of climate change and greenhouse gas emissions are focused on transportation. As an example, the European Union has recently presented the "Sustaninable and Smart Mobility Strategy" (2020), where a set of initiatives have been proposed for the period 2021-2025 in order to cut the 90% of transport related emissions by 2050 [4]. Typically, this and similar initiatives point out that effort is required around the following four axes to adequately attain targets for emissions reduction in transportation [5]:

(1) A structural shift in the modes used to move people and freight. In this concern, the reinforcement of public transport is understood as a necessary step. Indeed, public means of transport, such as urban buses or the different alternatives of railway mobility, enable the movement of passengers with a lower intensity of pollutant emissions (see Figure 1.2) [2, 6].

(2) A switch to low-carbon forms of energy. In this regard, the lower use of traditional fuels and the development and deployment of hybrid electric, full electric or hydrogen-based topologies is essential [1].

(3) An intensification of the research and development of key innovative technologies. According to the study in [1], nearly a 50% of the effort required for obtaining a net-zero emissions economy will come from technologies still under development, and

that share will be even higher for transportation. Related to the previous point, the report spotlights the research on technologies such as advanced batteries or hydrogen.

(4) Focus on using energy more efficiently. In a first step until new technologies are fully ready or behavioural changes are attained, the improvement on energy efficiency (e.g., measures in lightweighting or aerodynamics) can help in reducing emissions [5].

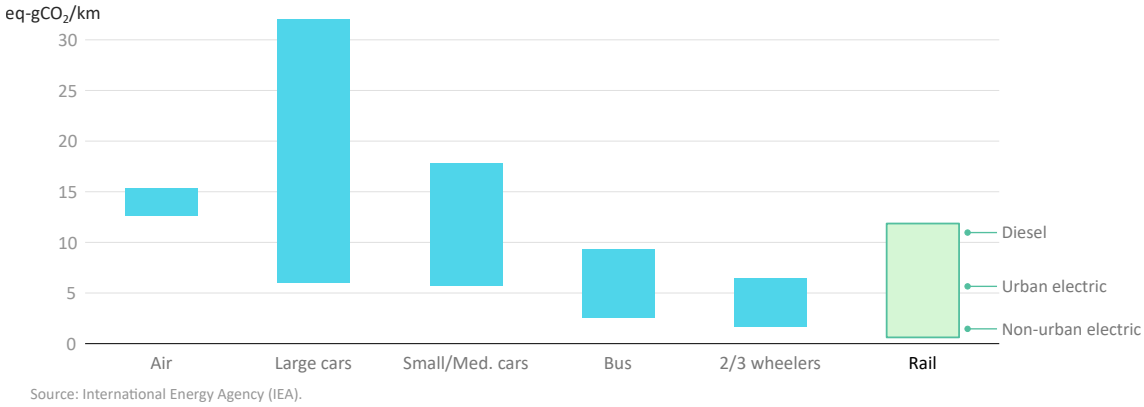

Figure 1.2: CO_2 emission intensity of passenger transport modes, adapted from [2].

In this context, railway mobility emerges as an important stakeholder in the path towards net-zero emissions. First of all, railway has the potential of being the transport mode with the lowest intensity on energy use and emissions, as already highlighted in Figure 1.2. In average, it only accounts for the 3% of transport energy use, while being responsible of the 9% of global motorised passenger movement and 7% of global freight transport [7]. From the energy efficiency point of view, rail sector has already made improvements in the past decades. The energy consumption of these vehicles was improved by nearly a 20% between 1990-2010 thanks to improvements in power electronics and motor drives [8]. However, not all the railway solutions are such efficient in terms of pollutant emissions, as this also depends on the primary energy source used to power the vehicle.

Traditionally, rail vehicles have been powered by either fossil fuels (steam at the beginnings, and diesel more recently) or electricity (catenary-based systems). During the last 50 years, an important effort to electrify railway lines has been conducted globally. However, electrification share is not expected to reach the 100% in the short term, mainly due to its high cost: the electrification of a rail track kilometer requires around 0.5-1.5 M€ [9]. Consequently, electrification is barely cost-efficient in some contexts, specially in low-traffic networks [10]. Nowadays, diesel still accounts for the 53% of the global railway sector energy use, and the 65% of rail tracks are not electrified yet [7]. In the context of the European Union, the 40% of the mainline network [11] and the 20% of the traffic [12] are not electrified yet. Figure 1.3 shows the evolution of the electrification share in different regions of the world [7].

Therefore, a switch to cleaner alternatives is also necessary in railway mobility. Accordingly, the interest of the rail industry on integrating innovative power sources on-board

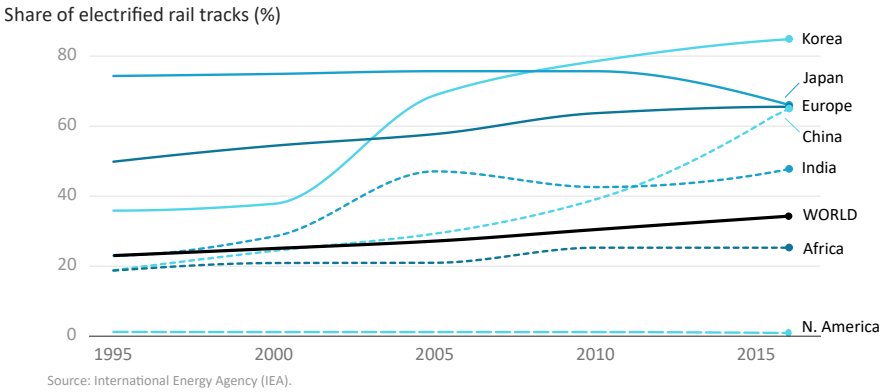

Figure 1.3: Evolution of rail tracks electrification in different regions, adapted from [7].

railway vehicles has increased in the last years, with the aim to substitute or supplement traditional fossil fuels powered traction systems [13–15]. However, the emergence of innovative powertrain architectures rises new technological challenges, which need to be solved in order to obtain cost-optimal solutions compared to conventional technologies.

The design process of a cost-optimal powertrain is conceived as a multi-layer system [16, 17]. Figure 1.4 shows the different levels of the cost-optimal powertrain design. The outermost level consists on the definition of the powertrain topology. Depending on which power sources are integrated on-board, the possible architectures and electrical/mechanical links may vary. Based on the selected topology, the next step consists on determining the sizes of the powertrain elements, including the power sources, converters and electric motors. Finally, the last level consists on the definition of the control strategies for the powertrain elements. Being the main objective of this Ph.D. Thesis the development of a methodology for a cost-effective powertrain design, the different levels depicted in Figure 1.4 will be approached.

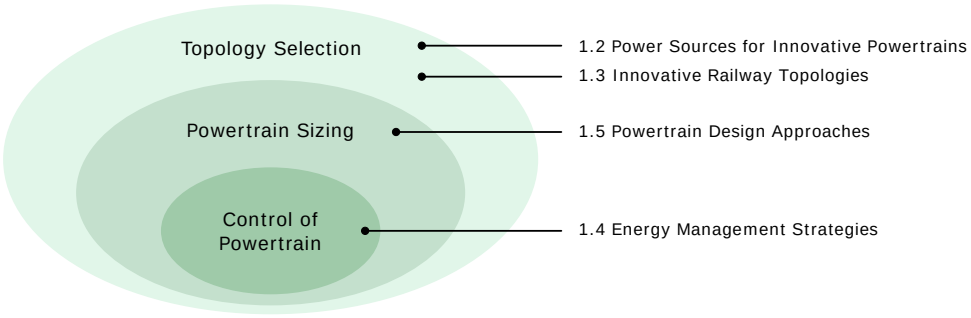

Figure 1.4: System-level design to achieve a cost-optimal powertrain [16].

In the following sections the literature related to each of the levels defined in Figure 1.4 is reviewed. First, the potential power sources to be integrated on-board railway vehicles are introduced, and the most appropriate options are selected (Section 1.2). Then, the potential innovative topologies that integrate the selected power sources are derived (Section 1.3). Based on this review, the topologies to be analysed in this Ph.D. Thesis are

defined. Then, the publications that propose powertrain control (Section 1.4) and sizing definition (Section 1.5) approaches for the considered rail topologies are also reviewed. Based on this analysis, some literature gaps are identified, which will eventually help define the main contribution of this Ph.D. Thesis (Section 1.6).

1.2 Power Sources for Innovative Powertrains

One of the most important technological challenges of the last decades has been the development of technologies that are able to replace Internal Combustion Engines (ICEs) in transport applications. Several devices have been proposed and developed, with uneven characteristics that make them be more appropriate for certain applications [18]. Power and energy rating, weight, volume, cost, response time, potential life or operating temperature are the typical characteristics to be considered in this approach [19].

Given the operational constraints of mobility applications, the most appropriate solutions to replace or assist ICEs are typically identified in the literature as Flywheel (FW), Electric Double Layer Capacitor (EDLC), Battery (BT) and Fuel Cell (FC) technologies [15, 20–22]. Some of these technologies are understood as generation systems (FC and ICE) and the other ones are storage devices (FW, EDLC and BT), also known as Energy Storage Systems (ESSs). Given that all the devices are able to provide traction power to drive transport applications, in this Ph.D. Thesis FC, ICE, FW, EDLC and BT systems will be referred as power sources.

Figure 1.5 shows a Ragone plot of the mentioned power sources. In the following subsections, the main characteristics, advantages and disadvantages of the technologies that are able to replace or assist conventional ICEs are reviewed. Eventually, the most appropriate solutions to be integrated on-board railway vehicles are identified.

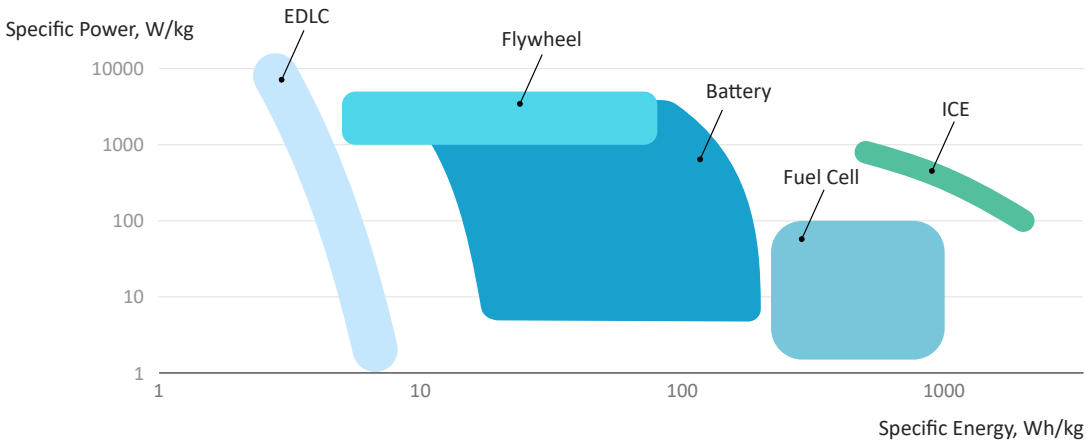

Figure 1.5: Ragone plot of typical power sources for transport, data from [15, 23–27].

1.2.1 Electric Double Layer Capacitors

EDLCs, also known as supercapacitors or ultracapacitors, are devices similar to normal capacitors, but with very high capacitance values up to kilo farads [21]. The high capacitance is achieved through the use of an electrochemical double layer and high surface area carbon electrodes, as seen in Figure 1.6a [19, 28].

Advantages of EDLC systems cover the high specific power (up to 10,000 W/kg, see Figure 1.5), high energy efficiency (up to 98%), long lifetime ($>10^6$ cycles) and rapid response [14, 29]. However, they show a low specific energy (see Figure 1.5), high self-discharge, and they involve a high cost [18]. These characteristics make EDLCs well suited for applications requiring a short-term and fast storage (e.g., regeneration of braking energy in mobility applications), but not for long-term or more energetic-oriented requirements.

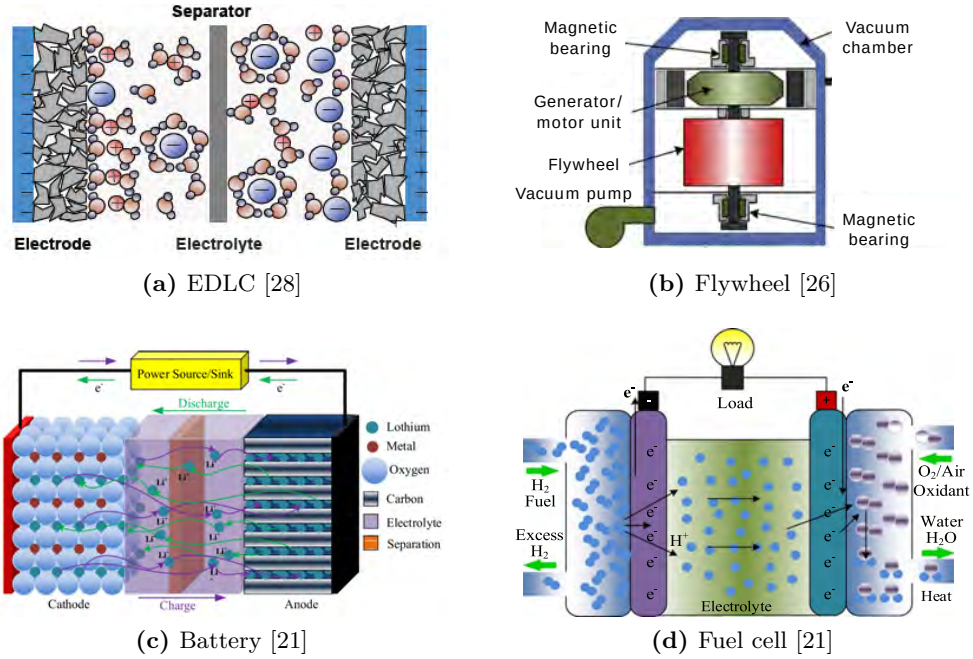

(a) EDLC [28] **(b)** Flywheel [26]

(c) Battery [21] **(d)** Fuel cell [21]

Figure 1.6: Working principle of the typical power sources for transport applications.

1.2.2 Flywheels

The FW is a mechanical ESS that stores (or maintains) the kinetic energy through the rotation of a body (i.e., the rotor) [30]. The storage system comprises the rotating body in a chamber (typically in a vacuum environment), a group of bearings, and the energy transmission device (i.e., a generator or motor unit) together mounted with a common shaft, as depicted in Figure 1.6b [26]. In short, the energy maintained by the constantly rotating flywheel is converted to electrical energy by means of the mentioned transmission device.

FW systems are characterized by the ability of providing a high power peak, as this feature is only limited by the coupled power converter [30]. In addition, it shows long lifespans compared to other technologies (>10^7 cycles) [21]. However, the safety issues related to the gyroscopic force and the high self-discharge are the main disadvantages when considering the introduction of FWs in mobility applications [22]. Mainly due to these reasons, FW systems have been barely introduced in transport applications, normally just in prototype or trial projects that are far from commercial implementation [26, 30].

1.2.3 Batteries

Rechargable or secundary BTs are devices that store electricity in the form of chemical energy and produce electricity through an electrochemical reaction process known as reduction-oxidation (Redox) [31]. As depicted in Figure 1.6c, they are constituted by an electrolyte, an anode and a cathode.

BT technologies are typically classified according to the materials used to build the battery cell, and they can be grouped in the following families: lead-based, nickel-based, sodium-based and lithium-based technologies [32]. As depicted in Figure 1.7, the development of these technologies has led to more energetic and powerful BTs, starting from the Lead-acid (Pb) technology in the 1850's, until the deployment of the Lithium-ion (Li-ion) technology in the 1990's. Nowadays, the Lithium-ion Battery (LIB) is the most common BT technology installed in mobility applications, due to its high specific energy and power (Figure 1.7), low rate of self-discharge, long lifetime, and high cost reduction in the last decade (nearly 79% drop between 2010-2017) [20, 27]. Emergent technologies such as solid-state and post-lithium batteries are expected to gain higher market penetration in the following years, but they are still in prototype and non-commercial stage [33, 34].

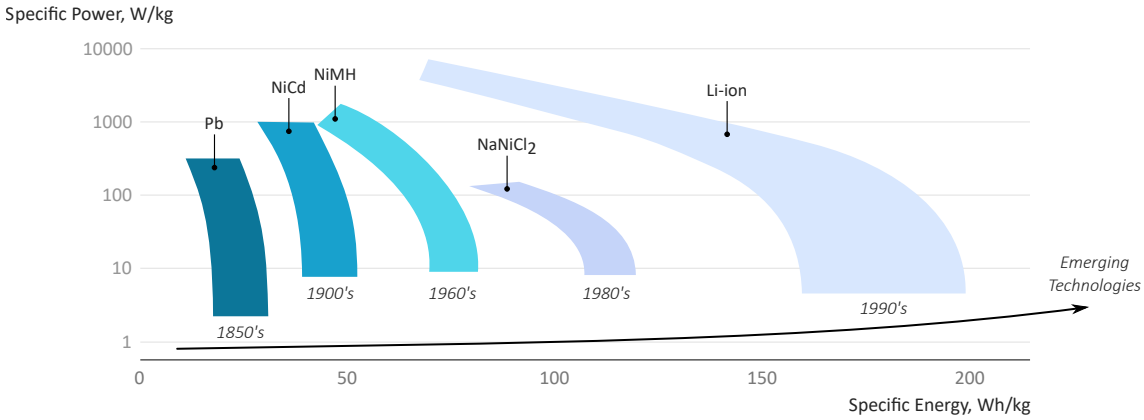

Figure 1.7: Ragone Plot of battery technologies, adapted from [24].

LIBs rely on insertion reactions from both electrodes, where lithium ions act as the charge carrier [35]. Different materials can be used in the fabrication process of the anode and cathode, what directly affects in features such as voltage, temperature performance, lifetime, safety or specific energy and power [36]. Typically, the cathode material is an

intercalated lithium compound. The most used cathode materials are Lithium Cobalt Oxide (LCO), Lithium Manganese Oxide (LMO), Lithium Iron Phosphate (LFP), Lithium Nickel Manganese Cobalt Oxide (NMC) and Lithium Nickel Cobalt Aluminium Oxide (NCA). Besides, the anode material is typically Graphite (G) based, Carbon (C) based, or Lithium Titanate (LTO) based [32, 35]. Figure 1.8 reviews the main features of the most used commercial combinations of anode and cathode materials, which are typically denoted as LIB chemistries [37].

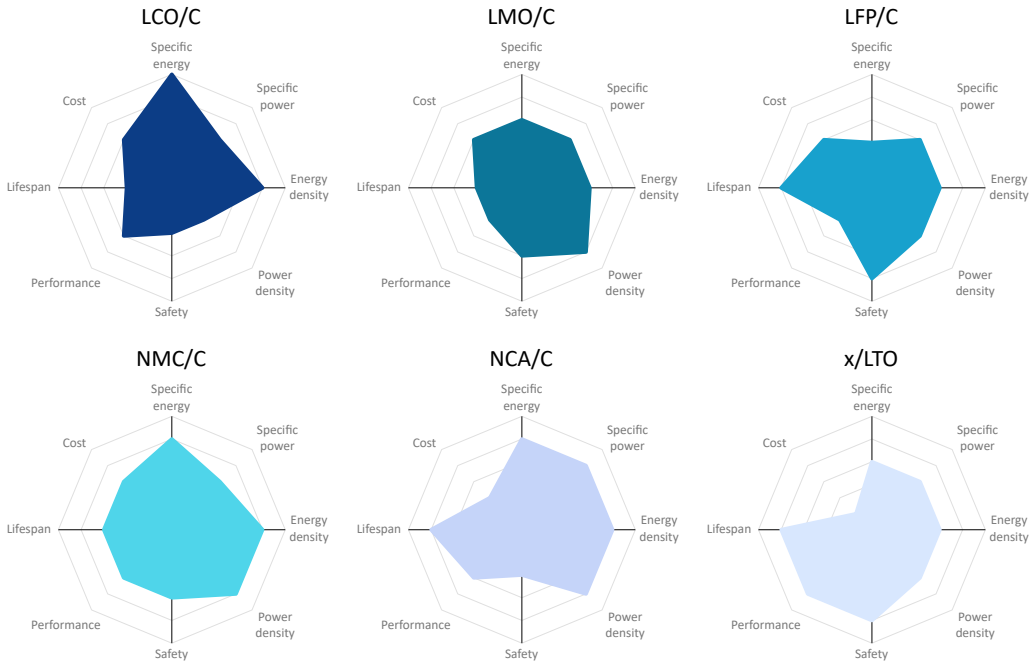

Figure 1.8: Main features of typical LIB chemistries (cathode/anode material), adapted from [37]. An outer value represents a better feature.

As it can be inferred from the figure, there is no chemistry that outperforms the rest of chemistries in all the considered features. Consequently, the selection of a specific cell for a certain application is typically made after seeking a compromise between the most limiting characteristics of each chemistry and the application requirements [36].

1.2.4 Fuel Cells

A FC is an energy conversion device that converts chemical energy from a fuel and an oxidizing agent into electric energy without a combustion [38]. It consists of two electrodes (anode and cathode) and an electrolyte separator, as shown in Figure 1.6d.

FCs are classified according to the nature of its electrolyte and the used fuel [27, 39]. Table 1.1 reviews the main characteristics of the commercially available FC technologies [40]. Among the depicted technologies, the Proton Exchange Membrane Fuel Cell (PEMFC) is considered as the most suitable FC for transportation applications, due to its low-temperature operation (<100ºC) and the better chemical characteristics of hydrogen

[41]. The PEMFC produces electricity from a reaction in which hydrogen and oxygen are combined, with usable heat and water as the principal by-products (Figure 1.6d). Due to the used fuel, PEMFCs are typically known as hydrogen FCs.

Table 1.1: Classification of FC technologies [27, 40].

FC type	Operation T (ºC)	FC efficiency (%)	Power density	Fuel options
AFC	50-230	50-60	High	Hydrogen
PAFC	150-220	40-50	Low	Natural Gas, Diesel, Hydrogen
MCFC	600-700	30-70	Medium	Natural Gas, Diesel, Hydrogen
PEMFC	65-85	40-60	Very High	Hydrogen
SOFC	500-1000	40-70	Low	Natural Gas, Diesel, Hydrogen

Main advantages of hydrogen FCs are the high specific energy (up to 1,000 Wh/kg, see Figure 1.5), the continuous power supply, and the emission-free operation [21, 38]. In fact, they combine the best features of ICE devices (operate as long as fuel is supplied) and batteries (provide electricity without combustion). On the contrary, main disadvantages of hydrogen FCs involve the low specific power, slow response, high cost, and the need of pure hydrogen [27, 41].

1.2.5 Review of Potential Power Sources for Railway Applications

In previous subsections, the potential power sources to be integrated in transport applications have been introduced. Table 1.2 reviews the main characteristics of these power sources. PEMFC technology has been defined for the FC case, since it has been claimed to be the most appropriate option for transport applications. Regarding BT technologies, LIB has been defined as the most relevant option for transport applications, due to its specific characteristics (Figure 1.7).

Table 1.2: Characteristics of potential power sources for transportation (shadowed cells represent technical limitations for railway applications) [15, 23–27].

	EDLC	FW	LIB	PEMFC
Specific Energy (Wh/kg)	<10	<80	<200	<1,000
Specific Power (W/kg)	<10,000	<5,000	<4,000	<100
Self-discharge (%/day)	20 - 40	100	0.1 - 0.3	0
Efficiency (%)	90 - 100	90 - 95	90 - 100	40 - 60
Capital Cost (€/kWh)	300 - 2,000	1,000 - 5,000	500 - 1,500	-
Capital Cost (€/kW)	100 - 300	250 - 350	1,200 - 4,000	600 - 2,500
Lifespan (cycles)	>1,000,000	>10,000,000	<30,000	-
Lifespan (hours)	-	-	-	<30,000
Safety Risk	Moderate	High	Moderate	Moderate

Additionally, Table 1.2 highlights the features that can limit the integration of each technology in rail vehicles (shadowed cells). FW and EDLC devices provide a low spe-

cific energy, specially comparing with traditional ICE-based powertrains (see Figure 1.5). Considering the space and weight limitations of rail vehicles, the potential energetic contribution of these technologies is found to be restricted, what complicates their integration as main power source especially in vehicles oriented to non-urban environments. In the case of FWs, the high self-discharge and the related safety issues are also defined as limitations for its integration in these vehicles. Regarding PEMFC devices, the low specific power is regarded as their main limitation. This issue can be solved with the hybridization of the PEMFC with a secondary power source, which is indeed necessary to solve the low response issue of this technology (this is addressed afterwards in Section 1.3).

Consequently, considering the analysed characteristics, PEMFC and LIB technologies are identified as the most appropriate power sources to be integrated in railway applications and substitute or supplement traditional ICE-based powertrains. For the sake of simplicity, in the remainder FC will refer to PEMFC technology, and BT will refer to LIB technology.

1.3 Traditional and Innovative Railway Topologies

This section reviews the possibilities for the integration of BT and FC systems in rail applications, focusing on how can they assist or replace traditional ICE-based topologies. First, the different rail transportation modes and vehicles are introduced to clarify the used terminology. Then, the evolution from traditional electric- and diesel-powered topologies to more innovative options is attained. The main characteristics, advantages, disadvantages and challenges of each option are discussed in detail.

1.3.1 Rail Transport Modes

A railway vehicle is defined as a vehicle that drives on a rail traction system. Different types of railway vehicles exist depending on its general characteristics, the provided service and the involved infrastructure [7]. Figure 1.9 depicts a proposal for the categorization of rail vehicles and rail transport modes, based on the contributions made in [7, 42]. It is worth to mention that there is no clear arrangement on the terminolology to be used when making a categorization of railway mobility. In this case the most generalized vehicles and transport modes have been considered, even if more categories could be added.

Typically, the first division in rail transport modes is made between freight and passenger transportation [7]. In the case of freight, locomotives are used, which consist of a single vehicle that gives traction to a set of carriages filled of goods. Besides, passenger rail is divided into several sub-sets, which are gathered into urban and non-urban transport.

Urban transport includes all the rail activities within cities and the immediately surrounding area [7]. The most common urban rail transport modes are light rail and metro. On the one hand, light rail refers to the urban rail transport systems that ride at street level, typically sharing the tracks with other urban transport modes. They are usually

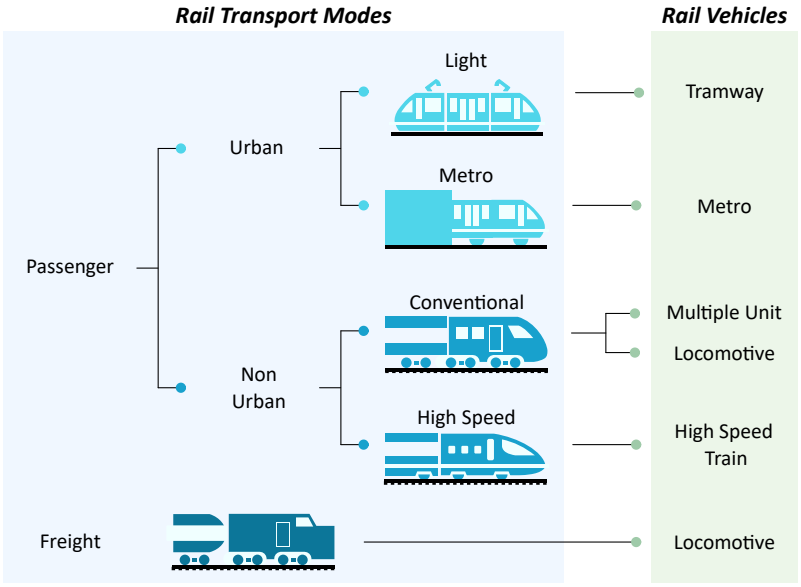

Figure 1.9: Classification of rail transport modes and vehicles, based on [7, 42].

lighter and shorter than rail vehicles driving on metro or interurban lines, and thus they offer a lower capacity and speed [42]. Light rail vehicles are also known as tramways. On the other hand, metro rail refers to the urban rail transport system that rides on exclusive righ-of-way, typically underground. Due to this fact, they reach higher speeds and can handle a higher passenger capacity compared to light rail [42]. However, metro systems are more expensive, especially considering the construction costs [2].

Non-urban rail transport includes conventional and high-speed railway systems. On the one hand, conventional rail includes medium- to long-distance journeys with a maximum speed under 250 km/h, and also suburban journeys that connect urban centres with surrounding areas [7]. Typical nomenclature for conventional rail services include also suburban, commuter, intercity or interurban modes. Conventional rail services can be provided by multiple units or locomotives. The main difference between both vehicles is that in the case of multiple units, the traction elements are distributed among the different carriages, while in the case of locomotives all the traction elements are included in a single vehicle unit [42]. On the other hand, high-speed rail is defined as the rail services that cover long distances and operate at a maximum speed above 250 km/h [7]. The vehicles that give these services are known as high-speed trains.

Nowadays, conventional services cover most of the global railway lines length (around 1,061 thousand km) and it also handles most of the transport activity (around 2,818 billion passenger-km), as it is shown in the breakdown of Figure 1.10 [7]. Even though the deployment of new high speed lines has increased in the last years, its transport activity only accounts for the 15.8%. Urban mobility moves more passengers than conventional and high-speed systems, but as the covered distances are lower, the involved transport activity is also low.

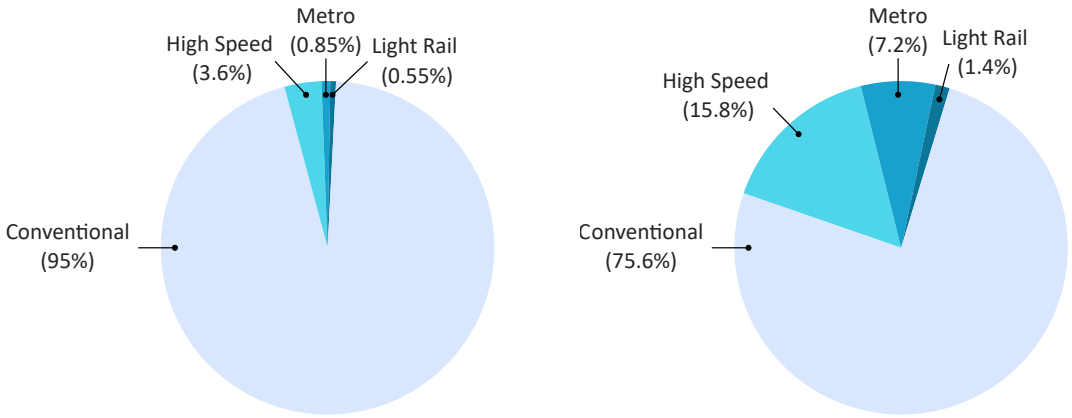

(a) Length of railway lines **(b)** Transport activity (passenger-km)

Figure 1.10: Share of main railway transport modes [7].

Table 1.3 shows the main characteristics of the introduced vehicles: tramways, metros, multiple units, locomotives and high speed trains [42]. As depicted, urban and high speed rail transport is driven electrically, thanks to the use of catenary or third rail systems. However, the vehicles used in conventional rail transport (multiple units and locomotives) are sometimes driven by diesel-based traction systems. This issue is further analised in Section 1.3.2.

Table 1.3: Characteristics of typical rail vehicles [42].

	Tramway	**Metro**	**Multiple Unit**	**Locomotive**	**High Speed**
Main Traction Source	Electric	Electric	Diesel Electric	Diesel Electric	Electric
Distributed Traction	Yes	Yes	Yes	No	Yes
Supply voltage (V DC)	600 750 900	750 1500	750 1500 3000	750 1500 3000	3000
Supply voltage (kV AC)	-	-	15 (16.7 Hz) 25 (50 Hz)	15 (16.7 Hz) 25 (50 Hz)	25 (50 Hz)
Electric Motor Size (kW)	75-150	150-250	200-600	340-1400	200-600
Converter Size (kW)	150-300	350-1000	200-1400	500-1400	200-1400
Electric Motors per Converter (-)	2-4	2-4	2-8	1-2	2-8
Carriages (-)	3-6	4-8	3-12	1	3-12
Weight (tons)	20-50	40	120-160	90-120	120-160
Top speed (km/h)	50-70	80	120-250	100-200	250-350

Therefore, it is found that conventional rail transport is an appropriate sector for the integration of innovative powertrain technologies, given that: (1) it is the sector accounting for most of the rail transport activity, and (2) it is the only sector where diesel-based traction systems are predominant yet. Hence, it is concluded that the developments of this Ph.D. Thesis will be oriented to the integration of innovative powertrain technologies

in conventional rail vehicles, specifically in multiple units.

1.3.2 Traditional Rail Vehicle Topologies

Nowadays, most of the powertrains of conventional multiple units are electrified, since they use a common DC link to transmit electrical power between the main power source and the traction motors [43]. As introduced in previous sections, the main power source can rely on diesel- or electric-based technologies (Table 1.3). In the case of the diesel-based topology, mechanical or hydraulic transmissions have also been used in the past [44], but they are not the main option nowadays [45].

In this section, and before introducing the possibilities offered by the integration of BT and FC systems in multiple units, the conventional topologies (depicted in Figure 1.11) are analysed in detail. These configurations are presented from a generic scope, and can be valid for nearly any rail vehicle. Anyway, as previously outlined, the developments of this Ph.D. Thesis are oriented to multiple units, and therefore the scope of this section is focused on these vehicles.

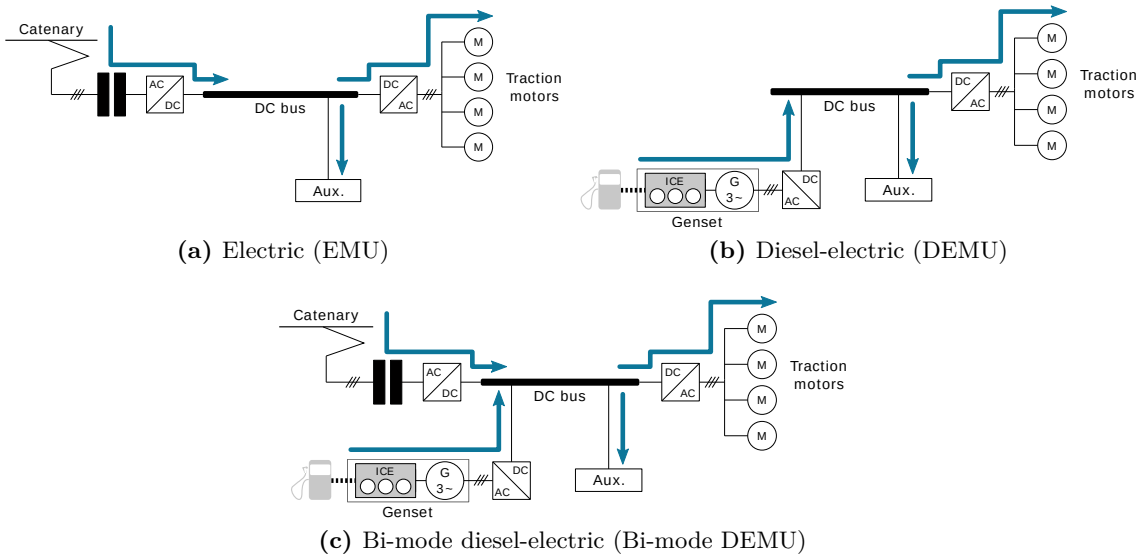

(a) Electric (EMU)

(b) Diesel-electric (DEMU)

(c) Bi-mode diesel-electric (Bi-mode DEMU)

Figure 1.11: Traiditional powertrain topologies for Multiple Units. Arrows represent potential power fluxes to/from DC bus.

The Electric Multiple Unit (EMU) obtains from the catenary system the required power for the auxiliaries and traction motors, as depicted in Figure 1.11a. The catenary systems can be different depending on the particular country or area where they are located, since the electrification of railway lines was developed differently according to the specific state-of-the-art technologies of each location [42]. Therefore, typically different AC and DC systems can be found, with different voltage amplitudes and frequencies (Table 1.3). Due to the fact that AC is easier to transmit over long distances, it is the preferred option

in long-distance rail lines. As the example of Figure 1.11a shows, in the case of an AC catenary system, a transformer and a converter are used to adapt the high voltage AC to adequate values for the DC link.

The second topology is the Diesel-Electric Multiple Unit (DEMU). The DC link of the DEMU is fed by a synchronous generator that converts the power generated by the diesel ICE, as it is depicted in Figure 1.11b. Both the ICE and the generator constitute the diesel generator set, also known as genset. In this topology, the voltage of the DC link can be adjusted depending on the design of the generator [42]. The DEMU is a typical choice for non-electrified railway lines, which nowadays constitute around the 65% of the global and 40% of the european rail networks (see Figure 1.3) [7, 11].

In some cases, rail vehicles serve services that drive through both electrified and non-electrified track sections. For these contexts, vehicles that are fed by both a catenary and a genset are required. This leads to the Bi-mode Diesel-Electric Multiple Unit (Bi-mode DEMU) topology, which is depicted in Figure 1.11c. As it is seen, the topology consists of a mixture between the EMU and the DEMU. In electrified sections, the catenary is the main power source, and in non-electrified sections the genset becomes the primary source. In some other cases, the term bi-mode is also used when referring to EMUs that drive through catenary systems of diverse characteristics (e.g., railway lines that include DC and AC track sections) [42].

1.3.3 Innovative Rail Vehicle Topologies

This subsection analyses the innovative topologies derived from the integration of BT and FC technologies in railway vehicles. Being an ESS, the BT can act both as a primary power source (replacing conventional technologies) or as a secondary power source (supporting conventional technologies). In contrast, the FC is understood as a generation device, and therefore it can only act as a primary power source, replacing conventional diesel- or catenary-based technologies. In the following subsections, the main features of each derived topology are reviewed, together with the commercial solutions already proposed by rail manufacturers.

1.3.3.1 BT as Primary Power Source

As mentioned, the BT can act as the primary and unique power source in a rail vehicle, what allows a 100% electric operation in non-electrified track sections. This topology is referred in the literature as the Battery Electric Multiple Unit (BEMU) [46], and it is depicted in Figure 1.12. In the cases where the vehicle drives in a railway line with both electrified and non-electrified track sections, the BT will be charged from the catenary using the same technology as in the EMU. Besides, in the cases where the vehicle drives exclusively in a non-electrified track, charging points are required to charge the battery. These charging points can be understood as very short catenary sections located in specific

points (e.g., the terminal station) [47]. Therefore, essentially both alternatives include the same elements, as it is depicted in Figure 1.12.

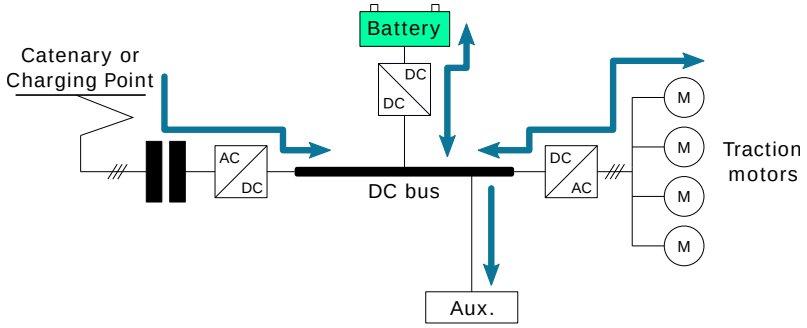

Figure 1.12: Battery Electric Multiple Unit (BEMU).

Some rail manufacturers have already proposed and developed the BEMU technology. Table 1.4 summarizes the projects that have ordered BEMUs for regular passenger use. The information has been obtained through a revision of the State of the Art and a compilation of press releases from railway manufacturers. The table includes the manufacturer of the vehicle, the operator that has ordered it, the year when the vehicle started the regular service, the BEMU model, the number of ordered vehicles, the deployed ESS technology, the capacity of the storage system, and the range of the vehicle in non-electrified sections. The cases in which an order has been signed but the commercial use has not started yet are specified with the year when the commercial use is expected to start. Trial or development projects are not included.

As seen in the table, the maximum provided ranges are around 120 km (Siemens' Mireo Plus B and Alstom's Coradia Continental) and 150 km (Stadler's Flirt Akku), what makes these vehicles impractical for long distance rail services without catenary support. The main barrier for the extension of the vehicle range is the limited available space and weight for the integration of big BT systems [12, 48]. In this sense, the development of BT technologies with a lower energy density and specific energy are required.

1.3.3.2 BT as Secondary Power Source

As second option, the BT can act as secondary power source to help the main supply of traditional topologies. This leads to the topologies known as Battery Hybrid Electric Multiple Unit (H-EMU) and Battery Hybrid Diesel-Electric Multiple Unit (H-DEMU). The hybridization offers some benefits and additional flexibility to the conventional EMU or DEMU vehicles. Among others, the following can be highlighted [43, 49, 50]:

- *Peak shaving:* Control of main source consumption to prevent power peaks. In the case of the H-EMU, this enables the possibility of downsizing the catenary power substations. In the case of the H-DEMU, it is possible to downsize the genset.
- *Backup mode:* Running capability when the primary source (catenary or genset) is

Table 1.4: Commercial projects involving BEMUs.

OEM	OPERATOR (Country)	YEAR	MODEL	QTY.	ESS (OEM)	QTY. (kWh)	RANGE (km)
J-TREC	JR East (JP)	2014 2017	EV-E301	1 3	LIB LMO (GS Yuasa)	190	*22.4* [2]
BOMBARDIER (ALSTOM)	Network Rail (UK)	2015	Electrostar Class 379	1	LIB LFP (Valence)	400	50
	SNCF (FR)	Expected (2023)	AGC [1]	5	LIB (Leclanché)	-	80
HITACHI	JR Kyushu (JP)	2016	BEC819	7	LIB LMO (GS Yuasa)	360	*10.8* [2]
	JR East (JP)	2017	EV-E801 Series	1	LIB LMO (Hitachi)	360	*26.6* [2]
SIEMENS	ÖBB (AT)	2019	CityJet Eco [1]	1	LIB LTO (Toshiba)	528	-
	NVBW (DE)	Expected (2023)	Mireo Plus B	20	LIB LTO (Toshiba)	-	120
	NEB (DE)	Expected (2024)	Mireo Plus B	26	LIB LTO (Toshiba)	-	120 *86* [2]
STADLER	Schleswig-Holstein (DE)	Expected (2022)	Flirt Akku	55	BT	-	150
	Wales & Borders (UK)	Expected (2022)	City Link BEMU	36	BT	-	*Short sections*
	Arriva (NL)	Expected (2025)	Wink BEMU	18	BT	180	*Short sections*
ALSTOM	VMS and ZVNL (DE)	Expected (2023)	Coradia Continental	11	LIB	-	120 *80* [2]
CAF	VRR and NWL (DE)	Expected (2025)	Civity BEMU	60	LIB	-	60-80

[1] Retrofitted models

[2] Values in italic represent length of non-electrified section, not the range of the vehicle

not available.

- *Energy Efficiency:* Energy recovery capability when braking (for both H-EMU and H-DEMU) and efficient operation of genset (for the H-DEMU).
- *Power Boost:* Increase of available power either for accelerating or for facing steep gradients.
- *Electric Mode:* 100% electric operation in low emission zones (e.g., in city centres).

Essentially, the H-EMU can be considered the same topology as the BEMU. As it was previously outlined, the BEMU requires of an external power source, which is typically a pantograph connected to a catenary (Figure 1.12). Therefore, the only difference between the H-EMU and the BEMU consists on how the different sources are operated: in the BEMU the battery works giving all the required demand, while in the H-EMU both power sources help in satisfying the demand. Indeed, some of the commercial vehicles depicted in Table 1.4 are expected to work also in H-EMU mode. In order to avoid potential

misunderstandings, in the remainder of this Ph.D. Thesis the term BEMU will refer to both alternatives.

Regarding the H-DEMU topology, the configuration is depicted in Figure 1.13. As it was outlined in Section 1.3.2, the H-DEMU can drive through railway lines with both electrified and non-electrified track sections. Therefore, the battery hybrid bi-mode DEMU is also possible. In order to simplify the terminology, H-DEMU will also refer to the battery hybrid bi-mode topology.

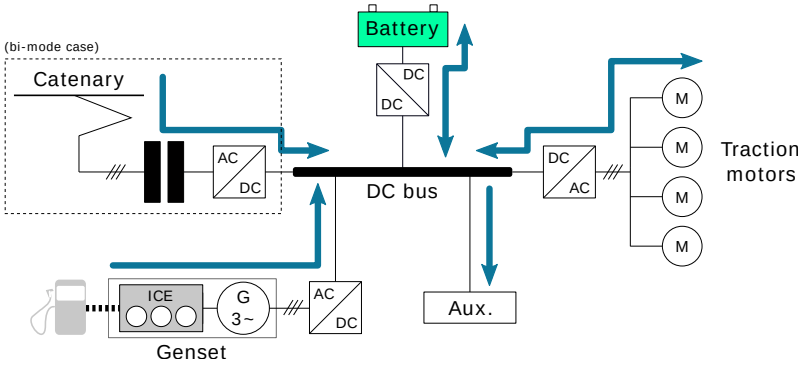

Figure 1.13: Battery Hybrid Diesel-Electric Multiple Unit (H-DEMU).

Table 1.5 reviews the commercial H-DEMU vehicles that are driving in regular passenger use (or are expected to). The table shows the manufacturer, the operator that has ordered the vehicle, the year when the commercial operation began, the H-DEMU model, the number of ordered vehicles, the storage technology, and the integrated storage capacity. Compared to the BEMU case, it can be noticed that smaller BT systems are integrated, due to the fact that the storage technology is not intended to be the main power source.

1.3.3.3 FC as Primary Power Source

An additional alternative for the electrification of railway vehicles is the integration of FC technology as primary energy source. The main benefit of this technology is that it allows a 100% electric operation. Moreover, if the hydrogen fuel is produced by an electrolysis driven by renewables, it can be considered that no pollution is generated [38].

However, the FC technology has also some disadvantages. The dynamic characteristic of the FC is relatevely low because of the auxiliary systems such as the air compressor, humidifier and cooler [51]. Accordingly, operating the FC with fast transients directly affects on its degradation [52, 53]. Therefore, the hybridization with a secondary power source is found to be essential for the correct integration of FC technology in railway vehicles [54, 55]. Following the analysis of the potential power sources developed in Section 1.2, it is concluded that a BT system is the most appropriate option for the auxiliary power source, even if hybridizations with EDLC systems have also been proposed in the past [56].

Table 1.5: Commercial projects involving H-DEMUs.

OEM	OPERATOR (Country)	YEAR	MODEL	QTY.	ESS (OEM)	QTY. (kWh)
J-TREC	JR East (JP) Koumi	2007	KiHa E200	3	LIB LMO (Hitachi)	15.2
	JR East (JP) Oito, Tsugaru, Ominato and Gono	2010	HB-E300 Series	5	LIB LMO (Hitachi)	-
	JR East (JP) Senseki-Tohoku	2015	HB-E210 Series	8	LIB LMO (Hitachi)	15.2
TOSHIBA	JR West (JP)	2017	Twilight Express Mizukaze	1	LIB LTO (Toshiba)	120
CRRC	Malaysia Rail Link (MY)	2020	Class 61	13	UC (CRRC)	-
STADLER	Arriva (NL)	2021	WINK	18	BT	180
	Wales and Borders (UK)	Expected (2023)	FLIRT Tri-mode	24	BT	-
ALSTOM	NASA (DE)	Expected (2021)	Coradia Lint	3	LIB	-
	SNCF (FR)	Expected (2022)	TER hybride (retrofitted)	1	LIB	-
PORTERBROOK[1]	Chiltern Railways (UK)	Expected (2021)	Turbostar Class 168-170	2	LIB	60.8
	Irish Rail (IE)	Expected (2021)	Class 22000	3	LIB	91.4
VIVARAIL[1]	Transport for Wales (UK)	Expected (2021)	Class 230	5	LIB NMC (Kokam)	200
SIEMENS	Amtrak (US)	Expected (2025)	Venture	9	LIB LTO (Toshiba)	-

[1] Porterbrook and Vivarail are companies oriented to the retrofitting of existing rail vehicles

Therefore, the configuration depicted in Figure 1.14 is found to be the most appropriate option for the integration of a FC in a multiple unit. Considering that a configuration with the FC as unique power source is not practical, and with the aim of simplifying the terminology, the depicted topology is defined as the Hydrogen Electric Multiple Unit (H_2EMU). As outlined in the previous section, railway vehicles can drive through lines with both electrified and not electrified track sections. In these cases, the bi-mode H_2EMU can be also deployed, as it is highlighted in Figure 1.14.

Some rail manufacturers have already proposed their concepts for the H_2EMU. As shown in Table 1.6, Alstom and Stadler have already won contracts to supply several H_2EMUs for regular passenger use. In the case of Alstom, two Coradia iLint vehicles are already driving in regular service since 2019. Additionaly, it is also known that companies such as Siemens (Mireo Plus H, which will be tested in Germany), CAF (Civity Hydrogen, which will be tested in Spain), Talgo (Vittal-One), Porterbrook and Vivarail are also working on their H_2EMU prototypes. As it is shown in the table, these vehicles are expected to have a driving range in non-electrified tracks of around 600-700 km, which

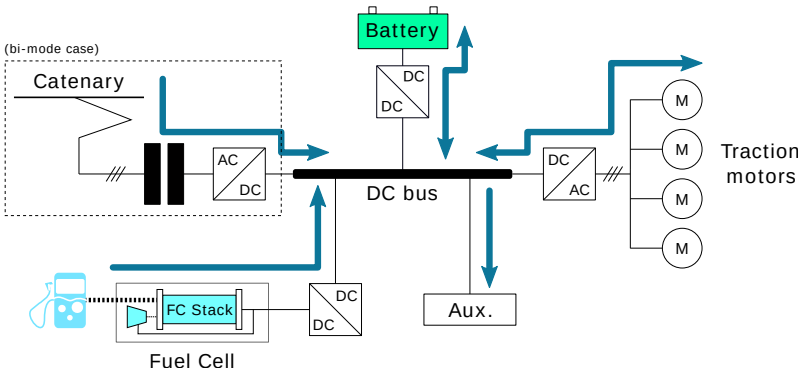

Figure 1.14: Hydrogen Electric Multiple Unit (H_2EMU).

is close to the ranges of diesel-based topologies. Therefore, H_2EMU vehicles become an appropriate alternative for long distance railway lines.

Table 1.6: Commercial projects involving H_2EMUs.

OEM	OPERATOR (Country)	YEAR	MODEL	QTY.	POWER SOURCES (OEM)	QTY.	RANGE (km)
ALSTOM	LNVG (DE)	2019	Coradia i-Lint	2	FC (Cummings) LIB NMC (Akasol)	FC 400 kW LIB 111 kWh	700
	LNVG (DE)	Expected (2022)	Coradia i-Lint	12	FC (Cummings) LIB NMC (Akasol)	FC 400 kW LIB 111 kWh	700
	FAHMA (DE)	Expected (2022)	Coradia i-Lint	27	FC (Cummings) LIB NMC (Akasol)	FC 400 kW LIB 111 kWh	700
	FNM (IT)	Expected (2023)	Coradia Polivalent	12	FC (Cummings) LIB NMC (Akasol)	-	600
	SNCF (FR)	Expected (2025)	Coradia Stream	6	FC (Cummings) LIB NMC (Akasol)	-	-
STADLER	Zillertalbahn (AT)	Expected (2022)	ÖBB Class 4090	5	FC BT	-	*32*[1]
	SBCTA (USA)	Expected (2024)	Flirt H2	5	FC BT	-	*14.5*[1]

[1] Values represent length of non-electrified section, not the range of the vehicle

1.3.3.4 Review of Innovative Topologies

Figure 1.15 reviews the evolution of the commercial projects involving the innovative railway topologies identified through Section 1.3.3: BEMU, H-DEMU and H_2EMU vehicles. The evolution is shown with the commulative number of ordered vehicles. The graph demonstrates that the interest of railway operators on innovative multiple unit topologies is exponentially increasing in the last few years.

As it has been highlighted, the integration of BT technologies in BEMU, H-DEMU and H_2EMU vehicles offers some advantages compared to the traditional EMU and DEMU topologies. However, some challenges do also emerge. The high cost of this technology, the involved additional weight, safety risks, temperature and degradation management,

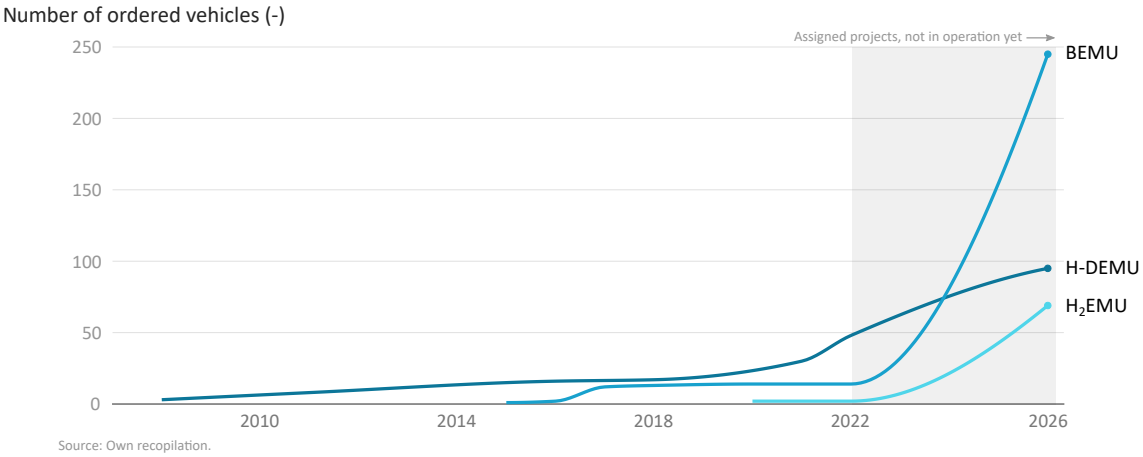

Figure 1.15: Evolution of commercial projects involving innovative powertrain technologies in rail vehicles (dates refer to the values at 1st January).

and the complexity of the energy management between the different sources are typically mentioned as the main challenges for the development of BT technology in rail vehicles [49, 57]. Accordingly, in the case of the H_2EMU, the integration of the FC involves additional challenges. Issues related to the FC cost, hydrogen supply, and the degradation that the FC suffers are commonly highlighted [58].

This Ph.D. Thesis will deal with the correct integration of FC and BT technologies on the mentioned multiple unit topologies. In this sense, the high cost of these technologies is identified as a crucial barrier not only for a wider deployment of BEMU, H-DEMU and H_2EMU vehicles, but also for the competitiveness of railway manufacturers. The literature typically identifies that for the optimal design of the powertrain, the size of their elements and the integrated control strategy need to be correctly defined (see Figure 1.4). Consequently, Section 1.4 and Section 1.5 analyse in detail the literature that deals with both issues. As already mentioned, the main contributions of this Ph.D. Thesis will be defined based on the conclusions extracted from these reviews.

1.4 Energy Management Strategies

The energy management is the control layer that organically coordinates the on-board energy sources in order to satisfy the power demand of the vehicle [59]. It is the outermost level in the hierarchy of control systems, as it is located above the power management and local control (see Figure 1.16) [18, 27]. The energy management plays a critical role in hybrid powertrain configurations (e.g., H-DEMU or H_2EMU), due to the fact that it is in charge of splitting the power supply between the different power and energy sources.

The energy management control is performed based on a strategy, which is denoted as the Energy Management Strategy (EMS). The design of the EMS is found to be one of the mayor challenges of hybrid powertrain configurations [16, 60, 61]. In order to

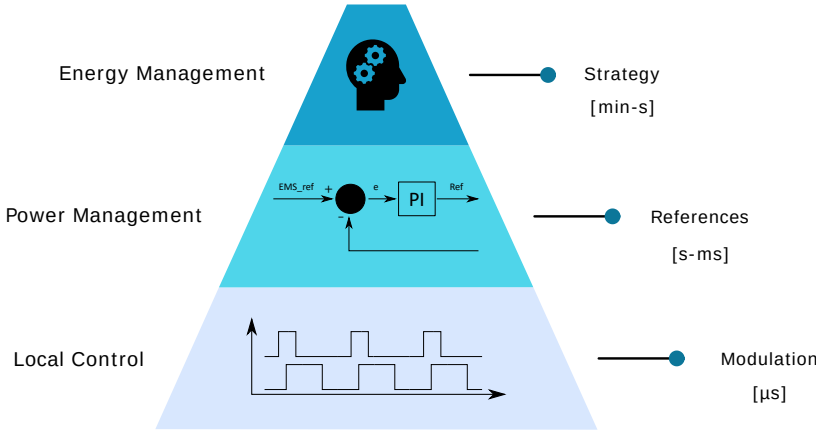

Figure 1.16: Control hierarchy in powertrain systems [18, 27].

obtain an efficient EMS, the strategy should be designed aiming certain objectives and ensuring the constraints or limitations of all the involved internal and external physical systems. Typically, the mentioned objectives include the improvement of fuel economy (both diesel or hydrogen), the increase of overall efficiency, the reduction of pollutant emissions, the maximization of the BT and/or FC lifetimes, or even a compromise among all the mentioned goals [16, 62–65]. Besides, the designed strategy should respect the operation constraints of each power source (i.e., the response time of the FC or the limits of the BT charge), it should exhibit resilience to possible external disturbances, it should be applicable under various driving conditions, and it should require a low computational burden in order to allow its implementation on a real-time controller [16, 66, 67]. Figure 1.17 reviews all the objectives and constraints for the design of an EMS.

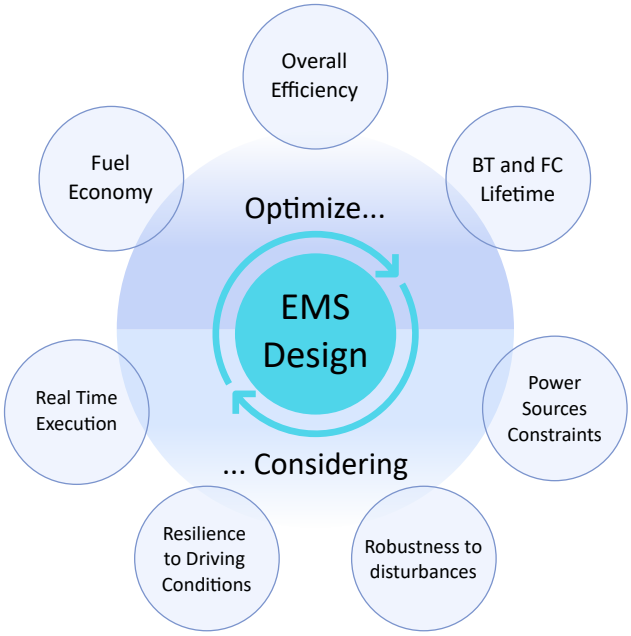

Figure 1.17: Objectives and considerations of EMS design.

All these requirements make the design of an efficient EMS a challenging task. This issue has been faced in the literature following different approaches, which are reviewed in the next subsections. First, the typical categorization of EMSs for hybrid vehicles is introduced in Section 1.4.1. Then, the specific literature related to EMSs for railway vehicles is reviewed in Section 1.4.2.

1.4.1 Classification of Energy Management Strategies

Figure 1.18 shows the generally accepted classification of EMSs, which includes three main categories: Rule-based (RB), Optimization-based (OB) and Learning-based (LB) strategies [16, 58]. Each category is further introduced in the following paragraphs.

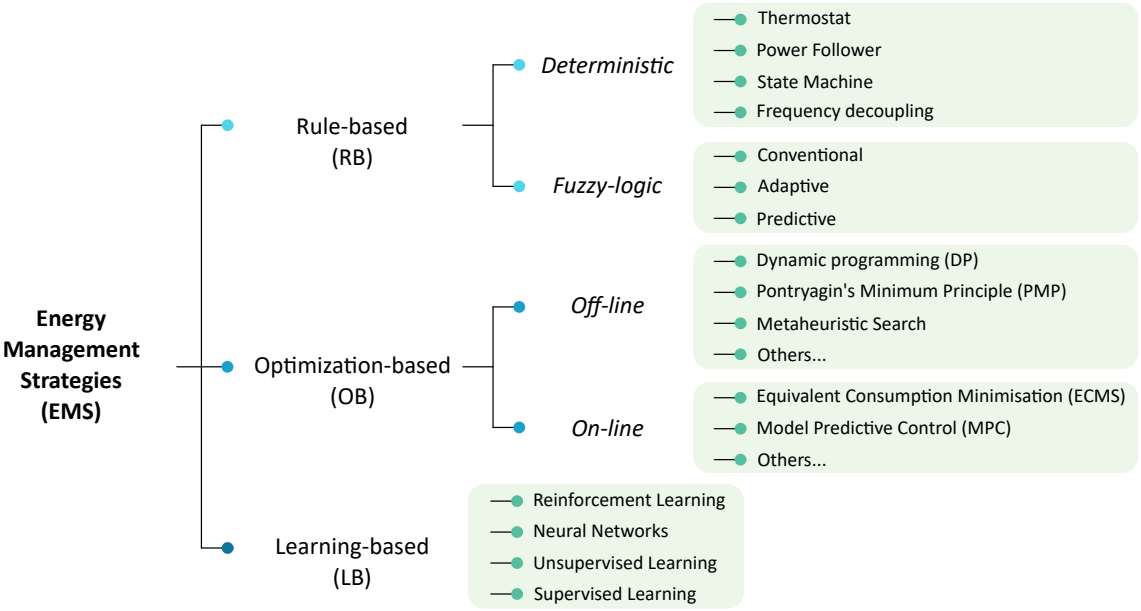

Figure 1.18: Classification of Energy Management Strategies [16, 58].

RB strategies define the power split based on predefined rules, which are designed based on heuristics, intuition, or human expertise [63, 65]. Therefore, they are simple to design and allow a feasible real-time implementation [64, 66]. However, in order to guarantee an optimal performance, a significant calibration effort is required, what typically leads to non-optimal or sub-optimal solutions [16, 62]. The rules can be either deterministic or fuzzy. Deterministic rules are useful for simple systems that can be easily interpreted or modelled. Besides, fuzzy rules are more oriented to complex systems, especially in the cases were linguistic knowledge can be efficiently implemented together with numerical data to model the controller [58]. Typical deterministic RB strategies include thermostat, power follower, state machine or frequency decoupling approaches; while fuzzy-logic RB strategies can be divided into conventional, adaptive or predictive approaches [16, 58].

OB strategies try to find the optimal control sequence that minimizes a cost-function [60, 63, 65]. This cost-function can be defined as the fuel consumption, BT lifetime, FC

lifetime, or even the life cycle cost of the system (which includes all the mentioned terms). OB strategies are further classified into off-line and on-line optimization.

On the one hand, off-line OB strategies perform a global optimization, which requires *a priori* information of the whole drive cycle and its conditions [60, 62]. Therefore, the minimum value of the objective function is obtained for the whole feasible space of the optimization problem [59]. However, these methods require high computational burden to be solved, what sometimes complicates their real-time implementation [59, 63]. The capacity to be implemented in real time, as well as the robustness of the OB strategy, also depends on the optimized variable: if the optimization returns a control sequence (e.g., a sequence of references for the FC or genset power), the solution is hard to be implemented in real time, and it will not be very robust against changes in the drive cycle. However, if the algorithm finds the optimal set of rules or thresholds for RB strategies, it is easier to implement, and it will be also robust to changes in the drive cycle (as long as the rules are designed to do so). Dynamic Programming (DP), Portryagin's Minimum Principle (PMP), and approaches based on metaheuristic search (e.g., genetic algorithms) are some of the typical off-line OB strategies [58].

On the other hand, on-line OB strategies perform a local optimization, which does not require *a priori* knowledge of the past and future driving conditions [16]. This is obtained by designing a cost-function that only depends on the present state of the system parameters [62, 65]. Therefore, the optimization can be implemented efficiently in real-time, but it only minimizes the cost-function for a limited space of the optimization problem. In some cases, in order to increase the space of the optimization problem, the use of predictive approaches is also proposed. Regarding the robustness, it depends on the used optimization algorithm. Equivalent Consumption Minimization Strategy (ECMS) and Model Predictive Control (MPC) are some well-known on-line OB strategies [16, 58].

Finally, LB strategies use advanced data mining methods, which allow deriving a control sequence based on historical, real-time and/or off-line optimized data [64, 65]. With data-driven and machine learning methods, causal and close-to-optimal strategies can be obtained, but a difficult and time-consuming approach to create an accurate database for the training step is required [58]. Neural network and reinforcement learning-based methods are some of the most used LB strategies in mobility applications [16, 58].

1.4.2 Energy Management in Hybrid Railway Vehicles

In the following paragraphs, the literature related to EMSs in railway applications is reviewed. The literature search has only been focused on hybrid diesel or hybrid FC topologies (e.g., H-DEMU or H_2EMU), considering their potential integration in innovative railway vehicles. Eventually, 42 research papers have been identified. In Figure 1.19, these publications are distributed according to the EMS type, publication year and the primary power source. As it can be noticed, only approaches dealing with RB and OB strategies

have been proposed for railway applications.

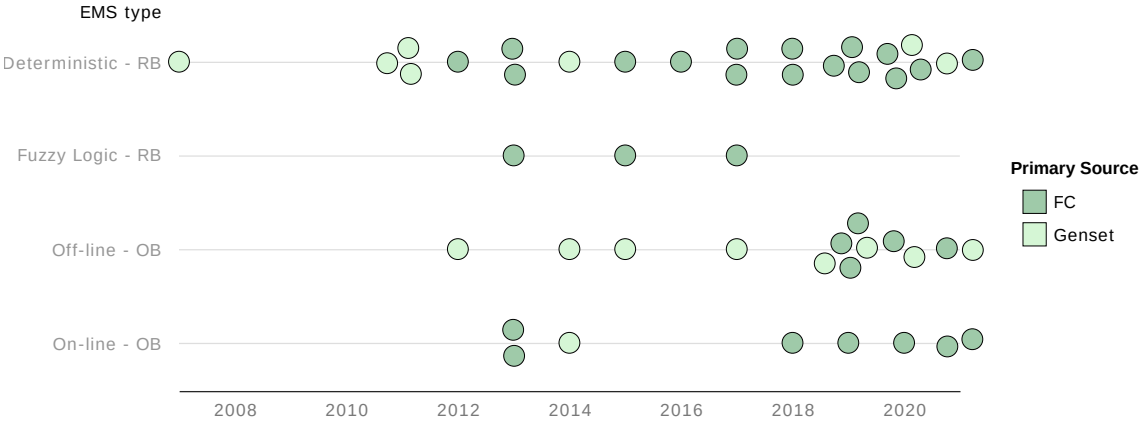

Figure 1.19: Identified literature according to EMS type and publication year.

1.4.2.1 Deterministic Rule-based Strategies

Regarding deterministic RB strategies, one of the most simple approaches consists on the thermostat strategy. The primary power source is turned on or turned off depending on the state of the auxiliary power source or power sources. This strategy is also referenced in the literature as the charge depleting and charge sustaining strategy. In the literature of hybrid railway systems, authors in [68] propose a thermostat strategy for a hybrid diesel-electric locomotive. They set the genset at its nominal operation point when the State of Charge (SOC) of the BT is below a certain threshold. On the contrary, when the SOC is above that threshold, the genset is turned off. In [69] a similar approach is proposed for a hybrid diesel-electric locomotive, but in this case the auxiliary ESS is composed of a BT and an EDLC. The thermostat controller defines the power output for the genset, and then a frequency decoupling strategy is proposed for splitting the remainder demand between the BT and EDLC.

Another typical deterministic RB strategy is the baseline control. This strategy consists on defining a constant power reference for the primary power source, so that the auxiliary system gives or absorbs the difference with the power demand. Indeed, it consists on the turned on state of the thermostat strategy. Authors in [54, 70] propose a baseline control for a hydrogen electric locomotive, and they define the constant operation point as the FC nominal power. Besides, the authors in [71] propose a similar approach for a hydrogen electric subway, but in this case the constant operation point of the FC is defined as the average power demand of the journey, so that the charge of the BT is sustained along the whole journey.

Some other simple deterministic RB strategies include the power follower and the frequency decoupling. The power follower is proposed in [72] for a hydrogen electric locomotive, and it consists on defining the FC power reference depending on the driving pattern (acceleration, cruising or braking). Besides, the frequency decoupling approach

consists on using a low-pass filter to split the power demand between different power sources. In [73] this strategy is proposed for a hybrid diesel-electric locomotive with an ESS composed of a BT and an EDLC. The genset works on its nominal operation point and then the low pass filter is used to split the rest of the demand between the auxiliary sources.

In some other publications, more complex deterministic RB strategies are proposed. A common approach is the state machine controller, which consists on varying the proposed rules depending on the state of the auxiliary power source. For instance, authors in [74, 75] propose a state machine controller for a H-DEMU with an EDLC as secondary power source. Three states are defined according to the SOC of the EDLC, and at each state a different power reference for the genset is set. Then, the same authors adapt this approach for a H_2EMU based on an EDLC [76]. A similar approach is proposed in [77] for a hydrogen electric locomotive, in which three states are defined depending on the SOC of the BT.

Some other authors combine a state machine controller with a droop control to split the demand in hybrid powertrains composed of three power sources. Authors in [78, 79] and in [80–82] have proposed separately similar approaches for hydrogen electric tramways with an ESS composed of a BT and an EDLC. They design a state machine controller with different states to define the FC power reference, and then a droop control adjusts the split between the BT and EDLC to maintain the voltage of the DC bus. Finally, in a more recent approach, authors in [52] design a state machine controller for a H_2EMU based on the results of a DP off-line optimization.

Another trend in deterministic RB strategies consists on designing a controller based on classic control theory. In some approaches, the controller is designed aiming a reduction of the error between a reference SOC and the real SOC of the auxiliary power source. Authors in [83] define this controller for a H_2EMU, authors in [84] for a diesel-electric locomotive, and authors in [85] for both a H-DEMU and a H_2EMU. Besides, some other authors have designed controllers to maintain the voltage of the DC bus in stable conditions, which is attained by means of a droop control. Authors in [86] propose this approach for a H_2EMU, and authors in [53, 87] for a hydrogen electric tramway. In both cases, the ESS is composed of a BT and an EDLC.

1.4.2.2 Fuzzy Logic Rule-based Strategies

The algorithm of a fuzzy logic controller is composed of three steps, as it is summarized in Figure 1.20. First, in the fuzzification approach the measurable variables (inputs) are translated to subjective or linguistic format. Then, this information is compared to heuristic rules, which are implemented with if-condition-then sentences. Finally, the defuzzification translates again from linguistic to measurable format in order to define the controller output [18].

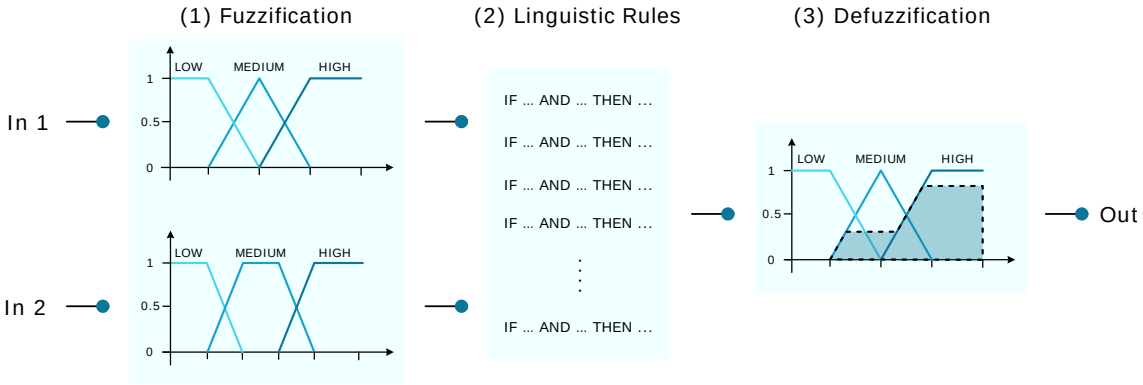

Figure 1.20: Working principle of Fuzzy Logic RB controller [18].

This scheme is followed in conventional fuzzy logic approaches. Authors in [79] proposed this EMS for a hydrogen electric tramway with BT and EDLC systems as auxiliary power sources. The SOC of both storage devices and the power demand are defined as the inputs of the fuzzy controller, and the FC reference and the change rate of the BT reference are defined as outputs. The obtained results are compared against a state machine controller (0.6% higher fuel consumption) and a couple of on-line OB strategies (2.6% higher fuel consumption than the best approach).

Besides, authors in [88] also propose a conventional fuzzy logic strategy for the same vehicle application. However, in this case the power demand is divided into different signals following a frequency decoupling approach. These signals, together with the SOC of both auxiliary power sources, are used as inputs to two fuzzy logic structures: the first one returns the FC reference, and the second controller the reference for the EDLC. The proposed strategy is compared to a frequency decoupling approach (11.4% overall efficiency improvement) and a fuzzy logic controller without frecuency decoupling (4.4% overall efficiency improvement).

Finally, a conventional fuzzy logic approach is also proposed in [72], in this case for a hydrogen electric locomotive. As in this case the powertrain is composed just of a FC and a BT, the controller is simplified: the power demand and the SOC of the BT are defined as inputs, and the FC reference as the output. The obtained results are compared against a power follower strategy, what unveils that 2.5% fuel reduction can be achieved.

In the case of the adaptive fuzzy logic approach, the parameters of the fuzzy-sets are weighted in order to vary the importance of a certain parameter or variable. The weight values are adapted depending on internal or external conditions (e.g., the driving environment). Besides, in predictive fuzzy logic approaches look-ahead windows are used to predict future states and take decisions based on this information. However, neither adaptive or predictive fuzzy logic approaches have been proposed for the hybrid railway vehicle topologies being analysed.

1.4.2.3 Off-line Optimization Strategies

One of the typical off-line OB strategies is the Dynamic Programming (DP) approach. This algorithm returns the optimal control trajectory to reduce a certain cost function based on Bellman's optimality principle. This principle states that an optimal decision can be derived by breaking down a complex problem into several subproblems [89]. A chart representing the working principle of DP is depicted in Figure 1.21. Typical DP optimization is proposed in [45] and [90] for a H-DEMU and in [77] for a hydrogen electric locomotive. In all cases, the secondary power source consists of a BT. In these publications the optimization aims a minimization of the fuel use (diesel or hydrogen), and it returns the optimal sequence of the split factor between the powertrain sources. DP results are compared against a state machine strategy (from 17% to 25% improvement in fuel use) in [45], and against a Quadratic Programming (QP) optimization (9.8% higher operation cost) in [77]. Besides, the authors in [91] propose a DP optimization for a H-DEMU that also returns the optimal sequence of the vehicle speed that minimizes the overall fuel consumption. The simulation results are compared against a traditional DEMU, obtaining a 33% reduction in the fuel consumption.

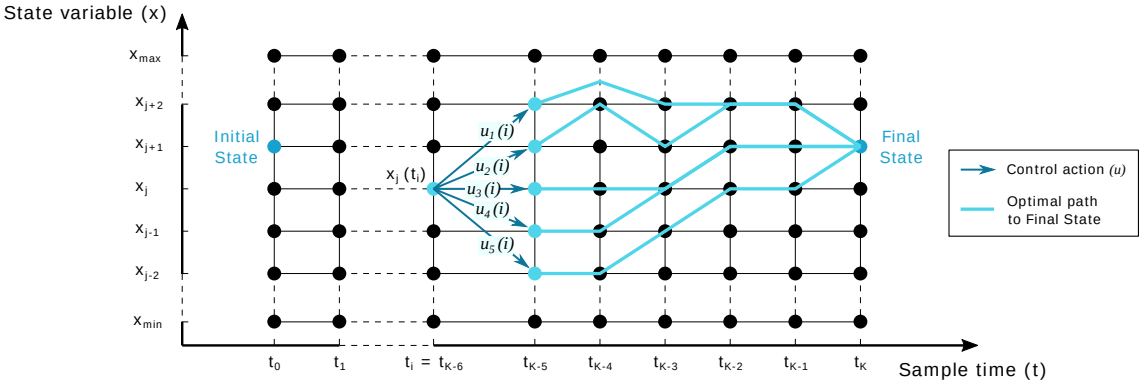

Figure 1.21: Dynamic Programming working chart.

The Pontryagin's Minimum Principle (PMP) is also a typical off-line OB approach proposed in the field of EMS problems. This principle relies on the idea that the optimal control sequence is obtained by solving the minimization of the Hamiltonian function [59]. The authors in [92] propose this approach for a H-DEMU with a BT as secondary power source. The algorithm returns the optimal control sequence for the genset aiming the minimization of the fuel consumption. The obtained results are compared against a RB state machine strategy, achieving a 7.3% reduction in the fuel use.

Some other non-linear optimization techniques have been proposed to solve the problem of the optimal EMS in hybrid railway vehicles. Authors in [77] propose the previously mentioned QP approach for a hydrogen electric locomotive with a BT as secondary power source. This method consists on a simplification of the typical DP approach in order to reduce the computational burden, but at the expense of the simplification and linearization of the cost function. Nevertheless, the simulation results unveil a 9.8% cost reduction

compared to DP. Besides, the method of Lagrange Multipliers is proposed in [93] to solve the optimal control sequence of the FC of a hydrogen electric tramway with an EDLC as secondary power source. This optimization also aims the reduction of the fuel use. The obtained hydrogen consumption is compared to that of a power follower strategy (2.5% reduction) and an ECMS (3.2% reduction). Finally, the authors in [94] apply the non-linear Simplex method to optimise the performance of a H-DEMU with a BT as secondary power source. In this case, the cost function includes both the fuel use and the deviation from a predetermined SOC value. The results unveil a 23% fuel reduction compared to a traditional DEMU.

The off-line OB approaches reviewed so far are typically used as benchmark to evaluate other strategies, since they return the global solution to the EMS optimization problem. However, and as it was already highlighted, the control sequences that these methods return are hardly implementable on-line, as they are optimized for a specific context or driving cycle. In other words, the replicability of these sequences in other driving cycles is limited. Nevertheless, some other optimization approaches can be proposed to optimize controllers that can be implemented on-line.

Metaheuristic search methods are typically implemented for this purpose. Authors in [95] propose a state machine controller for a hydrogen electric tramway with a BT and an EDLC as secondary power sources. The state machine relies on a series of thresholds for the power demand and SOC of both storage systems. These thresholds are optimized by two different evolutionary algorithms (Artificial Fish Swarm Algorithm and Multi-Population Genetic Algorithm), with the objective of reducing the operation costs of the tramway. The best result is obtained with the first evolutionary algorithm, achieving a 25% cost reduction compared to the non-optimized state machine strategy. Besides, an adaptive fuzzy logic controller for a hybrid diesel-electric locomotive is optimized in [96]. The auxiliary power system is composed of a BT and an EDLC. The membership functions of the fuzzy-logic controller are tuned based on a Genetic Algorithm (GA) optimization, which aims the reduction of the fuel use.

A more complex approach is proposed by the authors in [56]. In this case, an ECMS is proposed for a hydrogen electric tramway with a BT and an EDLC as auxiliary power sources. This on-line OB controller (introduced later in Section 1.4.2.4) returns the power references for the FC and BT, but they are later adjusted by a state machine controller. The balance factor that determines the performance of the ECMS-based controller is optimized by the Firefly Algorithm approach in order to reduce the operation costs of the tramway. The results are compared against a simple RB controller and the non-optimized ECMS, unveiling a reduction on the operation costs of the 39.6% and 13.8%, respectively.

In addition to metaheuristic search methods, non-linear optimization algorithms can also be used to optimize RB controllers. For instance, authors in [43] propose a classic control loop to control the SOC of the BT in a H-DEMU. Using a Direct Optimization approach, the controller parameters are optimized aiming a diesel use reduction. According

to the authors, a 16.5% fuel reduction can be achieved compared to a traditional DEMU. Besides, authors in [97] optimize a controller based on frequency decoupling for a H-DEMU with a BT and an EDLC as auxiliary power sources. The frequency decoupling based controller was already introduced in [73] (see Section 1.4.2.1). The authors propose a Sequential Quadratic Programming (SQP) approach to optimize the value of the low pass filter and the reference value for the genset power, with the aim of reducing the fuel use.

1.4.2.4 On-line Optimization Strategies

Regarding on-line OB strategies, the ECMS is one of the most used approaches. It consists on converting the electric consumption of the secondary power source (e.g., the BT) to the fuel consumption of the primary power source (e.g., the genset) at each sample time. In this way, the control action that minimizes the total equivalent fuel consumption can be defined [58].

Authors in [79] and authors in [98] have proposed an ECMS for a hydrogen electric tramway with a BT and an EDLC as auxiliary power sources. As the ECMS is designed for powertrains comprised of only two power sources, in both cases the optimization dismisses the equivalent consumption of the EDLC device. The controller returns the power reference for the BT, and then additional rules are set for the EDLC reference definition. The proposed strategies are compared against a series of RB strategies, and in both publications the ECMS is found to be a better option in terms of fuel consumption.

A similar approach is proposed in [99], but in this case instead of the equivalent fuel consumption, the equivalent efficiency of the secondary power source is calculated. The authors name this strategy the Equivalent Energy Consumption Minimization Strategy (EECMS), and they propose it for a hydrogen electric tramway with an EDLC as secondary power source. The strategy is tested in a Hardware in the Loop environment and in a trial operation of a real tramway. The obtained results are compared against the typical power follower strategy, obtaining a 2.4% and an 8.2% fuel improvement in the Hardware in the Loop and in the trial operation tests, respectively.

Another well-known on-line OB strategy is the Model Predictive Control (MPC), which is depicted in Figure 1.22. This approach consists on applying the predictive control theory to manage a hybrid powertrain system. At each sample time the controller makes the following steps: (1) it takes the current state as the initial state, (2) it predicts the model outputs and states over a specific horizon, (3) it optimizes the control actions over that horizon, and (4) it applies the optimized control action [100]. MPC is proposed for a hydrogen electric tramway with a BT and an EDLC as auxiliary power sources in [79]. They compare its performance against a series of RB strategies and the ECMS. The MPC strategy is a better option than the RB approaches in terms of fuel consumption, but it requires a longer computation time. Compared to ECMS, 1.8% higher fuel use is obtained, and it also requires a longer computation time. Besides, authors in [101] propose

a variation of the MPC for a H_2EMU with a BT as secondary power source. In this case, they add an online adaptively estimated co-state (as in PMP) to avoid the definition of a SOC reference for the controller. The results show a reduction of the 12.1% in the fuel use compared to a classic MPC.

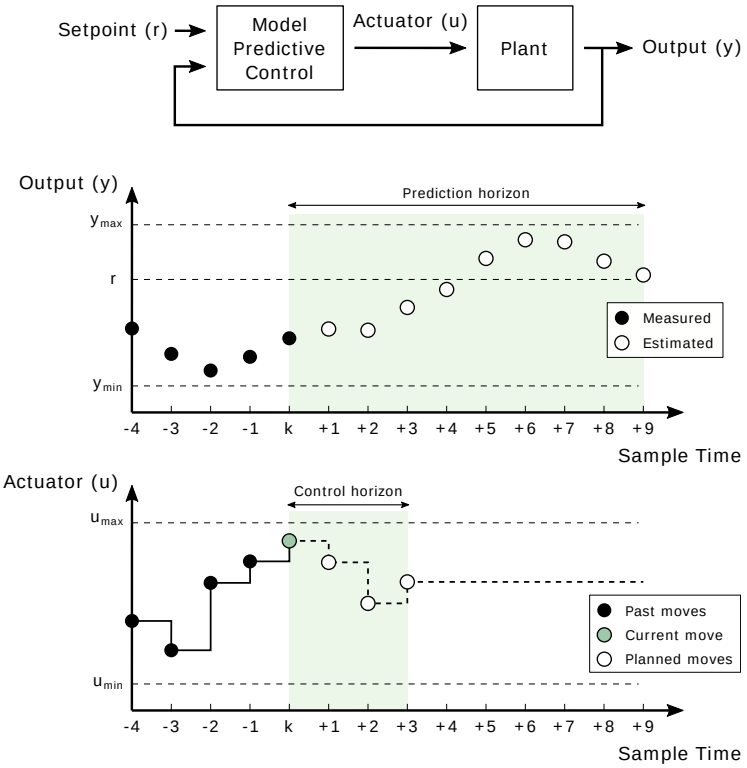

Figure 1.22: Model Predictive Control structure and working example [79].

Finally, authors in [102, 103] propose a novel on-line OB strategy based on the classic PMP. In this case, they propose an approach to regularly correct the co-state using an analytical formula derived from the energy conservation principle. This reduces the computational burden and allows the on-line implementation of the typically off-line computed PMP. They apply the proposed strategy to a H_2EMU with a BT as the secondary power source. The performance of the strategy is tested in a simulation environment and in a test bench, obtaining a maximum deviation on the fuel consumption of the 2.7% compared to the classic off-line optimized PMP.

1.4.3 Review of Energy Management in Railway Vehicles

The literature reviewed in this section has unveiled some limitations on the EMSs proposed for hybrid railway vehicles. These limitations are reviewed below:

(1) Most of the proposed strategies are designed aiming only one of the optimization objectives defined in Figure 1.17. A typical choice is to optimize the EMS just to reduce the fuel use, but without checking the overall efficiency or lifetime of the

other power sources. Only the approaches that propose to optimize the total cost of the vehicle (including acquisition and operation costs) consider together the three points mentioned above.

(2) Accordingly, most of the designed strategies do not analyse the design considerations highlighted in Figure 1.17. The analysis of the real time execution, the resilience to driving conditions or the robustness to potential disturbances are barely addressed in the reviewed literature, even if they are essential to develop adequate strategies.

(3) Publications analysing different EMSs and comparing their characteristics are scarce. Typically, the obtained results are just compared to a simple RB strategy or to the global optimization result given by the DP algorithm. This impedes the obtention of a real conclusion on which are the most appropriate strategies.

(4) LB strategies developed for the hybrid railway vehicles analysed in the current approach are missing. These EMSs become essential to replicate on-line the OB strategies that are hardy applicable in real operation (e.g., DP strategy).

In order to face the enumerated challenges, this Ph.D. Thesis proposes to develop and analyse different EMSs. This analysis will allow comparing the strategies according to the features highlighted in Figure 1.17. Among the proposed approaches, LB strategies will be developed, which will result in one of the contributions of the current Ph.D. Thesis.

1.5 Powertrain Design Approaches

The problem of finding the optimal EMS to control the different sources in a hybrid powertrain is closely coupled with the problem of finding the optimal size of the powertrain elements [63, 90]. Indeed, the performance of any control strategy is constrained by the capabilities and characteristics of the involved physical elements. Therefore, and as it has been already highlighted in Figure 1.4, an optimal design of the powertrain should consider in an integrated manner both levels: the sizing of the powertrain elements and the associated control strategy (or EMS) [17].

Ideally, the sizing approach should consider all the elements of the powertrain, including converters and traction motors (Figures 1.12, 1.13 and 1.14). However, the scope of this Ph.D. Thesis is solely focused on the design of the power sources (i.e., genset, FC or BT). It is assumed that the converters are associated to the size of each power source, and that the traction motors and related devices are designed to comply with the general features of the vehicle.

Different approaches can be followed in order to coordinate the powertrain sizing and powertrain control levels [16, 17]. A classification of these approaches is depicted in Figure 1.23. A typical procedure is to derive analytically the required sizing without deploying an optimization. In these cases, the EMS is designed *ad hoc* for the defined sizing, and

it can consist of an optimized or a non-optimized strategy (see Section 1.4). When an optimization is deployed for the sizing approach, different coordination architectures can be followed to handle the design and optimization of both levels. In the non-optimized EMS, only the powertrain sizing is optimized, with a predefined control strategy that is not altered by the obtained sizing. When a sequential optimization is followed, both levels are independently optimized. In the alternating optimization, the sizing and EMS optimization are deployed independently and alternatively until a certain convergence is reached. In the nested optimization, for each evaluation of a certain powertrain sizing the optimal EMS is derived. Finally, in the simultaneous optimization, both levels are optimized in a single approach.

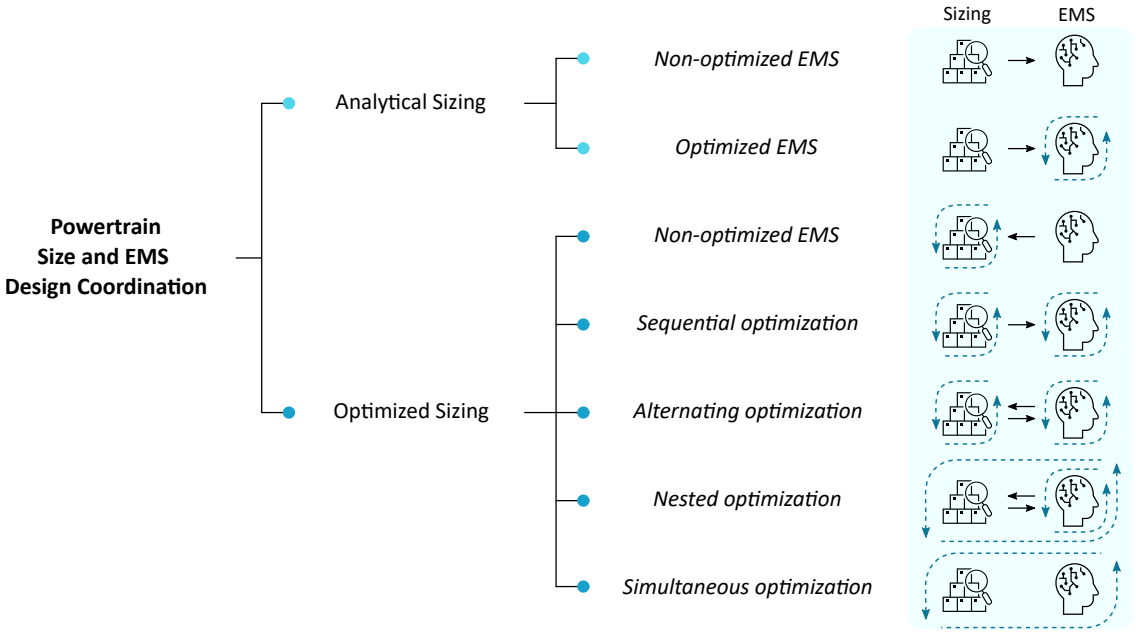

Figure 1.23: Powertrain design coordination concepts.

In most of the literature reviewed in Section 1.4.2, the sizing of the powertrain elements was predefined, as the main objective was the design of a novel control strategy. However, there are some other publications that deal together with the design of both the powertrain elements and the control strategy. In the following subsections these publications are reviewed.

1.5.1 Analytical Powertrain Designs in Hybrid Railway Vehicles

Regarding the analytical designs for hybrid railway powertrains, a simple approach consists on retrofitting previously designed conventional vehicles. For instance, authors in [84, 92] base their researches on existing diesel-electric vehicles. In both cases, half of the original gensets are removed, and in the released space BT packs are integrated. The followed sizing procedure consists on integrating the maximum amount of BT energy that the space or the weight limitations allow.

Another well-known analytical procedure consists on designing the primary power source considering that it will work most of the time on its nominal working point. One of the most deployed EMSs consists on the primary power source giving a constant power value around the average demand of the journey (baseline control, see Section 1.4.2). In these cases, the primary power source can be sized so its nominal operation point coincides with that average demand value. This approach is followed in [69] for a genset-based hybrid powertrain, and in [71, 78, 79, 86] for FC-based hybrid powertrains. In these cases, the secondary sources are designed so that they can provide the required power peaks or so that they do not perform deep charge and discharge cycles.

Besides, authors in [75] focus on designing the secondary power source (an EDLC) of a H-DEMU. They predefine the genset size, and based on an energetic simulation, they estimate the energy that the EDLC would absorb. A similar approach is followed in [43]. In this case, the secondary power source (a BT) of a H-DEMU is sized based on the braking energy that can be potentially recovered. Then, the genset size is defined considering the traction requirements and the maximum peak that the BT would give.

A more comprehensive approach is proposed in [73] for a hybrid diesel-electric locomotive. First, a relation between the EDLC and BT sizes and the EMS (frequency decoupling) is analytically derived. This allows obtaining the corresponding EDLC and BT sizes for each genset size. Then, the possible sizing combinations are analysed from the battery degradation, diesel use, powertrain volume and powertrain acquisition cost. A compromise between the analysed factors is found in order to select the most appropriate sizing of the powertrain. Therefore, it can not be considered that an optimization is deployed, as an analytical solution is deduced.

1.5.2 Optimized Powertrain Designs in Hybrid Railway Vehicles

The solutions obtained by the reviewed analytical approaches do not ensure optimality, as they are typically oriented just to comply with some minimum requirements (e.g., sizing the BT so it is able to recover all the braking energy). Therefore, some other works propose to implement an optimization to solve the most appropriate sizing for the power sources.

In most of the reviewed literature dealing with the optimization of the powertrain sizing, the EMS is independently designed and non-optimized. Authors in [54, 70] optimize the FC and BT sizes of a hydrogen electric locomotive by means of a Particle Swarm Optimization (PSO). The objective function considers the acquisition and replacement costs of the powertrain elements. In publication [70], the cost function additionally includes the cost related to the fuel use. Besides, authors in [72] propose the optimization of the FC, BT and traction motor sizes of a hydrogen electric locomotive by means of the bisection method. The deployment of a exhaustive search optimization is proposed in [76] to obtain the FC and EDLC sizes that involve the lowest acquisition costs for a H_2EMU.

A nested design optimization is proposed in [45] in order to handle together the EMS

and powertrain sizing problems for a H-DEMU. The genset size is predefined, so the optimization algorithm is focused on seeking the BT size that involves the lowest fuel consumption. The optimization is solved by an exhaustive search, since the feasible solution region is discretized. For each evaluation of a potential solution (i.e., for each BT size) the EMS is optimized by means of the DP algorithm.

Finally, authors in [97] deploy a SQP approach in order to simultaneously optimize the EMS (frequency decoupling) and the genset and BT sizes of a H-DEMU. As the EMS performance is defined by the value of the low pass filter, a single optimization algorithm can handle all the optimization variables together. The optimization aims the minimization of the powertrain acquisition costs.

1.5.3 Review of Powertrain Design Approaches

This section has reviewed the literature that handles together the sizing of the power sources and the design of the EMS. On the one hand, analytical procedures derive the required sizing without deploying any optimization. It has been found that most of the identified literature works propose analytical procedures. On the other hand, optimization approaches can be followed to derive the optimal sizing and/or EMS. In this case, different architectures can be followed to handle both levels together. It has been found that most of the publications that propose an optimization of the powertrain sizing do not consider the optimization of the EMS in an integrated manner. Considering that a cost-optimal powertrain design should consider together both approaches, nested or simultaneous optimization architectures are identified as the most appropriate ones.

Additionally, it is important to highlight that typically the powertrain is designed *ad-hoc* for a specific drive cycle and/or economic context. The effect of varying this environment has not been comprehensively addressed in the literature, what requires reproducing the optimization each time the drive cycle and economic context is varied. In order to overcome this issue, in this Ph.D. Thesis the interrelations between the cost-optimal powertrain design and the context related to the driving scenario and the economic model will be studied.

1.6 Conclusions and Main Gaps

The objective of the reviewed State of the Art has been to summarize the background knowledge related to the design and control of innovative powertrain technologies for railway vehicles. Therefore, this section aims to determine the challenges identified in this field, as well as to highlight the main lacks and possible improvements over the current research works. The obtained conclusions serve as basis for the definition of the contributions proposed by this Ph.D. Thesis.

Section 1.2 has reviewed the potential innovative technologies to replace ICE-based

powertrains. The characteristics of FW, BT, EDLC and FC devices have been analysed considering the specific requirements of railway applications. Due to the space and weight limitations of these vehicles, the need of technologies with high specific energy has been identified. Therefore, FC and BT systems have been found to be the most appropriate power sources to be integrated in railway applications and substitute or supplement traditional ICE-based technologies. Amidst FC systems, PEMFC technology shows the best characteristics for the integration in rail vehicles, while LIB technology is claimed to be the best option for BT systems. However, different LIB chemistries can be found in the market, which differ in terms of safety, specific energy and power, degradation or cost. The literature has barely addressed the issue of the most appropriate LIB chemistry for railway mobility applications.

Then, Section 1.3 has introduced a classification of the different railway transport modes and railway vehicles. Conventional rail accounts for most of the rail transport activity, and it is the only sector where diesel-based traction systems are predominant yet. Therefore, it has been defined that the developments of this Ph.D. Thesis will be oriented to conventional rail transportation, specifically to the vehicles denoted as multiple units. In a next step, the integration of FC and BT technologies in multiple units has been evaluated. A market evaluation of these topologies has unveiled that the interest of railway operators on deploying BEMU, H-DEMU and H_2EMU vehicles is exponentially increasing in the last few years. Consequently, it has been stated that this Ph.D. Thesis will be oriented to these powertrain architectures.

The emergence of innovative topologies rises new technological challenges, which need to be solved in order to obtain cost-optimal solutions compared to conventional technologies. The optimal design of a powertrain needs to consider the sizing of the power sources and the design of the integrated EMS if a cost-optimal solution is aimed. In Sections 1.4 and 1.5 the literature related to EMS and sizing approaches has been reviewed.

Regarding the concept of the EMS, the requirements that a control strategy should meet have been first identified: the optimization objectives that may be defined, and the constraints that should be considered. Then, an analysis of the existing literature related to this topic has been developed. The reviewed State of the Art has unveiled some limitations in the EMSs proposed for hybrid railway vehicles. First, most of the strategies are designed aiming only one of the identified optimization objectives. For instance, EMSs are typically designed just to consume the lowest possible fuel consumption, but other objectives such as overall efficiency or the degradation suffered by FC and BT devices are disregarded. Another limitation deals with the design constraints that should be checked for the correct implementation of an EMS. Specifically, the analysis of the real time execution, the resilience to driving conditions or the robustness to potential disturbances are barely addressed in the reviewed literature. Besides, publications analysing different EMSs and comparing their characteristics are scarce. Typically, the obtained results are just compared to a simple RB strategy or to the global optimization result, what impedes the obtention of a real conclusion regarding which are the most appropriate

strategies. Finally, LB strategies developed for hybrid railway vehicles have not been proposed yet. These EMSs become essential to replicate on-line the OB strategies that are hardy applicable in real operation.

Finally, Section 1.5 has reviewed the possible approaches to handle together the sizing of the power sources and the EMS design. This review has unveiled that recent researches have been more focused on analytical procedures, which do not derive an optimal solution. Moreover, most of the publications that propose an optimization of the powertrain sizing do not consider the optimization of the control strategy in an integrated manner. Considering that a cost-optimal powertrain design should consider together both approaches, nested or simultaneous optimization architectures are identified as the most appropriate ones. Additionally, it is necessary to highlight that the optimizations of both EMS and powertrain sizing are typically developed considering static conditions. That is to say, the powertrain is designed *ad-hoc* for a specific drive cycle and economic context. The effect of varying this environment is not comprehensively addressed in the literature, what requires reproducing the optimization each time the drive cycle and economic context is varied.

In order to handle all the identified challenges and literature gaps, this Ph.D. proposes the development of a **holistic design methodology for innovative railway vehicles focused on the definition of the power sources** (sizing and BT technology selection) **and the EMS or control strategy**. A comprehensive Life Cycle Cost (LCC) analysis is proposed in the next chapters, which aims finding the interrelations between the cost-optimal powertrain design and the context related to the driving scenario and the economic model. Considering the importance of the EMS design on the optimal powertrain solution, this Ph.D. Thesis proposes to develop and analyse different EMSs in order to compare their main features related to the identified optimization objectives (fuel use, power sources degradation and overall efficiency) and performance constraints (real time execution, resilience to driving conditions and robustness to potential disturbances).

2

Holistic Design Methodology for Rail Vehicles Powertrain and Operation Definition

Summary

The second chapter presents the holistic design methodology proposed as the main contribution of this Ph.D. Thesis. As it was concluded in Chapter 1, the methodology focuses on the design of the powertrain elements (sizing and technology definition) and the design of the energy management strategy. The holistic design methodology is based on an integral life cycle cost analysis composed of different steps. In this second chapter, all the models and methods required for the development of the life cycle cost analysis are explained in detail. As additional contribution of this Ph.D. Thesis, a chemistry-dependent battery degradation model is also presented in this chapter.

2.1 Introduction to Holistic Design Methodology

The objective of this Ph.D. Thesis is the development of tools and methodologies for the cost-effective integration of innovative technologies (FC and BT) in the powertrain of railway vehicles, specifically in H-DEMU and H_2EMU vehicles. The review developed in Chapter 1 has concluded that this research should focus on the design of the powertrain elements (sizing and technology definition) and control strategy (EMS), considering also the impact of the context (driving cycle and economic parameters) on that design. In order to face the identified challenges, in this Ph.D. Thesis a holistic design methodology based on an integral LCC analysis is proposed, which is depicted in Figure 2.1.

The proposed analysis considers holistically the effect that all the features mentioned above have on the LCC of the innovative vehicles: rail topology, EMS design, BT chemistry, size of power sources, driving scenario and parameters of the economic model. The ultimate goal of the LCC analysis is the identification of the parameters and/or features most dependent and most transversal to the context characteristics (i.e., to the driving scenario and to the parameters of the economic model). Based on these conclusions, a tool for the optimal design of the powertrain elements (technology and sizing) and the control strategy (EMS) based on the context characteristics could be developed for each of the analysed vehicle topologies. In the following sections, the integral LCC analysis is explained in detail, including all the models and methods required for this approach.

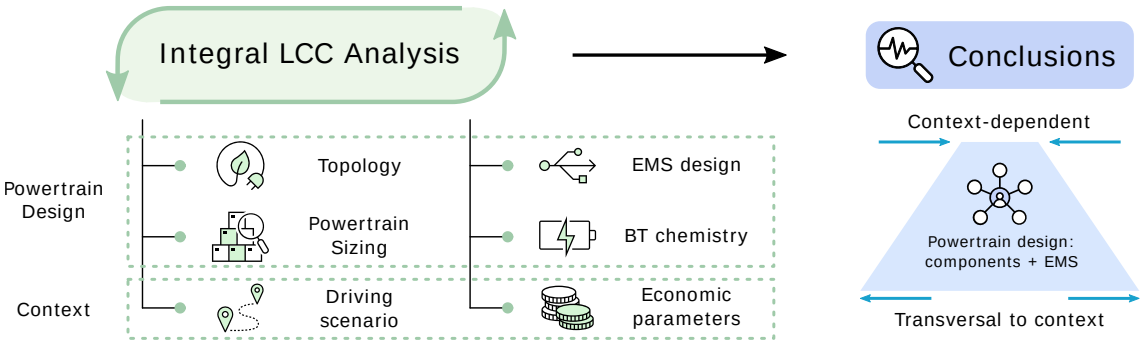

Figure 2.1: General overview of the methodology proposed in the Ph.D. Thesis.

2.2 Structure of Integral Life Cycle Cost Analysis

The LCC analysis should consider the effect of all the parameters and features highlighted in Figure 2.1. Developing a sensitivity analysis that considers together the variations of all the parameters or features is a time-consuming and therefore unviable approach. Consequently, the LCC analysis proposed in this Ph.D. Thesis is divided into different steps, as depicted in Figure 2.2. The entire LCC analysis presented in the following paragraphs is developed individually for each of the vehicle topologies to be analysed: H-DEMU and H_2EMU.

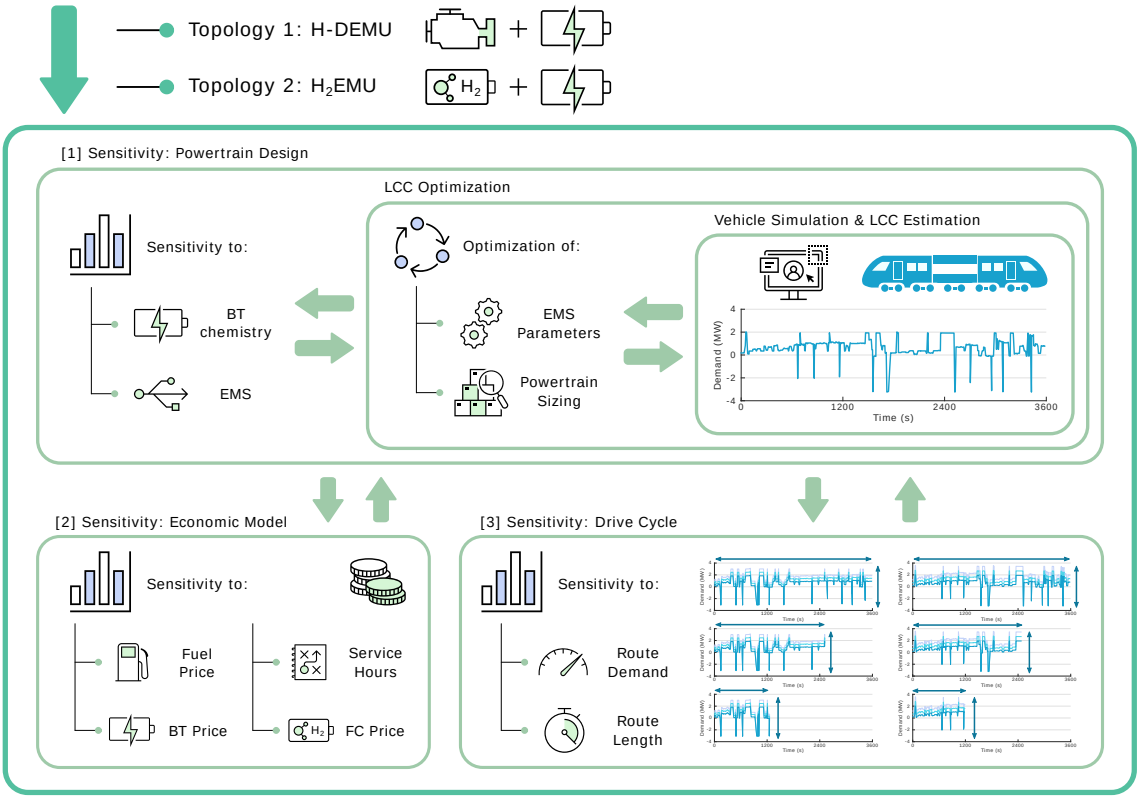

Figure 2.2: Detailed Methodology for Integral LCC analysis.

First of all, a sensitivity analysis is developed for the nominal case, that is to say, for a specific context defined as the nominal case study. A fixed drive cycle and economic model is defined for this nominal case. This first sensitivity analysis is focused on the design of the powertrain: different BT chemistries and EMSs are compared, as it is shown in the upper rectangle of Figure 2.2. As previously discussed in Chapter 1, it can be considered that each EMS is related to an optimal sizing of the powertrain sources. Therefore, instead of analysing the sensitivity of the LCC to the powertrain sizing, an optimal sizing is solved for each combination of BT chemistry and EMS. This corresponds to the inner rectangle of the previously mentioned upper part of Figure 2.2. In the cases of the optimized EMSs, the optimization approach also considers the optimization of the internal parameters of the control strategy, as it will be further discussed in the following sections of Chapter 2.

Once the analysis of the nominal case is completed, the next step consists on evaluating the replicability of the obtained conclusions in different contexts. For this approach, two independent sensitivity analyses are developed: on the one hand, a sensitivity analysis to the parameters of the economic model (lower-left rectangle of Figure 2.2); and on the other hand, a sensitivity analysis to the driving cycle (lower-right rectangle of Figure 2.2). The sensitivity analysis to the parameters of the economic model includes variabilities to the fuel price (hydrogen or diesel), BT price, FC price, and total service hours during the useful life. Besides, the aim of the sensitivity analysis to the driving cycle is to evaluate

routes with different average demands and lengths.

In the following sections, the different steps of the integral LCC analysis are explained in detail. In short, the proposed LCC analysis is based on two approaches: on the LCC value estimation, and on the optimization of this LCC value. Therefore, the remainder sections of this chapter are organized following this sequence:

- In a first step, Section 2.3 presents the methodology for the calculation of the LCC value of each case being analysed. This methodology includes a simulation model for the evaluation of the vehicle performance in a certain drive cycle, the technical verification of the simulation results, and a model for the economic evaluation. An important step of this model consists on the estimation of the BT and FC lifetimes. Therefore, the used lifetime estimation models are also introduced.
- Then, in a second step, Section 2.4 introduces the optimization methodologies used to obtain the cost-optimal powertrain sizing for each case being analysed. Depending on the EMS being analysed, the number of optimization variables may vary. Therefore, different methodologies are proposed to solve the optimization problem.
- Finally, Section 2.5 reviews the main methods and models presented in this chapter, and the main conclusions and the links with the following chapters are derived.

2.3 Calculation of Life Cycle Cost

The core of the LCC analysis proposed in Section 2.2 consists on the LCC evaluation of each case being analysed and/or optimised. For this approach, a simulation-based methodology is proposed, which is depicted in Figure 2.3. The methodology obtains the LCC value of each case l, being l any combination of vehicle topology, EMS, BT chemistry, powertrain sizing, driving scenario and economic parameters. The LCC calculation is divided into three main steps: vehicle simulation, technical verification, and economic evaluation.

For the vehicle simulation step, an electric model of the powertrain has been developed and implemented in a Matlab environment (Section 2.3.1). This model allows to evaluate the performance of different powertrain configurations in diverse driving scenarios. Once the vehicle has been simulated, the obtained results are technically verified to check if the proposed powertrain configuration can provide a feasible performance in the evaluated driving scenario (Section 2.3.2). Finally, the simulation results are extrapolated to the whole vehicle lifetime in order to calculate the LCC of the case being analysed. For this approach, a LCC model has been proposed, which includes costs related to the acquisition, operation and maintenance of the vehicle (Section 2.3.3). Among operation costs, the replacement of the power sources (specifically FC and BT systems) cannot be ignored. In order to include these costs in the LCC model, lifetime estimation models for FC and BT systems have been developed (Section 2.3.4 and Section 2.3.5, respectively). The BT lifetime estimation model is one of the novel contributions of this Ph.D. Thesis.

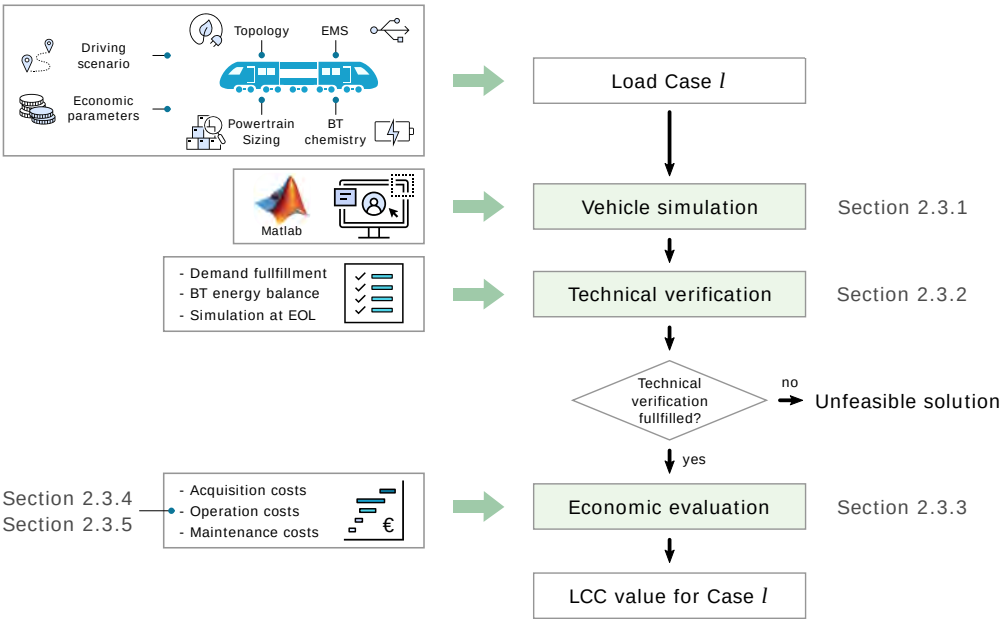

Figure 2.3: Diagram for LCC calculation approach.

2.3.1 Vehicle Simulation Model

Modelling the vehicle is a fundamental step in any study approaching an energy and/or power analysis of a hybrid powertrain system [104]. The vehicle simulation model developed for this Ph.D. Thesis is partially based on the ITINER tool previously developed by CAF I+D [105]. This tool allows the simulation of diverse rail vehicles and routes, and it enables an energetic analysis of the vehicle performance by post-processing the returned results. Specifically, some ITINER modules have been extracted from the main tool, and they have been set up to work independently.

The deployed simulation model is of quasi-static nature, what means that during each discrete time step k the values of the variables are considered constant [18, 106]. Besides, the model is based on the backward or wheel-to-engine approach: the signals flow from the power consumed by the vehicle through the powertrain elements in one way [27]. Considering that the analysis proposed in this Ph.D. Thesis is focused on the energy management level (see Figure 1.16), and that a compromise between the simulation detail and the computational cost has to be reached, a time step of $\Delta t = 1s$ has been selected. This time step also coincides with the one used in ITINER.

As previously mentioned, the developed model has been implemented in a Matlab environment. The diagrams of Figure 2.4 show which elements of the H-DEMU and H_2EMU vehicles have been modelled. As already mentioned, the model input consists on the power demanded by the vehicle, which has to be filled by the rest of the powertrain elements. In the following subsections each component of the simulation model is introduced in detail. As the arquitecture of the powertrain differs depending on the vehicle topology being

analysed, in this section the model is explained in a generic way. The models will be particularized for the H-DEMU in Chapter 3 and for the H_2EMU in Chapter 4.

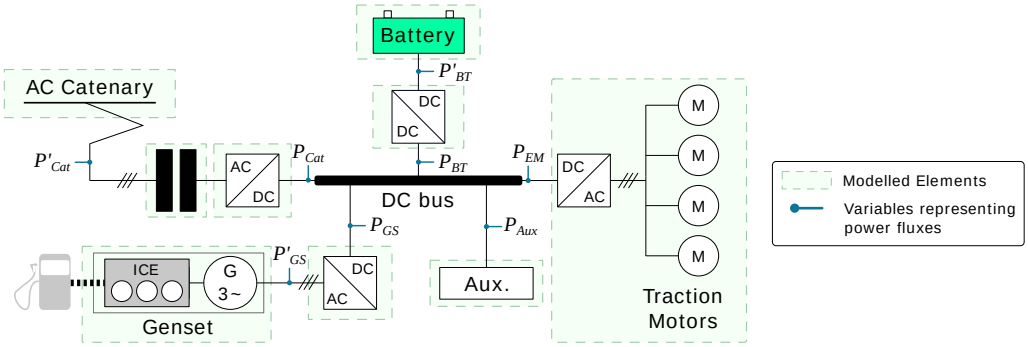

(a) Bi-mode H-DEMU

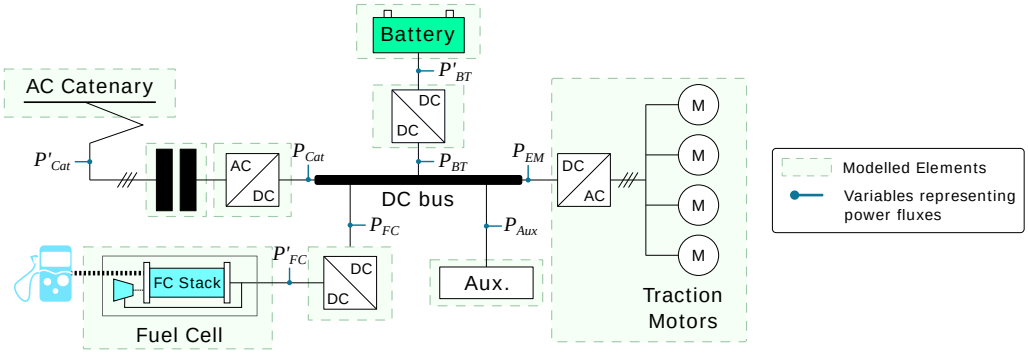

(b) Bi-mode H_2EMU

Figure 2.4: Block diagrams of the modelled powertrain architectures.

As it was already mentioned in Chapter 1, BT and FC systems lose performance capabilities during their useful life due to ageing phenomena. Due to the suffered degradation, they cannot offer the same power or energy capabilities at Beginning of Life (BOL) conditions and at End of Life (EOL) conditions. Therefore, it becomes relevant to check if the proposed powertrain configuration is able to provide a feasible performance when the BT and FC are both at BOL and EOL conditions. Consequently, for each Case l being evaluated, two simulations are developed. Firstly, BT and FC characteristics are set at BOL, and secondly, the characteristics are set at EOL. Further information regarding BOL and EOL conditions is given in the following subsections.

2.3.1.1 Traction Demand

The power demanded by the traction motors (P_{EM} $[W]$) constitutes the input of the quasi-static simulation model. The adopted sign convention considers a positive power value when there is an electrical power demand or mechanical traction ($P_{EM} > 0$) and a negative value when there is an electrical power absorption or mechanical braking ($P_{EM} < 0$). The P_{EM} profiles used in the current Ph.D. Thesis have been provided by CAF Power and Automation and CAF I+D. Figure 2.5 shows an example of a P_{EM} profile for the

railway line “Badajoz - Madrid”, which is located in Spain. The profiles used in each of the case studies are introduced in Chapter 3 and Chapter 4.

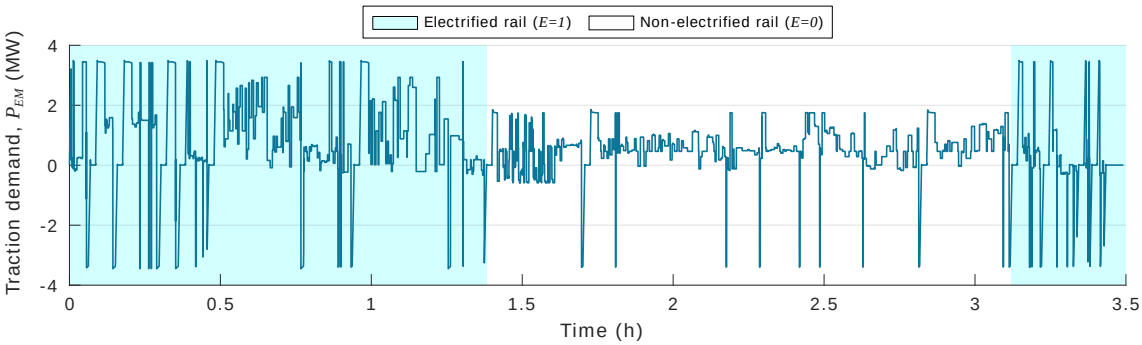

Figure 2.5: Example of input for the vehicle simulation model: P_{EM}.

2.3.1.2 Power Split

The power demand P_{EM} has to be provided/absorbed by the remainder powertrain elements, except the auxiliaries converters, which always absorb power to feed the auxiliary systems (e.g., lights, cooling or air conditioner). Therefore, the total power demand to be provided/absorbed by the power sources is defined as:

$$P_{Dem}(k) = P_{EM}(k) + P_{Aux}(k) \tag{2.1}$$

being P_{Dem} $[W]$ the total power demand at the DC bus, and P_{Aux} $[W]$ the power demanded by the auxiliaries converters at the DC bus.

As it was reviewed in Section 1.4, the EMS is the control unit in charge of splitting the power demand P_{Dem} at each time step. However, the deployed strategy varies depending on the characteristics of the track section where the rail vehicle is driving, as the available power sources may differ. As depicted in the example of Figure 2.5, a railway line can be composed of electrified ($E = 1$) and non-electrified ($E = 0$) sections. When a line combines both scenarios, bi-mode vehicles are required, as the ones modelled in the current approach (see Figure 2.4).

In non-electrified sections, the genset (in the H-DEMU) or the FC (in the H_2EMU) becomes the primary power source, and it works together with the BT, which works as secondary source. In electrified sections, the genset or the FC is turned off, and the catenary becomes the primary power source. In these conditions, the BT remains as secondary power source. Besides, in any of the working modes introduced so far, when there is an electrical power absorption ($P_{Dem} < 0$), the braking resistors may be activated to burn the power that cannot be absorbed by the remainder powertrain elements. In short, the power split is realized meeting the following conditions, being (2.2) the case of the H-DEMU and (2.3) the case of the H_2EMU:

$$P_{Dem}(k) = \begin{cases} P_{GS}(k) + P_{BT}(k) & \text{for } E(k) = 0,\ P_{Dem}(k) > 0 \\ P_{GS}(k) + P_{BT}(k) + P_{Res}(k) & \text{for } E(k) = 0,\ P_{Dem}(k) < 0 \\ P_{Cat}(k) + P_{BT}(k) & \text{for } E(k) = 1,\ P_{Dem}(k) > 0 \\ P_{Cat}(k) + P_{BT}(k) + P_{Res}(k) & \text{for } E(k) = 1,\ P_{Dem}(k) < 0 \end{cases} \tag{2.2}$$

$$P_{Dem}(k) = \begin{cases} P_{FC}(k) + P_{BT}(k) & \text{for } E(k) = 0,\ P_{Dem}(k) > 0 \\ P_{FC}(k) + P_{BT}(k) + P_{Res}(k) & \text{for } E(k) = 0,\ P_{Dem}(k) < 0 \\ P_{Cat}(k) + P_{BT}(k) & \text{for } E(k) = 1,\ P_{Dem}(k) > 0 \\ P_{Cat}(k) + P_{BT}(k) + P_{Res}(k) & \text{for } E(k) = 1,\ P_{Dem}(k) < 0 \end{cases} \tag{2.3}$$

where P_{GS} $[W]$ is the power provided by the genset, P_{BT} $[W]$ is the power provided/absorbed by the BT, P_{Cat} $[W]$ is the power provided/absorbed by the catenary, P_{Res} $[W]$ is the power absorbed by the braking resistors, and P_{FC} $[W]$ is the power provided by the FC. All these variables represent the power fluxes at the DC bus. The objective of the EMS is to define these power targets at each time step.

As it was already discussed in Chapter 1, the developments of this Ph.D. Thesis are focused on non-electrified sections. The EMSs proposed for non-electrified sections will be introduced in Chapter 3 and Chapter 4, as they differ depending on the vehicle topology and case study. Regarding electrified sections, it is assumed that due to the characteristics of the catenary system (unlimited power to be provided) it is not necessary to use the BT to provide traction power. Consequently, the design of the EMS will barely affect on the LCC, what reduces the need of developing a precise EMS to split the demand.

Due to these reasons, in this Ph.D. Thesis a simple RB strategy is proposed for the electrified sections, which is depicted in Figure 2.6. Essentially, the catenary is in charge of providing all the traction demand ($P_{Dem} > 0$), while the BT recovers the regenerative power ($P_{Dem} < 0$). If the BT cannot recover all the power, the braking resistors are activated. However, as it can be deduced by the available regenerative power in Figure 2.5, the energy generated in the braking stage may not be enough for the BT to recover the SOC value in which it started the previous non-electrified section. Therefore, the EMS adds an additional feature, which consists on charging the BT from the catenary, in case this is necessary to recover the mentioned SOC value. This value is defined as P_{BT-cat} $[W]$ in Figure 2.6. Besides, at the same time, the EMS is in charge of ensuring that the BT charging does not accelerate its degradation.

In order to ease this task, and considering that this EMS is not the main focus of this Ph.D. Thesis, it is assumed that the strategy knows in advance the P_{Dem} profile of the whole electrified section. Therefore, the EMS is able to calculate which will be the amount of energy recovered by the regenerative braking trough all this section ($E_{braking}$ $[Wh]$). Based on this value, the catenary will be just in charge of providing the remainder energy required to recover the aimed SOC (E_{BT-cat} $[Wh]$). In order to ensure a low degradation,

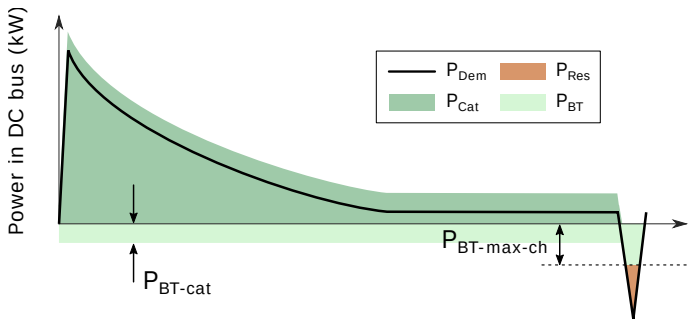

Figure 2.6: EMS for electrified sections ($E = 1$).

this energy should be provided at the lowest possible current. Therefore, E_{BT_cat} is proportionally distributed through all the electrified section. In short, Equations (2.4)-(2.6) introduce the expressions to calculate at each time step which should be the power provided by the catenary to charge the BT:

$$P_{BT-cat}(k) = \frac{E_{BT-cat}(k)}{t_{res}(k)} \tag{2.4}$$

$$E_{BT-cat} = \frac{E_{BT} \cdot \Big(SOC_{ref} - SOC(k)\Big) \cdot \eta_{eff} - E_{braking}(k)}{t_{res}(k)} \tag{2.5}$$

$$E_{braking}(k) = \sum_{k}^{K} P_{Dem} \cdot (P_{Dem} < 0) \cdot \Delta t \tag{2.6}$$

being t_{res} $[s]$ the remaining time until the end of the electrified section, η_{eff} [%] the coefficient to consider the efficiency of battery charging, E_{BT} $[Wh]$ the nominal energy of the BT, and SOC_{ref} [%] the SOC value to be recovered. As the efficiency may vary due to different reasons, it is assumed that the P_{BT-cat} value may not be always enough to recover the aimed SOC. In order to avoid this issue, the EMS updates P_{BT-cat} at each time step. In this way, the possible deviations can be corrected, as the required remainder energy to charge the battery is also updated at each time step (in the end, the EMS acts as a controller to recover the defined SOC reference).

2.3.1.3 Power Electronic Devices

The current study is focused on simulating the power flows through the powertrain elements. Hence, all the power converter devices have not been modelled in detail. Specifically, an average fixed efficiency value has been used for the transformer and the AC/DC rectifier of the catenary (η_{tr_cat} [%] and η_{inv_cat} [%]), the DC/DC converter of the battery (η_{conv_BT} [%]), the AC/DC rectifier of the genset (η_{inv_GS} [%]) and the DC/DC converter of the FC (η_{conv_FC} [%]). Therefore, the power values calculated at the DC bus are translated to the power values provided/absorbed by each powertrain element following these expressions:

$$P'_{cat}(k) = \frac{P_{cat}(k)}{\eta_{tr\_cat} \cdot \eta_{inv\_cat}} \tag{2.7}$$

$$P'_{GS}(k) = \frac{P_{GS}(k)}{\eta_{inv\_GS}} \tag{2.8}$$

$$P'_{FC}(k) = \frac{P_{FC}(k)}{\eta_{conv\_FC}} \tag{2.9}$$

$$P'_{BT}(k) = P_{BT}(k) \cdot \eta_{conv\_BT}^{-sgn(P_{BT}(k))} \tag{2.10}$$

being P'_{cat} $[W]$, P'_{GS} $[W]$, P'_{FC} $[W]$ and P'_{BT} $[W]$ the power provided/absorbed by each powertrain element, and $sgn(x)$ a function that returns the sign of the argument x. All these power values were also depicted in Figure 2.4. Table 2.1 shows the considered efficiency values.

Table 2.1: Efficiency of modelled converters.

Element	Efficiency
Catenary transformer (η_{tr_cat})	97 %
Catenary AC/DC rectifier (η_{inv_cat})	92 %
Genset AC/DC rectifier (η_{inv_GS})	95 %
Fuel Cell DC/DC converter (η_{conv_FC})	95 %
Battery DC/DC converter (η_{conv_BT})	95 %

It is worth to mention that the converter efficiency may differ depending on the voltage and current flowing on the device. Therefore, some constraints have been considered on the operation of the BT system to avoid a poor energy conversion, as it is further detailed in the section related to its modelling (Section 2.3.1.7).

2.3.1.4 Auxiliary Consumptions

The consumptions of the auxiliary loads (e.g., air conditioning, air compressor, cooling pump, power steering or lights) have been modelled by a constant average value (P_{aux}) for the entire journey.

2.3.1.5 Genset Model

The genset is a power device composed by an ICE and an electric generator, which are connected mechanically by a clutch. In this Ph.D. Thesis, the genset has been modelled based on efficiency maps, and therefore the dynamics related to its operation have not been addressed.

The input for the genset model is the power target defined by the EMS (P_{GS}), which is translated to the value P'_{GS} once the AC/DC inverter efficiency is considered. This value can be obtained by different combinations of ICE rotational speed (ω_{ICE} $[\frac{rad}{s}]$) and torque (T_{ICE} $[Nm]$). Each combination of rotational speed and torque leads also to a different fuel mass consumption ($\dot{m}_f$ $[g/s]$). Figure 2.7 shows the genset consumption

map considered in the current Ph.D. Thesis, represented by the required fuel mass per generated energy unit ($\dot{m}'_f$ $[g/kWh]$). It is worth to mention that the depicted $\dot{m}'_f$ values are calculated considering the generated energy at the genset output (E_{GS} $[kWh]$), so they also consider the efficiency of the electric generator.

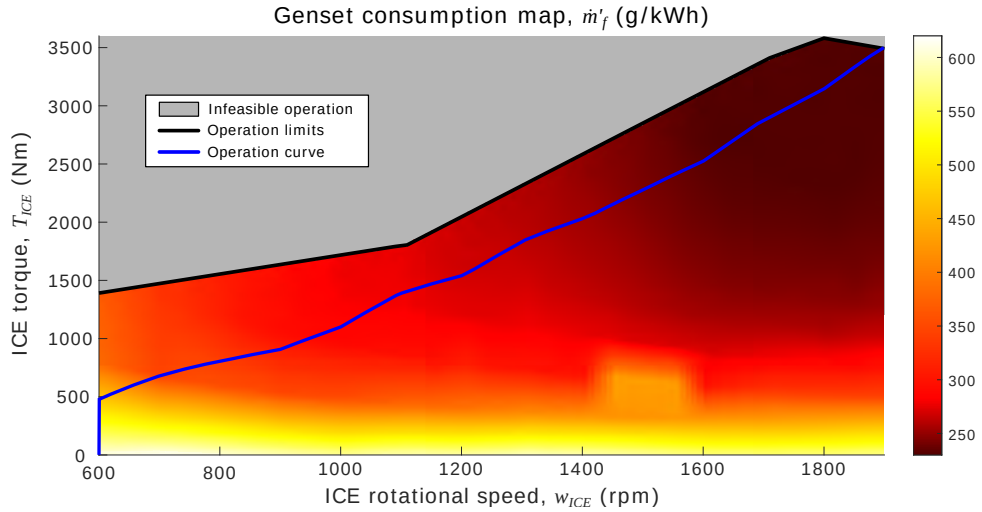

Figure 2.7: ICE efficiency map. Source: CAF Power and Automation.

In order to improve the efficiency of the genset operation, an operation path has been defined (depicted blue line in Figure 2.7). This path assigns a fixed ω_{ICE} and T_{ICE} value for each ICE output power (P_{ICE} $[W]$). Both the depicted map and operation curve have been provided by CAF Power and Automation, and correspond to a 700 kW genset. In the optimization approaches presented in Section 2.4, different genset sizes are evaluated. For each sizing evaluation, the operation curve will be proportionally scaled.

2.3.1.6 Fuel Cell Model

A FC system is composed of the FC stack and a series of auxiliary or balance of plant devices [107]. The FC system has been modelled based on the efficiency curves given in [108], which are depicted in Figure 2.8. The curves correspond to a 60 kW system, and therefore they are proportionally scaled when different sizes are evaluated (Section 2.4).

The input to the FC model is the power target assigned by the EMS (P_{FC}), which is translated to the value P'_{FC} once the efficiency of the DC/DC power conversion is considered. As it was already highlighted in Chapter 1, the dynamic properties of FC systems are poor [51]. In order to avoid fast transients on the FC operation point, P'_{FC} is subjected to the following constraints:

$$P'_{FC}(k) < P'_{FC}(k-1) + \Delta P_{FC\_max} \cdot \Delta t \tag{2.11}$$

$$P'_{FC}(k) > P'_{FC}(k-1) - \Delta P_{FC\_max} \cdot \Delta t \tag{2.12}$$

being ΔP_{FC_max} $[W/s]$ the maximum deviation of the FC operation point per time unit.

Additionally, a minimum operation point (P'_{FC_min} $[W]$) is also defined to avoid poor FC performance.

From the P'_{FC} value the corresponding FC current (I_{FC} $[A]$) and FC efficiency (η_{FC} $[\%]$) are obtained, following the curves depicted in Figure 2.8a and Figure 2.8b, respectively. Once the system efficiency is obtained, the fuel mass consumption of the FC is deduced from the following expression:

$$\dot{m}_{H_2}(k) = \frac{P'_{FC}(k)}{\eta_{FC}(k) \cdot LHV} \tag{2.13}$$

being $\dot{m}_{H_2}$ $[g/s]$ the hydrogen mass consumption and LHV $[J/g]$ the low heating value of hydrogen.

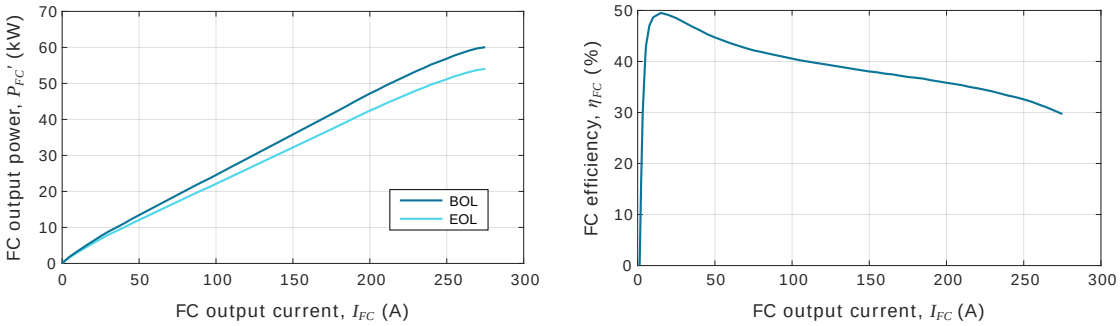

(a) Power curve **(b)** Efficiency curve

Figure 2.8: Fuel Cell model [108].

The components that constitute the FC tend to suffer from aging phenomena, what makes the FC lose performance capability during its useful life. Among the diverse effects, the degradation causes a drop of the FC voltage for the same generated current [109]. Therefore, a degraded FC will generate a lower power P'_{FC} value for each current I_{FC}, as depicted in Figure 2.8a. A typical convention adopted in the literature defines the EOL of FCs at the moment when the voltage decreases a 10% from the initial rated value [109–111]. Hence, in the current approach the power curve will be reduced a 10% in the EOL simulation. Further information regarding FC degradation is given in Section 2.3.4.

Table 2.2 shows the considered parameters for the FC modelling. As specified, the values refer to a 60 kW module, and therefore they will be proportionally scaled when different sizes are evaluated (Section 2.4).

Table 2.2: Fuel cell parameters (reference values for 60 kW module).

Parameter	Value
ΔP_{FC_max}	7.8 kW/s
P_{FC_min}	7 kW
LHV	120,000 J/g

2.3.1.7 Battery Model

BT systems are characterized by internal, complex and non-linear chemical processes, what complicates building accurate models to adequately describe and simulate their performance [112]. Different approaches have been proposed in the literature to model BT systems, with uneven accuracy levels and computational requirements [113]. In order to find a compromise between the accuracy and computational cost, in this Ph.D. Thesis an equivalent circuit model based on an open-circuit voltage source (V_{ocv}) connected in series with and an internal resistance (R_{int}) is proposed. This model is typically denoted as the Rint model [18, 27], and its diagram is depicted in Figure 2.9.

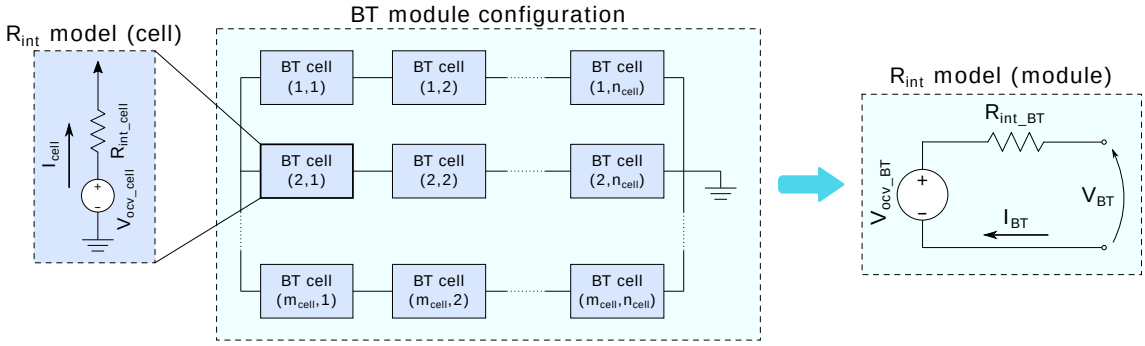

Figure 2.9: Battery model: from cell to module.

As it is shown, the model is based on an equivalent circuit of the BT module, which considers the connection of n_{cell} cells in series and m_{cell} cells in parallel. Therefore, the open-circuit voltage and internal resistance values at module level are obtained as follows:

$$V_{OCV\_BT}(k) = V_{OCV\_cell}(k) \cdot n_{cell} \tag{2.14}$$

$$R_{int\_BT}(k) = R_{int\_cell}(k) \cdot \frac{n_{cell}}{m_{cell}} \tag{2.15}$$

being V_{OCV_BT} $[V]$ the open circuit voltage value at module level, V_{OCV_cell} $[V]$ the open circuit voltage value at cell level, R_{int_BT} $[\Omega]$ the internal resistance value at module level and R_{int_cell} $[\Omega]$ the internal resistance value at cell level. Both V_{OCV_cell} and R_{int_cell} are non-linear functions of the SOC and charging condition (charge/discharge), as the example depicted in Figure 2.10 shows. It is worth to mention that these curves may differ depending on the BT chemistry.

The input of the BT model is the power assigned by the EMS once the converter efficiency is considered (P'_{BT}). In order to evaluate the state of the BT, it is necessary to obtain the current ($I_{BT}\,[A]$) and voltage ($V_{BT}\,[V]$) values of the system. The electric model is solved to obtain these values, what leads to the following expressions:

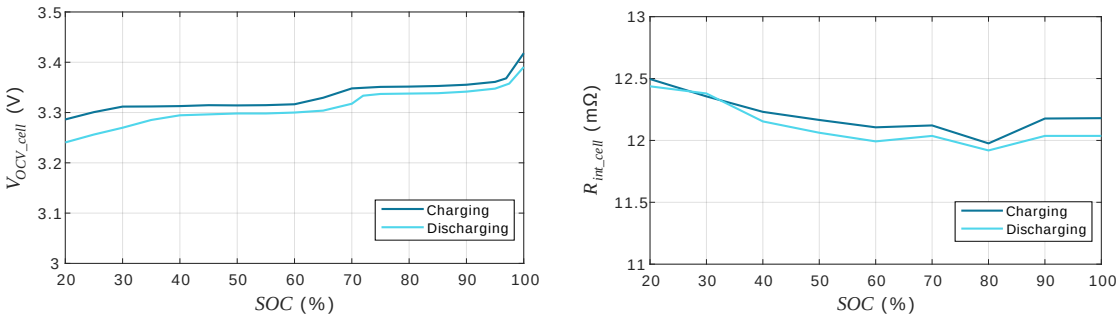

(a) Open circuit voltage **(b)** Internal resistance

Figure 2.10: State-of-charge dependency of BT parameters [32].

$$I_{BT}(k) = \frac{V_{OCV\_BT}(k) - \sqrt{V_{OCV\_BT}(k)^2 - 4 \cdot R_{int\_BT}(k) \cdot P'_{BT}(k)}}{2 \cdot R_{int\_BT}(k)} \tag{2.16}$$

$$V_{BT}(k) = V_{OCV\_BT}(k) - I_{BT}(k) \cdot R_{int\_BT}(k) \tag{2.17}$$

where a positive current means that the BT is discharging ($I_{BT} > 0$) and a negative current means that it is charging ($I_{BT} < 0$).

Both values are constrained by the maximum and minimum allowable BT current and voltage, as defined in expressions (2.18) and (2.19). Therefore, if the EMS asks a P'_{BT} value that bring I_{BT} and/or V_{BT} out of their bounds, the BT will not be able to provide or absorb the targeted power.

$$I_{BT\_max\_ch} < I_{BT}(k) < I_{BT\_max\_dch} \tag{2.18}$$

$$V_{BT\_min} < V_{BT}(k) < V_{BT\_max} \tag{2.19}$$

being $I_{BT\_max\_ch}$ $[A]$ the maximum current allowed when charging the BT, $I_{BT\_max\_dch}$ $[A]$ the maximum current allowed when discharging the BT, V_{BT_min} $[V]$ the minimum allowed BT voltage, and V_{BT_max} $[V]$ the maximum allowed BT voltage.

V_{BT_min} and V_{BT_max} are defined to ensure an optimal converter operation. Besides, $I_{BT\_max\_ch}$ and $I_{BT\_max\_dch}$ are defined according to the maximum charging and discharging C-rates recommended by the BT manufacturer. The C-rate (C $[h^{-1}]$) is a BT current value normalized against the battery capacity, and therefore it represents also the charging or discharging speed. Therefore, the maximum current values are defined as:

$$I_{BT\_max\_ch} = \frac{C_{max\_ch}}{Q_{BT}(k)} \tag{2.20}$$

$$I_{BT\_max\_dch} = \frac{C_{max\_dch}}{Q_{BT}(k)} \tag{2.21}$$

where C_{max_ch} $[h^{-1}]$ refers to the maximum charging C-rate, C_{max_dch} $[h^{-1}]$ refers to the maximum discharging C-rate, and Q_{BT} $[Ah]$ refers to the actual battery capacity.

Once the BT current and voltage are calculated, the model updates the SOC [%] of the BT using the Coulomb counting method [114], as depicted in Equation (2.22). The expression reflects the need of defining a SOC value for the initial time step, which is defined as SOC_0.

$$SOC(k) = SOC(k-1) - I_{BT}(k) \cdot \frac{\Delta t}{Q_{BT}(k)} \cdot 100 \tag{2.22}$$

Very high and low SOC values are not recommended for BT systems. Therefore, the BT is not allowed to be further discharged if the charge is below SOC_{min} [%], and it is not allowed to be further charged if the charge is above SOC_{max} [%]. Consequently, I_{BT} is also constrained by the BT SOC:

$$I_{BT}(k) = \begin{cases} 0 & \text{for } SOC(k) < SOC_{min},\ P_{BT}(k) > 0 \\ 0 & \text{for } SOC(k) > SOC_{max},\ P_{BT}(k) < 0 \\ I_{BT}(k) & \text{otherwise} \end{cases} \tag{2.23}$$

It is worth to mention that the BT capacity value (Q_{BT}) may change during the battery life due to the degradation that it suffers. The State of Health (SOH) reflects the loss of BT performance capability in relation to the initial conditions. It can be related to different variables, such as the loss of capacity or the increase of the internal resistance. In the approach of the current Ph.D. Thesis, the SOH is defined by the loss of capacity, being the most typical choice in the literature [36]:

$$SOH_{BT}(k) = \frac{Q_{BT}(k)}{Q_{BT\_0}} \cdot 100 \tag{2.24}$$

where SOH_{BT} [%] refers to the BT SOH, and Q_{BT_0} [Ah] refers to the BT capacity at BOL, when the SOH_{BT} is defined at the 100%.

The typically adopted convention defines the EOL of a BT system at the 80% of SOH [36]. Additionally, in the current approach the BT will be simulated at EOL conditions with the internal resistance (R_{int_BT}) increased to the 150%. Further information regarding BT degradation and SOH evolution is given in Section 2.3.5.

2.3.1.8 Catenary Model

As previously highlighted, the scope of this Ph.D. Thesis is oriented to the analysis of rail vehicles operation in non-electrified sections. Therefore, the AC catenary has been modelled as a linear system in which the electricity consumption (E_{Cat} [Wh]) is calculated based on an average transmission efficiency factor (γ_{cat} [%]). The value for the transmission efficiency factor has been set at the 95% [11]:

$$E_{Cat}(k) = \frac{P'_{Cat}(k) \cdot \Delta t}{\gamma_{cat}} \tag{2.25}$$

2.3.2 Technical Verification

Once the simulation is finished, in the next step the obtained results are verified to check if the simulated powertrain configuration (Case l) is feasible for the proposed driving scenario. Specifically, the results are evaluated following the demand fulfilment and the energy balance criteria:

- On the one hand, the backwards nature of the simulation model and the limitations defined in the operation of FC and BT systems do not ensure that the demand is filled at each time step. Therefore, in the technical verification step the simulation results are analysed to check if the expressions defined in (2.2) and (2.3) are met for all time steps, from $k = 1$ to $k = K$ (being K the total number of time steps).
- On the other hand, the energy balance of the BT must be ensured. If the SOC of the BT is lower at the end of the simulation (end of the trip) compared to the beginning of the simulation (beginning of the trip), it can not be ensured that in a second trip the vehicle will perform similarly. Therefore, the final SOC must be constrained as follows:

$$SOC(k = K) \geq SOC(k = 0) \tag{2.26}$$

As previously mentioned in Section 2.3.1, for each Case l being evaluated two simulations are launched: the first one, with BT and FC characteristics set at BOL (nominal conditions); and the second one, with BT and FC characteristics set at EOL (P'_{FC} curve downgraded a 10%, Q_{BT} reduced a 20%, and R_{int_BT} increased a 50%). Therefore, the evaluated powertrain configuration is only considered feasible if the demand fulfilment and energy balance criteria are met in both simulations.

2.3.3 Economic Evaluation Model

After the simulation results are checked to ensure the feasibility of the powertrain configuration being analysed, in the next step the LCC of Case l is calculated. This section introduces the economic model for the calculation of the LCC. The objective of the model is to estimate all the costs related to the useful lifetime of the rail vehicle starting from the simulation results of a single trip.

The LCC is divided into acquisition, operation and maintenance costs, as Equation (2.27) shows:

$$LCC(l) = C_{acq}(l) + C_{op}(l) + C_{maint} \tag{2.27}$$

being C_{acq} [€] the acquisition costs, C_{op} [€] the operation costs, and C_{maint} [€] the maintenance costs. In the following subsections, each of the LCC terms is further defined. As it will be explained, C_{acq} and C_{op} depend on Case l, while C_{maint} does not.

2.3.3.1 Acquisition Costs

Acquisition costs include all the costs related to the initial investment of the vehicle and the powertrain elements. In order to ease the expression, all the invariable costs are gathered into the term C_{train} [€], which is not dependent of Case l. The rest of the terms refer to the variable acquisition costs, including genset (C_{GS} [€]), FC system (C_{FC} [€]) and BT system (C_{BT} [€]) costs, as shown in Equation 2.28. Logically, in the case of the H_2EMU the genset cost is not considered, and in the case of the H-DEMU the FC cost is not considered.

$$C_{acq}(l) = C_{train} + C_{GS}(l) + C_{FC}(l) + C_{BT}(l) \tag{2.28}$$

The terms related to the powertrain sources are calculated based on their size:

$$C_{GS}(l) = n_{GS}(l) \cdot S_{GS} \cdot c_{GS} \tag{2.29}$$
$$C_{FC}(l) = n_{FC}(l) \cdot S_{FC} \cdot c_{FC} \tag{2.30}$$
$$C_{BT}(l) = n_{BT}(l) \cdot S_{BT} \cdot c_{BT} \tag{2.31}$$

being n_{GS} [−] the number of gensets deployed in the vehicle, n_{FC} [−] the number of FC modules deployed in the vehicle, n_{BT} [−] the number of BT modules deployed in the vehicle, S_{GS} [kW] the size of a genset, S_{FC} [kW] the size of a FC module, S_{BT} [kWh] the size of a BT module, c_{GS} [€/kW] the referential cost of the genset, c_{FC} [€/kW] the referential cost of the FC, and c_{BT} [€/kWh] the referential cost of the BT module.

2.3.3.2 Operation Costs

Regarding operation costs, they include the costs related to the fuel consumption (either diesel or hydrogen), catenary consumption, and replacement of BT and FC elements. Equation 2.32 shows the related expression. The replacement costs of the power sources could also be included as maintenance costs. However, as the degradation speed of both BT and FC systems is influenced by the way they are operated, in the approach of the current Ph.D. Thesis they are considered as operation costs:

$$C_{op}(l) = C_f(l) + C_{H_2}(l) + C_{cat}(l) + C_{FCrepl}(l) + C_{BTrepl}(l) \tag{2.32}$$

being C_f [€] the costs related to the diesel consumption (only in the H-DEMU), C_{H_2} [€] the costs related to the hydrogen consumption (only in the H_2EMU), C_{cat} [€] the costs related to the catenary consumption, C_{FCrepl} [€] the costs related to the FC replacements

(only in the H_2EMU), and C_{BTrepl} [€] the costs related to the BT replacements.

The costs related to the consumptions from the irreversible power sources (i.e., C_f, C_{H_2} and C_{cat}) are calculated annualizing the daily consumptions obtained at simulation:

$$C_f(l) = \sum_{y=1}^{Y} \left(L_{f\_day}(l) \cdot c_f\right) \cdot t_{op} \cdot (1+I)^{-y} \tag{2.33}$$

$$C_{H_2}(l) = \sum_{y=1}^{Y} \left(L_{H_2\_day}(l) \cdot c_{H_2}\right) \cdot t_{op} \cdot (1+I)^{-y} \tag{2.34}$$

$$C_{cat}(l) = \sum_{y=1}^{Y} \left(E_{Cat\_day}(l) \cdot c_{cat}\right) \cdot t_{op} \cdot (1+I)^{-y} \tag{2.35}$$

being L_{f_day} $[L]$ the daily diesel consumption, $L_{H_2\_day}$ $[kg]$ the daily hydrogen consumption, E_{Cat_day} $[kWh]$ the daily electricity consumption from catenary, c_f [€/L] the referential diesel cost, c_{H_2} [€/kg] the referential hydrogen cost, c_{cat} [€/kWh] the referential electricity cost, t_{op} $[\frac{days}{year}]$ the numer of operation days per year, I [%] the discount rate, y $[year]$ the current year, and Y $[years]$ the vehicle service life.

It is worth to mention that for the calculation of the daily fuel and electricity consumptions, the results of both BOL and EOL simulations are considered. Ideally, the fuel and electricity consumptions may differ each time the FC or the BT degrades. For instance, when the BT losses capacity, the genset or FC may increase its consumption. In order to reduce the number of performed simulations, in this approach it is assumed that the daily consumptions will approximate to the average of the BOL and EOL consumptions. That is to say, the consumptions may change linearly when the power sources degrade. Therefore, the expressions for L_{f_day}, $L_{H_2\_day}$ and E_{Cat_day} are obtained as follows:

$$L_{f\_day}(l) = \frac{L_{f\_BOL}(l) + L_{f\_EOL}(l)}{2} \cdot n_{trips} \tag{2.36}$$

$$L_{H_2\_day}(l) = \frac{L_{H_2\_BOL}(l) + L_{H_2\_EOL}(l)}{2} \cdot n_{trips} \tag{2.37}$$

$$E_{Cat\_day}(l) = \frac{E_{Cat\_BOL}(l) + E_{Cat\_EOL}(l)}{2} \cdot n_{trips} \tag{2.38}$$

where L_{f_BOL} $[L]$ and L_{f_EOL} $[L]$ refer to the diesel consumptions in BOL and EOL simulations, respectively (which are computed from $\dot{m}_f$); $L_{H_2\_BOL}$ $[kg]$ and $L_{H_2\_EOL}$ $[kg]$ refer to the hydrogen consumptions in BOL and EOL simulations, respectively (computed from $\dot{m}_{H_2}$); E_{Cat_BOL} $[kWh]$ and E_{Cat_EOL} $[kWh]$ refer to the electricity consumptions from catenary in BOL and EOL simulations, respectively (computed from E_{Cat}); and n_{trips} $[\frac{trips}{day}]$ refers to the number of trips that the vehicle undertakes in a day.

Regarding the replacements of the power sources, they are calculated following these expressions:

$$C_{FCrepl}(l) = \sum_{r_{FC}=1}^{R_{FC}(l)} n_{FC}(l) \cdot S_{FC} \cdot c_{FC} \cdot (1+I)^{-r_{FC} \cdot y_{FC}(l)} \tag{2.39}$$

$$C_{BTrepl}(l) = \sum_{r_{BT}=1}^{R_{BT}(l)} n_{BT}(l) \cdot S_{BT} \cdot c_{BT} \cdot (1+I)^{-r_{BT} \cdot y_{BT}(l)} \tag{2.40}$$

being R_{FC} $[-]$ the total number of FC replacements, R_{BT} $[-]$ the total number of BT replacements, r_{FC} $[-]$ the current FC replacement, r_{BT} $[-]$ the current BT replacement, y_{FC} $[years]$ the estimated FC lifetime, and y_{BT} $[years]$ the estimated BT lifetime.

R_{FC} and R_{BT} are calculated considering the estimated lifetimes of each source (y_{FC} and y_{BT}) and the service life of the vehicle (Y). Regarding the approaches used to estimate both FC and BT lifetimes, they are explained in detail in Sections 2.3.4 and 2.3.5, respectively.

2.3.3.3 Maintenance Costs

The costs related to the maintenance of the vehicle can be diverse, but it is assumed that they are not affected by the vehicle operation. Consequently, they are calculated based on an average vehicle maintenance cost per year, as represented in the following expression:

$$C_{maint} = \sum_{y=1}^{Y} c_{maint} \cdot (1+I)^{-y} \tag{2.41}$$

where c_{maint} $[€/year]$ refers to the average maintenance cost per year.

2.3.4 Fuel Cell Lifetime Estimation

As mentioned in Section 2.3.3, the proposed economic model considers the replacements of the FC system during the vehicle useful life. For this approach, it is necessary to estimate the FC lifetime from the operation profiles obtained in simulation. In this section, first the principles behind the degradation of FC systems are reviewed, and then the degradation model and lifetime estimation approach proposed for the development of the Ph.D. Thesis are explained.

2.3.4.1 Fuel Cell Degradation Principle

The durability is yet an essential milestone for the widespread commercialization of FC systems. The degradation of a FC is related to the deterioration of the components constituting the cell. The typical components subject to the mentioned degradation are the membrane, the electrocatalyst, the catalyst layer, the gas diffusion layer, the bipolar plates and the sealing gaskets [115, 116]. These elements can be affected by different

degradation modes (including mechanical, chemical or thermal degradation), which can be accelerated due to different causes. Table 2.3 overviews the main FC components subject to degradation, the degradation or failure modes they suffer, and the involved causes [115].

Table 2.3: Major failure modes of FC components [115].

Component	Failure Modes	Causes
Membrane	Mechanical Degradation	- Mechanical stress due to non-uniform press pressure, inadequate humidification or penetration of the catalyst and seal material traces
	Thermal Degradation	- Thermal Stress - Thermal Cycles
	Chemical/Electrochemical Degradation	- Contamination - Radial attack
Electrocatalyst or Catalyst Layer	Loss of activation	- Sintering or de-alloying of catalyst
	Conductivity loss	- Corrosion of electrocatalyst support
	Decrease in reactants mass transport rate	- Mechanical stress
	Loss of reformate tolerance	- Contamination
	Decrease in water management ability	- Change in hydrophobicity of materials due to Nafion or PTFE dissolution
Gas Diffusion Layer	Decrease in mass transport	- Degradation of backing material
	Decrease in water management ability	- Mechanical stress - Change in the hydrophobicity of materials
	Conductivity loss	- Corrosion
Bipolar Plate	Conductivity loss	- Corrosion - Oxidation
	Fracture/deformation	- Mechanical stress
Sealing Gasket	Mechanical failure	- Corrosion - Mechanical stress

Depending on the way the FC is operated, the degradation causes and failure modes introduced on Table 2.3 will be enhanced or dismissed. Besides, some of the causes can be mitigated by a correct balance-of-plant system. In short, the application in which the FC is integrated restricts its life expectancy. For instance, a considerable lifetime difference between FCs integrated in stationary and in transport applications is typically denoted. This is caused more due to the significantly different operation conditions, rather than due to the inherently different designs for the two applications [117].

In the case of transport applications, as it is the case of the current Ph.D. Thesis, the drive cycle of the vehicle has a direct impact on the degradation that the FC suffers. The FC operation modes and related drive cycle segments that influence FC degradation are listed below [118]:

(1) Constant load current or galvanostatic operation during constant speed.

(2) Current cycling or load changing during speeding up or slowing down.

(3) Low current or open circuit voltage during idling.

(4) High current during rapid acceleration.

Additionally, as in the H_2EMU the FC is hybridized with a BT, the deployed EMS also influences the FC ageing. Indeed, a correct designed EMS can mitigate some of the degradation modes reviewed above. Some of the potential actions that the EMS may adopt in order to maximize the FC lifetime are listed below [119]:

(1) Avoid running at very low currents to limit the reduction of the electrochemical active surface area.

(2) Ensure that the current demand does not exceed reactant supply limitations to prevent reactant starvation.

(3) Avoid excessive transient loading to maintain a stable temperature and humidity.

(4) Limit start-up/shut-down cycling to prevent localised starvation.

2.3.4.2 Fuel Cell Degradation Model

As it has been reviewed, the degradation suffered by FC systems may be originated by diverse causes and affect in different components, what inevitably complicates its modelling. FC degradation models can be divided into empirical (also called data-driven) and physical models [62]. Empirical models rely on mathematical functions that relate health indicators and stress factors observed in degradation tests, while physical models detail the degradation phenomena of FCs from a more physical, chemical and/or electrochemical scope. Typically, physical models try to model the degradation of one of the FC components, such as the catalyst [120–122] or the membrane [123–125]. Regarding empirical models, the main trend in the literature consists on approaches that relate FC operating conditions and the decrease of the voltage curve [110, 111, 119, 126]. Besides, some other approaches also propose empirical fittings that integrate physical or chemical basis, which are known as a semi-empirical models [127].

Considering that physical models require high computational effort and that a high detail of the degradation suffered by the FC is not required, in this Ph.D. Thesis an empirical degradation model is used to estimate FC lifetime. The used model was first proposed by Pei *et al.* in [110], and it considers that the voltage degradation is linear with time. This degradation is affected by four operation conditions, which are denoted as load change, start-stop, idle and high power. Figure 2.11 shows an example of the mentioned operation conditions.

Therefore, the FC lifetime can be obtained from the following expression:

$$y_{FC} = \frac{\Delta V_{FC}}{\delta_{FC}} \tag{2.42}$$

being ΔV_{FC} $[V]$ the voltage decrease at EOL and δ_{FC} $[\frac{V}{year}]$ the degradation rate.

As it was already mentioned in Section 2.3.1.6, the typically adopted convention defines the EOL at the moment when the voltage decreases a 10% from the initial rated point

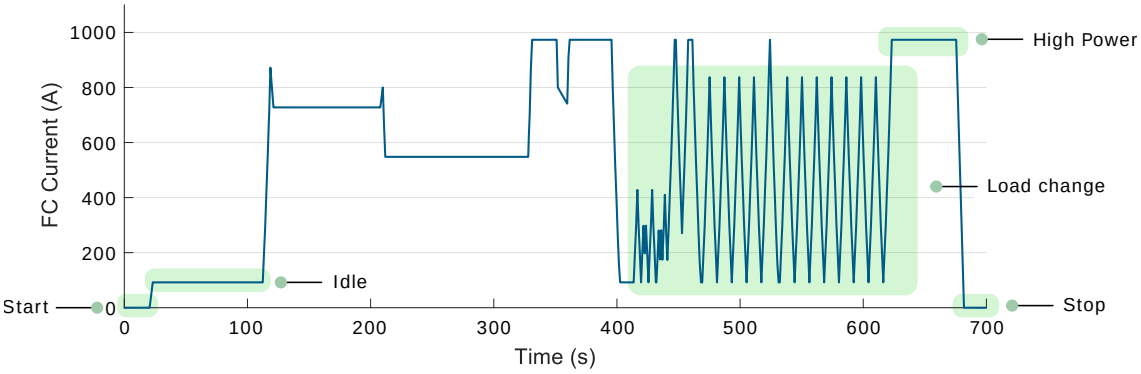

Figure 2.11: Operation conditions affecting FC degradation.

[109–111]. Besides, the degradation rate is obtained quantifying the effect of the four operation conditions, as the following expression defines:

$$\delta_{FC} = p_0 \cdot (p_1 \cdot w_1 + p_2 \cdot w_2 + p_3 \cdot w_3 + p_4 \cdot w_4) \tag{2.43}$$

where p_0 $[-]$ is the accelerating coefficient, p_1 $[\frac{V}{cycle}]$ is the degradation rate resulted by load change cycling, p_2 $[\frac{V}{cycle}]$ is the degradation rate resulted by start-stop cycles, p_3 $[V/s]$ is the degradation rate resulted by idle operation, p_4 $[V/s]$ is the degradation rate resulted by high power load condition, w_1 $[\frac{cycles}{year}]$ is the number of load changing cycles, w_2 $[\frac{cycles}{year}]$ is the number of start-stop cycles, w_3 $[\frac{s}{year}]$ is the time in idle operation, and w_4 $[\frac{s}{year}]$ is the time in high power load condition.

The degradation rate coefficients p_0, p_1, p_2, p_3, and p_4 have been adapted from the values proposed in [109–111] in order to better fit with the lifetimes claimed by FC manufacturers nowadays [128, 129]. Table 2.4 shows the degradation rate coefficients implemented in the model of the current Ph.D. Thesis.

Table 2.4: Coefficients for FC degradation model.

Coefficient	Value
p_0 [-]	1
p_1 $[\mu V/cycle]$	0.2092
p_2 $[\mu V/cycle]$	3.45
p_3 $[\mu V/h]$	2.166
p_4 $[\mu V/h]$	2.5

Regarding the variables related to the operation time at each condition, w_2, w_3 and w_4 are obtained straightforward from the operation profile. Besides, w_1 is obtained calculating the equivalent number of full cycles that the FC performs. A full cycle is considered as a cycle from idle operation to maximum power condition, and back to idle operation. Figure 2.12 shows an example of different load changing cycles and their representation into variable w_1.

As it was already mentioned, the introduced FC lifetime estimation model will be used

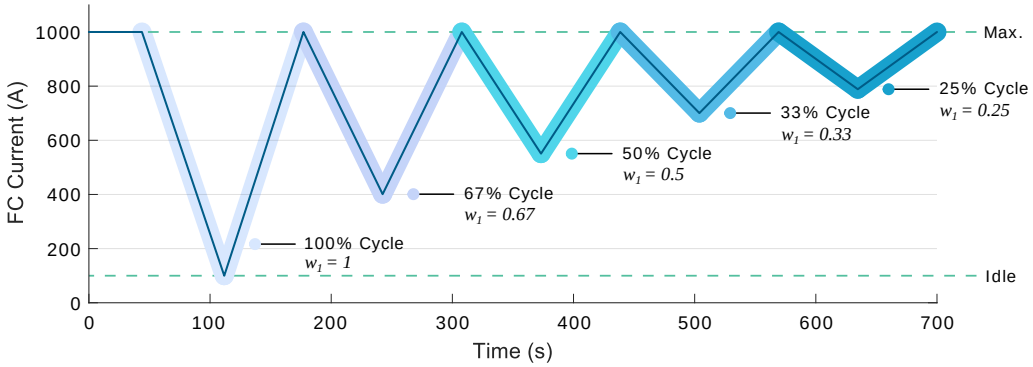

Figure 2.12: Different load changing cycles and the equivalent w_1 values.

during the developments of the current Ph.D. Thesis to infer the number of required FC replacements during the lifetime of a railway vehicle.

2.3.5 Battery Lifetime Estimation

As it was explained in Section 2.3.3, the proposed economic model considers the number of BT replacements during the vehicle useful life. For this approach, it is necessary to estimate the BT lifetime from the operation profiles obtained in simulation. In this section, first the principles behind the degradation of BT systems are reviewed. Then, the degradation model and lifetime estimation approach proposed in this Ph.D. Thesis are explained. It is worth to mention that the development and parametrization of the BT degradation model is one of the contributions of this Ph.D Thesis.

2.3.5.1 Battery Degradation Principle

Due to the occurring internal chemical reactions, BT systems irrevocably suffer from performance decline over time and use. The suffered degradation is not generated from a single cause. High and low temperatures, high charge and discharge currents, mechanical stresses, high and low operation voltages, and even the course of time are considered the main BT ageing stress factors [130, 131]. These stress factors accelerate diverse degradation mechanisms, including the Solid Electrolyte Interphase (SEI) growth, SEI decomposition, electrolyte decomposition, lithium plating, or particle cracking [132–136]. An illustration of the diverse degradation mechanisms is given in Figure 2.13 [137]. Eventually, these mechanisms cause Loss of Lithium Inventory (LLI), Loss of Active Material (LAM) and Ohmic Resistance Increase (ORI), which are considered the main degradation modes of BT systems [138].

From a macroscopic point of view, the degradation induces a capacity decay and an internal resistance increase, which are typically established as the health indicators for evaluating the remaining useful life of BT systems [139]. For a straightforward evaluation of the degradation, the EOL is defined as the moment when the capacity decays below

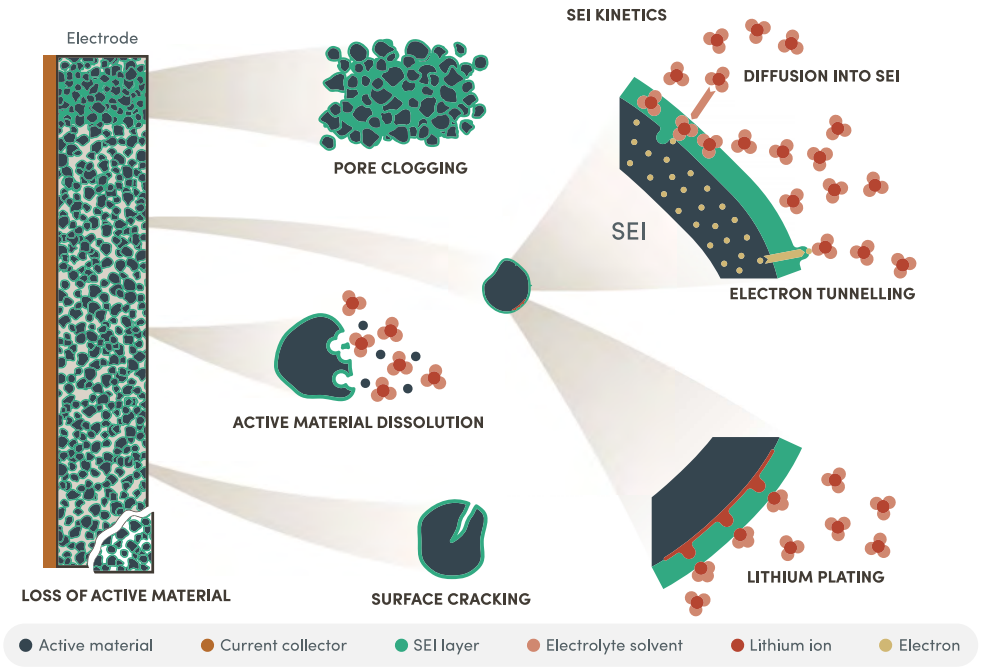

Figure 2.13: Graphical illustration of the various degradation mechanisms [137].

a certain value (e.g., 80% of the initial value) or the resistance increases above a certain value (e.g., 150% of the initial value) [140, 141]. As it was already defined in Section 2.3.1, in this Ph.D. Thesis a capacity decay of the 20% has been defined as the EOL criteria.

As previously mentioned, a BT can suffer from degradation both when being at rest (what is known as calendar ageing) and when being in use (what is known as cycling ageing). Figure 2.14 shows a series of examples of the capacity decay at different conditions. These capacity decay curves correspond to laboratory tests held at specific conditions (as indicated in the graphs), and have been compilated from different research works [142, 143].

On the one hand, Figure 2.14a depicts the ageing that a BT cell suffers when being at rest at different temperatures and SOCs. Indeed, temperature and SOC are considered the main stress factors accelerating calendar ageing [144]. The degradation evolution is expressed by the number of days. On the other hand, Figure 2.14b depicts the ageing that a BT cell suffers when being cycled at different temperatures, Depth of Discharges (DODs), charge and discharge C-rates, and middle SOCs. These are considered the main stress factors accelerating cycling ageing [145]. The DOD is defined as the SOC difference in a cycle, and the middle SOC is the average value of that cycle (e.g., a cycle between 20%-80% SOC is defined as a 60% DOD and a 50% middle SOC). In this case, the degradation evolution is expressed by the number of Full Equivalent Cycles (FECs). One FEC is defined as a full charge and full discharge cycle, that is to say, a cycle with a 100% DOD.

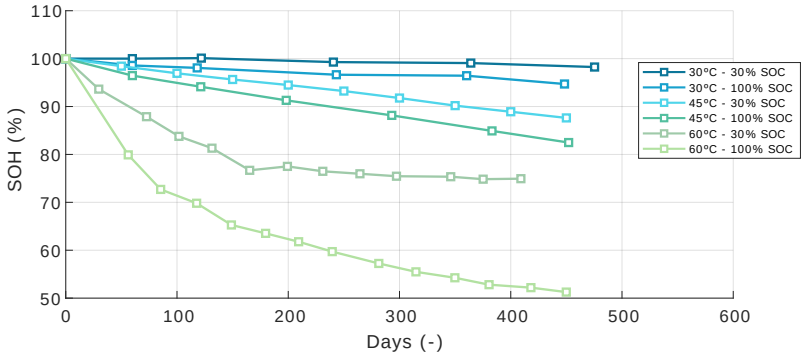

(a) Calendar ageing [142].

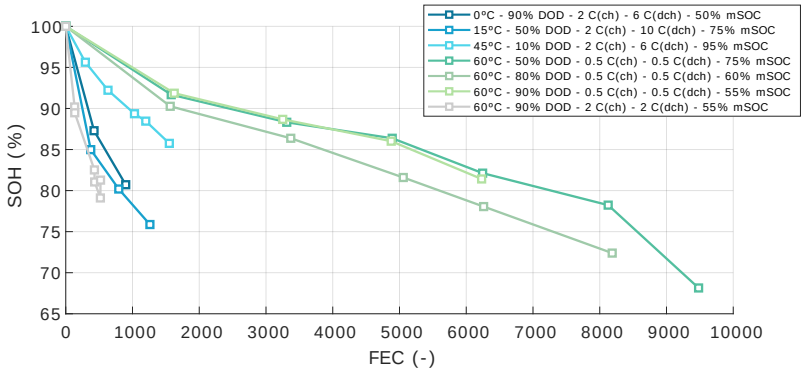

(b) Cycling ageing [143].

Figure 2.14: BT capacity decay at different conditions.

2.3.5.2 Classification of Battery Degradation Models

BT degradation models are developed in order to replicate, estimate or predict the ageing that BT systems suffer. Several models have been proposed in the literature, with uneven levels of complexity, accuracy and representativeness of the internal physics and chemical processes occurring in these devices [146].

The typical categorization of BT degradation models results in physical and empirical models [147]. On the one hand, physical models detail the degradation phenomena occurring within BTs from a physical, chemical, mechanical and/or electrochemical scope. However, this requires an increased level of complexity and computational cost, which leads to complications when implementing these models in real applications [148]. On the other hand, empirical models consist of building up a mathematical function relating the health indicators and stress factors observed in the degradation tests. The main strength of empirical models is their potential effectiveness in real applications. However, they lack of generality if enough degradation tests are not deployed, and they are not as robust as physical models [137].

Considering that the degradation detail level required for the methodology proposed in this Ph.D. Thesis is not high, it is assumed that for the current approach empirical

models are the most appropriated option. Therefore, as in the case of the FC, an empirical degradation model will be used to estimate the BT lifetime.

Related also to the estimation of the BT lifetime, one of the objectives of this Ph.D. Thesis is the comparison of different BT chemistries for the specific case of railway mobility. Among other characteristics, BT chemistries differ in terms of degradation phenomena, what unveils the necessity of developing a degradation model for each specific BT chemistry. A review of the BT degradation models proposed in the literature [143, 149–157] concludes that most of them are based on degradation tests held to a single BT reference (defined as a specific product from a BT manufacturer). Even if based on the same combination of cathode and anode materials, BT references of the same chemistry can show different degradation behaviour due to differences in the manufacturing process.

Consequently, this Ph.D. Thesis proposes the development of a BT degradation model that will be parametrized for different BT chemistries. This parametrization will be set based on data from multiple BT references. Considering that this is a novel approach in the literature, this degradation model is presented as one of the contributions of the current Ph.D. Thesis.

2.3.5.3 Proposed Battery Degradation Model

This section introduces the chemistry-dependent empirical BT degradation model developed in this Ph.D. Thesis. As previously mentioned, the development consists on two steps: (1) the empirical degradation model is set, and (2) the model is parametrized for different BT chemistries. In the following paragraphs, the main ideas behind this degradation model are reviewed. Further details of the methodology followed for this development can be found in the publication by Olmos *et al.* [36], which was written in the framework of this Ph.D. Thesis.

First of all, the degradation will be divided into the terms related to the calendar and cycling ageing. As already introduced in Equation (2.24), the degradation will be measured by the SOH evolution. Considering that the SOH starts at the 100% and reduces its value depending on the calendar and cycling terms, the following expression is proposed for the evolution of the SOH:

$$SOH_{BT}(t, FEC) = 100 - \Delta SOH_{BT\_cal}(t) - \Delta SOH_{BT\_cyc}(FEC) \tag{2.44}$$

being ΔSOH_{BT_cal} [%] the capacity decay due to calendar ageing and ΔSOH_{BT_cyc} [%] the capacity decay due to cycling ageing. As it was already introduced in Figure 2.14, calendar ageing is expressed by the course of the time (t [$days$]), and cycling ageing is expressed by the number of FECs that the battery has performed (FEC [−]).

On the one hand, considering that the main focus of this Ph.D. Thesis is the analysis of rail vehicles operation, the calendar part will be assumed to be similar in all cases being

analysed. Consequently, the term ΔSOH_{BT_cal} is modelled just with a linear capacity decay over time:

$$\Delta SOH_{BT\_cal} = \delta_{BT\_cal} \cdot t \tag{2.45}$$

where δ_{BT_cal} $[\%/day]$ refers to the BT degradation rate due to calendar ageing. One δ_{BT_cal} value will be defined for each of the BT chemistries being analysed.

On the other hand, the modelling and parametrization of the cycling degradation will be the main contribution of the developed chemistry-dependent BT degradation model. The model considers the effect of the main stress factors conditioning cycling degradation: temperature (T $[K]$), depth of discharge (DOD $[\%]$), charge C-rate (C_{ch} $[h^{-1}]$), discharge C-rate (C_{dch} $[h^{-1}]$) and middle SOC ($mSOC[\%]$). A huge batch of degradation tests is required in order to develop and parametrize a degradation model that considers diverse stress factors, BT chemistries and BT references. Developing all these tests in a laboratory environment is a time- and cost-consuming approach. Therefore, the model developed in the current Ph.D. Thesis is based on a compilation of nearly 500 degradation tests available in the literature [32, 139, 143, 145, 153–182].

Table 2.5 summarizes the data batches obtained for each BT chemistry, together with the stress factors that can be modelled at each case. It can be checked that it is only possible to parametrize an accurate degradation model that considers all the defined stress factors in the case of NMC and LFP chemistries. Therefore, the degradation model has been first developed based on the data from NMC and LFP, and then it has been parametrized for each of the BT chemistries depicted in Table 2.5.

Table 2.5: Collected data batch for each BT chemistry.

BT chemistry	Number of tests	Analysed factors	References
NMC	285	T, DOD, C_{ch}, C_{dch}, $mSOC$	[139, 145, 157–168]
LFP	131	T, DOD, C_{ch}, C_{dch}, $mSOC$	[32, 143, 153, 155, 169–173]
LCO	30	T, DOD, C_{ch}, C_{dch}	[154, 174–178]
NMC-LMO	27	T, DOD, C_{dch}, $mSOC$	[179]
LTO	16	T, DOD, C_{ch}, C_{dch}	[180]
NCA	10	T, C_{dch}	[181, 182]

Based on the gathered data, a methodology for the development and parametrization of the chemistry-dependent degradation model has been proposed. Figure 2.15 presents the main steps of this methodology, which it is further detailed in the following lines:

(1) *Data conditioning.* This step consist on removing noisy, incomplete or inconsistent data sets (e.g., initial capacity increases are removed). Additionally, tests set at extreme conditions are withdrawn from the data batch (e.g., too high temperatures or C-rates), as they are not representative of the typical recommended safe operation conditions.

(2) *Regression to $SOH(FEC)$ curves.* This step consists on defining a general expression

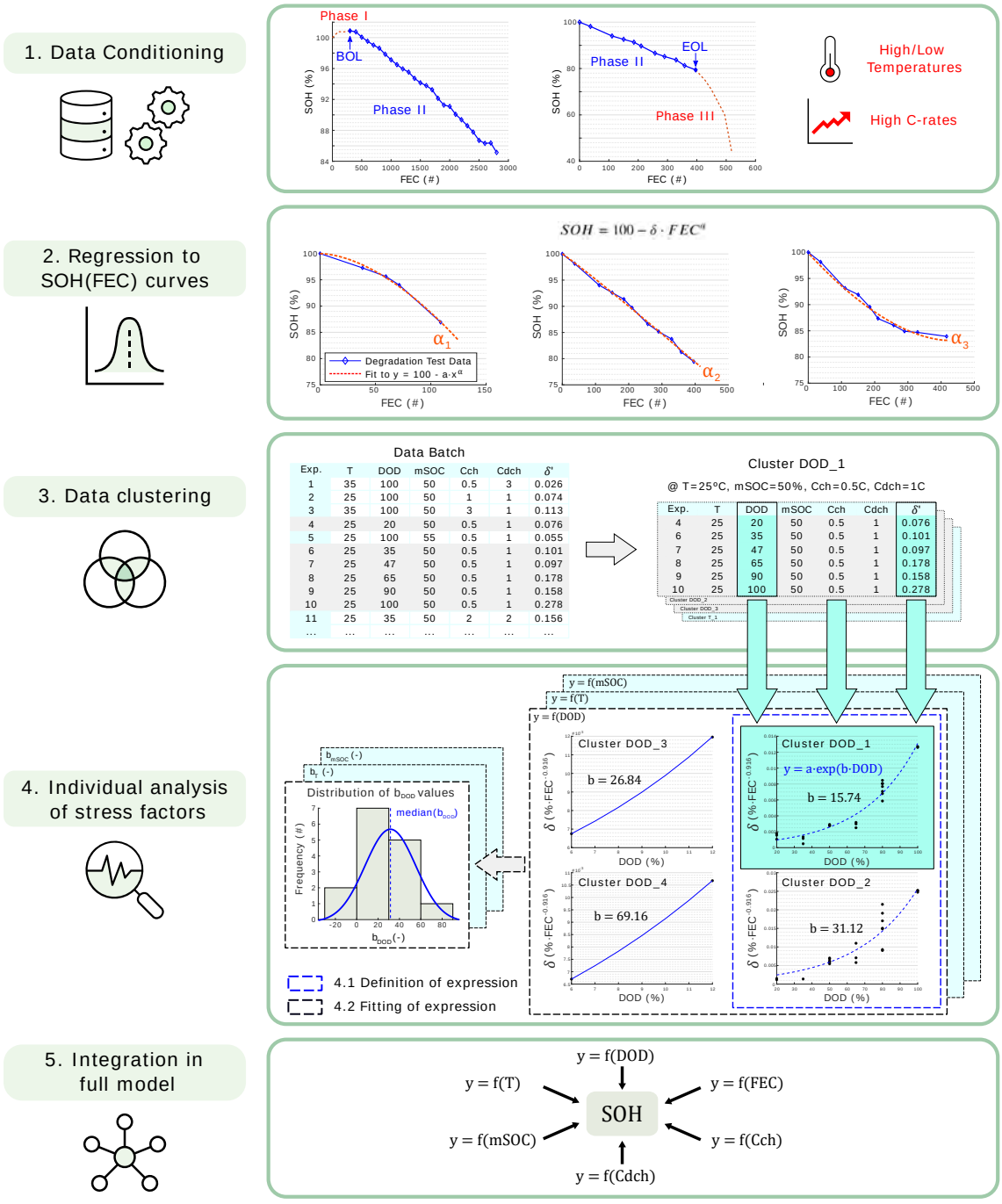

Figure 2.15: Methodology for the degradation model development and parametrization.

for the curve $y = SOH(FEC)$, which is the format typically used to represent the degradation tests results (see Figure 2.14). As the graphs inside the second rectangle of Figure 2.15 show, these curves can show different trends. Therefore, the objective of this step is finding a trend that it is well adjusted to the majority of the curves. This trend is defined by coefficient α $[-]$. Once this coefficient is defined, a degradation rate factor (denoted as δ_{BT_cyc} $[\%/FEC]$) is assigned to each test from

the data batch. The objective of the following steps of the methodology is to relate the value δ_{BT_cyc} to the degradation stress factors.

(3) *Data clustering.* In order to individually analyse the effect of the stress factors, this step consists on clustering the degradation tests in groups that share four equal stress factors, so the fifth factor can be analysed independently from the other four. In the third rectangle of Figure 2.15 an example of a cluster at $T = 25°\text{C}$, $C_{ch} = 0.5\text{C}$, $C_{dch} = 1\text{C}$, and $mSOC = 50\%$ is presented. In the example, this cluster is used in the next step to analyse the relation between the DOD and the degradation rate δ_{BT_cyc}, as seen in the graph "Cluster DOD 1".

(4) *Individual analysis of stress factors.* Once a series of graphs have been obtained for each stress factor, the aim of this step is to obtain an expression that models the effect of each stress factor. For this approach, the step is divided into two parts, which are presented in Figure 2.15. First, an expression is proposed for each stress factor by analysing the most representative clusters ("4.1 Definition of expression" in Figure 2.15). Then, the proposed expression is fitted to all the clusters of each stress factor, in order to define the appropriate model parameters ("4.2 Fitting of expression" in Figure 2.15).

(5) *Integration in full model.* The last step consists on gathering together all the expressions obtained for each stress factor. This is made by fitting the parameter β [−] with all the degradation tests of the data batch.

It is worth to mention that step 4.1 has only been implemented with LTO and NMC chemistries, as they are the only ones that provide enough data to model all the stress factors. For the remainder chemistries, the expressions proposed with LTO and NMC have been directly used in step 4.2 to parametrize the model. Eventually, the implementation of the methodology has lead to the definition of the following expression for ΔSOH_{BT_cyc}:

$$\Delta SOH_{BT\_cyc} = \beta \cdot exp\Big(k_1 \cdot \frac{T - k_2}{T} + k_3 \cdot DOD + k_4 \cdot C_{ch} + k_5 \cdot C_{dch}\Big) \cdot \Big[1 + k_6 \cdot mSOC \cdot \Big(1 - \frac{mSOC}{k_7}\Big)\Big] \cdot FEC^{\alpha} \tag{2.46}$$

being k_1 [−] and k_2 [K] the coefficients related to the temperature, k_3 [$\%^{-1}$] the coefficient related to the DOD, k_4 [h] the coefficient related to the charging C-rate, k_5 [h] the coefficient related to the discharging C-rate, and k_6 [$\%^{-1}$] and k_7 [%] the coefficients related to the middle SOC.

As mentioned before, once the general expression for the degradation model is set, the next step consists on obtaining the model parameters for each of the BT chemistries being analysed. The results obtained after deploying the proposed parametrization methodology are depicted in Table 2.6. These values allow implementing the proposed degradation model with each of the BT chemistries for which data was gathered, which is an important step of the holistic design methodology proposed in the current Ph.D. Thesis.

Table 2.6: Parameters for the chemistry-dependent degradation model.

Parameter	NMC	LFP	LCO	NMC-LMO	LTO	NCA
δ_{BT_cal}	0.003653	0.005479	0.005479	0.005479	0.002740	0.005479
β	0.001673	0.003414	0.047368	0.118470	0.022528	0.407644
k_1	21.67	5.8755	9.1716	6.3173	16.3118	-6.1342
k_2	293	293	293	293	293	293
k_3	0.022	-0.0046	0	0.0043	-0.0049	0
k_4	0.2553	0.1038	0.0849	0	0.0125	0
k_5	0.1571	0.296	0.4522	0.0895	0.0125	-0.1798
k_6	-0.0212	0.0513	0	0	0	0
k_7	42	42	1	1	1	1
α	0.915	0.869	0.841	0.652	0.541	0.698

2.3.5.4 Integration of Battery Degradation Model in LCC Calculation

Once the chemistry-dependent BT degradation model is built, another important step consists on integrating in the LCC calculation methodology proposed in this Ph.D. Thesis. For this approach, it is necessary to derive the BT lifetime value (y_{BT}) from the developed empirical degradation model. This is carried out by iteratively calling Equations (2.44), (2.45) and (2.46) until the EOL criteria is met (i.e., the SOH reaches the 80%). The stress factors affecting the expression of Equation (2.46) may change at each simulation time step k. Consequently, it is necessary to deduce for each time step the values of T, DOD, C_{ch}, C_{dch} and $mSOC$, as well as the cumulative number of FECs. A post processing of the simulation results is required for this approach.

The most challenging step of the post processing consists on the estimation of the DOD and $mSOC$ that the battery is doing at each time step. Different approaches can be followed to estimate these variables. In the current Ph.D. Thesis, the use of the Rainflow algorithm is proposed. The process carried out by this algorithm is depicted in Figure 2.16, and it can be summarized as follows [18]:

(1) First, the SOC profile obtained in simulation is analysed beginning from the highest value and making an always decreasing path until the lowest SOC value is found (Figure 2.16, green path 1).

(2) Then, the algorithm restarts from the next highest SOC value and it repeats the process until the next lowest SOC value is found, without overlapping the previous path (Figure 2.16, green path 2). The process is repeated as many times as necessary until all the discharging semi-cycles are analysed (Figure 2.16, all green paths).

(3) Once the discharging semi-cycles are analysed, the same process is repeated, but analysing the charging semi-cycles. Therefore, the algorithm starts from the lowest SOC value and makes an always increasing path until the highest SOC value is found (Figure 2.16, blue paths).

(4) Finally, the charging and discharging semi-cycles are grouped in cycles with the same DOD and $mSOC$ (e.g., discharge cycle 1 and charge cycle 1 in Figure 2.16).

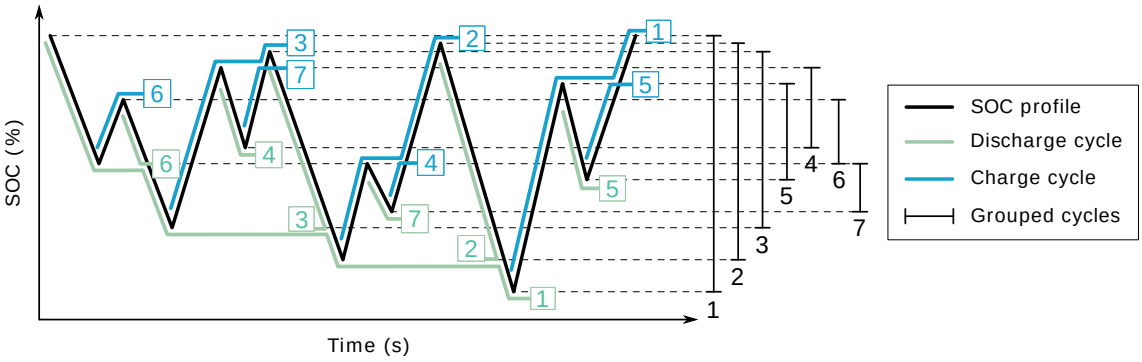

Figure 2.16: Rainflow algorithm working principle [18].

With this approach, each simulation time step has a DOD and $mSOC$ value assigned. However, Equation (2.46) requires also the assignment of a C_{ch} value and a C_{dch} value for each time step. Obviously, it is not possible for a battery to be charging and discharging at the same time. A possible solution is setting one of the values to zero, but as the degradation model was not built considering this circumstance, this is not a feasible solution. In order to solve this issue, the approach presented in Figure 2.17 is proposed. The figure follows the same example depicted in Figure 2.16, focusing on the charge/discharge cycle 1. The approach is further detailed in the following lines:

- If the current time step is part of a discharging semi-cycle (case depicted in Figure 2.17), the C_{dch} value corresponds to the C-rate that the BT is giving in the current time step. For the C_{ch} value, the root mean square of all the C_{ch} values of the linked charging semi-cycle is calculated, and then it is used in the model.

- If the current time step is part of a charging semi-cycle, the C_{ch} value corresponds to the C-rate that the BT is receiving in the current time step. For the C_{dch} value, the root mean square of all the C_{dch} values of the linked discharging semi-cycle is calculated, and then it is used in the model.

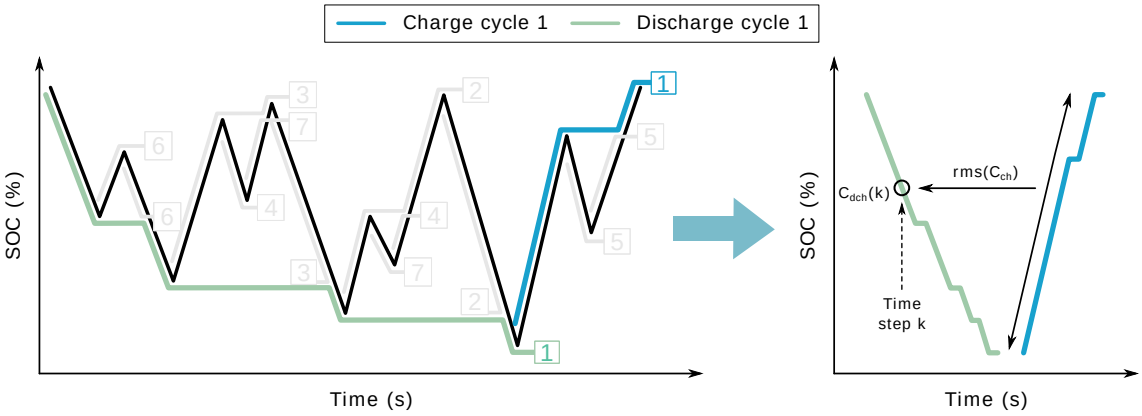

Figure 2.17: C_{dch} and C_{ch} definition at each time step (example of discharge semi-cycle).

2.4 Optimization of Life Cycle Cost

Once all the details of the LCC calculation approach have been given in Section 2.3, including all the methods and simulation models, this section is focused on explaining how is the LCC optimized.

As it was explained in Section 2.2, for each case being analysed in a sensitivity analysis, an optimization of the LCC is carried out (see inner rectangle in the upper part of Figure 2.2, "LCC optimization"). The main objective of this optimization is obtaining the cost-effective sizing of the powertrain sources, as it is assumed that each EMS is related to a different optimal sizing. However, some other parameters related to the EMS operation are also optimized in the LCC optimization approach. Specifically, the initial SOC in which the BT starts the journey is also optimized. This variable is considered important as it limits the absolute quantity of energy that the BT can absorb/provide during the whole journey. Additionally, in some optimization-based EMSs some parameters that define the internal rules of the strategy will be also optimized.

In short, the following optimization variables are defined: number of gensets (n_{GS}, only in the case of the H-DEMU), number of FC modules (n_{FC}, only in the case of the H_2EMU), number of BT modules (n_{BT}), initial SOC (SOC_0) and the EMS internal parameters (gathered in variable p_{EMS}). p_{EMS} can represent a different amount of optimization variables depending on the specific EMS being analysed. These specific optimization variables will be detailed in Chapter 3 and Chapter 4 together with the introduction of the corresponding EMSs. In this section, the generic p_{EMS} variable will be used to represent them.

In order to face the optimizations, in this Ph.D. Thesis the use of two different methodologies is proposed: an exhaustive search-based optimization, and a GA-based optimization. The reason of this split is the different amount of variables that can be found in the proposed optimization problems. Indeed, as more optimization variables, the number of feasible solutions increases exponentially, what complicates or even makes unfeasible the use of methodologies such as the exhaustive search.

In the cases when the internal parameters of the EMS are not optimized, the problem consists of 3 variables: n_{FC}/n_{GS}, n_{BT} and SOC_0. For these cases, it is considered that a methodology based on an exhaustive search is an appropriate approach to solve the problem. Indeed, with an appropriate discretization of the optimization variables, the number of potential solutions can be maintained in a feasible value without compromising the obtention of a solution close to the global optimal one. The methodology for the optimization based on exhaustive search is further detailed in Section 2.4.1.

Besides, in the cases when the internal parameters of the EMS are optimized, at least 4 variables have to be optimised: n_{FC}/n_{GS}, n_{BT}, SOC_0 and all the variables that compose p_{EMS}. Due to the increased number of feasible solutions, it is considered that a

GA-based methodology is more suitable for these cases. The GA is a metaheuristic search method widely implemented in the literature related to optimization-based EMSs, as it was reviewed in Section 1.4.2. Being an stochastic solving method, the GA does not ensure reaching the global optimal solution [18]. However, compared to the exhaustive search method, the number of iterations to reach the optimal solution is reduced significantly. The methodology for the GA based optimization is further detailed in Section 2.4.2.

2.4.1 Exhaustive Search Based Optimization

Figure 2.18 depicts the general diagram for the optimization by exhaustive search. The methodology is based on four main steps, and basically it consists on an iterative process in which all the feasible solutions (denoted as j) are evaluated. The steps are further described in the following lines:

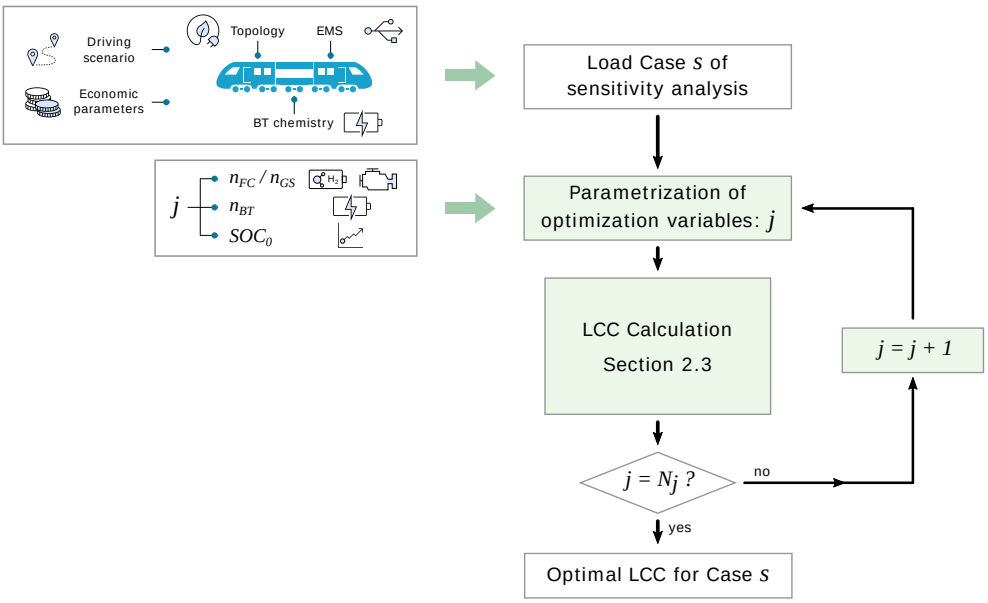

Figure 2.18: Diagram for optimization by exhaustive search.

(1) The first step consists on the initialization of the characteristics of the sensitivity analysis case that is being currently analysed. This case is denoted as s, being s any combination of vehicle topology, EMS, BT chemistry, driving scenario and economic parameters.

(2) Once the characteristics of Case s are set, the iterations of the exhaustive search optimization are initialized. At each iteration, a specific combination of the optimization variables is set (j). As mentioned before, each j consists on n_{FC}/n_{GS}, n_{BT} and SOC_0. All the optimization variables are discretized in order to obtain a manageable number of solutions (N_j).

(3) Each combination of optimization variables j is evaluated following the LCC calculation approach explained in Section 2.3, which corresponds to the optimization cost

function. Therefore, a LCC value is assigned to each j.

(4) Once all the feasible solutions N_j are evaluated, the methodology returns the optimal LCC and the combination of variables that have led to that optimal value for the Case s being evaluated.

2.4.2 Genetic Algorithms Based Optimization

The GA is a metaheuristic optimization solving method based on the concept of natural selection [183]. The algorithm is based on the concepts of individuals (i) and generations (x). One individual is a feasible solution (i.e., a combination of optimization variables, equal to j in the exhaustive search optimization), while a generation is a set of individuals. In short, the algorithm repeatedly modifies the sets of individual solutions to create new generations. From each generation, the GA selects the best features of the current individuals and uses them as parents to produce new children (i.e., a new generation). The algorithm evolves until it is allowed, hence the obtained solution will be closer to the optimal solution depending on the defined degree of evolution [18].

Figure 2.19 depicts the general diagram for the optimization by GA, which is mainly based on two iteration layers that are composed of different steps. These steps are further described in the following lines [184]:

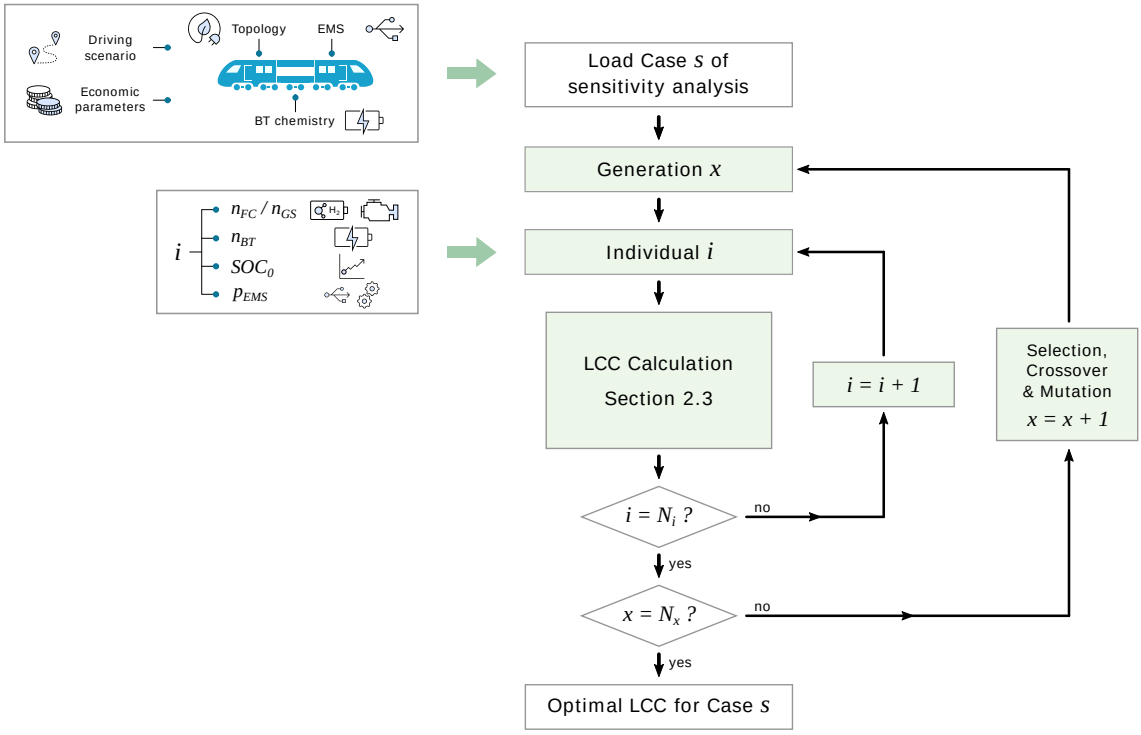

Figure 2.19: Diagram for optimization by genetic algorithms.

(1) As in the exhaustive search optimization, the first step consists on initializing the characteristics of the Case s of the sensitivity analysis.

(2) Once Case s is set, the outer iteration loop of Figure 2.19 is initialized. For this approach, the first generation is created. This generation is based on a random initial population of N_i individuals, which generally represents the search domain.

(3) At each generation, the inner loops depicted in Figure 2.19 are run. The aim of these iterations is to evaluate all the individuals from the current generation, based on the optimization cost function. As previously mentioned, the fitness function consists on the LCC value, whose calculation was widely explained in Section 2.3. Therefore, a LCC value is assigned to each i.

(4) Once all the N_i individuals have been evaluated, the next step consists on the selection of the best individuals from the current generation, based on the obtained fitness function. According to the evolutionary theory, the best individuals have the highest probability to join the next population.

(5) The last step before starting with the new generation consists on the generation of the new individuals. Three types of individuals are created: elite, crossover and mutation. Elite individuals are the solutions selected in step (4), and therefore they can be considered the parents of the next generation. Crossover individuals are created by combining characteristics of the parents or elite individuals. Finally, mutation individuals are created by introducing random changes to a single parent.

(6) In order to finalize the algorithm, steps (3)-(5) are repeated until the desired number of generations (N_x) is reached. Once these number of generations is reached, the optimization methodology returns the optimal LCC and the combination of variables related to that optimal value for Case s of the sensitivity analysis.

2.5 Conclusions

This chapter has presented the holistic design methodology proposed as the main contribution of this Ph.D. Thesis. This methodology has been developed based on the conclusions derived from Chapter 1, and it will be implemented in Chapter 3 for the H-DEMU case study and in Chapter 4 for the H_2EMU case study.

Section 2.1 has introduced the general overview of the proposed methodology, which is based on an integral LCC analysis. This analysis considers holistically the effect that the features identified in Chapter 1 have on the LCC of innovative railway vehicles. These features are defined as (i) the rail topology, (ii) the EMS design, (iii) the BT chemistry, (iv) the size of the power sources, (v) the driving scenario, and (vi) the parameters of the economic model. The aim of the LCC analysis is the identification of the features most dependent and most transversal to the context characteristics.

The structure of the LCC analysis has been presented in Section 2.2. Developing a sensitivity analysis that considers together all the features identified above is an unviable

approach. Consequently, the LCC analysis is divided into several steps. First, a sensitivity analysis is developed for the specific context defined as the nominal case. This first sensitivity analysis is focused on the design of the powertrain, as different BT chemistries and EMSs are compared. For each combination of BT chemistry and EMS, the optimal sizing of the powertrain sources is also solved. Once the analysis of the nominal case is finished, in a second step the replicability of the obtained conclusions in different contexts is evaluated. On the one hand, the sensitivity to the parameters of the economic model is developed. On the other hand, the sensitivity to different driving scenarios is developed.

Section 2.3 has presented the approach to calculate the LCC value of each case being analysed. This approach is divided into three main steps. First, the vehicle is simulated in a Matlab environment. Therefore, the proposed powertrain electric model has been explained in this section. Then, the results obtained in simulation are verified technically to check if the proposed powertrain configuration can provide a feasible performance. Finally, the LCC of the case being analysed is estimated from simulation results by means of an economic model. The different terms of the economic model have been explained in detail. An important step of the economic model is the estimation of the BT and FC lifetimes. Therefore, the algorithms used to estimate their lifetimes have also been introduced. In the case of the BT, a chemistry-dependent degradation model has been proposed, which constitutes one of the additional contributions of the current Ph.D. Thesis. In order to define the FC and BT lifetime estimation algorithms to be used in the current approach, a literature review of the existing models has also been performed. This review has complemented the State of the Art presented in Chapter 1, but focusing on the specific needs of the proposed holistic design methodology.

As mentioned in the introduction of the LCC analysis, the proposed methodology includes the optimization of the LCC to obtain the cost-optimal powertrain sizing for each case being analysed in a sensitivity analysis. Section 2.4 has introduced the different approaches to solve this optimization. A differentiation in the optimization solving methods has been defined due to differences in the number of optimization variables of the different cases. For the cases where 3 optimization variables are defined, an exhaustive search approach is proposed. Besides, for the cases with more than 3 variables (i.e., the cases where the parameters of the EMS are also optimized), an optimization based on GA is proposed. Both solving methods have been introduced in this section.

The methodology presented in this Chapter has been introduced from a generic view, and in the following chapters it will be particularized for each of the case studies proposed in this Ph.D. Thesis: for the H-DEMU in Chapter 3 and for the H_2EMU in Chapter 4. Specifically, at each case study all the cases of the sensitivity analysis will be defined, including the different control strategies, BT chemistries, parameters of the economic model, and driving cycles to be analysed.

3

Case Study A: Hybrid Diesel-Electric Multiple Unit

Summary

In this third chapter the first case study of this Ph.D. Thesis is developed. The holistic design methodology described in Chapter 2 is implemented with the vehicle topology denoted as the Bi-mode Hybrid Diesel-Electric Multiple Unit. On the one hand, the methodology is particularized for the current case study: the different cases of the sensitivity analysis are introduced, and the details of the optimization problems are given. On the other hand, the results of the different sensitivity analyses are explained: the sensitivity analysis to the powertrain design, the sensitivity analysis to the economic parameters, and the sensitivity analysis to the driving cycle.

3.1 Introduction

This chapter deals with the first case study of the current Ph.D. Thesis. The chapter aims the implementation of the methodology proposed in Chapter 2 with the vehicle topology denoted as the Bi-mode H-DEMU. The bi-mode vehicles will drive in rail lines that combine electrified and non-electrified sections, what becomes important for the design and analysis of the control strategies.

Figure 3.1 shows the powertrain architecture of the vehicle topology analysed in the current Chapter. The vehicle can be powered by a genset (which was modelled in Section 2.3.1.5), a BT (modelled in Section 2.3.1.7) or a catenary (modelled in Section 2.3.1.8). As already specified in Chapter 2, the genset and BT characteristics are proportionally scaled when analysing different sizings, and the BT parameters are defined depending on the chemistry being analysed (this will be defined in Section 3.2.2).

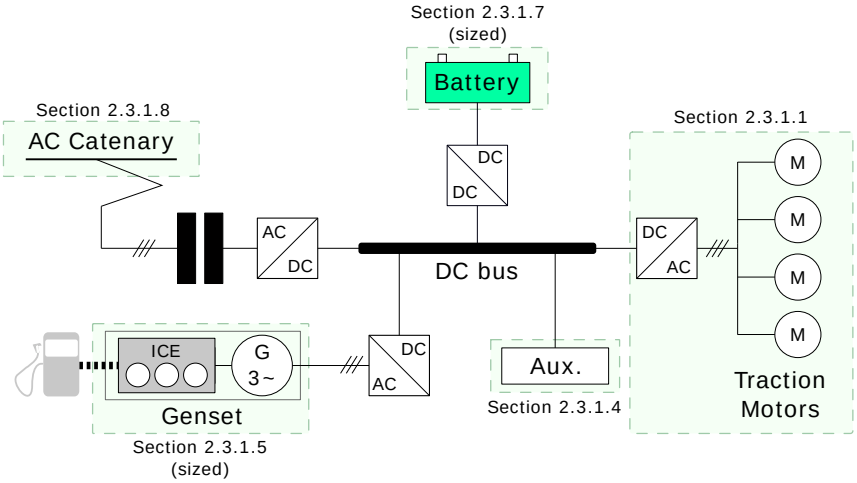

Figure 3.1: Considered Bi-mode H-DEMU architecture.

Additionally, Table 3.1 shows the general characteristics of the simulated vehicle, which is based on the CIVITY vehicle family manufactured by CAF [185].

Table 3.1: General information of modelled Bi-mode H-DEMU.

Parameter	Value
Length	86 m
Weight	124 t
Number of traction motors	4
Maximum speed	210 km/h
Maximum traction power at wheel	4.4 MW
DC Bus voltage	3,000 V
AC Catenary voltage	22.5 kV
Auxiliaries consumption	165 kW

The remainder of the chapter is organized as follows. First, Section 3.2 presents all the cases of the sensitivity analyses developed as part of the holistic design methodology.

Specifically, the different EMSs, BT chemistries, parameters of the economic model and driving cycles are detailed. Section 3.3 also particularises the generic optimization problems presented in Section 2.4 to the specific case study analysed in the current chapter.

Then, the holistic design methodology proposed as the main contribution of this Ph.D. Thesis is implemented step by step in Sections 3.4 to 3.6. First, the sensitivity analysis is focused on the powertrain design (different BT chemistries and EMSs, Section 3.4); then, on the parameters of the economic model (Section 3.5); and finally on the driving cycles (Section 3.6). At each step, the obtained results are discussed in detail to derive the main conclusions related to the design of H-DEMU vehicles.

3.2 Overview of Sensitivity Analyses

As a previous step before implementing the holistic design methodology, this section introduces all the cases of the sensitivity analyses that compose the mentioned methodology. The proposed control strategies, BT chemistries, parameters of the economic model and driving cycles are detailed in the following subsections.

3.2.1 Energy Management Strategies

Starting with the control strategies, the review of the State of the Art developed in Chapter 1 concluded that in this Ph.D. Thesis Rule-Based (RB), Optimization-Based (OB) and Learning-Based (LB) strategies will be developed and analysed. Specifically, in the current case study 5 strategies are based on rules, 3 strategies are based on an off-line optimization approach, and an additional strategy is based on a learning approach.

In all the cases, the EMS defines time step by time step the operation point of the genset (P_{GS}). Therefore, the BT will give or absorb (P_{BT}) the power difference between the defined genset operation point and the power demand (P_{Dem}). If the BT cannot absorb all the defined power, the braking resistors will be activated. Therefore, the description of each EMS will be focused on how the strategy defines the genset operation point.

For the design of the RB strategies, the efficiency curve of the genset has been taken into account. This curve has been generated considering the optimal path defined in the genset efficiency map (Figure 2.7), and it is depicted in Figure 3.2. Three regions have been defined in the efficiency curve: low, medium and high efficiency. The objective of the RB strategies will be to maximize the operation time in the high efficiency region. Therefore, for the design of the rules, the thresholds P_{GS1} and P_{GS2} will be considered, together with the maximum efficiency operation point (P_{GS-eff}) and the maximum load operation point (P_{GS-max}).

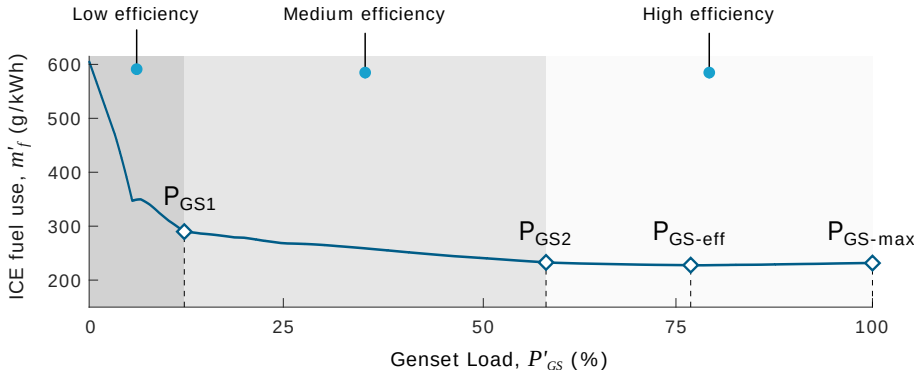

Figure 3.2: Genset efficiency curve, extracted from the efficiency map of Figure 2.7.

3.2.1.1 RB - Baseline Control (RB1)

The first strategy is called the Baseline Control. Figure 3.3 depicts the working principle of this strategy. Basically, the Baseline Control consists on defining a constant operation point for the genset, which is the most simple control approach. In order to enhance the efficiency of the main traction source, this reference is defined at the maximum efficiency point, P_{GS-eff}. However, as the figure shows, there are some conditions that force to alter this operation point. These conditions are enumerated below:

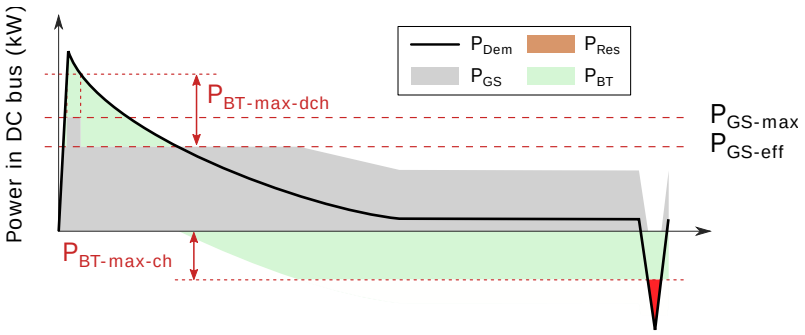

Figure 3.3: Baseline Control (RB1).

(1) In high demand conditions (e.g., in an acceleration peak), it may happen that the BT is not able to give all the required peak, as the difference between P_{GS-eff} and P_{Dem} may be higher than $P_{BT\_max\_dch}$. When this happens, the genset power is increased to P_{GS-max} in order to comply with the vehicle demand. This is shown at the left part of Figure 3.3.

(2) In low demand conditions (e.g., when the vehicle maintains its speed or brakes), the BT receives from the genset the power difference between P_{GS-eff} and P_{Dem}. In these conditions, it may happen that the BT is not able to receive all that power, either because it exceeds the maximum BT charge power ($P_{BT\_max\_ch}$) or because the BT is totally charged ($SOC > SOC_{max}$). When this happens, the genset operation point is reduced in order to avoid an unnecessary diesel waste. This is shown at the right part of Figure 3.3.

In order to ease the classification of the different strategies, in the remainder of the chapter this strategy will be denoted as RB1.

3.2.1.2 RB - Improved Baseline Control for Charge Sustaining (RB2)

The second strategy is known as the Improved Baseline Control for Charge Sustaining. As the name indicates, the strategy is understood to be an improvement of the Baseline Control. The objective of this improvement is to adapt the genset operation point to the demand, but maintaining a nearly constant and high efficient operation. For this approach, the operation point is switched between P_{GS-max} and P_{GS2}, instead of working constantly at P_{GS-eff}. Indeed, all these operation points are located at the high efficiency area of the genset, as it was shown in Figure 3.2. Therefore, it is understood that the global efficiency will not be much lower than in RB1, and at the same time the BT will give and receive lower peaks.

Figure 3.4 depicts the working principle of the strategy, which can be divided into three operation conditions, similarly to the case of RB1. These conditions are listed below:

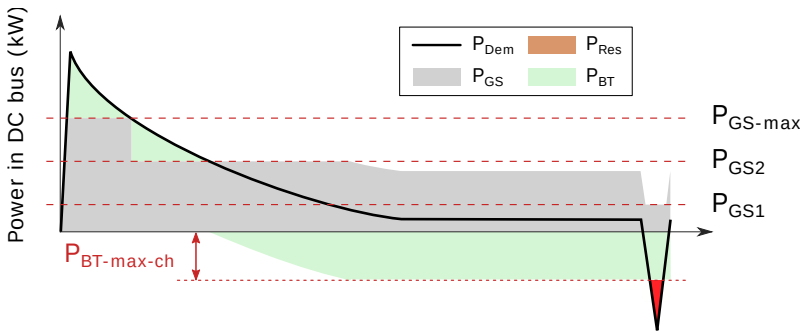

Figure 3.4: Improved Baseline Control for Charge Sustaining (RB2).

(1) In normal operation, the genset is fixed at P_{GS2}, which is the lower limit of the genset high efficiency zone. This condition is shown in the middle part of Figure 3.4.

(2) When the demand is higher than P_{GS-max}, the genset operation point is fixed at full load (P_{GS-max}). This prevents a situation when the BT is not able to give all the required power, for instance when an acceleration peak happens. This condition is shown in the left part of Figure 3.4.

(3) In low demand conditions (e.g., when the vehicle maintains the speed or brakes), the BT receives from the genset the power difference between P_{GS-eff} and P_{Dem}. In this condition, it may happen that the BT is not able to receive all that power, either because it exceeds $P_{BT\_max\_ch}$ or because the BT is totally charged. When this happens, the genset operation point is reduced. However, contrary to the case of RB1, in this case the lowest genset operation point is limited at P_{GS1}. This prevents the genset from working at the low efficiency operation area of Figure 3.2. This condition is shown in the right part of Figure 3.4.

In order to ease the classification of the different strategies, in the remainder of the chapter this strategy will be denoted as RB2.

3.2.1.3 RB - Improved Baseline Control for Charge Depleting (RB3)

The third strategy is known as the Improved Baseline Control for Charge Depleting. As the name indicates, this EMS is based on the previously introduced RB1 and RB2 strategies. One of the characteristics of RB1 and RB2 is that in low demand sections (which are common in rail operation) the BT is charged from the genset. In the case study being analysed in this chapter, the BT can also be charged from the catenary when an electrified section starts, which in terms of diesel use is a more efficient way of charging it. Therefore, the objective of this EMS is to reduce the energy transferred from the genset. To do so, the genset is allowed to work at lower operation points, including the medium efficiency zone of Figure 3.2. Consequently, the efficiency of the genset is sacrificed; but at the same time, the use of diesel is reduced, as the BT is now charged from the catenary when the non-electrified section ends.

Figure 3.5 depicts the working principle of this strategy, which can be divided into four operation conditions. These conditions are listed below.

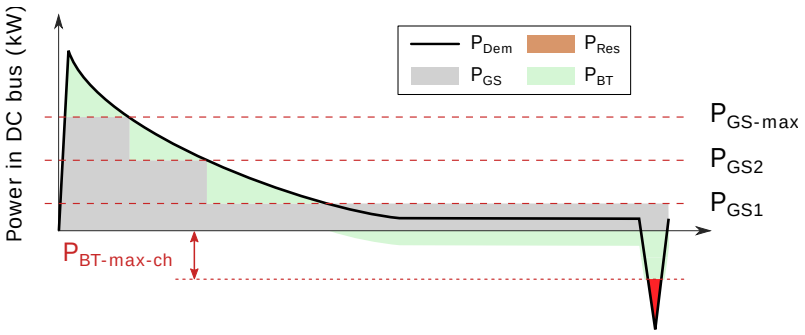

Figure 3.5: Improved Baseline Control for Charge Depleting (RB3).

(1) In normal operation, the genset is fixed at P_{GS1}, which is the lower limit of the middle efficiency zone. This condition is shown at the middle part of Figure 3.5.

(2) When the demand is higher than P_{GS2}, but lower than P_{GS-max}, the genset operation point is increased to P_{GS2}, which is the lower limit of the high efficiency zone. This condition is shown at the left-middle part of Figure 3.5.

(3) When the demand is higher than P_{GS-max}, the genset operation point is fixed at full load (P_{GS-max}), as it was done in the case of RB2. This prevents a situation when the BT is not able to give all the required power, for instance when an acceleration peak happens. This condition is shown at the left part of Figure 3.5.

(4) As it was highlighted in previous strategies, in low demand conditions (e.g., when the vehicle brakes), it may happen that the BT is not able to receive all the power

from the genset. In this circumstance, the genset operation point is not reduced to avoid the low efficiency zone of Figure 3.2. This condition is shown at the right part of Figure 3.5.

As it can be deduced from the comparison of Figures 3.4 and 3.5, the BT SOC will fall faster in the case of the current strategy. That is the reason to call this EMS "Improved Baseline Control for Charge Depleting", while RB2 is called "Improved Baseline Control for Charge Sustaining". In order to ease the classification of the different strategies, in the remainder of the chapter the Improved Baseline Control for Charge Depleting will be denoted as RB3.

3.2.1.4 RB - State Machine Controller (RB-SM) and OB - Optimized State Machine Controller (GA-SM)

Both alternatives for the Improved Baseline Control (RB2 for charge sustaining and RB3 for charge depleting) have some advantages and disadvantages: RB2 uses more diesel but maintains the charge of the BT, while RB3 uses less diesel but discharges faster the BT. In order to combine the characteristics and avoid the disadvantages of both alternatives, a strategy based on a State Machine (SM) controller is proposed.

Figure 3.6 shows the different states of the SM controller, which are defined according to the current SOC of the BT. Specifically, the SM states are divided according to the thresholds k_{SM1} [%], k_{SM2} [%], k_{SM3} [%] and k_{SM4} [%]. Each of the states is further detailed below:

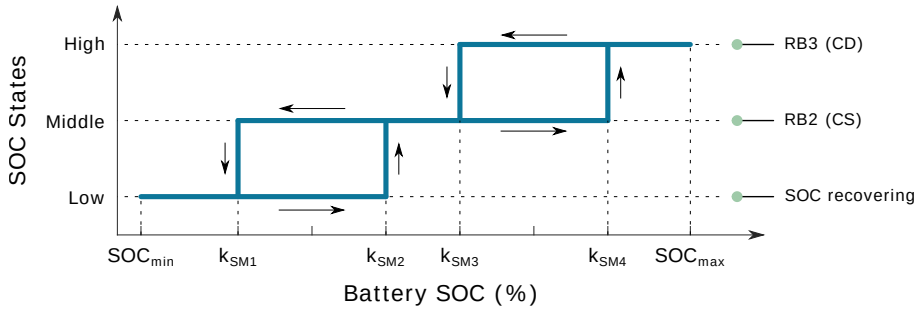

Figure 3.6: State Machine Controller (SM).

(1) When the SOC is high, it is considered that more energy can be asked to the BT, as the risk of running out of energy is low. Therefore, RB3 strategy is adopted in this state.

(2) When the SOC is in a medium value, more energy is asked to the genset to reduce the contribution of the BT. Therefore, RB2 strategy is adopted in this second state.

(3) Finally, when the SOC is low, it is considered that the priority is recovering the BT energy to avoid a traction power shortage. Therefore, a SOC recovering mode

is applied in this state. Figure 3.7 shows the working principle of this last mode: nominally, the genset works at full load (P_{GS-max}), and this power reference is only reduced when the BT cannot be further charged.

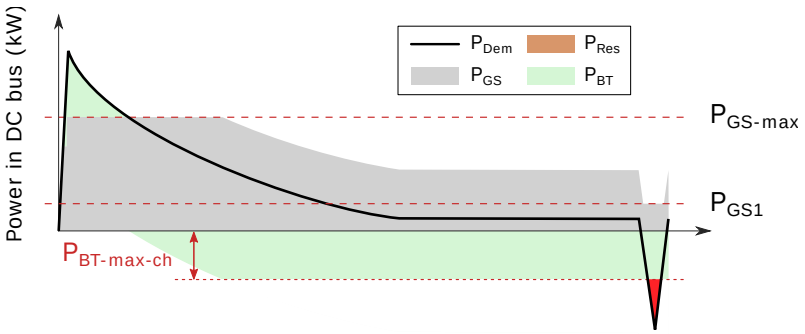

Figure 3.7: SOC recovery mode for low SOC state in State Machine Controller (SM).

As it can be deduced, thresholds k_{SM1}, k_{SM2}, k_{SM3} and k_{SM4} may influence the performance of the SM-based EMS. In a first approach, these thresholds have been defined based on the conclusions obtained after some first tests. Precisely, values 50%, 60%, 70% and 80% have been defined, respectively. However, this parametrization does not ensure an optimal operation. Therefore, in a second approach these values are optimized by means of a GA-based optimization method. Further information regarding how is this optimization approach coupled with the powertrain design optimization is given in Section 3.3.

In order to differentiate between both parametrizations, the strategy with the hand-tuned values will be denoted as the Rule Based State Machine (RB-SM), and the strategy with the optimized values will be denoted as the Optimized State Machine (GA-SM).

3.2.1.5 RB - Fuzzy Logic Based Controller (RB-FL) and OB - Optimized Fuzzy Logic Based Controller (GA-FL)

Another option for the RB strategies is to develop a controller based on Fuzzy Logic (FL) theory. A first introduction to FL based controllers was made in Chapter 1. As highlighted there, FL is an attractive option to control complex systems, especially in the cases were linguistic knowledge can be efficiently implemented together with numerical data. The main advantage of these controllers is that they avoid the mathematical stiffness of the rules defined in the typical deterministic RB strategies.

The process carried out by the controller is called the Fuzzy Inference System (FIS). In this Ph.D. Thesis, a Sugeno FIS is proposed, as this methodology requires less computational time and becomes more appropriate for dynamic non-linear systems [186, 187]. The block diagram of the Sugeno FIS is depicted in Figure 3.8. The objective of the controller is to define the genset operation point for the current time step (P_{GS}). This is made based on the current SOC of the BT (SOC), the current power demand (P_{Dem}), and the previous time step genset operation point (P_{GS_k}). The input variables have been

selected based on the FL controller proposed by Lopez-Ibarra *et al.* in [186]. To obtain the output value, the FIS is composed of three main steps, as it was already introduced in Figure 1.20: fuzzification, inference (use of linguistic rules), and defuzzification.

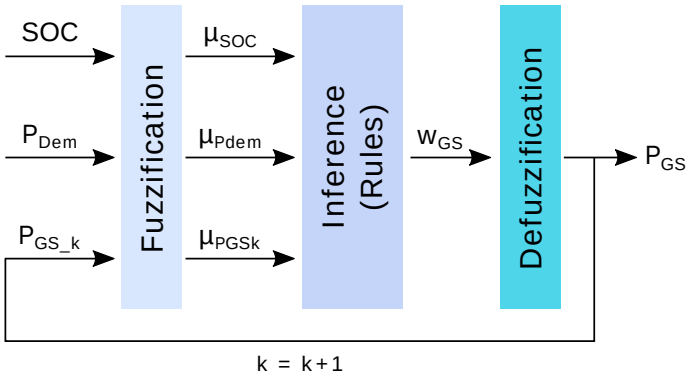

Figure 3.8: Block diagram of Sugeno fuzzy inference system.

In the first step, different fuzzy sets are defined for each input variable in order to derive the degree of membership of each variable (defined as $\mu_{SOC}\,[-]$, $\mu_{PDem}\,[-]$ and $\mu_{PGSk}\,[-]$). The membership functions and fuzzy sets defined for each input variable are presented in Figure 3.9. As depicted, trapezoidal shapes have been used. The definitions of the fuzzy sets and membership functions for each variable are given as follows:

- BT state of charge (SOC). This first input is considered to evaluate if the BT needs to be charged or it is able to provide energy. For this approach, 4 fuzzy sets are proposed: Very Low (VL), Low (L), Medium (M) and High (H). As depicted in Figure 3.9a, the transitions from one fuzzy set to another have been defined around the thresholds k_{FL1} [%], k_{FL2} [%] and k_{FL3} [%]. Besides, the ramps of the trapezoidal shapes have a width defined by variable k_{FL4} [%].

- Vehicle power demand (P_{Dem}). The aim of this variable is to define a different response depending on the power required for traction. This becomes crucial due to the high power peaks occurring in heavy-duty applications such as the one being analysed. As depicted in Figure 3.9b, 5 fuzzy sets are defined: Negative (N), Very Low (VL), Low (L), Medium (M) and High (H). N is intended for negative power demands (i.e., for regenerative braking), VL for power demands around the auxiliaries consumption (defined by threshold k_{FL5} [%]), L for a demand lower than 1/3 of the typical power peak (P_{peak} [W]), M for a demand lower than 2/3 of P_{peak}, and H for a demand around P_{peak}. k_{FL5} is also defined as the percentage in relation to P_{peak}. The ramps of the trapezoidal shapes have a width of just 1 kW in the case of the transitions from N to VL and from VL to L. As seen in the figure, this means that a fast transition is made between these fuzzy sets. For the rest of cases, the ramps of the trapezoidal shapes have a width of 300 kW.

- Genset operation point of previous time step (P_{GS_k}). This variable is used as an input in order to smooth the transitions of the genset operation point. As depicted

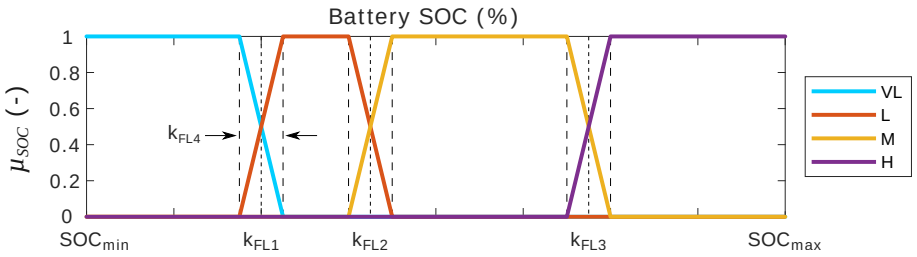

(a) Battery state-of-charge.

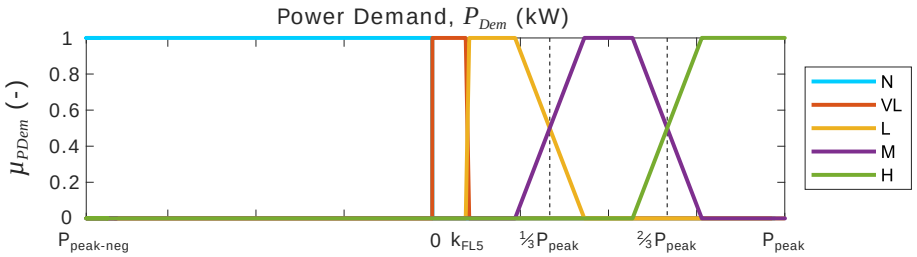

(b) Vehicle power demand.

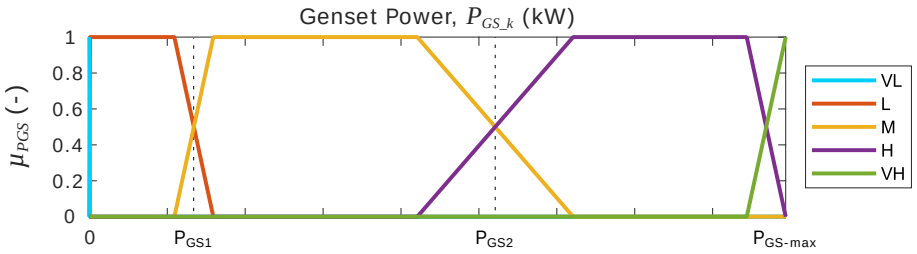

(c) Genset operation point.

Figure 3.9: Membership functions of Fuzzy Logic based controller.

in Figure 3.9c, 5 fuzzy sets are defined: Very Low (VL), Low (L), Medium (M), High (H), and Very High (VH). L, M and H are designed to refer to the low, medium and high efficiency regions of Figure 3.2, respectively. Besides, VL refers to the genset idle operation point, and VH to the maximum load operation point. As Figure 3.2 depicted, the limit between the medium and the high efficiency zone is quite smooth, as the efficiency does not differ much from one zone to the next one. Due to this reason, the transition between M and H is wider. Specifically, the ramp of the trapezoidal shape has a width that is defined as the 20% of the genset maximum load. In the other two cases, that width is defined as the 5% of the maximum load.

Apart from the input variables, it is also necessary to define the fuzzy sets and membership functions for the output variable P_{GS}. As P_{GS} coincides with the input variable P_{GS_k} (the only difference between them is the shift of one time step), the same fuzzy sets are defined for P_{GS_k}: Very Low (VL), Low (L), Medium (M), High (H) and Very High (VH). However, the P_{GS} membership functions do not coincide with the P_{GS_k} ones (which were defined in Figure 3.9c), since in the case of Sugeno type FIS the output membership functions are defined as linear or constant functions. Indeed, in the current approach the use of constant functions is proposed. Specifically, the following values have

been defined for each fuzzy set: VL refers to an idle genset operation, L to an operation in P_{GS1}, M to an operation in the middle point of the medium efficiency region, H to an operation in P_{GS-eff}, and VH to an operation in P_{GS-max}

Once the membership function degrees are obtained, the next step consists on applying the if/then rules that relate the input variables (SOC, P_{Dem} and P_{GS_k}) and output variable (P_{GS}). The tables depicted in Figure 3.10 summarize all the relations between the input and output variables.

Demand H	SOC			
Genset	VL	L	M	H
VL	M	M	M	M
L	M	M	M	M
M	H	H	H	H
H	VH	VH	H	H
VH	VH	VH	H	H

Demand M	SOC			
Genset	VL	L	M	H
VL	M	M	M	M
L	M	M	M	M
M	H	H	H	M
H	VH	VH	H	M
VH	VH	VH	H	H

Demand L	SOC			
Genset	VL	L	M	H
VL	M	M	M	L
L	M	M	M	L
M	H	H	M	L
H	VH	H	M	M
VH	VH	H	H	H

Demand VL	SOC			
Genset	VL	L	M	H
VL	M	M	L	VL
L	M	M	L	VL
M	H	H	L	VL
H	VH	H	M	M
VH	VH	H	H	H

Demand N	SOC			
Genset	VL	L	M	H
VL	VL	VL	VL	VL
L	VL	VL	VL	VL
M	VL	VL	VL	VL
H	M	M	M	M
VH	H	H	H	H

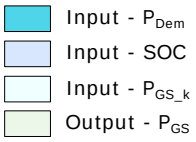

Figure 3.10: Rules of fuzzy logic controller.

The processing of the rules is performed by a series of statistic functions. In the current Ph.D. Thesis, the approach based on the error propagation function is proposed [186]. This function is computed to obtain the weigth (w_{GS_i}) that defines the contribution of the FL rules (w_{rule_n}) to each genset output power value (GS_i):

$$w_{GS\_i} = \sqrt{w_{rule\_1}^2 + w_{rule\_1}^2 + ... + w_{rule\_N}^2} \tag{3.1}$$

Finally, the defuzzification approach derives the value of the output variable (P_{GS}) from all the weights (w_{GS_i}) obtained in the previous step. For this approach, the use of the weighted arighmetic mean statistic function is proposed, as Equation (3.2) shows. The calculated value is the output value of the EMS.

$$P_{GS} = \frac{\sum_{i=1}^{N}(w_{GS\_i} \cdot GS_i)}{\sum_{i=1}^{N} w_{GS\_i}} \tag{3.2}$$

As it can be deduced, parameters k_{FL1}, k_{FL2}, k_{FL3}, k_{FL4} and k_{FL5} may affect the effectiveness of the FL-based controller. As in the case of RB-SM, in a first approach these values have been defined based on the conclusions of some first tests. Precisely, values 30%, 42.5%, 67.5%, 5% and 10% have been selected for each parameter, respectively.

However, this parametrization does not ensure an optimal operation. Therefore, in a second approach these values are optimized by means of a GA-based optimization method, as in the case of the SM-based controller. Further detail regarding how is this optimization approach coupled with the powertrain design optimization is given in Section 3.3.

In order to differentiate between both parametrizations, the strategy with the hand-tuned values will be denoted as the Rule Based Fuzzy Logic (RB-FL), and the strategy with the optimized values as the Optimized Fuzzy Logic (GA-FL).

3.2.1.6 OB - Dynamic Programming (DP)

As it was already introduced in Chapter 1, the DP approach consists on an algorithm that, based on Bellman's optimality principle, returns the optimal control trajectory that minimizes a certain cost function. In order to run the DP algorithm, it is necessary to define the control variable(s) Φ, the state variable(s) ι, the cost function(s) J, and the optimization constraint(s).

First of all, the control variable Φ is the optimized variable, which in the current approach is also the output of the DP-based EMS: the genset operation point, P_{GS}. Therefore, Φ is defined as follows:

$$\Phi(k) = P_{GS}(k) \tag{3.3}$$

The state variable ι is the variable that represents the dynamic state of the system, which is affected by the control actions taken so far. In the current case, this dynamic state is represented by the SOC of the BT. Therefore, ι is defined as follows:

$$\iota(k) = SOC(k) \tag{3.4}$$

The cost function J is the function to be minimized by the DP approach. In the current approach, J is defined as the amount of fuel that the H-DEMU consumes during a certain driving cycle. In other words, DP aims the definition of control actions that minimize the diesel consumption. J is defined as follows:

$$J = \sum_{k=0}^{K-1} \dot{m}_f(\Phi(k)) \cdot \Delta t \tag{3.5}$$

where $K\,[-]$ is the total number of time steps of the simulation. As determined, the cost function considers the cost ($\dot{m}_f(k)$) of performing a certain control action ($\Phi(k)$).

Finally, the optimization problem also requires the specification of some constraints, which are related to Φ and ι. First, in order to be initialized, DP requires the definition of the initial and final states of the system, that is to say, the initial and final SOC values.

Besides, a feasible space of state variables has to be also defined. In the current approach, the SOC is constrained by the maximum and minimum allowable values (90% and 20%, respectively). Apart from the constraints related to the state variable, a feasible space of control variables has to be also defined. In this case, P_{GS} is allowed to vary between the idle load point and the full load point. The following equation resumes the defined optimization constraints:

$$\begin{cases} \iota(0) = SOC_0 \\ \iota(K) = SOC_K \\ 20 \leq \iota(k) \leq 90 \\ 0 \leq \Phi(k) \leq P_{GS-max} \end{cases} \tag{3.6}$$

being SOC_K [%] the BT SOC at the last time step K.

It is worth to mention that in the current case study a compromise has to be reach to define the most suitable SOC_K value. Indeed, a low SOC_K is understood to reduce more the fuel consumption, but increase the BT degradation (due to the high DOD). However, a high SOC_K is understood to reduce the BT degradation, but increase the fuel consumption. In order to overcome this issue and find a compromise, variable SOC_K is optimized. Further detail regarding how is this optimization approach coupled with the powertrain design optimization is given in Section 3.3.

In conclusion, DP returns the optimal sequence of P_{GS} values that minimizes the diesel consumed by the H-DEMU. However, this sequence of the control variable is only valid for the specific context (i.e., specific drive cycle) for which the optimization is deployed. This makes the on-line implementation of DP practically unfeasible. Due to this reason, DP results are commonly used just as baseline for benchmarking other strategies. It is worth to mention that the DP algorithm integrated in the current Ph.D. Thesis is based on the function and scripts developed in [188] and available in [189].

3.2.1.7 LB - Neuro-Fuzzy Learning based Controller (ANFIS)

In order to overcome the main disadvantage of DP optimization, in this Ph.D. Thesis the use of a LB strategy is proposed. The selected LB approach is the Adaptive Neuro Fuzzy Inference System (ANFIS), which has been proposed for similar applications in previous research works [27, 190, 191]. The objective of the ANFIS approach is to train a FL-based controller with data obtained from DP optimizations, so the controller is able to replicate in real-time the operation proposed by DP. Figure 3.11 shows the general overview of the ANFIS based learning technique.

As in any learning approach, the first step consists on generating the data required for the training process. The trained ANFIS controller should be robust to different contexts, i.e., to different drive cycles. Therefore, the DP data generated for the training step is

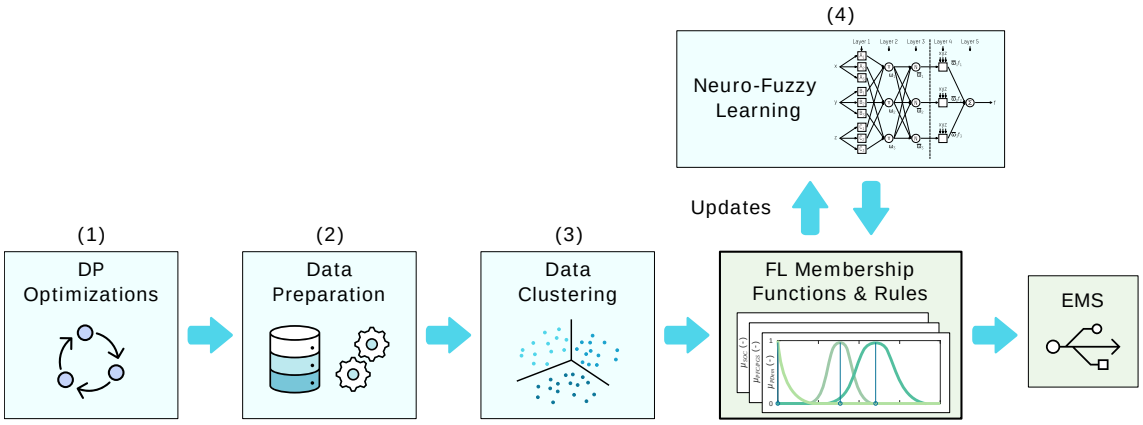

Figure 3.11: Overview of ANFIS based learning technique [27].

obtained optimizing the H-DEMU operation under different drive cycles. These drive cycles are generated varying the number of passengers and the auxiliaries consumption set in the nominal scenario, which will be presented in Section 3.2.4. Specifically, the number of passengers will be varied in a ±7%, and the auxiliaries in a ±30%, leading to a 3x3 matrix of 9 driving cycles.

Once the DP optimizations are completed, the second step consists on processing the data required by the ANFIS training step. The training process requires a set of inputs and outputs, which will be the inputs and outputs required by the controller during real operation. Specifically, the BT SOC, length-ratio, and P_{Dem} profiles are set as the inputs, and the P_{GS} profile as the output. The inputs and outputs are normalized within the range [0,1].

The next step consists on the generation of the initial FL design, which is developed based on the subtractive-clustering technique of the datasets. This FL structure includes the initial designs for the membership functions and rules. However, this initial FL structure is not trained yet, and therefore it can not be used as EMS.

Once the initial FL design is obtained, the next step consists on the ANFIS training. The training step aims tuning the membership functions and refining the rules originally proposed by the data sub-clustering. For this approach, the 80% of the original DP data is used, as the remainder 20% is used to test the effectiveness of the learning approach. Figure 3.12 shows the architecture used for the ANFIS learning step. As it is depicted, the tuning stage is a hybrid learning algorithm in conformity with back-propagation and least-squares methods [27]. The architecture is composed of 5 layers. Nodes x, y and z in layer 1 represent the system inputs (SOC, length-ratio, and P_{dem}), while the node in layer 5 refers to the system output P_{GS}. The output of each layer is represented as shown in Equation 3.7.

Layer 1 $O_i^1 = \mu_{A_i}$ is an adaptive layer that represents the fuzzification process, which is performed according to Gaussian membership functions. In the example given in Equation

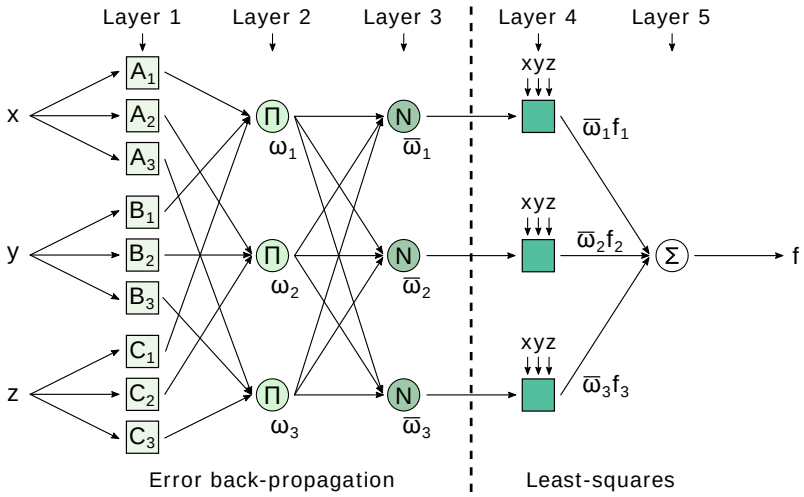

Figure 3.12: ANFIS architecture [27].

3.7, x represents one of the input varibles, and the Gaussian shape is defined by parameters $\{a, b\}$. The same equation should be applied to relate input variables y and z with their Gaussian membership functions (B and C). Layer 2 $O_i^2 = \omega_i$ and Layer 3 $O_i^3 = \bar{\omega}_i$ are fixed layers that represent the FL inference or evaluation of rules. In Layer 2 each rule weight is determined multiplying each node by the input signals, and in Layer 3 each rule weight is normalized. Layer 4 $O_i^4 = \bar{\omega}_i \cdot F_i$ is an adaptive layer where $\{p, q, r, m\}$ parameters define the fuzzy set designs for the defuzzification. As Equation 3.7 shows, $\{p, q, r, m\}$ parameters represent a linear membership function. Finally, Layer 5 $O^5 = F$ performs the defuzzification.

$$\begin{cases} O_i^1 = \mu_{A_i} = e^{-\left(\frac{x-a}{b}\right)^2}, \quad i = 1,2,3 \\ O_i^2 = \omega_i = \mu_{A_i}(x) \cdot \mu_{B_i}(y) \cdot \mu_{C_i}(z), \quad i = 1,2,3 \\ O_i^3 = \bar{\omega}_i = \frac{\omega_i}{\sum_{j=1}^{i} \omega_i}, \quad i = 1,2,3 \\ O_i^4 = \bar{\omega}_i \cdot F_i = \omega_i \cdot (p_i \cdot x + q_i \cdot y + r_i \cdot z + m_i), \quad i = 1,2,3 \\ O^5 = F = \sum_{j=1}^{3} \bar{\omega}_j \cdot f_j = \frac{\sum_{j=1}^{3} \omega_j \cdot f_j}{\sum_{j=1}^{3} \omega_j} \end{cases} \tag{3.7}$$

Eventually, once the training step is finalized, the FL-based controller is obtained, which can be implemented online in the H-DEMU. In order to ease the understanding and differentiate this FL-based controller from the RB-FL and GA-FL strategies, the current EMS will be denoted as ANFIS.

3.2.2 Battery Chemistries

Once all the proposed EMSs have been presented, this subsection deals with the BT chemistries that will be evaluated in this case study. As already reviewed in Chapter 1,

different BT chemistries exist depending on the deployed anode and cathode material. In this case study, the analysis of the following BT chemistries is proposed: LTO, NMC and LFP. Table 3.2 shows the parameters related to the characterization of each BT chemistry. These values are required by the BT simulation model (Section 2.3.1.7), and refer to the parametrization at cell level and at BOL. V_{oc} and R_{int} curves have been obtained from characterization tests carried out in collaboration between Ikerlan and CAF Power and Automation.

Table 3.2: Characterization of BT cells.

Parameter	LFP	NMC	LTO
Q_{BT_0}	28 Ah	46 Ah	23 Ah
V_{BT_nom}	3.2 V	3.7 V	2.3 V
R_{nom}	1.8 mΩ	1.9 mΩ	1.2 mΩ
V_{BT_max}	3.6 V	4.2 V	2.7 V
V_{BT_min}	2.5 V	3 V	1.7 V
C_{max_ch}	4 C	3 C	4 C
C_{max_dch}	6.5 C	5 C	4.5 C
SOC_{max}	90 %	90 %	90 %
SOC_{min}	20 %	20 %	20 %

BT cells are arranged in series and parallel to build BT modules. In the LCC optimization step the number of BT modules is optimized (variable n_{BT}). In order to obtain a fair comparison between the different BT capacities, modules with the same nominal energy (20 kWh) are built with the cells introduced in Table 3.2.

Table 3.3 shows the characteristics of the obtained BT modules. As it was specified, n_{cell} refers to the number of cells connected in series, while m_{cell} refers to the number of cells connected in parallel. Key parameters of the built modules are the volumetric and energetic densities, defined as ρ_{BT_L} $[Wh/L]$ and ρ_{BT_E} $[Wh/kg]$, respectively. These values limit the maximum amount of BT nominal energy that can be integrated in the vehicle, which is a constraint of the optimization problem that will be detailed in Section 3.3. Both values have been estimated from commercial BT packs of the considered chemistries [192–194].

Table 3.3: Characterization of BT modules.

Parameter	LFP	NMC	LTO
E_{BT}	20 kWh	20 kWh	20 kWh
n_{cell}	112	118	189
m_{cell}	2	1	2
ρ_{BT_L}	81.1 Wh/L	112.2 Wh/L	52.8 Wh/L
ρ_{BT_E}	47.9 Wh/kg	86.9 Wh/kg	53.3 Wh/kg

Regarding the lifetime estimation of each BT chemistry, the degradation model introduced in Section 2.3.5 and the parametrizations given in Table 2.6 are used.

3.2.3 Economic Model Parametrizations

After the control strategies and BT chemistries, in this subsection the parameters of the economic model used in the different sensitivity analyses are introduced. Two different parametrizations are defined depending on the sensitivity analysis being performed. On the one hand, a nominal parametrization is defined. This parametrization is used in the sensitivity to the powertrain design and in the sensitivity to the drive cycle. On the other hand, some of these parameters are selected and their sensitivity is also analysed in the sensitivity to the parameters of the economic model (see Figure 2.2 for the general chart of sensitivity analyses).

3.2.3.1 Nominal Parametrization

Table 3.4 presents the values defined for the nominal parametrization. These values have been selected based on the proposals made in similar literature works [11, 27, 48, 195, 196]. The parameters without a reference are own assumptions. These assumptions have been defined together with CAF Power & Automation, based on the typical characteristics of H-DEMU applications.

Table 3.4: Nominal parameters for economic evaluation.

	Parameter	**Value**	**Reference**
General Parameters	Y	30 years	-
	I	2.5 %	-
	t_{op}	320 days/year	-
	t_{day}	14 h/day	-
Acquisition Costs	C_{train}	8,000,000 €	-
	c_{BT} - LTO	1500 €/kWh	[27, 195]
	c_{BT} - NMC	800 €/kWh	[27, 195]
	c_{BT} - LFP	1040 €/kWh	[48]
	c_{GS}	500 €/kW	[48]
Operation Costs	c_f	1.1 €/L	[196]
	c_{cat}	0.06 €/kWh	[11]
Maintenance costs	c_{maint}	200,000 €/year	-

3.2.3.2 Scenarios for Sensitivity Analysis to Economic Model

Some of the parameters defined in the nominal parametrization are identified as unsteady, or as probable to vary from context to context. Specifically, the daily operation hours (t_{day}) may vary depending on the railway line or railway project, the BT price (c_{BT}) may vary depending on the selected manufacturer, and the diesel price (c_f) may vary depending on the country or even the socio-economic context.

In order to develop the sensitivity analysis, for each parameter a Low Scenario (LS), a Medium Scenario (MS) and a High Scenario (HS) have been defined. The values at each scenario have been defined based on the variability that each parameter may suffer. Table

3.5 shows the values proposed for each parameter and scenario. In the following lines the reasons behind these values are enumerated:

Table 3.5: Sensitivity to parameters of economic model.

Parameter	Low	Medium	High
t_{day}	7 h/day	10.5 h/day	14 h/day
c_{BT} - LTO	1200 €/kWh	1500 €/kWh	1800 €/kWh
c_{BT} - NMC	640 €/kWh	800 €/kWh	960 €/kWh
c_{BT} - LFP	520 €/kWh	1040 €/kWh	1560 €/kWh
c_f	0.65 €/L	1.1 €/L	1.55 €/L

- In the case of t_{day}, it is understood that values higher than the one defined in the nominal scenario (14 h/day) are less probable. Therefore, the nominal value is defined at the HS. For the MS and LS, reductions of the 25% and 50% have been defined, respectively, based on the typical working hours of a H-DEMU.
- In the case of c_{BT} different variabilities have been defined for each BT chemistry. Based on an analysis of prices from different manufacturers, it is concluded that the prices can increase or decrease compared to the nominal parametrization. Therefore, the nominal value has been defined in the MS. The values for the LS and HS have been defined based on the mentioned market analysis: ±20% variability for LTO and NMC, and ±50% variability for LFP.
- Finally, in the case of c_f the nominal parametrization is also defined in the MS. Even if the diesel price evolution in the last years shows an upwards trend, it is understood that analysing low prices is also interesting. Therefore, a ±40% variability is set for the definition of LS and HS.

3.2.4 Driving Cycles

After analysing the proposed EMSs, BT chemistries and parametrizations of the economic model, the last subsection deals with the driving cycles to be used in the different sensitivity analyses. As in the case of the economic model, first a nominal case is defined, which is used when analysing the sensitivity to the powertrain design and the sensitivity to the parameters of the economic model. Then, a series of driving profiles with different characteristics are proposed to develop the sensitivity to the driving cycle.

3.2.4.1 Nominal Driving Cycle

The nominal case is based on an existing railway line, which is called “A Coruña - A Coruña” line. Figure 3.13 shows the map of the circular line and Figure 3.14 depicts the corresponding speed profile, which corresponds to the round trip route. In both cases the locations of the stations are specified. The round trip route is composed of 768.5 km and 14 stations, and it is completed in 7 hours.

Figure 3.13: Journey of "A Coruña - A Coruña" railway line.

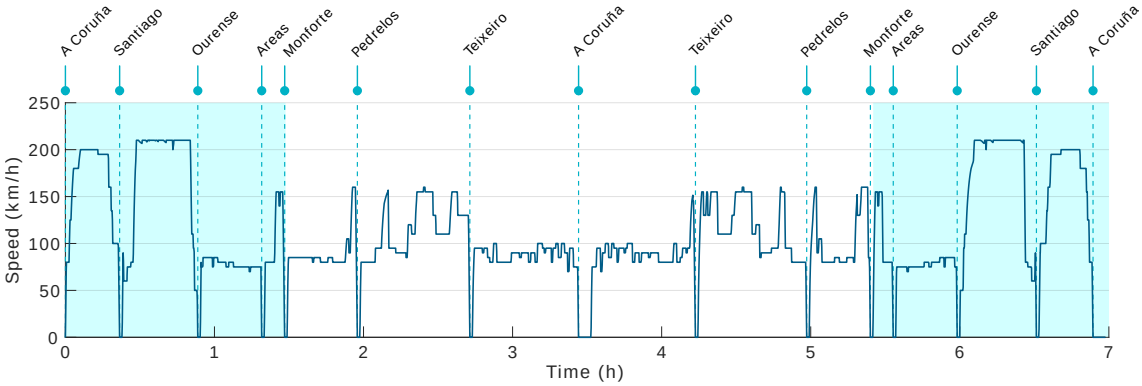

Figure 3.14: Speed profile of "A Coruña - A Coruña" railway line. Shadowed section represents electrification.

As it was stated in Section 2.3.1, the input required for the simulation model is the traction demand profile (P_{EM}). Figure 3.15 depicts the P_{Dem} profile provided by CAF Power and Automation, which already considers the demand from the auxiliaries ($P_{Dem} = P_{EM} + P_{Aux}$). It is worth to mention that for the simulation the start of the route has been defined at the beginning of the non-electrified section (station "Monforte"). The reason is that in order to obtain a representative comparison of different SOC_0 values, it is better to start the simulation from the beginning of the non-electrified section. Therefore, Figure 3.15 shows the demand profile starting from the station of "Monforte".

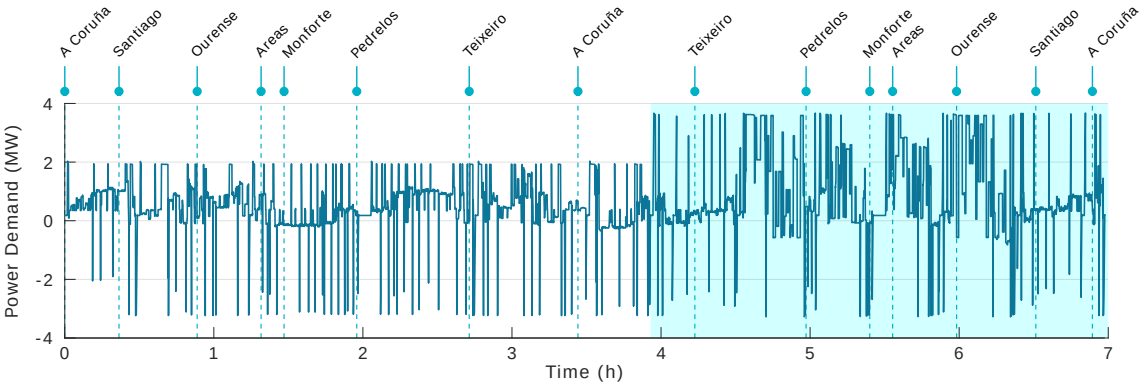

Figure 3.15: Power demand profile of "A Coruña - A Coruña" railway line. Shadowed section represents electrification.

3.2.4.2 Scenarios for Sensitivity Analysis to Driving Cycle

For the development of this sensitivity analysis, driving cycles of different characteristics are required. Due to the difficulty of obtaining information from many real railway lines, it has been decided to use synthetic cycles. That is to say, new driving cycles will be generated from the routes already presented. An advantage of this approach is also the possibility of generating driving cycles of pre-defined specific characteristics.

As the aim of this Ph.D. Thesis is the analysis of non-electrified sections, the objective of the synthetic cycles will be obtaining driving profiles of different characteristics for these sections. In the case of electrified sections, it is considered that it is not necessary to analyse driving cycles with different characteristics, as they barely affect the optimal design and operation of the powertrain. The only exception would be a case in which the electrified section is so short that the BT cannot recover its initial SOC. However, it is considered that this scenario is out of the scope of the current case study. Therefore, the design of the synthetic cycles will be oriented to the non-electrified sections.

Two variables have been defined as the design criteria of the generated synthetic cycles, as they are representative of the characteristics of the driving cycles: the average power demand and the total energy demand. From a macroscopic view, the average power demand is related to the average speed and size of the vehicle, and also to the cumulative slope of the route. In short, this variable defines the demand level of each driving profile, what affects in the optimal sizing and operation of the powertrain sources, particularly of the genset. Regarding the total energy demand, it is related to the average power demand, but also to the duration of the route. As in the current scenario the BT is expected to deplete its charge during the non-electrified section, the running time in this section will inevitably affect in the optimal operation and sizing of the powertrain sources, particularly of the BT. As the average power demand and the total energy demand are correlated, the duration of the route will be used as design criteria instead of the total energy demand.

In order to generate the synthetic cycles, the non-electrified sections of the already

introduced “Madrid-Badajoz” (Figure 2.5 in Chapter 2) and “A Coruña - A Coruña” (Figure 3.15 in the current chapter) routes have been used. These profiles are divided into station to station sub-profiles. Then, the sub-profiles are combined so as to obtain driving cycles of different durations and average power demands.

In order to obtain a sufficient disparate matrix of cases, 4 different average power demands and 4 different running times are proposed, what has led to 16 cases. In the case of the power demands, the following values have been proposed: 200 kW, 400 kW, 600 kW and 800 kW. Indeed, it is considered that values lower than 200 kW or higher than 800 kW are not very likely for the analysed application, since only the auxiliaries provide 135 kW, and very high demands are only possible in very mountainous routes. In the case of the running times, values 0.5 h, 1.5 h, 2.5 h and 3.5 h have been proposed for the non-electrified sections. For the electrified sections, equal running times are proposed, and therefore the real durations of the routes are 1 h, 3 h, 5 h and 7 h, respectively.

As the number of potential combinations of the sub-profiles is limited, the exact proposed values can not be obtained. Figure 3.16 depicts the real matrix of the generated driving cycles. For each driving cycle, the total energy demand is also given. The obtained approximation is understood to be appropriate, as the aim of this approach is not to analyse the operation of the H-DEMU in drive cycles of exact characteristics. The graphs of the generated synthetic profiles can be found in Appendix A.

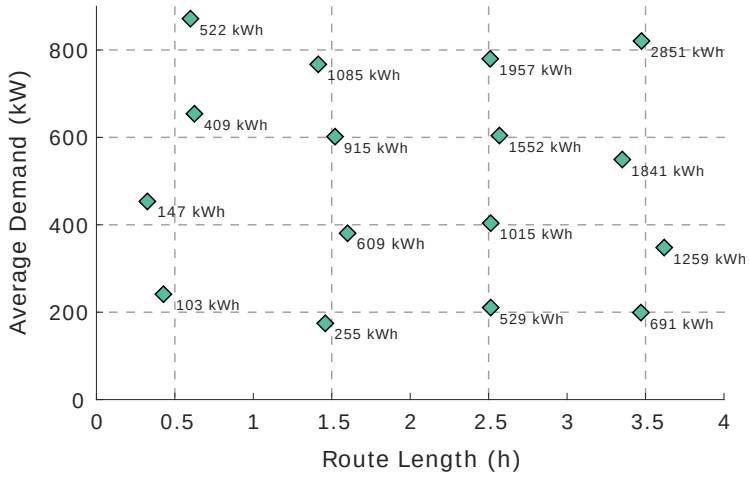

Figure 3.16: Matrix of generated synthetic driving cycles.

3.3 Definition of Optimization Problem

Once all the cases of the sensitivity analysis have been introduced, this new section focuses on the optimization problem deployed as part of the holistic design methodology. As it was explained in Chapter 2, the methodology of the current Ph.D. Thesis includes the LCC optimization of each case being analysed in a certain sensitivity analysis. This LCC optimization is focused on obtaining the cost-efficient powertrain sizing (n_{BT} and

n_{GS}), initial BT SOC (SOC_0), and in some cases also the optimal EMS parameters.

Generic methodologies to solve this optimization problem were introduced in Section 2.4. As it was specified, the optimization problem may differ depending on the strategy being analysed. Therefore, in this section these generic optimization methodologies are particularized to the EMSs introduced in this case study. Figure 3.16 shows the classification of optimization problems according to the EMS, which is further detailed below:

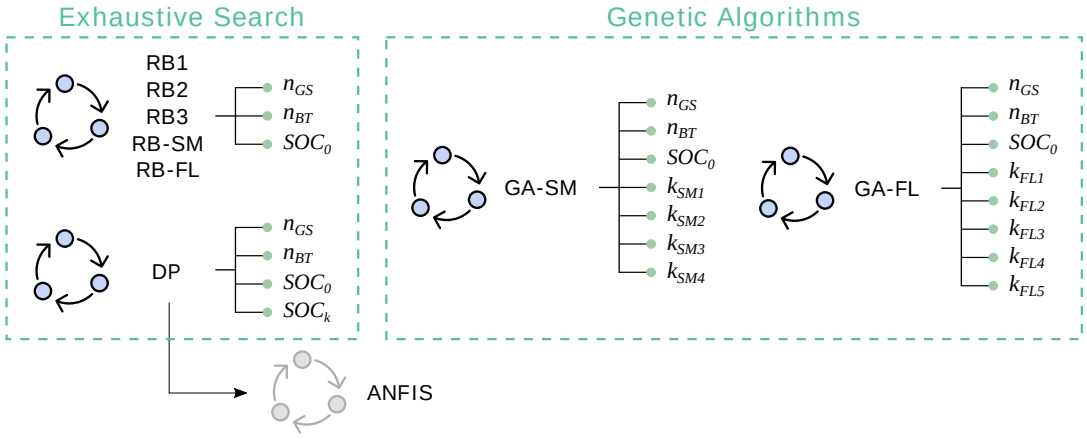

Figure 3.17: Distribution of Optimization approaches according to EMS.

(1) In the case of RB strategies (RB1, RB2, RB3, RB-SM and RB-FL), the EMS is not optimized. Therefore, as the number of optimization variables is low (n_{BT}, n_{GS} and SOC_0), the exhaustive search based optimization introduced in Section 2.4.1 is deployed. This generic problem will be particularized in the following Section 3.3.1.

(2) In the case of OB strategies, different design coordination concepts are deployed. On the one hand, in the case of DP the optimization is realized in two levels. In the outer level, the powertrain sizing (n_{BT} and n_{GS}) and initial and final SOC values (SOC_0 and SOC_K) are optimized. In the inner level, the DP optimization (presented in Section 3.2.1.6) is deployed for the specific n_{BT}, n_{GS}, SOC_0 and SOC_K values being evaluated in the outer level. Therefore, a nested optimization is deployed. Considering the number of optimization variables of the outer level, the exhaustive search based optimization introduced in Section 2.4.1 is deployed. The generic problem introduced in that section will be particularized in Section 3.3.2 for the DP case.

(3) On the other hand, in the case of GA-SM and GA-FL the optimization is realized in a single level, as all the variables can be optimized together. Therefore, a simultaneous optimization approach is deployed. Due to the increased number of optimization variables, in this case the GA-based approach introduced in Section 2.4.2 is deployed. The generic problem introduced in that section will be particularized in Section 3.3.3 for GA-SM and in Section 3.3.4 for GA-FL.

(4) Finally, the ANFIS strategy is understood to be the real-time implementation of DP. Therefore, no optimization is deployed in this case, as the n_{BT}, n_{GS}, SOC_0

and SOC_K values obtained in the case of DP are used to calculate the LCC.

The fitness function is the same in all the mentioned optimization problems, as it consists on the LCC minimization. Therefore, the fitness function is defined as follows:

$$minimize\ LCC(X)\ \mid\ X \in \Pi \tag{3.8}$$

where X represents the vector containing the optimization variables, and Π represents the space of feasible solutions. X and Π vary depending on the specific optimization problem, and therefore they are introduced in the following subsections.

It is worth to mention that in all the optimization problems, each n_{BT} refers to a 20 kWh BT module, and each n_{GS} to a 500 kW genset. The definition of the remainder variables depends on the specific optimization problem, and therefore they are independently introduced in the following subsections.

3.3.1 Exhaustive Search Optimization

The exhaustive search optimization is deployed when analysing the RB1, RB2, RB3, RB-SM and RB-FL strategies. The optimization variables vector X_{ES} and the space of feasible solutions Π_{ES} are defined as in Equations 3.9 and 3.10. Being this an exhaustive search-based approach, Π_{ES} has to be discretized into a feasible number of cases. This is the reason to define SOC_0 between 50% and 90% in steps of 10%. The limits have been defined based on the conclusions obtained after some first tests. Regarding n_{GS} and n_{BT}, they are defined as natural numbers. n_{GS} ranges between 0 and the maximum number of gensets (N_{GS} [−]), as in this way the BEMU is considered also as a possible option. Besides, n_{BT} ranges between 1 and the maximum number of BT modules (N_{BT} [−]), since the DEMU is not considered as a possible option.

$$X_{ES} = \begin{bmatrix} n_{BT} \\ n_{GS} \\ SOC_0 \end{bmatrix} \tag{3.9}$$

$$\Pi_{ES} = \begin{cases} 1 \leq n_{BT} \leq N_{BT} \ \rightarrow n_{BT} \in \mathbb{Z} \\ 0 \leq n_{GS} \leq N_{GS} \ \rightarrow n_{GS} \in \mathbb{Z} \\ 50 \leq SOC_0 \leq 90 \ \rightarrow SOC_0 \in \{50, 60, ... \ 90\} \end{cases} \tag{3.10}$$

N_{GS} and N_{BT} are a key constraint for the optimization problem. In order to obtain realistic values, it is assumed that there is a maximum available space and weight in the vehicle for the integration of the gensets and BT modules, which is common for both elements. From this assumption, it is concluded that N_{BT} depends on n_{GS}, or that N_{GS} depends on n_{BT} (both dependencies rely on the same idea). That is to say, depending on the number of gensets that are being analysed, the maximum number of BT modules changes (and vice versa).

The maximum volume and weight allowable for the powertrain elements, and the volume and weight of a single genset have been provided by CAF Power and Automation. From these values, it is concluded that the maximum number of gensets are 4 ($N_{GS} = 4$), in an scenario with no space for BTs ($N_{BT} = 0$). Then, considering the energetic and volumetric densities of each BT chemistry (see Table 3.3), the relation between N_{BT} and n_{GS} is derived. Figure 3.18 depicts this relation. The same graph can be depicted to represent the relation between N_{GS} and n_{BT}.

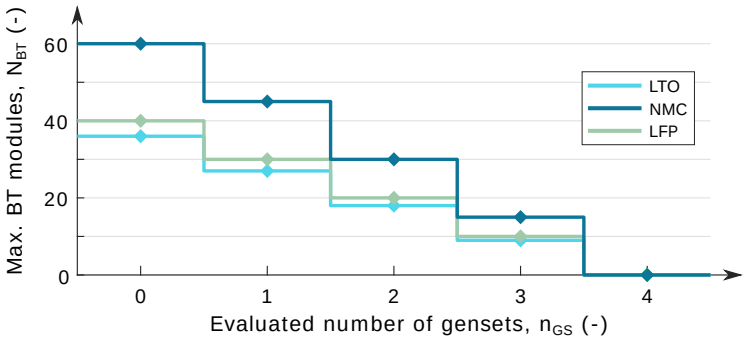

Figure 3.18: Relation of maximum number of gensets and BT modules.

3.3.2 Exhaustive Search Optimization - Dynamic Programming

A variation of the exhaustive search optimization introduced in the previous subsection is deployed when analysing the DP strategy, due to the fact that in this case SOC_K is also optimized. The optimization variables vector X_{DP} and the space of feasible solutions Π_{DP} are defined in Equations 3.11 and 3.12. The space of n_{GS}, n_{BT} and SOC_0 is defined as in the previous exhaustive search optimization problem. Regarding SOC_K, it is also defined in steps of 10%, and after some first tests it has been decided to be constrained between 20% and 50%.

$$X_{DP} = \begin{bmatrix} n_{BT} \\ n_{GS} \\ SOC_0 \\ SOC_K \end{bmatrix} \tag{3.11}$$

$$\Pi_{DP} = \begin{cases} 1 \leq n_{BT} \leq N_{BT} \ \rightarrow n_{BT} \in \mathbb{Z} \\ 0 \leq n_{GS} \leq N_{GS} \ \rightarrow n_{GS} \in \mathbb{Z} \\ 50 \leq SOC_0 \leq 90 \ \rightarrow SOC_0 \in \{50, 60, ... \ 90\} \\ 20 \leq SOC_K \leq 50 \ \rightarrow SOC_K \in \{20, 30, ... \ 50\} \end{cases} \tag{3.12}$$

3.3.3 GA-SM Optimization

The generic GA optimization introduced in Section 2.4.2 is particularized in this section for the case of the GA-SM strategy. The optimization variables vector X_{GASM} and the

space of feasible solutions Π_{GASM} are defined in Equations (3.13) and (3.14). As in this case Π_{GASM} does not affect the feasibility of the problem, a wider space is defined for SOC_0, which coincides with the maximum and minimum allowable SOC values. The same constraints are defined for k_{SM1}, k_{SM2}, k_{SM3} and k_{SM4}. Besides, some additional constraints are defined in order to ensure a soft change from state to state (see Figure 3.6). These constraints are introduced in Equation (3.15). It is considered that a 2% difference between k_{SM1} and k_{SM2}, k_{SM3} and k_{SM4}, k_{SM1} and k_{SM3}, and k_{SM2} and k_{SM4} ensures the mentioned soft control.

$$X_{GASM} = \begin{bmatrix} n_{BT} \\ n_{GS} \\ SOC_0 \\ k_{SM1} \\ k_{SM2} \\ k_{SM3} \\ k_{SM4} \end{bmatrix} \tag{3.13}$$

$$\Pi_{GASM} = \begin{cases} 1 \leq n_{BT} \leq N_{BT} \ \rightarrow n_{BT} \in \mathbb{Z} \\ 0 \leq n_{GS} \leq N_{GS} \ \rightarrow n_{GS} \in \mathbb{Z} \\ 20 \leq SOC_0 \leq 90 \ \rightarrow SOC_0 \in \mathbb{R} \\ 20 \leq k_{SM1} \leq 90 \ \rightarrow k_{SM1} \in \mathbb{R} \\ 20 \leq k_{SM2} \leq 90 \ \rightarrow k_{SM2} \in \mathbb{R} \\ 20 \leq k_{SM3} \leq 90 \ \rightarrow k_{SM3} \in \mathbb{R} \\ 20 \leq k_{SM4} \leq 90 \ \rightarrow k_{SM4} \in \mathbb{R} \end{cases} \tag{3.14}$$

$$subject\ to: \begin{cases} k_{SM1} + 2 < k_{SM2} \\ k_{SM3} + 2 < k_{SM4} \\ k_{SM1} + 2 < k_{SM3} \\ k_{SM2} + 2 < k_{SM4} \end{cases} \tag{3.15}$$

Table 3.6 shows the relation of the parameters required by the GA. The population size is defined as 10 times the number of optimization variables, and for the elite count and crossover fraction the typically recommended values are defined [18]. In order to avoid a long running time, a maximum number of generations, stall generations and optimization time are set. The defined values are considered to provide an appropriate balance between the required optimization time and the optimality of the obtained solution.

Table 3.6: Parameters for the Genetic Algorithm in GA-SM optimization.

Parameter	**Value**	**Parameter**	**Value**
Population size	70	Max. generations	100
Elite count	5 %	Max. stall generation	50
Crossover fraction	80 %	Max. optimization time	24 h

3.3.4 GA-FL Optimization

The generic GA optimization introduced in Section 2.4.2 is particularized in this section for the case of the GA-FL strategy. The optimization variables vector X_{GAFL} and the space of feasible solutions Π_{GAFL} are defined in Equations (3.16) and (3.17), respectively. k_{FL1}, k_{FL2} and k_{FL3} follow the same constraints as SOC_0, as they refer to specific SOC values. k_{FL4} is restricted in a way that the trapezoidal shapes are not too wide or too narrow, and the feasible space of k_{FL5} ensures the correct order of the fuzzy sets (see Figure 3.9). Besides, as in the case of GA-SM, some additional constraints are defined. These constraints ensure maintaining the trapezoidal shape of the fuzzy sets: the difference between k_{FL1} and k_{FL2} is at least two times the width of the ramp defined by k_{FL4}. The same happens for k_{FL2} and k_{FL3}.

$$X_{GAFL} = \begin{bmatrix} n_{BT} \\ n_{GS} \\ SOC_0 \\ k_{FL1} \\ k_{FL2} \\ k_{FL3} \\ k_{FL4} \\ k_{FL5} \end{bmatrix} \tag{3.16}$$

$$\Pi_{GAFL} = \begin{cases} 1 \leq n_{BT} \leq N_{BT} \ \rightarrow n_{BT} \in \mathbb{Z} \\ 0 \leq n_{GS} \leq N_{GS} \ \rightarrow n_{GS} \in \mathbb{Z} \\ 20 \leq SOC_0 \leq 90 \ \rightarrow SOC_0 \in \mathbb{R} \\ 20 \leq k_{FL1} \leq 90 \ \rightarrow k_{FL1} \in \mathbb{R} \\ 20 \leq k_{FL2} \leq 90 \ \rightarrow k_{FL2} \in \mathbb{R} \\ 20 \leq k_{FL3} \leq 90 \ \rightarrow k_{FL3} \in \mathbb{R} \\ 1 \leq k_{FL4} \leq 10 \ \rightarrow k_{FL4} \in \mathbb{R} \\ 0 \leq k_{FL5} \leq 33 \ \rightarrow k_{FL5} \in \mathbb{R} \end{cases} \tag{3.17}$$

$$subject\ to: \begin{cases} k_{FL1} + 2 \cdot k_{FL4} < k_{FL2} \\ k_{FL2} + 2 \cdot k_{FL4} < k_{FL3} \end{cases} \tag{3.18}$$

Table 3.7 shows the relation of the parameters required by the GA. Compared to the GA-FL optimization, the only variation comes in the population size, which is increased due to the higher number of variables.

Table 3.7: Parameters for the Genetic Algorithm in GA-FL optimization.

Parameter	Value	Parameter	Value
Population size	80	Max. generations	100
Elite count	5 %	Max. stall generation	50
Crossover fraction	80 %	Max. optimization time	24 h

3.4 Results of Sensitivity Analysis to Powertrain Design

After providing all the details required to launch the different sensitivity analyses, this section presents the results obtained in the sensitivity analysis to the powertrain design. As it was specified in the methodology presented in Chapter 2, this sensitivity analysis is focused on comparing the LCC of different control strategies and BT chemistries. Figure 3.19 shows where it is located this sensitivity analysis in the methodology proposed in this Ph.D. Thesis. The results of this sensitivity analysis have been obtained for the nominal parametrization of the economic model, and simulating the nominal driving cycle.

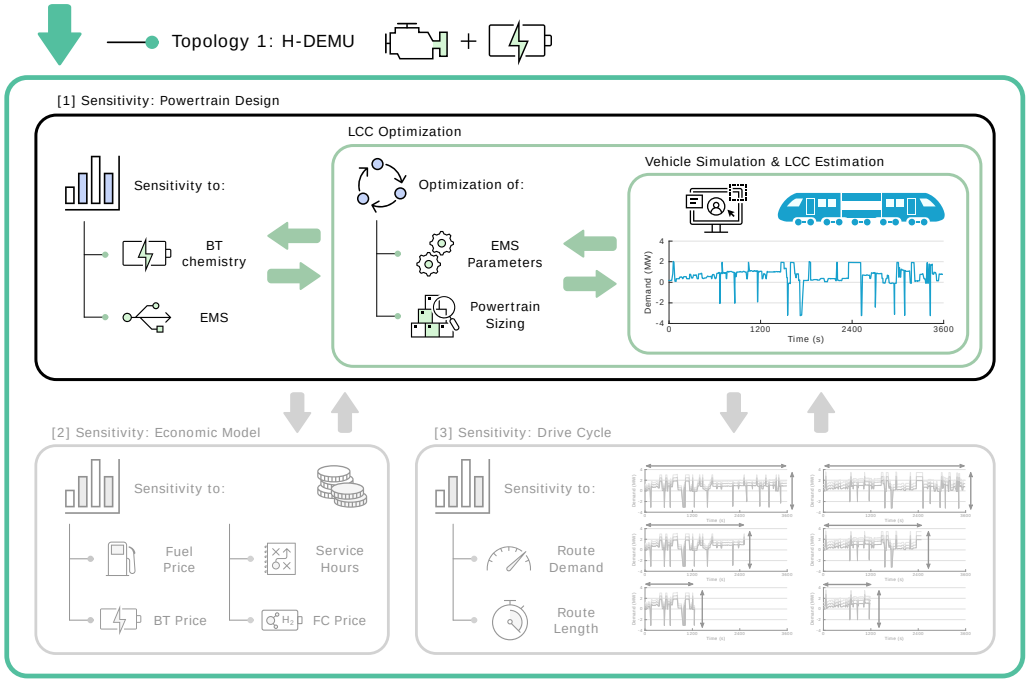

Figure 3.19: Current step of holistic design methodology.

In order to improve the evaluation of the obtained results, the analysis is divided into several subsections. First, the results of the LCC optimization will be presented in general terms in Section 3.4.1. In Section 3.4.2, the analysis will be focused on comparing the LCC values of the different EMS and BT chemistries. This analysis will give a general idea regarding the most appropriate control strategies and BT chemistries. The reasons behind the results obtained by each EMS and BT chemistry will be also addressed. Then, the relation between the optimal values of the optimization variables and a lower LCC value will be analysed in Section 3.4.3. The influence that the costs that can vary (C_{GS}, C_{BT}, C_f and C_{BTrepl}) have on the final LCC will be also addressed in Section 3.4.4. This analysis will unveil which costs become crucial to reduce the overall LCC.

As it was highlighted in Chapter 1, it is important to consider different features when evaluating an EMS. Besides the optimality in relation to the fuel use or the BT lifetime (which in the proposed approach are gathered in the LCC), it is important to consider

also the real time execution and the robustness to potential disturbances, as they limit the efficiency of the EMS when implementing in a real application. Therefore, in Section 3.4.5 the robustness and real time execution of the proposed control strategies will be analysed. Finally, in Section 3.4.6 the main conclusions of the first sensitivity analysis will be reviewed.

3.4.1 Results of LCC Optimization

A review of the obtained optimization results is given in Table 3.8. Each row presents a case of the sensitivity analysis, i.e., a combination of BT chemistry and EMS. Additionally, in the first row the results of a conventional DEMU are given. The DEMU is sized with a genset of 2000 kW, and it is used as reference to compare the results of the sensitivity analysis. It is worth to mention that no results are given for RB3, due to the fact that no feasible solution is obtained with this strategy.

At each column of the table a representative parameter is given. First, the obtained fitness function value is introduced, i.e., the LCC value. The LCC of each case is given in per units (p.u.) in relation to the LCC of the DEMU. In the next columns the optimization variables shared in all the cases are given: n_{GS}, n_{BT} and SOC_0. n_{GS} and n_{BT} are given in kW and kWh, respectively, and SOC_0 in percentage (%). Table 3.8 also shows a breakdown of the LCC value into the costs that can vary between the different cases: genset acquisition cost (C_{GS}), BT acquisition cost (C_{BT}), fuel use cost (C_f) and BT replacement cost (C_{BTrepl}). The values of these variables are also given in p.u. in relation to the LCC of the DEMU. C_{train} and C_{maint} are not given, as they are the same in all the cases. The cost related to the catenary use (C_{cat}) may vary between the different cases due to variations in the use of electricity to charge the BT. However, as the obtained differences are residual in comparison to the variations of the other costs, C_{cat} is left out of this analysis. This is the reason why the sum of the cost terms given in the table does not coincide with the overall LCC value. Finally, the last column gives the results returned by the BT lifetime estimation model. The lifetime is provided in years.

Moreover, and as additional information, the specific optimization variables of strategies GA-SM, GA-FL and DP are given in Table 3.9. In the case of GA-SM and GA-FL, RB refers to the RB-SM and RB-FL parametrizations, which are the same for the different BT chemistries.

In this subsection a qualitative analysis of the optimization results has been provided. In the following subsections a quantitative analysis of the variables presented in this subsection will be developed.

Table 3.8: Representative results of sensitivity analysis to the powertrain design.

		LCC $(p.u.)$	n_{GS} (kW)	n_{BT} (kWh)	SOC_0 (%)	C_{GS} $(p.u.)$	C_{BT} $(p.u.)$	C_f $(p.u.)$	C_{BTrepl} $(p.u.)$	y_{BT} $(years)$
DEMU		1.000	2000	-	-	0.038	-	0.369	-	-
LTO	**RB1**	0.996	1000	280	90	0.019	0.016	0.356	0.022	10.3
	RB2	0.965	1000	300	90	0.019	0.017	0.326	0.020	12.6
	RB3	-	-	-	-	-	-	-	-	-
	RB-SM	0.970	1000	360	90	0.019	0.021	0.325	0.023	13.2
	GA-SM	0.960	1000	320	89.9	0.019	0.019	0.318	0.021	12.7
	RB-FL	0.967	1000	360	90	0.019	0.021	0.320	0.025	12.1
	GA-FL	0.966	1000	360	88.7	0.019	0.021	0.319	0.024	12.3
	DP	0.953	1000	360	90	0.019	0.021	0.305	0.025	11.8
	ANFIS	0.963	1000	360	90	0.019	0.021	0.314	0.026	11.5
NMC	**RB1**	1.016	1500	280	90	0.029	0.009	0.366	0.029	5.3
	RB2	0.973	1000	480	90	0.019	0.015	0.326	0.030	7.9
	RB3	-	-	-	-	-	-	-	-	-
	RB-SM	0.971	1000	540	90	0.019	0.017	0.320	0.032	8.6
	GA-SM	0.966	1000	580	89.3	0.019	0.018	0.313	0.033	8.8
	RB-FL	0.976	1500	300	90	0.029	0.009	0.331	0.025	6.5
	GA-FL	0.972	1000	600	86.8	0.019	0.019	0.316	0.035	8.6
	DP	0.959	1000	600	90	0.019	0.019	0.282	0.052	6.1
	ANFIS	0.977	1000	600	90	0.019	0.019	0.301	0.051	6.3
LFP	**RB1**	1.052	1500	200	90	0.029	0.008	0.365	0.067	2.4
	RB2	1.009	1500	200	90	0.029	0.008	0.358	0.031	4.8
	RB3	-	-	-	-	-	-	-	-	-
	RB-SM	1.013	1500	200	90	0.029	0.008	0.344	0.049	3.3
	GA-SM	1.003	1500	200	89.3	0.029	0.008	0.350	0.034	4.4
	RB-FL	1.054	1000	400	90	0.019	0.016	0.314	0.122	2.6
	GA-FL	1.021	1500	200	86.8	0.029	0.008	0.351	0.050	3.1
	DP	1.048	1000	400	90	0.019	0.016	0.298	0.132	2.5
	ANFIS	1.085	1000	400	90	0.019	0.016	0.313	0.153	2.1

Table 3.9: Additional optimization variables of GA-SM, GA-FL and DP.

		Optimization variables
GA-SM	**RB**[1]	k_{SM1}=50.0%, k_{SM2}=60.0%, k_{SM3}=70.0%, k_{SM4}=80.0%
	LTO	k_{SM1}=22.7%, k_{SM2}=30.3%, k_{SM3}=56.5%, k_{SM4}=81.8%
	NMC	k_{SM1}=22.7%, k_{SM2}=48.7%, k_{SM3}=58.8%, k_{SM4}=78.1%
	LFP	k_{SM1}=26.4%, k_{SM2}=56.2%, k_{SM3}=82.8%, k_{SM4}=89.1%
GA-FL	**RB**[2]	k_{FL1}=30.0%, k_{FL2}=42.5%, k_{FL3}=67.5%, k_{FL4}=2.5%, k_{FL5}=10.0%
	LTO	k_{FL1}=23.9%, k_{FL2}=42.1%, k_{FL3}=85.7%, k_{FL4}=3.5%, k_{FL5}=11.4%
	NMC	k_{FL1}=25.8%, k_{FL2}=55.5%, k_{FL3}=80.2%, k_{FL4}=1.6%, k_{FL5}=14.6%
	LFP	k_{FL1}=48.1%, k_{FL2}=82.4%, k_{FL3}=87.4%, k_{FL4}=2.4%, k_{FL5}=30.1%
DP	**LTO**	SOC_K=25%
	NMC	SOC_K=25%
	LFP	SOC_K=25%

[1] Refers to the parametrization of RB-SM

[2] Refers to the parametrization of RB-FL

3.4.2 Analysis of LCC Values

This subsection focuses on comparing the LCC values of the different BT chemistries and EMSs. In order to ease the analysis, different graphs are depicted in Figures 3.20 and 3.21. On the one hand, Figure 3.20 plots the LCC values grouped according to the BT chemistry, with the shapes and colours representing different control strategies. The x-axis represents the LCC, and therefore the values located at the left refer to a better solution. On the other hand, in Figure 3.21 the LCC value of each case of the sensitivity analysis is divided into the key cost terms: C_{GS}, C_{BT}, C_f and C_{BTrepl}.

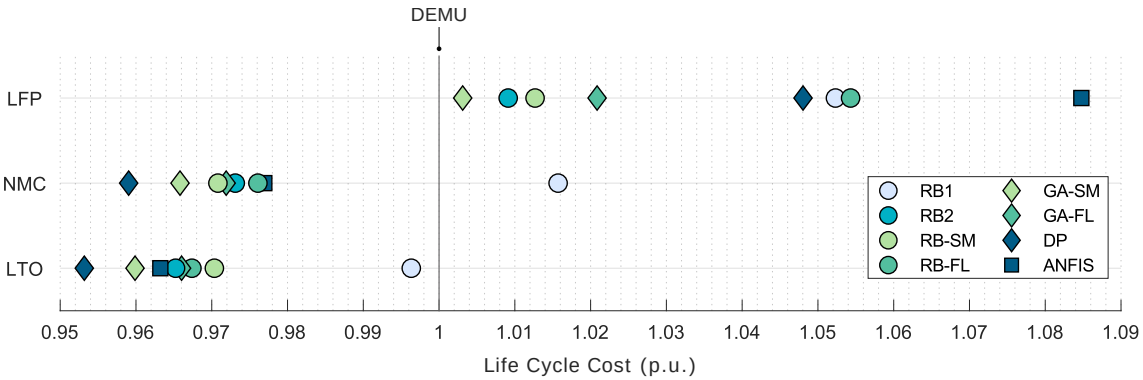

Figure 3.20: LCC results for different EMSs and BT chemistries.

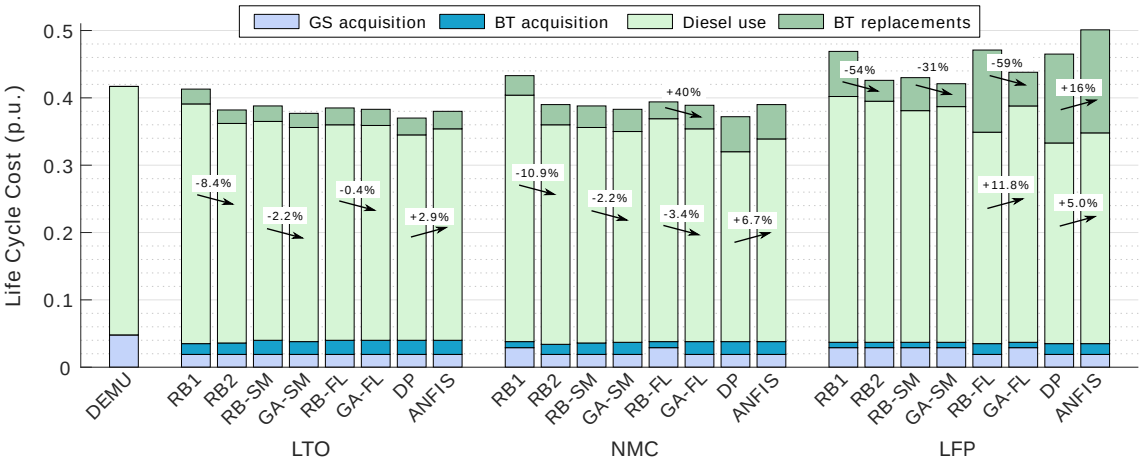

Figure 3.21: LCC breakdown into key cost terms.

3.4.2.1 Comparison of BT Chemistries

The first observation when analysing the results of the different BT technologies is that the LCC values of the vehicles integrating LFP chemistry are far from those of the other two chemistries. The LCC of the best strategy with LFP is nearly 4% higher than the best strategy with NMC, and 5% higher than the best strategy with LTO (see Figure 3.20). In addition, none of the strategies with LFP obtain a cost-efficient solution compared to the conventional DEMU (all the cases obtain a higher LCC). Looking to the graph depicted

in Figure 3.21, it can be concluded that the main cause of this higher LCC is the high C_{BTrepl} values obtained with this chemistry. In order to reduce the degradation of the BT, a possible initiative is to minimize its use, e.g., by reducing the DOD that it performs. However, a DOD reduction is normally translated into an increased diesel use. This is the reason why the solutions with LFP chemistry obtain also a higher fuel use in comparison to LTO or NMC options (compare c_f values of Table 3.8).

Looking to Figure 3.20, it can be also noticed that the results with LTO are slightly better than the results with NMC. Indeed, in all the strategies the LCC is always higher in NMC, even if the difference is kept relatively low: in RB1 2% higher, in RB2 0.8% higher, in RB-SM 0.1% higher, in RB-FL 1% higher, in GA-SM 0.6% higher, in GA-SL 0.6% higher, in DP 0.6% higher, and in ANFIS 1.4% higher. Therefore, the difference is always lower than 2%, and in most of the cases lower than 1%.

In the case of LTO, all the strategies improve the result of the DEMU, and in the case of NMC only RB1 obtains a LCC higher than the conventional diesel vehicle. It can be noticed that in most of the cases the fuel use cost is lower in NMC compared to LTO (see c_f values of Table 3.8), thanks to the possibility of integrating bigger BT systems. Indeed, as bigger is the BT size, less energy is required from the genset. However, LTO compensates this disadvantage due to a lower C_{BTrepl} value. Even if the LTO acquisition cost is higher, C_{BTrepl} is lower due to the fact that the lifetimes are much longer compared to NMC. Therefore, it can be foreseen that in scenarios with different fuel prices or BT acquisition costs, the chemistry with the best result could vary.

3.4.2.2 Comparison of Control Strategies

In order to add further information to the comparison of the different EMSs, in this subsection the simulation results of all the cases of the sensitivity analysis are depicted in Figures 3.22 to 3.25. The graphs represent the SOC evolution in the non-electrified section of the simulated railway line, and correspond to the BOL simulation.

Starting from the simple RB strategies, the improvement of RB2 over RB1 is notorious in the three chemistries: 3.1% LCC improvement in LTO, and 4.3% improvement in both NMC and LFP (see Table 3.8). In the cases of LTO and NMC, the LCC reduction is obtained due to the lower fuel use (8.4% and 10.9%, respectively). In the case of LFP, the reduction is due to the increase of the BT life, which is doubled (see Figure 3.21 and Table 3.8). Checking the simulation results depicted in Figure 3.22, the fuel use reduction of LTO and NMC can be linked to the higher use of the BT. Indeed, in RB1 the SOC is maintained around 85-90% at the end of the non-electrified section, while in RB2 that value is reduced until 60-65%. In the case of LFP, the final SOC value is kept close to 90% in both strategies, what explains the low difference in the diesel use. However, thanks to a softer battery operation (reduction of peak power values and performed DOD), the BT lifetime is doubled.

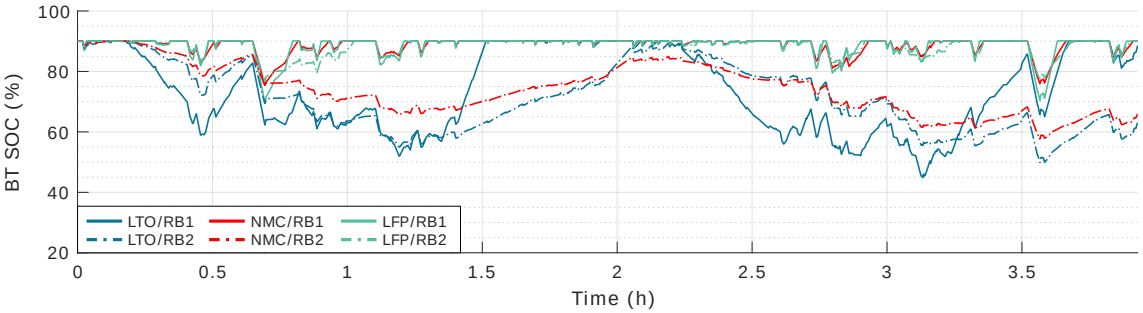

Figure 3.22: Simulation results of RB1 and RB2 strategies.

As it was previously highlighted, RB3 does not obtain a feasible solution. The reason is that in this case the genset reference might be lower compared to RB1 and RB2 (see Figure 3.5), what makes the BT be faster discharged. In order to obtain a feasible solution, a big BT is required. However, due to the space limitations for the integration of the BT, that feasible solution cannot obtained. The main disadvantage of RB3 is compensated in RB-SM/GA-SM thanks to the variation of the strategy when the SOC starts to deplete.

Continuing with RB-SM, it only improves RB2 in the case of NMC, with a LCC reduction of just the 0.2%. In LTO, RB-SM is 0.5% behind RB2, and in LFP 0.4% behind (see Table 3.8). This evidences that the first parametrization of SM strategy is not the most appropriated one, as it was designed to improve the performance of RB2 and RB3.

When optimizing the parameters of the strategy (from RB-SM to GA-SM), the improvement is remarkable: 1% lower LCC in LTO and LFP, and 0.5% lower LCC in NMC. In LTO and NMC the improvement comes due to the fuel use reduction (2.2% in both cases), and in LFP due to the BT life improvement (which is increased a 33%). With these results, GA-SM turns to be the second best strategy in NMC and LTO (0.7% behind DP in both cases) and the best strategy in LFP. Therefore, this evidences that GA-SM is the second option in terms of LCC, just after DP.

Figure 3.23 helps understanding how is this improvement achieved. In the case of LTO, the lower diesel use is linked to the depletion of the BT charge (the difference in the final SOC is around 20%). The higher BT depletion does not affect much in the BT lifetime (it is just reduced a 3.8%), as LTO is not very sensitive to high DODs. On the contrary, in the case of NMC the DOD is maintained (indeed, the SOC evolution profile is very similar), but the diesel use reduction comes from an increase of the BT size (from 540 kWh to 580 kWh). Finally, in the case of LFP the improvement in the BT lifetime is obtained thanks to a reduction of the performed highest DOD (from 25% in RB-SM to 15% in GA-SM). This is translated into an increase of the diesel use (around 1.7%), but it is compensated due to the reduction of the BT replacement cost (around 30%).

Looking to the results of RB-FL and GA-FL, it can be checked that they are not able to improve the results of the SM-based strategies. RB-FL obtains a lower LCC compared

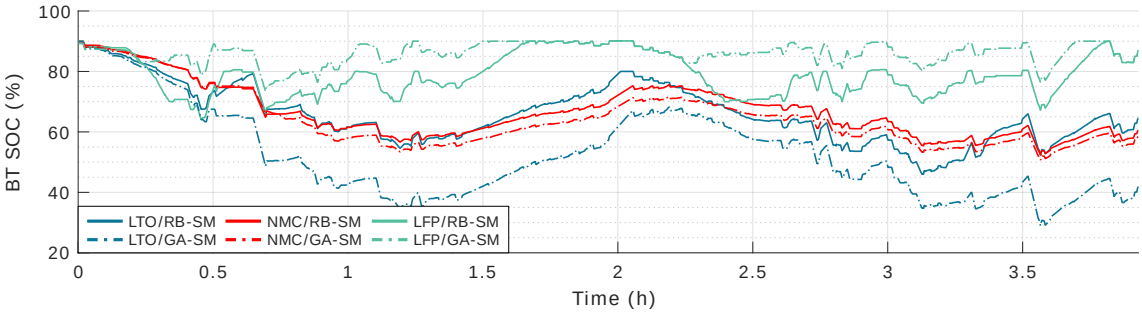

Figure 3.23: Simulation results of RB-SM and GA-SM strategies.

to RB-SM only in the case of LTO. However, when optimizing the parameters by the GA approach, GA-SM turns to be a better option than GA-FL in every chemistry. There is no case where the diesel use is lower in GA-FL compared to GA-SM, what inevitably penalises the final LCC value. Looking to the simulation graphs in Figure 3.24, it can be checked that the operation of these FL-based strategies is close to the charge depleting/charge maintaining approach: the SOC is reduced fast in the first 2500 seconds, and then it is nearly maintained until the end of the non-electrified section.

Regarding the LCC reductions obtained with the GA parametrization, a 0.1% improvement is obtained in LTO, a 0.4% improvement in NMC, and a 3.3% improvement in LFP. In LTO the difference is almost non-existent, what means that the parametrization of RB-FL was already appropriate. This issue can be also noticed in Figure 3.24, where the BT operation is found to be very similar in RB-FL and GA-FL. In the case of NMC, the improvement comes mainly thanks to a 4.5% reduction of the fuel use, which is caused due to the reduction of the genset size (from 1500 kW in RB-FL to 1000 kW in GA-FL). Consequently, the BT size is higher, what increases its replacement cost a 40%. However, this increase is compensated by the mentioned fuel use reduction. Finally, in the case of LFP the cost reduction comes due to the reduction of the BT replacement cost. Contrary to the NMC case, the optimization recommends to increase the genset size and reduce the BT size. This is translated into a 59% reduction of the BT replacement cost, which eventually compensates the 11.8% fuel use increase.

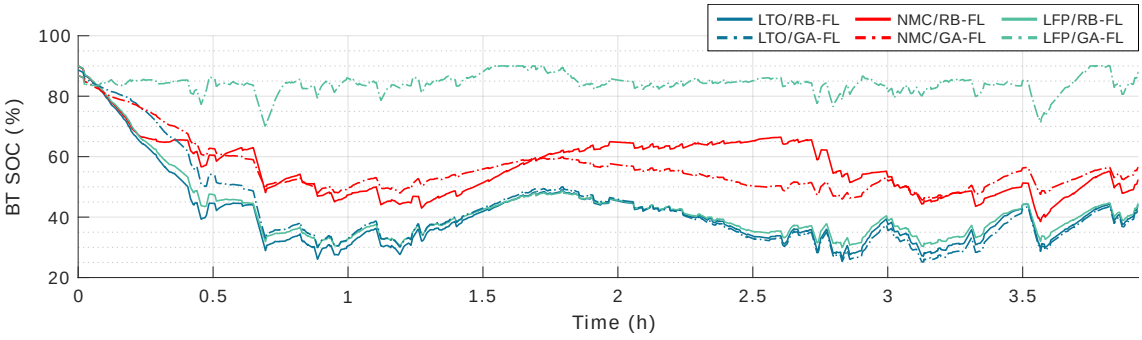

Figure 3.24: Simulation results of RB-FL and GA-FL strategies.

Regarding DP strategy, it is found to be the best option in both NMC and LTO cases, which are the chemistries with the best results. In the three chemistries DP is the strategy obtaining the lowest diesel use, what is a logical conclusion considering that minimizing the diesel use is the objective of DP optimization. Indeed, compared to the DEMU, the fuel use is reduced 17.4% in LTO, 23.6% in NMC, and 19.3% in LFP. As it can be seen in the simulation results of Figure 3.25, in DP the BT is depleted more than in the strategies previously analysed. This explains in part the obtained diesel consumption values. As it has been already highlighted, enhancing the DOD that the BT performs can negatively affect its lifetime. In the case of LTO, it barely affects the BT degradation: compared to the next best strategy (GA-SM), the BT lifetime is just reduced a 7.1%. In the case of NMC, the BT lifetime is affected more (31% reduction compared to GA-SM), but the fuel use reduction compensates this higher cost. Finally, in the case of LFP the BT replacement cost is increased overmuch (compared to GA-SM, this cost is almost 4 times higher), what inevitably increases the LCC. This makes DP be far from the best strategies in the case of LFP (4.5% higher than the best strategy, GA-SM). Therefore, it can be concluded that DP is the best option as long as a chemistry with a relatively long BT lifetime is integrated.

As DP is hardly implementable in the real vehicle, the ANFIS learning technique is proposed to replicate its results. Looking to the graphs of Figure 3.25, it can be observed that the BT operation profiles are similar in DP and ANFIS. However, the small variations (which are inevitable, as a 0% training error is not possible) are translated into higher LCC values compared to DP: in LTO a 1% higher, in NMC a 1.9% higher, and in LFP a 3.5% higher. In the cases of LTO and NMC, the higher LCC value comes due to the increased diesel use (2.9% and 6.7% higher, respectively), as the BT lifetimes barely vary compared to the DP case. Besides, in the case of LFP both the diesel use (5.0% higher) and BT replacement cost (16% higher) are increased. Compared to the rest of strategies, the result of ANFIS is only good in the case of LTO, where it is just behind DP and GA-SM. In the case of NMC, the replication of DP is worse, what makes ANFIS obtain higher LCC than DP, GA-SM, RB-SM, GA-FL, RB2 and RB-FL strategies. Finally, in the case of LFP, ANFIS obtains the worst result. This evidences that a better replication of DP results is necessary, as even a relatively small training error can be translated into an increased diesel use and BT degradation.

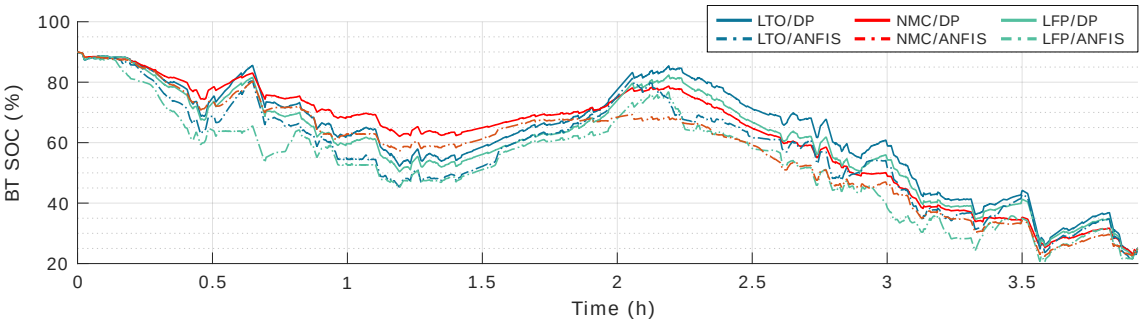

Figure 3.25: Simulation results of DP and ANFIS strategies.

In short, the comparison of the different control strategies with different BT chemistries has shown that DP is the best option in most of the cases, at least when long BT lifetimes are obtained (such as in LTO or NMC). The replication of DP with ANFIS has not shown good results, as it is not able to improve the performance of GA-SM strategy at any case. GA-SM has obtained the best result in LFP, and in LTO and NMC it is just a 0.7% behind DP, being the second best strategy. Therefore, it is also concluded that GA-SM is an appropriate strategy. The comparison of the different strategies will be further extended in Section 3.4.5 with the analysis of the robustness and real time execution.

3.4.3 Analysis of Optimization Variables

In this subsection an analysis of the optimization variables returned by the LCC optimization approach is developed. In order to help in this analysis, Figure 3.26 depicts the relation between the three optimization variables (n_{GS}, n_{BT} and SOC_0) and the final LCC of each case of the sensitivity analysis. The colours represent the different BT chemistries, as the constraints for n_{BT} vary depending on the chemistry. Some tendencies are highlighted by the dotted rectangles.

Regarding the genset size, Figure 3.26a shows that the solutions with a lower LCC propose a genset of 1000 kW. The main reason is that a higher genset leads to a higher diesel consumption, what penalises the final LCC. As gensets lower than 1000 kW do not comply the minimum traction requirements, this size turns to be the best option. It can be also observed that in the case of LFP chemistry most of the solutions propose a genset of 1500 kW. As it was previously analysed, the main disadvantage of this chemistry is its short lifetime compared to LTO and NMC. In order to reduce the costs derived from the BT replacements, the optimal solutions for LFP propose small BT systems, which require of bigger gensets in order to comply with the traction requirements.

Figure 3.26b shows that the solutions with a lower LCC tend to propose bigger BT sizes. Considering that in NMC and LTO the optimal genset size is 1000 kW, the maximum allowable BT sizes turn to be 600 kWh and 360 kWh, respectively. The solutions with a lower LCC are close to these values, as it is highlighted in the mentioned graph. Considering the importance of reducing the fuel use to obtain a low LCC, the option of a big BT is reasonable, as it can help more in traction and reduce the contribution of the genset (and consequently, the diesel use). In the case of LFP, the proposed sizes are also the biggest possible ones, both when the optimal genset size is 1500 kW and 1000 kW.

Eventually, Figure 3.26c shows that the optimal initial SOC values are close to 90%. Depending on the optimization approach, SOC_0 is a discrete or continuous variable. Anyway, even in the cases when it is a continuous variable, the optimal values are between 86-90%. Therefore, the optimal values coincide with the most conservative option, which consists of starting the non-electrified section with the BT totally charged.

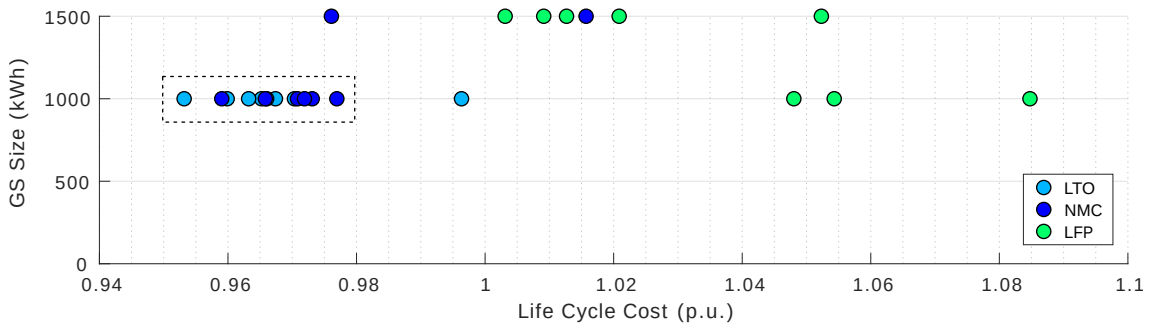

(a) Optimal GS size

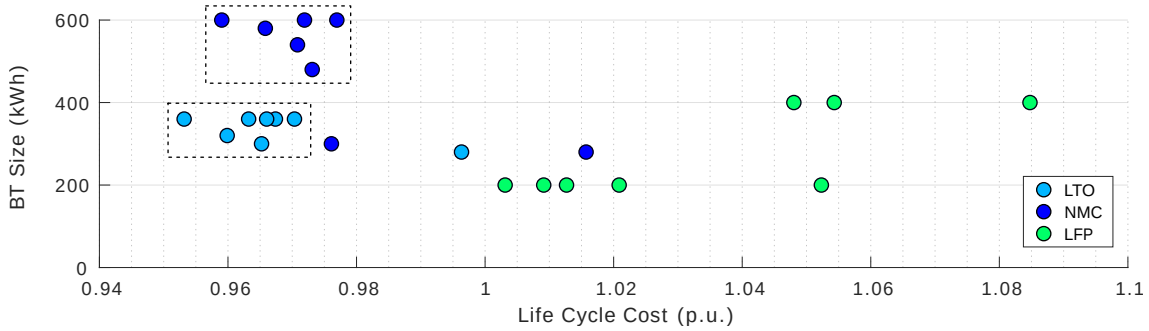

(b) Optimal BT size

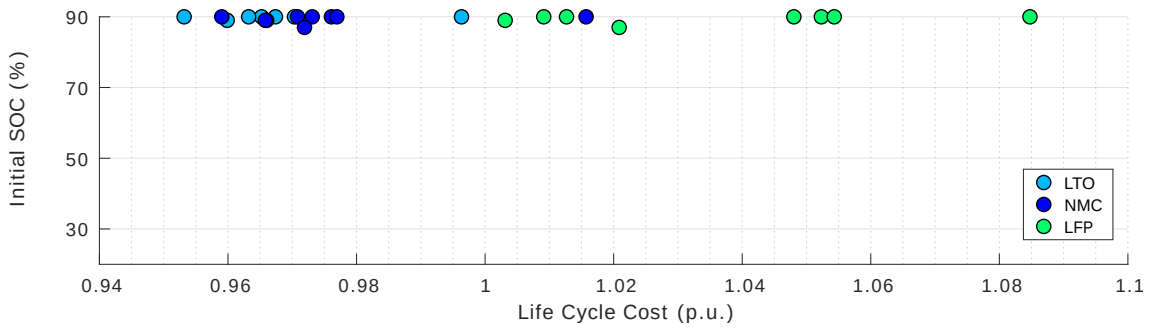

(c) Optimal initial SOC

Figure 3.26: Influence of optimization variables on LCC.

3.4.4 Influence of Key Cost Terms on Overall LCC

Once the optimization results and the LCC values of the different EMS and BT chemistries have been analysed, in this subsection a detailed analysis of the cost terms of the LCC model is developed. The aim of this approach is to identify the most influential terms of the cost model. That is to say, to identify which are the cost terms with a higher correlation with the LCC, as they are the ones that have to be minimized in order to reduce the overall LCC. Figure 3.27 depicts for each case of the sensitivity analysis the relation between the final LCC value and the previously mentioned cost terms (C_{GS}, C_{BT}, C_f and C_{BTrepl}). All figures respect the same scale in the y-axis, since in this way it is easier to identify which is the cost term with the highest correlation with the LCC. As in the previous figure, the different colours represent the analysed BT chemistries, and the

dotted lines highlight some of the identified trends.

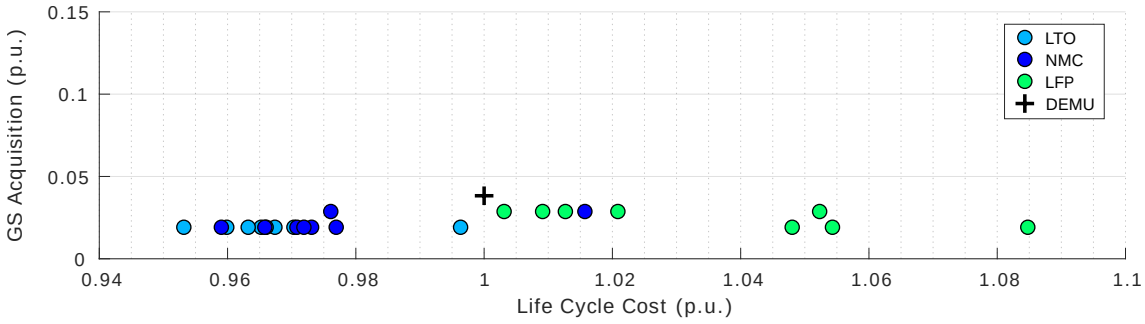

(a) Cost of GS acquisition, C_{GS}

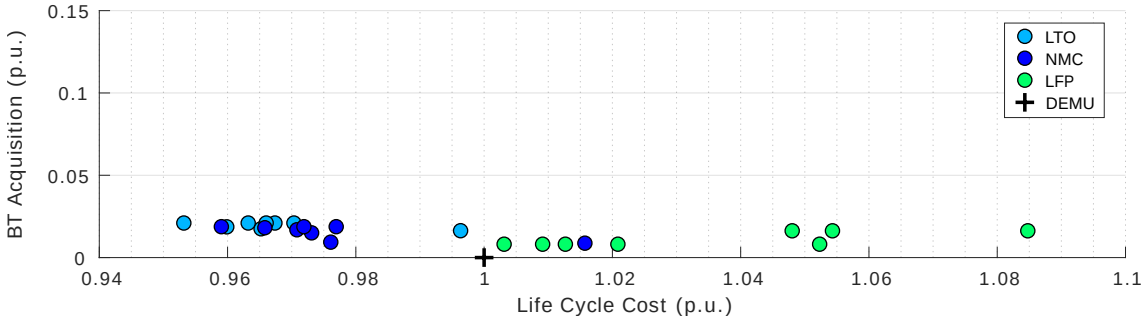

(b) Cost of BT acquisition, C_{BT}

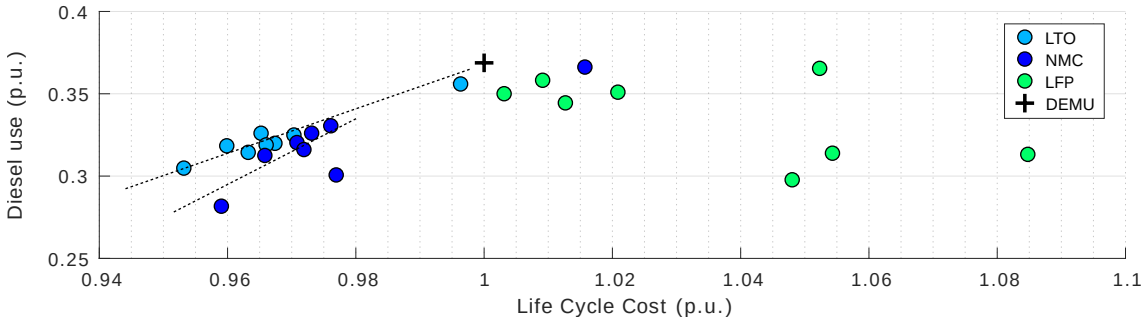

(c) Cost of diesel use, C_f

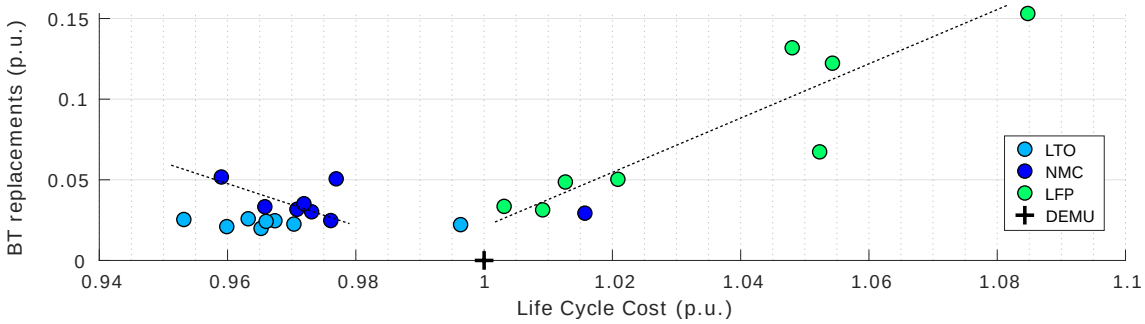

(d) Cost of BT replacements, C_{BTrepl}

Figure 3.27: Relation between LCC and LCC terms.

First of all, it can be observed that the genset and BT acquisition costs represent a small fraction of the LCC, and that they show small variability. Indeed, the C_{GS} and C_{BT} values depicted in Figures 3.27a and 3.27b do not represent more than the 3% of the referential DEMU cost. Moreover, there is not noteworthy relation between these variables and the LCC, what unveils that their influence is limited. In the case of Figure 3.27a the best options have a lower C_{GS} value. However, as it was discussed before, this is more related to the fact that a smaller genset leads to a smaller diesel consumption.

As it was already highlighted in the bar plots of Figure 3.21, the diesel cost represents the major proportion of the LCC variable terms (between 28-37% of the DEMU referential cost). As it is seen in Figure 3.27c, there are clear trends that relate a lower C_f with a lower LCC in both NMC and LTO results. Compared to the other terms, it can be stated that C_f is the most influential factor for the cases of NMC and LTO chemistries. This enforces the idea that an EMS has to be designed aiming a fuel use reduction.

Regarding the BT replacement costs, Figure 3.27d shows that it is the most influential factor in the case of LFP. This trend was already noticed in the analysis of Section 3.4.2. The main disadvantage of LFP is that the reduction of C_{BTrepl} is made at the expense of increasing the diesel use, what inevitably limits the obtention of a competitive LCC. In the case of LTO the cost of the BT replacements is always below 3% of the referential DEMU cost. Even if the raw cost of LTO technology (c_{BT}) is the highest one, the long lifetimes (always above 10 years) compensate this disadvantage. Regarding NMC chemistry, it is noticed that the solutions with a lower LCC tend to increase C_{BTrepl}. As it was previously highlighted, this can be related to the fact that it is necessary to deplete more the BT in order to reduce the diesel consumption. This leads to a higher DOD, what inevitably affects the lifetime of NMC.

In short, it can be concluded that in the cases when an strategy successes in limiting the BT degradation (as in the cases of NMC and LTO), the potential reduction of the diesel use becomes the most important parameter of the LCC model. In these cases, if an EMS is able to reduce the diesel use, it will success in obtaining a competitive LCC. The effect of C_{GS} and C_{BT} on the final LCC has been found to be low. However, this does not mean that the genset and BT sizes do not affect in the LCC, as they indirectly influence in the other costs (C_f and C_{BTrepl}).

3.4.5 Analysis of EMS Robustness and Real Time Execution

As it was previously mentioned, in this subsection the evaluation of the different EMSs is extended. In this case, the analysis is focused on the robustness and real time execution possibilities of the proposed strategies. Besides the LCC analysis, the current evaluation becomes also crucial to define which control strategy turns to be the most appropriate, as the mentioned features could limit the efficiency of an EMS when integrating in a real application.

3.4.5.1 EMS Robustness

In a first step, the analysis is focused on the robustness evaluation. Indeed, each of the cases of the sensitivity analysis has been optimized for a specific driving cycle. However, this driving cycle is prone to vary while in real operation, so the EMS must be able to give a feasible solution also under these circumstances, and not only under the scenario used for the design. In this context, it is considered that DP is not robust, as even the smallest variation in the driving cycle requires the deployment of a new optimization. Therefore, DP is kept out of the robustness analysis.

For the proposed analysis, the 24 optimal solutions obtained in the sensitivity analysis (see Table 3.8) have been simulated again under new driving cycles. The new driving cycles are variations of the nominal scenario (presented in Figure 3.15), as they aim at representing potential disturbances that may occur in real operation. In order to vary the nominal scenario, the number of passengers and the auxiliaries consumption are altered a ±7% and ±30%, respectively, what leads to 8 additional driving cycles. These driving cycles coincide with the scenarios used to train the ANFIS controller.

In a first row of simulations, it was identified that some cases turned to be unfeasible due to the fact that the BT charge dropped below the minimum allowable value (20%). However, it is important to point out that the BT is able to provide energy even below that value. Therefore, it is reasonable to use a higher SOC_{min} value for the design step (to be more conservative), but allow a lower value during real operation. Indeed, in a second row of simulations the SOC has been allowed to drop until 15%. The results introduced in this section refer to these second case. For a first evaluation of the obtained results, Figure 3.28 shows for each of the analysed control strategies how many of the deployed simulations returned an unfeasible solution. For each EMS, 27 simulations were deployed, which correspond to the combination of 9 driving cycles and 3 chemistries.

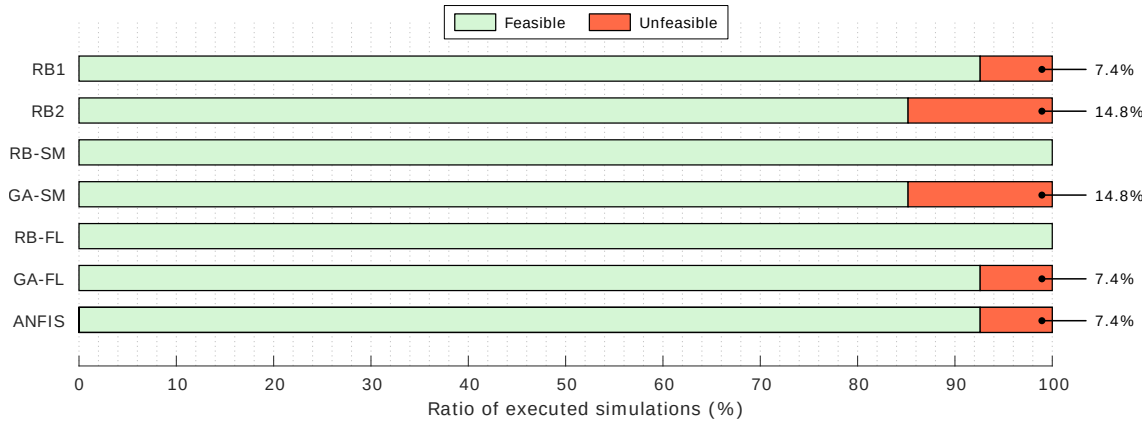

Figure 3.28: Analysis of EMS feasibility in different scenarios.

The results show that only RB-SM and RB-FL are able to provide a feasible solution in all the proposed scenarios. However, in both cases the strategy turns to be less robust

when optimizing by the GA. This demonstrates that the rules are pushed to the limits of the feasibility in order to optimize the EMS. An example of this can be appreciated in GA-SM, as k_{SM1} tends to be reduced compared to the RB case (see Table 3.9). A low k_{SM1} may be valid for the nominal scenario, but in more demanding driving cycles the BT might be overdischarged. A similar conclusion is obtained in GA-FL with the parameter k_{FL1}. In both cases it would be necessary to adapt in real time the values of the internal parameters in order to improve the feasibility of the strategy.

In the case of RB1 and RB2, they are not able to provide a feasible solution in all the scenarios. The rules specified in these strategies were not designed aiming to be adaptive to the scenario (e.g., adaptive to the SOC), hence the low robustness is reasonable. Finally, the results show that ANFIS also obtains some unfeasible solutions. In this case, the main cause is the error obtained when trying to replicate the DP result. As seen in Figure 3.25, there is a route section where the SOC nearly drops to the 20%. Therefore, when trying to replicate the DP result, even a small error in the SOC tracking makes the BT energy drop bellow the allowable value.

In addition, it is also interesting to analyse how is the LCC altered under the new driving cycles. Indeed, if the strategy provides a feasible solution but increases overmuch the LCC, it can be considered that it is not very robust. Figure 3.29 depicts for each case of the sensitivity analysis (excluding DP) the distribution of the LCC values under the proposed driving cycles. In order to make a reasonable comparison, the LCC under each new scenario is normalized in relation to the best case of the sensitivity analysis (DP with LTO) under that same scenario. In addition, the 'x' marks represent the LCC values of the nominal case. In short, the figure allows evaluating if the majority of the cases stay close to the results obtained in the original optimization, and how close do they stay.

The figure shows that the strategies with the lowest variability are RB-FL, GA-FL and ANFIS, specially in the case of LTO. In the case of NMC and LFP, there is sometimes a slightly higher LCC variability, due to the fact that the number of BT replacements differs in relation to the original scenario. This demonstrates that these strategies are able to provide an appropriate genset operation also under different driving scenarios, what does not lead to an increased diesel use.

Besides, RB-SM and GA-SM show a higher variability than previous cases, what demonstrates again that they are less robust than the FL-based strategies. Moreover, in the majority of cases the results are worsened compared to the original case. This means that RB-SM and GA-SM tend to increase the diesel use and/or the BT degradation under the new scenarios.

Finally, RB1 and RB2 are the strategies showing the highest LCC variability. This demonstrates again the importance of designing control strategies that try to recover the BT SOC, as it is done in the cases of RB-SM, GA-SM, RB-FL, GA-FL and ANFIS (in this last EMS, indirectly while trying to follow the DP operation).

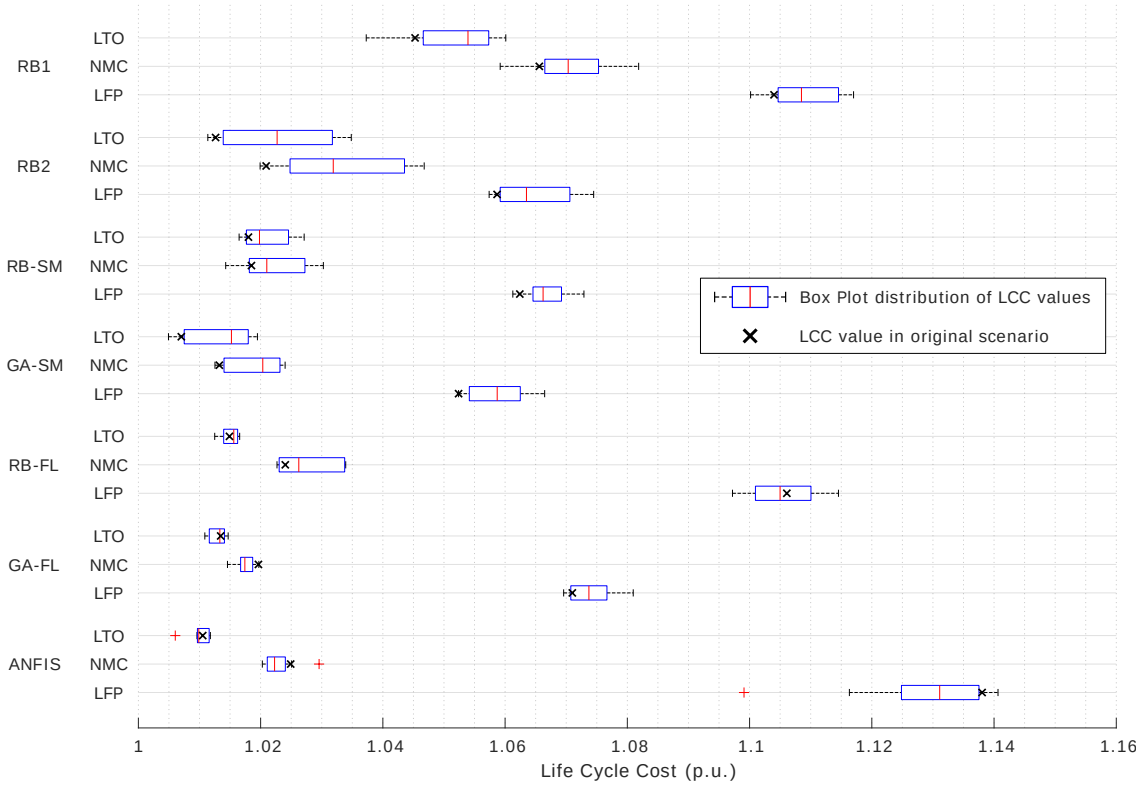

Figure 3.29: Box plot representing the LCC variability under different scenarios.

3.4.5.2 EMS Real Time Execution

As a second step of this subsection, the time required for the execution of the simulations has been analysed. The objective of this analysis is to evaluate the real time performance of the different EMSs. Logically, the simulation execution time can not be considered as an exact approximation to the real time performance, but it helps understand which strategies will require higher or lower execution times and computational burden. Therefore, their feasibility can be estimated. Anyway, it has to be considered that the analysis of this section is a bare approximation.

Specifically, the time required for the simulations of the EMS robustness analysis have been considered (27 simulations per each strategy). Figure 3.30 shows a box plot of the obtained execution times. The values are represented in p.u. in relation to the time required to execute the DEMU simulation, which does not have EMS.

The results show that RB1, RB2 and both SM-based strategies require simulation times near to the DEMU. Therefore, it can be concluded that their real time execution will not derive additional problems. RB-FL and GA-FL require nearly 20% more execution time compared to the previous strategies, as they are based on much more rules and calculations. Anyway, it can be considered that their execution times are reasonable. In the case of ANFIS, it is also based on FL, but as the number of membership functions and rules is

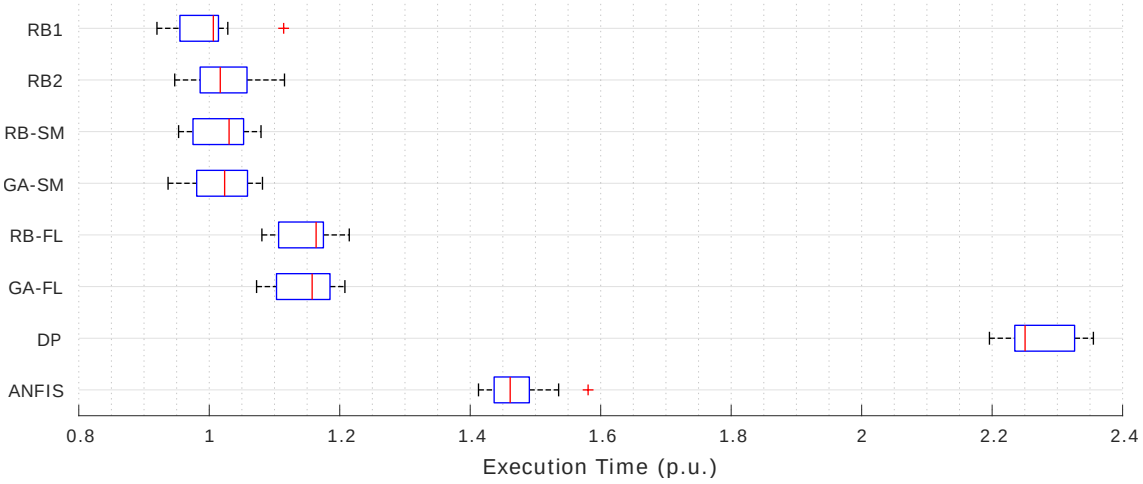

Figure 3.30: Box Plot representing the execution time of each EMS.

much higher, the required simulation time is between 40-50% higher than in the simple RB strategies. Finally, DP is the strategy that requires the highest simulation time (more than two times compared to the DEMU), due to the long time required for solving the optimization.

Therefore, from this analysis it can be concluded that DP and ANFIS are not optimal options from the computational point of view due their high execution time requirements.

3.4.6 Review of Sensitivity Analysis to Powertrain Design

In this subsection the main conclusions obtained in the sensitivity analysis to the powertrain design are reviewed. This analysis has been focused on evaluating the proposed EMSs and BT chemistries. In a first step, the LCC values obtained by each solution have been compared, and the reasons behind the results of each EMS and BT chemistry have been investigated and discussed in detail. In the case of the control strategies, their analysis has been extended by addressing their robustness and execution time. Then, the analysis has been focused on the obtained optimal values for the optimization variables and their relation with better LCC values. Additionally, the influence of the key cost terms (C_{GS}, C_{BT}, C_f and C_{BTrepl}) on the obtained LCC has also been analysed.

Regarding the analysis of BT chemistries, Table 3.10 reviews the capabilities of LTO, NMC and LFP in order to: (1) reduce the LCC, (2) minimize the diesel use, and (3) reduce the cost related to the BT replacements. More filled bullets refer to a better capability.

The main conclusions are reviewed as follows:

- LTO is the chemistry that obtains the best results, even if the LCC difference with NMC is most of the times below the 1%.
- LTO is not able to improve NMC in terms of diesel use, but this is compensated

Table 3.10: Main capabilities of analysed BT chemistries.

	LCC	Diesel use	BT lifetime
LTO	●●●●●	●●●●◐	●●●●●
NMC	●●●●◐	●●●●●	●●●●○
LFP	●○○○○	●●●○○	●○○○○

thanks to the lower BT replacement costs of LTO.

- The results of LFP are the worst ones, as its LCC turns to be always around 4-5% higher than NMC and LTO. The main disadvantage of this chemistry is its higher degradation compared to the other chemistries.

Besides, Table 3.11 resumes the main characteristics of the proposed and analysed strategies. The table follows the same format as Table 3.10, and the characteristics related to the robustness and execution time have also been included. To estimate the capability to reduce the LCC, only the results of NMC and LTO have been considered, as they are more representative of the potential that each strategy has to improve that value.

Table 3.11: Main capabilities of analysed EMSs.

	LCC	Diesel use	BT lifetime	Robustness	Execution time
RB1	●○○○○	●○○○○	●●●●○	●●●◐○	●●●●●
RB2	●●●●○	●●●○○	●●●●○	●●○○○	●●●●●
RB-SM	●●●●○	●●●○○	●●●●○	●●●●◐	●●●●●
GA-SM	●●●●◐	●●●◐○	●●●●◐	●●●○○	●●●●●
RB-FL	●●●◐○	●●●○○	●●●●○	●●●●◐	●●●●◐
GA-FL	●●●●○	●●●○○	●●●●◐	●●●●○	●●●●◐
DP	●●●●●	●●●●●	●●○○○	○○○○○	●○○○○
ANFIS	●●●●○	●●●●○	●●○○○	●●●●○	●●●○○

The main conclusions are reviewed as follows:

- The best strategy in terms of LCC is DP. However, the long execution time and null robustness prevent its integration in a real application.

- The replication of DP by means of the ANFIS approach obtains satisfactory results in terms of LCC and diesel use, and makes it possible to integrate it in a real application (even if the robustness and computational requirements should be improved).

- Overall, the SM-based strategies obtain a better result compared to the FL-based strategies in terms of LCC and diesel use. The optimization by means of the GA turned to be effective to improve the LCC. The case of GA-SM can be highlighted, as it is the strategy closest to DP in terms of LCC. However, special attention must be given to the possibility of obtaining a non-robust controller in the cases optimized by the GA approach.

- RB2 obtains a good result in terms of LCC, however its main problem consists on the robustness. This strategy is not designed to be adapted to possible disruptions in the SOC, so it easily leads to non-feasible solutions when the route demand increases.
- A similar conclusion is derived when analysing the results RB1, and in this case even worst LCC and diesel use results are obtained.

After concluding with the analysis of the BT chemistries and EMSs, some other conclusions can be highlighted regarding the analysis of the optimization results:

- The solutions with a lower LCC propose a genset of 1000 kW, which coincides with the lowest feasible size. The main reason is that a smaller genset allows to integrate a bigger BT, and therefore the potential diesel reduction is higher.
- Regarding the BT size, the solutions with a lower LCC propose to integrate the maximum allowable energy with the genset of 1000 kW (600 kWh in the case of NMC and 360 kWh in the case of LTO). The reason is again linked to the capability of reducing the diesel use, as long as the BT lifetime is maintained.
- The optimal initial SOC coincides with the most conservative option: starting a new trip with the BT totally charged.

Finally, the analysis of the influence of C_{GS}, C_{BT}, C_f and C_{BTrepl} terms in the overall LCC has unveiled some additional conclusions:

- When an strategy successes in limiting the BT degradation (as in the cases of NMC and LTO), the potential reduction of C_f becomes the most important parameter of the LCC model. In these cases, if an EMS is able to reduce the diesel use, it will success in obtaining a competitive LCC.
- In the case of LFP, the reduction of C_{BTrepl} becomes the most important parameter of the LCC model. This unveils that in the case of a chemistry with a fast degradation, trying to improve its lifetime becomes essential.
- There is not a noteworthy relation between C_{GS} and C_{BT} costs and the overall LCC, as their effect is relatively low.

3.5 Results of Sensitivity Analysis to Economic Model

This section presents and evaluates the results of the sensitivity analysis to some of the parameters of the economic model. As it was specified in the methodology presented in Chapter 2, this second sensitivity analysis is focused on evaluating how do the results and conclusions of the H-DEMU powertrain design (Section 3.4) differ when varying some parameters of the economic model. Figure 3.31 shows where it is located this sensitivity analysis in the methodology proposed in this Ph.D. Thesis. As defined in Section

3.2.3, the variability of the operation hours (t_{day}), BT price (c_{BT}, independently for the 3 chemistries) and diesel price (c_f) will be analysed in this case study. The results are obtained for the nominal drive cycle also used in the previous sensitivity analysis.

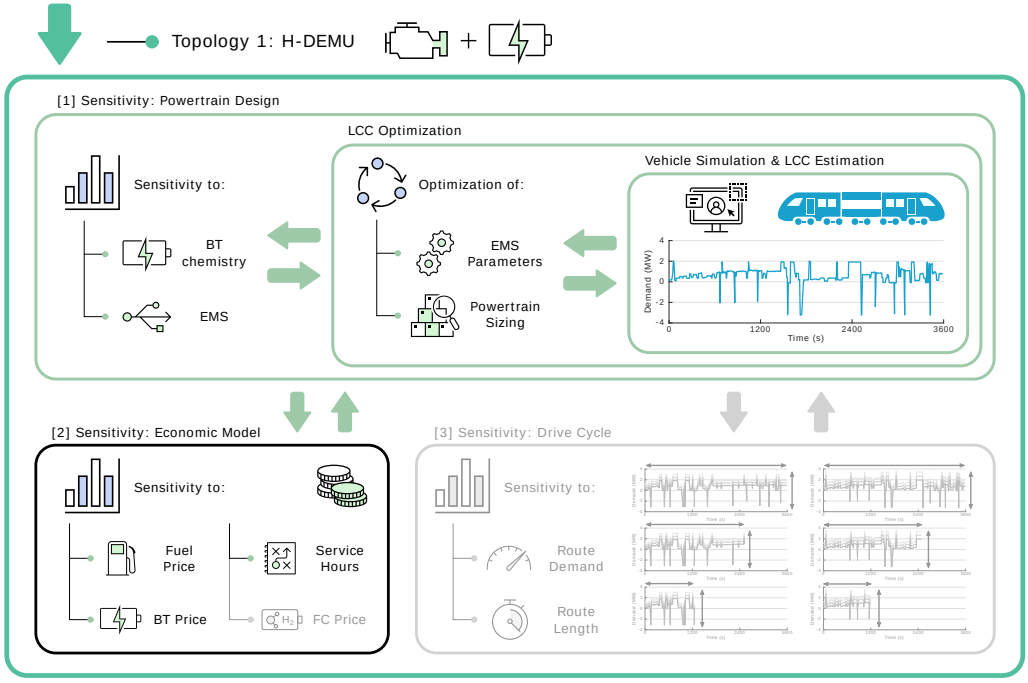

Figure 3.31: Current step of holistic design methodology.

In order to simplify the analysis of the results, the number of considered EMSs has been reduced. Firstly, the effectiveness of the GA-based strategies to improve the performance of RB strategies has been already demonstrated. Therefore, RB-SM and RB-FL strategies are kept out of the analysis of this section. Secondly, the effectiveness of ANFIS operation has also been evaluated. However, as deploying this strategy in many scenarios requires a long training step, it is kept out of the analysis of this section. It is understood that the results of DP are enough to estimate the potential performance of ANFIS in the proposed new contexts.

The analysis of the economic parameters is divided into different subsections, according to the parameter whose sensitivity is analysed: operation hours, diesel price and BT price.

3.5.1 Sensitivity to Operation Hours

In a first step, the sensitivity analysis is focused on the operation hours that the rail vehicle is driving each day (t_{day}). As previously specified, in the High Scenario (HS) the vehicle operates 14 h/day, in the Medium Scenario (MS) 10.5 h/day, and in the Low Scenario (LS) 7 h/day. The analysis of the obtined results will be divided into three independent sections, as it was done in the case of the sensitivity analysis to the powertrain design. First, the LCC values obtained at the different cases are analysed. Then, the

analysis focuses on the variables returned by the different optimization approaches. And finally, the analysis focuses on the how do the cost terms of the economic model vary.

3.5.1.1 Analysis of LCC Values

The LCC values obtained at each scenario are depicted in Figure 3.32. Logically, a change in t_{day} means that the LCC varies considerably from one scenario to another. As the main objective of the current analysis is not to compare the LCC in absolute terms, the values of each scenario are normalized in relation to the result of DP strategy with LTO chemistry (which in the nominal scenario of Section 3.4 turned to be the best option). Then, the results are grouped by each chemistry, as it is easier to see the effect of varying t_{day}. As the legend shows, each marker refers to a different EMS. The results will be analysed from two points of view: focusing on the comparison of the EMSs, and focusing on the comparison of the BT chemistries.

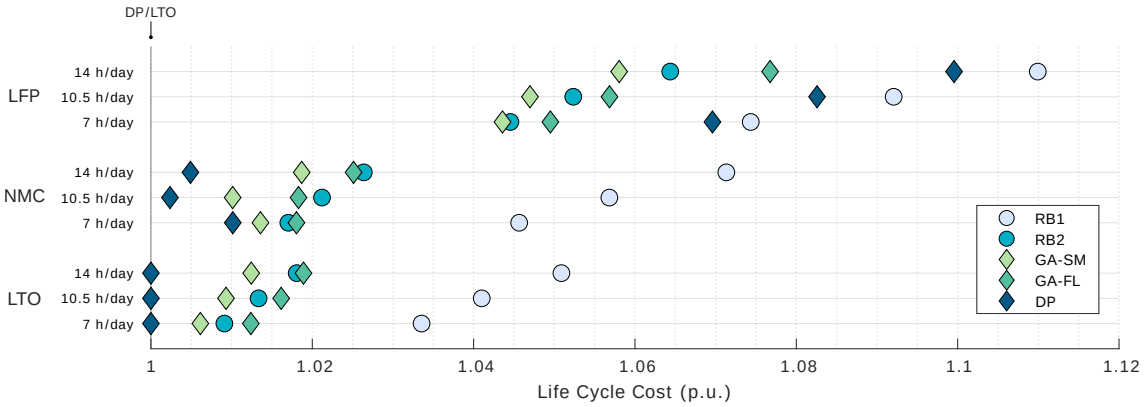

Figure 3.32: Sensitivity of LCC values when varying t_{day}.

Regarding the results obtained by the different EMSs, it can be checked that in general the relative differences between them are reduced as the operation hours are reduced. For instance, in HS/LTO the difference between DP and RB1 is 5.1%, while in LS/LTO the difference is reduced up to the 3.8%. Anyway, in general this reduction is similar in all the strategies. That is to say, with a few exceptions, the order of the EMSs is barely changed from scenario to scenario: DP continues being the best option with LTO and NMC, and GA-SM is the best option with LFP (and the second best option with LTO and NMC).

Regarding the results of the different BT chemistries, similar conclusions can be obtained. The relative difference between the results of the chemistries is reduced when reducing t_{day}. However, this reduction does not affect in the general conclusions obtained in the previous section. The difference between LTO and NMC continues being low, but with LTO always ahead. In the case of LFP, it continues being far from the results of the other two chemistries: even in LS, the difference of the best LFP strategy (GA-SM) and the best LTO strategy (DP) is higher than the 4%.

3.5.1.2 Analysis of Optimization Variables

Besides the LCC values, more variations can be observed when analysing the optimization variables obtained in the different scenarios. Figure 3.33 depicts the relation between the optimization variables and the LCC for each scenario. The upper graphs represent the results of HS, the middle graphs represent the results of MS, and the lower graphs represent the results of LS. The left-side graphs show the relation of the optimal genset sizes, while the right-side graphs present the results of the optimal BT sizes. The LCC values of each graph are normalized in relation to the best option of each scenario, as the objective of these figures is not to analyse how do the exact LCC values vary from one scenario to another. The SOC_0 values returned by the optimization are not depicted, as in all the scenarios the same conclusion obtained in Section 3.4 is maintained (SOC_0 values around 90% are the optimal option).

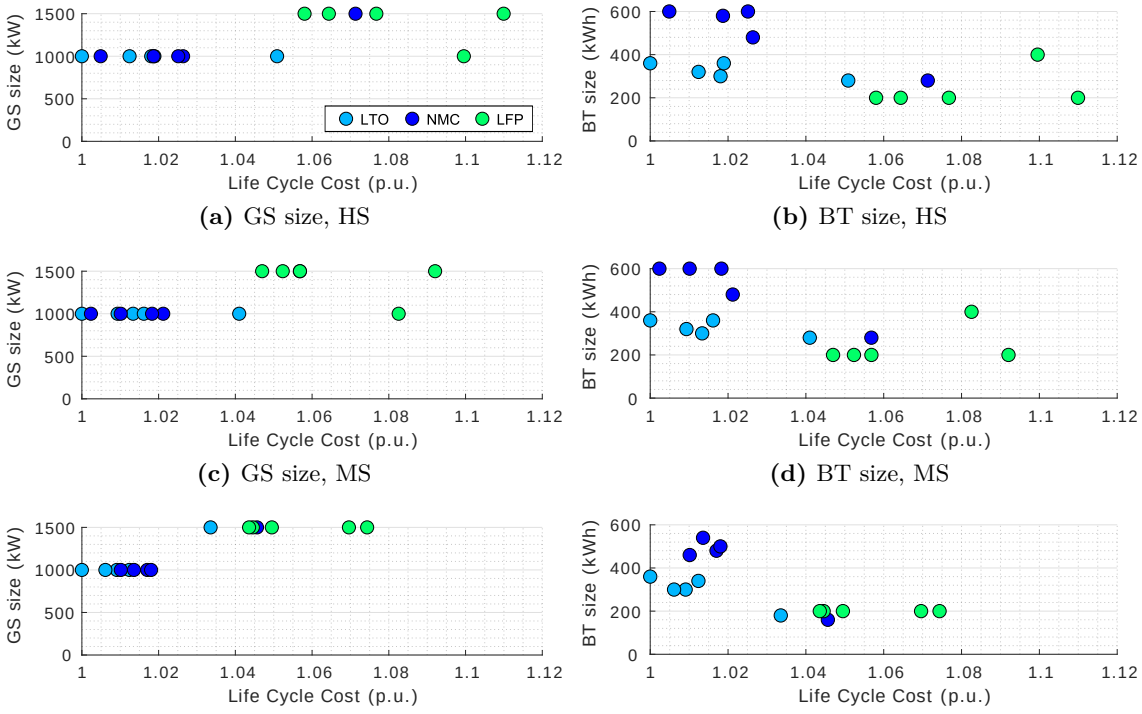

(a) GS size, HS **(b)** BT size, HS

(c) GS size, MS **(d)** BT size, MS

(e) GS size, LS **(f)** BT size, LS

Figure 3.33: Sensitivity of optimal sizing values to t_{day}.

A first general observation shows that the biggest variation in the optimal sizing values is made when changing from MS to LS, rather than from HS to MS. Anyway, some general tendencies can be derived from these results. Regarding the optimal genset, it can be seen that when reducing t_{day}, the cases with a better LCC continue proposing the genset size of 1000 kW. In the LS there are more options that propose the genset of 1500 kW, however these are always the options with a higher LCC.

Besides, the tendency on the BT sizes shows that when reducing the operation hours,

the solutions with a better LCC start proposing optimal BT sizes with lower values. In the nominal scenario (HS), the best results (those of LTO and NMC) proposed BT sizes near the maximum allowable values (360 kWh and 600 kWh, respectively, considering that the optimal genset size was 1000 kW). However, it can be observed than when reducing the daily operation hours to 7 h (LS), the optimal BT sizes start being closer to 300 kWh in the case of LTO and to 500 kWh in the case of NMC. On the contrary, the results of LFP stay on their own when reducing the daily operation hours (200 kWh).

3.5.1.3 Influence of Key Cost Terms on Overall LCC

Finally, the analysis of this subsection focuses on how does the influence of the key cost terms (C_{GS}, C_{BT}, C_f and C_{BTrepl}) change when varying the daily operation hours. This analysis also helps understanding the LCC and optimal sizing values obtained in the analysis of this subsection. Figure 3.34 shows the relation between the LCC and the mentioned cost terms, following a similar format as Figure 3.27: each colour refers to a BT chemistry, and all graphs use the same scale in the y-axis to better identify the correlations between the cost terms and the overall LCC. The different subplots have been arranged so it is easier to compare the results in HS, MS and LS individually for each cost term: subplots a, c and e show the three scenarios to evaluate the genset acquisition cost (C_{GS}), subplots b, d and f the three scenarios to evaluate the BT acquisition cost (C_{BT}), subplots g, i and k the three scenarios to evaluate the diesel use cost (C_f), and finally subplots h, j and l the three scenarios to evaluate the BT replacement cost (C_{BTrepl}). At each graph, both variables are normalized in relation to the LCC value of the best case.

In the following lines, each of the variable cost terms are analysed in detail. First of all, it can be stated that when reducing t_{day}, the relative contribution of the acquisition costs (both C_{GS} and C_{BT}) increases a little. This is a logical conclusion, since when reducing t_{day} the operation costs decrease, while the acquisition costs are kept constant. However, this contribution continues being low compared to the rest of terms, as they do not represent more than the 5% of the referential LCC in any case. Besides, there is not noteworthy relation between C_{GS}, C_{BT} and the LCC.

Regarding the diesel use cost (C_f), its relative contribution inevitably decreases when reducing the daily operation hours, as less diesel is consumed during the useful life of the vehicle: from accounting around 30-40% of the referential LCC in HS to around 20-25% in LS. Anyway, it can be stated that reducing the diesel use continues being the key to obtain a good LCC: as more is C_f reduced, a lower LCC is obtained, even in LS.

Regarding the variation of the BT replacement costs (C_{BTrepl}), it can be checked that their relative contribution is also reduced. With a lower t_{day}, longer BT lifetimes can be achieved, what inevitably reduces the importance of C_{BTrepl}. Anyway, this decrease is lower than in the case of C_f, as the BT life does not increase proportionally to the reduction of t_{day}. Besides, it can be checked that even in the LS, in order to obtain a good

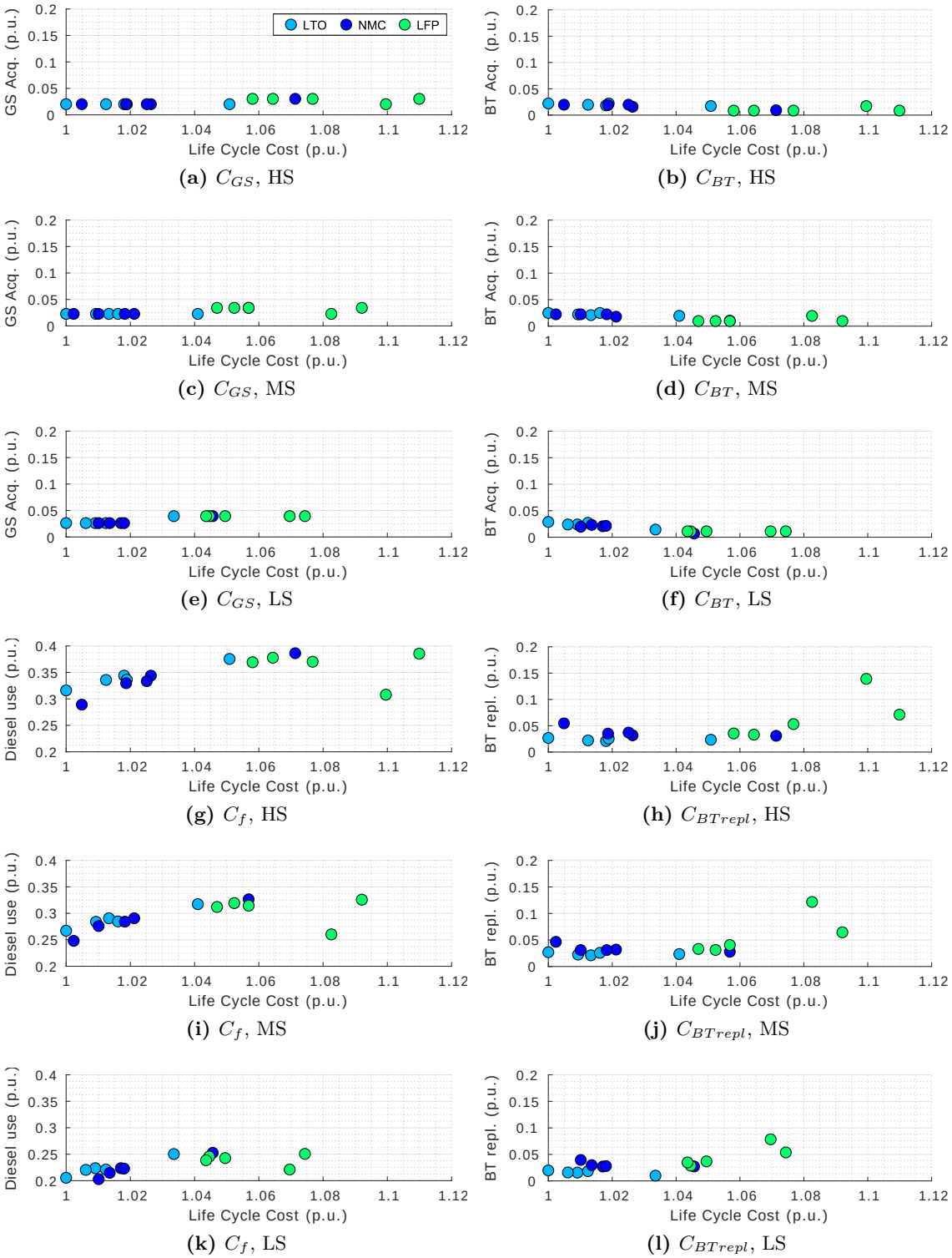

(a) C_{GS}, HS **(b)** C_{BT}, HS

(c) C_{GS}, MS **(d)** C_{BT}, MS

(e) C_{GS}, LS **(f)** C_{BT}, LS

(g) C_f, HS **(h)** C_{BTrepl}, HS

(i) C_f, MS **(j)** C_{BTrepl}, MS

(k) C_f, LS **(l)** C_{BTrepl}, LS

Figure 3.34: Sensitivity of the key cost terms to t_{day}.

LCC it is important to reduce the BT degradation.

The reduction in the importance of the diesel use is the cause behind the lower BT sizes proposed when reducing t_{day}. Indeed, in the nominal scenario (HS) the reason behind integrating big BT systems was that they could reduce more the diesel use, what compensates the higher BT acquisition and replacement costs of these systems. However, when the importance of C_f is reduced (in this case, a little more than the importance of C_{BTrepl}), the benefits of integrating big BT systems disappear, as the higher C_{BT} and C_{BTrepl} costs are not compensated. In addition, the reduction of the importance of both C_f and C_{BTrepl} is the cause of the LCC results previously analysed in Figure 3.32. As the importance of both cost terms is reduced similarly (even if in the case of C_f is more notorious), there is not EMS or BT chemistry that improves its performance compared to the rest of cases (similar results were obtained in the three cost scenarios).

In short, it can be concluded that when reducing t_{day}, it continues being crucial to reduce C_f, but always keeping a reasonable C_{BTrepl} value.

3.5.2 Sensitivity to Diesel Price

In this subsection, the sensitivity of the powertrain design to the diesel price (c_f) is analysed. As previously specified, in HS this price is kept at 1.55 €/L, in MS at 1.10 €/L, and in LS at 0.65 €/L. As with previous results, the analysis is divided into different steps. First, the LCC values of the different cases are analysed. Then, the analysis focuses on the optimization results, and finally, on the influence of the cost terms.

3.5.2.1 Analysis of LCC Values

First of all, Figure 3.35 depicts the LCC obtained by each EMS and BT chemistry at the three cost scenarios. The figure follows the same format as Figure 3.32: the LCC values are normalized in relation to DP/LTO, the results are grouped by each BT chemistry, and each marker refers to an EMS. The results are analysed from two points of view: focusing on the comparison of control strategies and focusing on the comparison of BT chemistries.

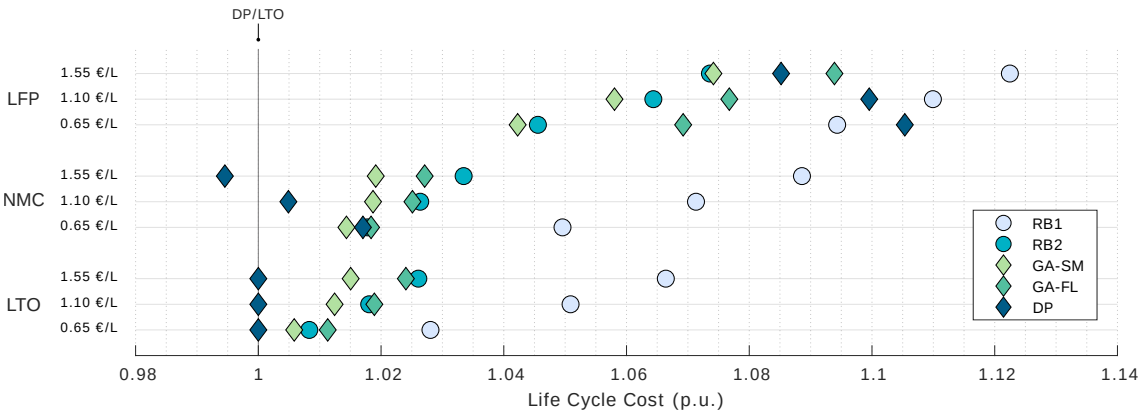

Figure 3.35: Sensitivity of LCC values when varying c_f.

Regarding the results of the different EMSs, it can be checked that as lower c_f is, the relative differences between the strategies are reduced. That is to say, all the strategies get closer in terms of LCC when reducing c_f. For instance, in the case of LTO, the difference between the best and worst strategies is 6.6% in HS, but 2.8% in LS. Similar conclusions are obtained focusing on the results of NMC and LFP.

Besides, it can be also checked that when c_f is reduced, DP worsens its results compared to the remainder EMSs. This is specially notorious in the case of LFP and NMC: when reducing c_f, DP is the only strategy that increases the relative LCC, that is to say, it is the only strategy that goes to the right in the graph. In the case of LTO, this is more difficult to identify because the result of DP is used as baseline to calculate the relative LCC. However, it can be seen that the rest of the strategies get much closer to DP when c_f is reduced.

Finally, it can be also noticed that RB2 tends to improve its result with low c_f values, specially in LTO and NMC. Indeed, with these chemistries, RB2 outperforms GA-FL in the lower price scenarios. The remainder strategies obtain similar performances in all the proposed scenarios.

Regarding the BT chemistries, it is checked that with a higher c_f, NMC is able to get closer to the results of LTO. In HS, NMC improves LTO in the case of DP (0.6% lower LCC), and in the remainder strategies it stays close to the results of LTO (closer than in MS). Anyway, a further c_f increase than the one proposed in HS is necessary for NMC to become clearly the best option. On the contrary, in LS the difference between LTO and NMC is clearly beneficial for LTO. Finally, regarding LFP chemistry, there is no notorious difference compared to the nominal scenario. As the main disadvantage of this chemistry is its high degradation, it is barely affected by the variation of c_f.

3.5.2.2 Analysis of Optimization Results

As it was checked in the previous subsection, the results of the optimization variables can also vary when increasing or decreasing c_f. Figure 3.36 depicts the relation between the optimal genset and BT sizes and the LCC values of each case. The figure follows the same arrangement of graphs defined for Figure 3.33, and the LCC is normalized in relation to the best option of each scenario. The optimal SOC_0 values are not depicted as there are not changes in relation to the nominal scenario already analysed in Section 3.4.

On the one hand, the results of the optimal genset size (left-side graphs) show that when increasing c_f, most of the options propose a genset of 1000 kW (even when integrating LFP). Besides, when reducing c_f, there are more options that propose the genset of 1500 kW. Anyway, even in LS, the cases with the best LCC values continue proposing the genset of 1000 kW. As it will be analysed afterwards, the reason is that in the cases with a low c_f, the importance of obtaining low C_{BTrepl} values increases, what can be obtained integrating lower BT sizes (and consequently, higher genset sizes).

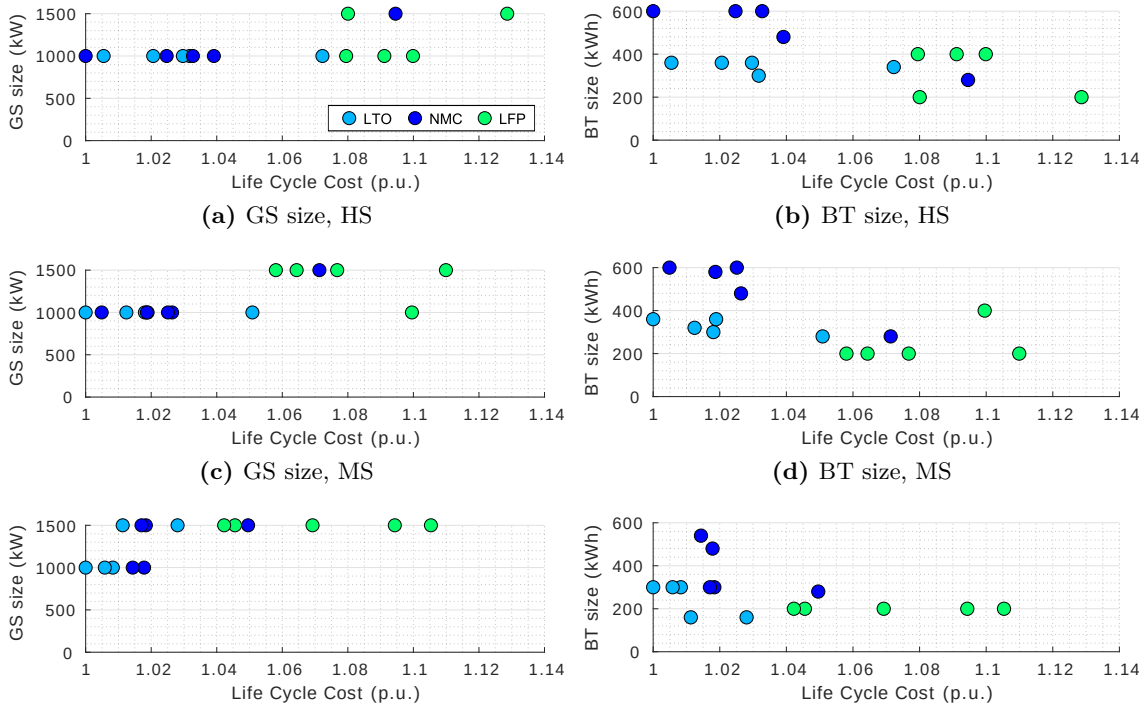

(a) GS size, HS **(b)** BT size, HS

(c) GS size, MS **(d)** BT size, MS

(e) GS size, LS **(f)** BT size, LS

Figure 3.36: Sensitivity of optimal sizing values to c_f.

On the other hand, when analysing the results of the optimal BT sizes (right-side graphs), it can be derived that as higher c_f is, higher sizes are proposed. In HS, most of the NMC cases propose a BT size of 600 kWh, most of the LTO cases a BT size of 360 kWh, and most of the LFP cases a BT size of 400 kWh (all are the maximum allowable sizes with the genset of 1000 kW). However, when reducing c_f, the optimal BT sizes are lower. In the case of LFP they are maintained around the maximum allowable values, but in the case of NMC and LTO they are hardly around these values. As previously stated, this is due to the increase of C_{BTrepl} importance when reducing c_f: in order to reduce the costs related to the replacement of BT systems, the optimizations decide to reduce the BT sizes. This is analysed in detail in the following subsection.

3.5.2.3 Influence of Key Cost Terms on Overall LCC

In a last step to analyse the sensitivity to c_f, Figure 3.37 depicts the relations between the obtained LCC values and the key cost terms of the economic model (C_{GS}, C_{BT}, C_f and C_{BTrepl}) in the different cost scenarios. These graphs help evaluating how do the influence of these terms change when varying the diesel price. The figure and suplots follow the same arrangement as Figure 3.34. As in that figure, all the graphs share the same scale in the y-axis, as in this way it is easier to identify correlations. At each graph, both variables are normalized (p.u.) in relation to the case with the lowest LCC.

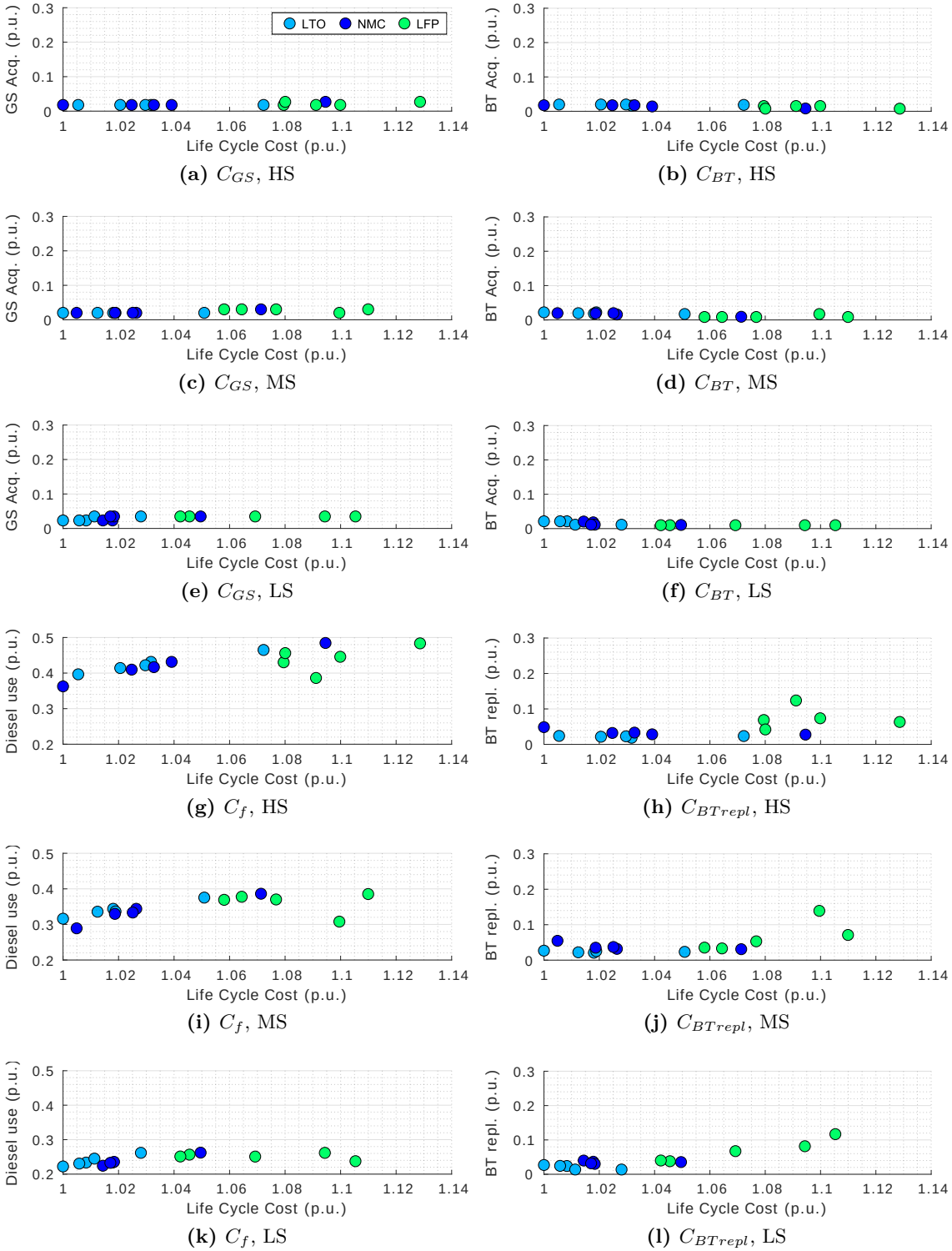

(a) C_{GS}, HS **(b)** C_{BT}, HS

(c) C_{GS}, MS **(d)** C_{BT}, MS

(e) C_{GS}, LS **(f)** C_{BT}, LS

(g) C_f, HS **(h)** C_{BTrepl}, HS

(i) C_f, MS **(j)** C_{BTrepl}, MS

(k) C_f, LS **(l)** C_{BTrepl}, LS

Figure 3.37: Sensitivity of key cost terms to c_f.

Regarding the influence of the acquisition costs, it can be checked that neither C_{BT} or C_{GS} start to be more influential when varying the diesel price. Besides, in any of the cases

the contribution of these terms is higher than the 5% of the referential LCC. In the case of C_{GS}, a small increase is denoted in LS, but it is more related to the fact that higher gensets are proposed in that scenario.

Logically, C_f is the term that it is most affected by the change in the diesel price. In HS it accounts to the 35-50% of the referential LCC, but in LS these values are reduced to the 20-30%. This reduction has two effects. On the one hand, the influence of C_f is reduced a little, but does not disappear, as seen in Figure 3.37k. Indeed, there is still a relation between a lower C_f and a lower LCC. On the other hand, the influence of C_{BTrepl} is increased. The contribution of C_{BTrepl} to the final LCC barely changes when reducing c_f. However, as the contribution of C_f is reduced, the proportion of C_{BTrepl} in relation to C_f is increased. Consequently, the influence of C_{BTrepl} increases when reducing the diesel price. This can be checked in Figure 3.37l. That is to say, compared to the nominal scenario (MS), in LS it becomes more important to reduce the BT degradation.

This increase in the C_{BTrepl} importance has some side effects, which were already identify during this subsection. As DP tends to increase the degradation of the BT (the BT makes a higher DOD with this strategy), it obtains worse results when reducing c_f. Besides, LTO generally obtains lower C_{BTrepl} values compared to NMC. Therefore, LTO improves over NMC in terms of LCC.

On the contrary, in HS the importance of reducing the diesel use is even higher. This inevitably makes the importance of C_{BTrepl} be reduced, contrary to the case of LS. Consequently, the BT chemistries and EMSs that most reduce C_f (even if that goes against BT degradation) turn to obtain better results than in the lower scenarios. The good results of NMC chemistry and DP strategy in HS are a clear example of this trend.

3.5.3 Sensitivity to BT Price

The last parameter to be analysed in the sensitivity analysis to the economic model is the price of the BT technology (c_{BT}). Each BT chemistry has a different c_{BT}, therefore the sensitivity to the prices of each chemistry has to be analysed individually. As it was previously specified, in the case of LTO 1200-1500-1800 €/kWh prices are proposed for each scenario (LS-MS-HS, respectively), in the case of NMC 640-800-960 €/kWh, and in the case of LFP 520-1040-1560 €/kWh. As with previous sensitivity analysis, the evaluation of the results will be divided into three steps. First, the analysis will focus on the LCC values, then on the optimization results, and finally on the influence of the cost terms.

3.5.3.1 Analysis of LCC Values

Figure 3.38 depicts the LCC values of the scenarios proposed in this analysis. Varying c_{BT} for one chemistry does not affect in the results of the other chemistries. However, in order to better understand what happens when varying the price of a single chemistry,

one graph is depicted for the variation of each chemistry price: Figure 3.38a shows the obtained results when varying LTO price, Figure 3.38b the results when varying NMC price, and Figure 3.38c the results when varying LFP price. In order to better identify the chemistry that is being analysed, the chemistries with no variation have a grey background. Following the format of the previously introduced Figures 3.32 and 3.35, in all the cases the LCC values are normalized in relation to the DP/LTO result. This is the reason why in the case of Figure 3.38a the values of LFP and NMC change from one scenario to another: the absolute LCC values do not change, but as the reference LCC has changed, the normalized LCC values are different.

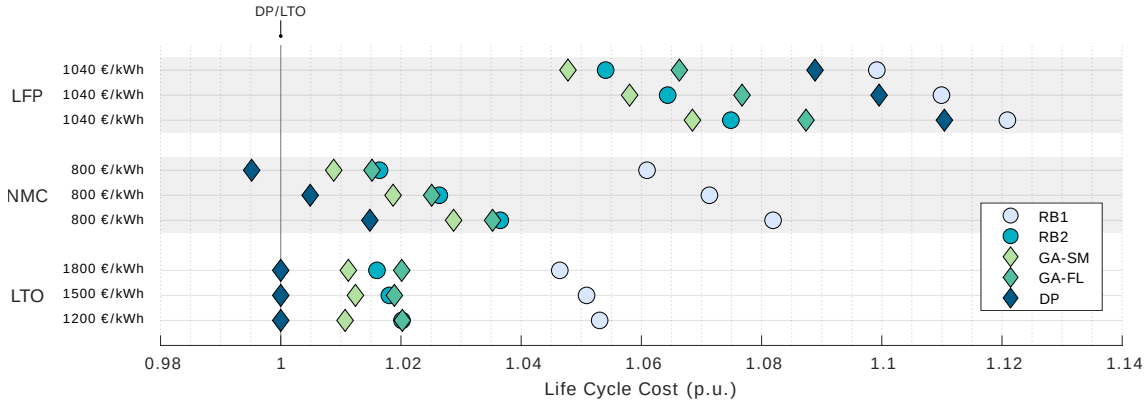

(a) Variation of LTO price

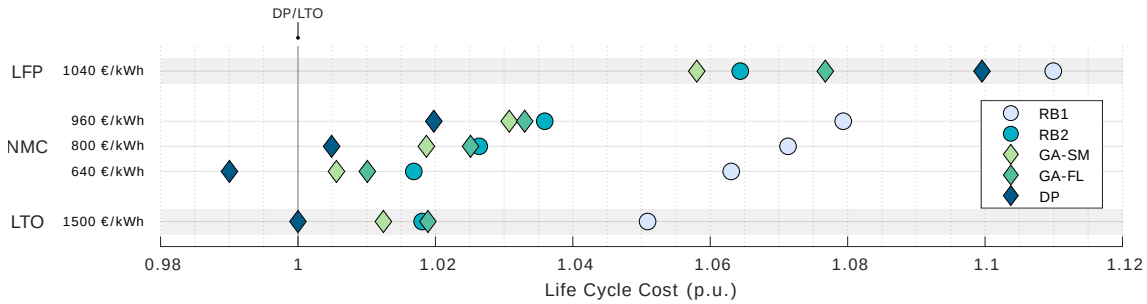

(b) Variation of NMC price

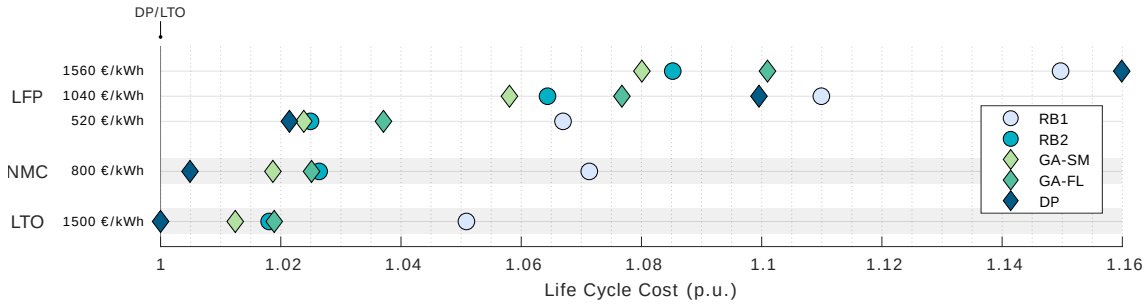

(c) Variation of LFP price

Figure 3.38: Sensitivity of LCC values to c_{BT} of each chemistry.

Firstly, the results can be analysed focusing on the comparison of the different EMSs. In the case of the LTO price variation, it can be checked that the same trend is maintained

in all the scenarios. That is to say, there is no EMS that performs better/worse when increasing/decreasing LTO price. However, in the case of NMC and LFP price variation, some changes can be perceived. Specifically, in these two chemistries it can be noticed that DP improves its result as lower is the BT price. In the case of NMC, DP increases the difference with GA-SM, and in the case of LFP, it becomes the best strategy. The reason is that when the BT price is reduced, the importance of C_{BTrepl} is also reduced. Consequently, the strategies that degrade more the BT (DP is a clear example) improve their results. In the case of LTO this is not noticed, mainly because the BT degradation does not change much from one strategy to another, contrary to the cases of NMC/LTO.

Secondly, the results can be analysed focusing on the comparison of the different BT chemistries. For this evaluation, each BT chemistry is analysed only in the case when its cost is altered, as this variation does not affect the performance of the other chemistries. Regarding LTO (Figure 3.38a), it can be checked that when reducing its price (LS), it improves its performance in relation to the remainder chemistries. It increases its distance with NMC up to the 1.5% in the case of the best strategy, and with LFP this distance is increased up to the 4.8%. On the other side, when increasing the price (HS), NMC starts to be the best option in some of the strategies (with DP a 0.5% lower LCC, with GA-SM a 0.3% lower LCC, and with GA-FL a 0.5% lower LCC). Therefore, it is demonstrated that LTO price has to be increased more than in the proposed HS so NMC can become clearly the most appropriate option.

Regarding NMC chemistry (Figure 3.38b), it can be checked that reducing its price has a similar impact as increasing LTO price. In LS, NMC becomes the main chemistry option in most of the strategies (with DP a 1% lower LCC, with GA-SM a 0.5% lower LCC, and with GA-FL a 0.8% lower LCC). In addition, increasing NMC price has a similar impact as reducing LTO price: LTO becomes clearly the best option, as in almost all the strategies the options with LTO reduce the LCC more than a 1% in relation to their counterparts.

In the case of LFP (Figure 3.38c), increasing its price logically enlarges its distance with the other chemistries. However, when reducing its price (in this case the price reduction is higher than in NMC and LTO) it gets much closer to the other chemistries, specially to NMC. However, it only success in obtaining a better result than NMC in the cases of RB1 (0.4% lower LCC) and RB2 (0.2% lower LCC), which are indeed the strategies with the worst result. Therefore, it is demonstrated that besides a LFP price decrease, a scenario in which NMC or LTO prices are also increased is necessary for LFP to become a reasonable option.

3.5.3.2 Analysis of Optimization Variables

After evaluating the obtained LCC values, the next analysis focuses on the optimization variables returned by the optimization at each cost scenario. Figure 3.39 shows the relation

between the optimal genset and BT sizes and the LCC values of each cost scenario. The subplots are arranged as in the previously introduced Figure 3.33 and Figure 3.36.

The objective of this figure is to evaluate the variations of the optimal sizing values, rather than the comparison of the LCC values. Due to this reason and in the sake of simplicity, at each cost scenario (HS, MS and LS) the results of each chemistry refer to the results obtained when solely varying their price. That is to say, in Figure 3.39a the results refer to the case when all the BT prices are in the HS: the results of LTO refer to the increase of its cost to 1800 €/kWh, the results of NMC to the increase of its cost to 960 €/kWh, and the results of LFP to the increase of its cost to 1560 €/kWh.

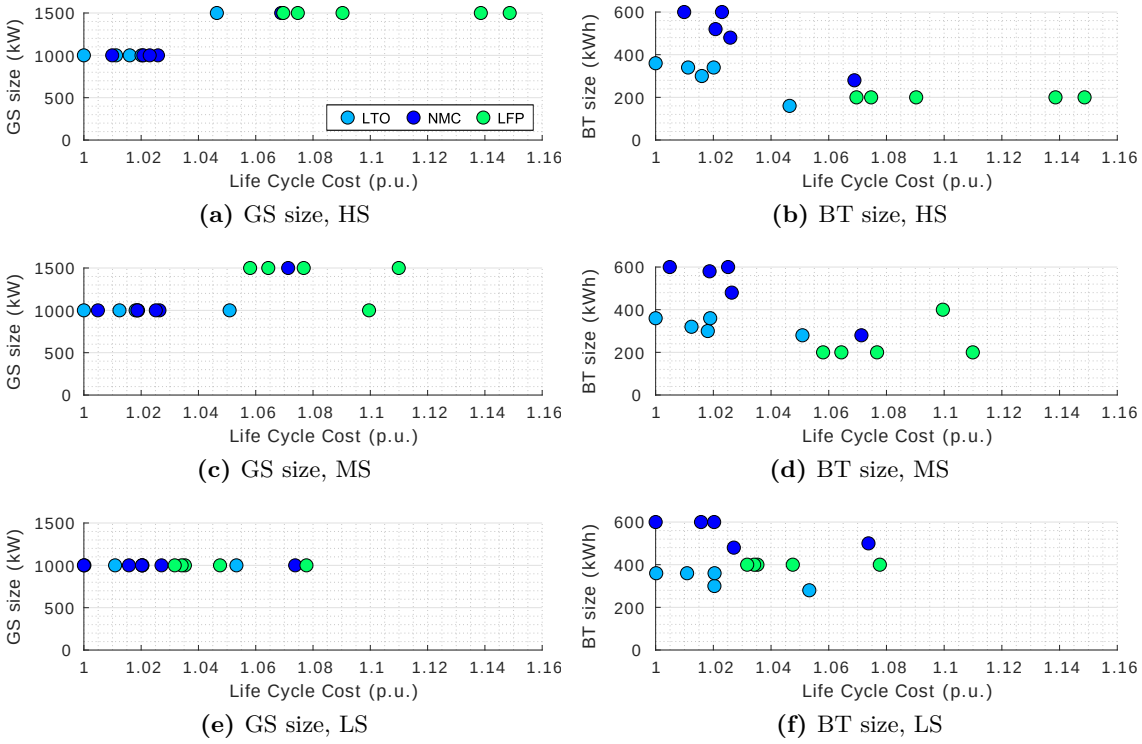

(a) GS size, HS **(b)** BT size, HS

(c) GS size, MS **(d)** BT size, MS

(e) GS size, LS **(f)** BT size, LS

Figure 3.39: Sensitivity of optimal sizing values to c_{BT}.

Regarding the variation in the results of LTO, it can be noticed that they are not very sensible to the change of c_{BT}. In the case of the optimal genset size, there is just one option in HS that proposes the 1500 kW size, and it turns to be the strategy with the worst result. Besides, in the case of the optimal BT size, just some minor changes are noticed: while the price goes down, slightly higher BT sizes are proposed, even if in the original scenario (MS) they were already near the maximum allowable sizes.

In the case of NMC, the results of the optimal genset size are maintained (1000 kW), as in comparison to the original scenario (MS) just one change is noticed. Besides, regarding the optimal BT results, some minor changes are found, similar to the case of LTO: when reducing the BT price, the proposed sizes tend to be slightly bigger, but the difference is

minimum. A higher c_{BT} increase or decrease is required to vary the sizing results to a considerable extent.

Finally, in the case of LFP, the major differences are found in the proposed genset sizes. As lower c_{BT} is, the optimal options tend to propose the genset of 1000 kW. The reason behind this variation will be further analysed afterwards, but it is related to the fact that when reducing the BT price, the effect of the BT replacement cost is reduced. This increases the importance of reducing the diesel use, and therefore, of reducing the genset size. Besides, the BT sizes are only affected by the genset size. Indeed, in all the cases the proposition is to integrate the maximum allowable BT size: 200 kWh with the genset of 1500 kW, and 400 kWh with the genset of 1000 kW.

3.5.3.3 Influence of Key Cost Terms on Overall LCC

In order to complete the analysis of the BT price sensitivity, Figure 3.40 shows a series of graphs that relate the obtained LCC values and the key cost terms (C_{GS}, C_{BT}, C_f and C_{BTrepl}) for the different cost scenarios. The figure and subplots follow the same arrangement as the previously introduced Figure 3.34 and Figure 3.37. Moreover, as in the last analysis, the results of each chemistry refer only to the variation of their price. That is to say, the depicted LCC values are not convenient to compare the performance of the different BT chemistries or EMSs, as the aim is to identify the correlations between a certain cost term and the overall LCC. All the graphs share the same scale in the y-axis, as in this way it is easier to identify the mentioned correlations.

Regarding the variation of LTO price, it can be checked that it barely affects in the values of the different cost terms. Even if c_{BT} is increased or reduced, C_{BT} and C_{BTrepl} are barely affected, and therefore their influence is not increased. Consequently, the importance of C_f is unchanged. This is the reason why only minor changes have been found in the results of the LCC and optimal variables of LTO during this subsection.

Besides, the results of NMC unveil some minor changes in the effect of the cost terms. When c_{BT} is increased, the major change is found in C_{BTrepl}. However, the best EMSs continue being the ones that reduce more the diesel use (DP), what demonstrates that the importance of reducing C_f (and thus, the importance of C_{BTrepl}) is not varied.

Eventually, the results of LFP are the ones that show more variability from one scenario to another. This is also a reasonable conclusion, as the price of LFP is varied more than the price of the other two chemistries. As in the case of NMC, C_{BTrepl} is the most affected cost factor when varying c_{BT}: when reducing the BT price, the contribution of C_{BTrepl} is also reduced. Consequently, C_f starts having more influence: in LS, the strategies with lowest diesel consumption end up being the best ones (e.g., DP). On the contrary, when increasing c_{BT}, the contribution and importance of C_{BTrepl} are enhanced even more than in the original scenario (MS).

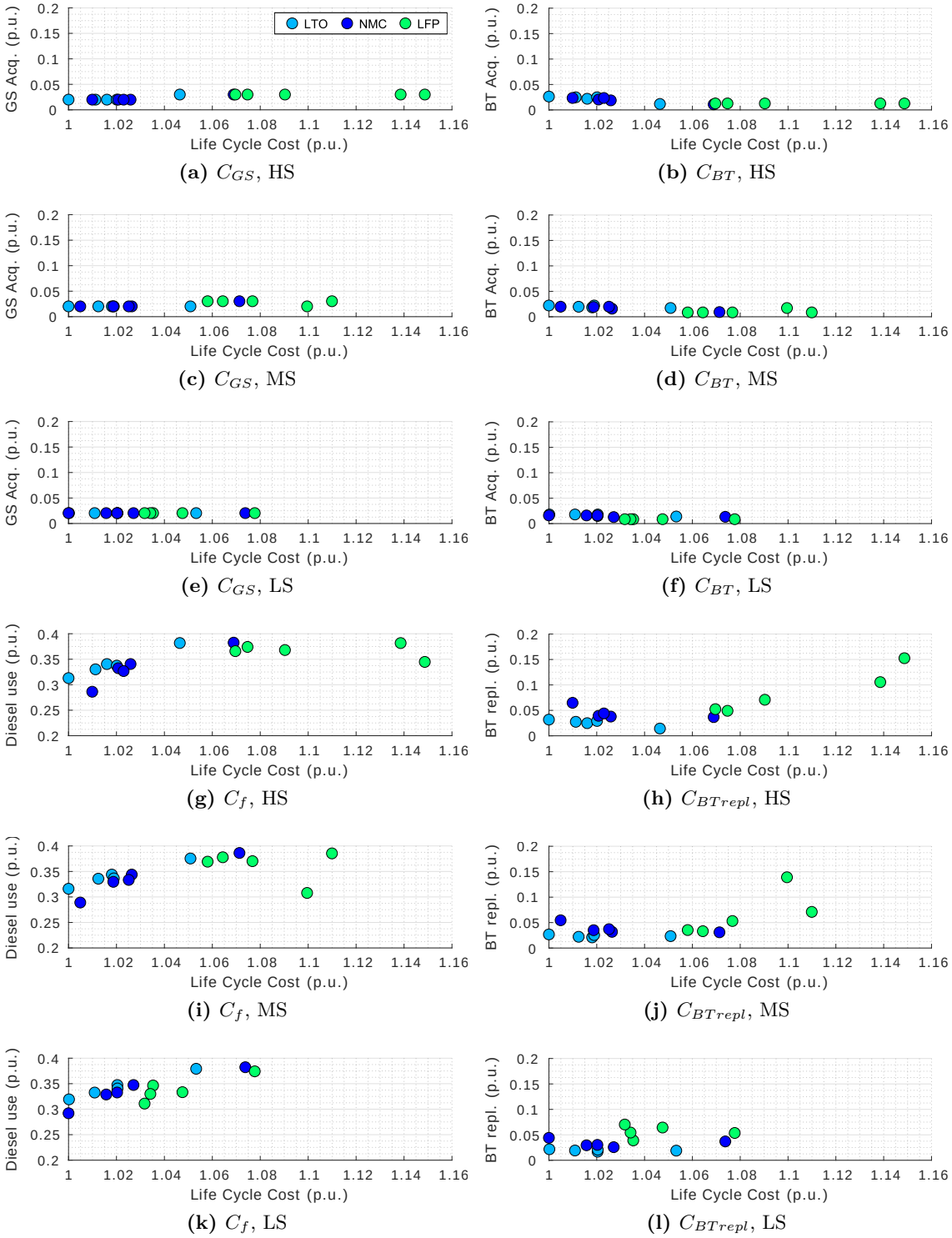

(a) C_{GS}, HS **(b)** C_{BT}, HS

(c) C_{GS}, MS **(d)** C_{BT}, MS

(e) C_{GS}, LS **(f)** C_{BT}, LS

(g) C_f, HS **(h)** C_{BTrepl}, HS

(i) C_f, MS **(j)** C_{BTrepl}, MS

(k) C_f, LS **(l)** C_{BTrepl}, LS

Figure 3.40: Sensitivity of key cost terms to c_{BT}.

3.5.4 Review of Sensitivity Analysis to Economic Model

In this section the effect of varying the daily operation hours (t_{day}), the diesel price (c_f), and the BT price (c_{BT}) has been evaluated. The analysis has been focused on identifying

how is the optimal powertrain design affected when varying the mentioned parameters of the economic model. Specifically, the variations in the LCC value of the different EMSs and BT chemistries, the variations in the returned optimization variables (BT size, genset size and SOC_0), and the variations in the influence of the economic model terms (C_{GS}, C_{BT}, C_f and C_{BTrepl}) have been evaluated.

Table 3.12 reviews the main conclusions obtained in this section. At each column, the effect of the different parameters of the economic model are listed; and at each row, the analysed design decisions. In short, the value of each cell refers to how much the specific design decision has changed when varying the specific parameter of the economic model (e.g., how much have changed the results of the optimal BT size when varying the operation hours). At each cell, the superscript number refers to the comment at which each conclusion is further discussed. The comments and conclusions are listed below.

Table 3.12: How much does the variation of each parameter influence the optimal design of the H-DEMU powertrain.

	Operation hours	**Diesel price**	**BT price**
Optimality of EMSs	●○○(01)	●○○(02)	●○○(03)
Optimality of BT chemistries	○○○(04)	●○○(05)	●●●(06)
Optimal genset size	●○○(07)	●●○(08)	●●○(09)
Optimal BT size	●●●(10)	●●●(11)	●○○(12)
Optimal SOC_0	○○○(13)	○○○(13)	○○○(13)
Influence of cost terms	●●●(14)	●●○(15)	●○○(16)

(1) The LCC distances between the different EMS are reduced when reducing t_{day}, but there is no EMS that overtakes another one compared to the nominal scenario.

(2) The relative performance of DP in comparison with the rest of EMSs is improved when increasing c_f, and it is reduced when decreasing c_f. In all the cases it remains the best strategy, and the order between the remainder EMSs is barely varied.

(3) Changes are noticed in the cases that integrate NMC and LFP: as lower c_{BT} is, the performance of DP is enhanced, as the relative influence of C_{BTrepl} is reduced (it is the main drawback of DP). No notable changes are noticed in the remainder strategies.

(4) LTO remains the best chemistry. No noticeable changes have been identified when varying the operation hours.

(5) As the importance of reducing the diesel use is increased when increasing c_f, NMC improves its results (it can integrate higher BT sizes, which allow a higher diesel use reduction). However, NMC does not outperform LTO in the defined LS. In the opposite scenarios, LTO gains more distance against NMC and LFP.

(6) When slightly increasing LTO price or slightly reducing NMC price, NMC becomes the best option in most of the strategies. However, it does not become clearly the best option, as LTO stays always close. In the opposite scenario, LTO gains more distance

against NMC. Even if LFP price is reduced much, it does not become competitive.

(7) The general tendency is maintained when reducing t_{day}. Some slight changes unveil that at lower operation hours, the genset of 1500 kW starts being the optimal option in some cases. Anyway, the options with lowest LCC continue proposing the 1000 kW genset.

(8) When reducing c_f, the importance of reducing the diesel use is reduced, and consequently many options propose the genset of 1500 kW. Anyway, the options with lowest LCC continue proposing the 1000 kW genset.

(9) In NMC and LTO there are not nearly changes in the optimal genset size. In LFP, when reducing much c_{BT}, the option of 1000 kW becomes clearly the optimal one.

(10) When reducing t_{day}, minimizing the fuel use losses importance. Therefore, integrating big BT systems is no longer cost-efficient: the optimal BT sizes are reduced.

(11) The same conclusion as in point (10) is obtained: when reducing c_f, minimizing the fuel use losses importance. Consequently, lower BT sizes are proposed. On the contrary, when increasing c_f, the optimal sizes are even closer to the maximum allowable values with the genset of 1000 kW.

(12) In LTO there are not changes, and in NMC and LFP just slight variations: the size of NMC is slightly reduced when increasing c_{BT}, and in the case of LFP the changes are influenced by the optimal genset size (the maximum allowable BT size is always proposed).

(13) The optimal initial SOC is always 90%, even when varying the H-DEMU operation hours, the diesel price and the BT price.

(14) C_f losses influence when reducing t_{day}, and a slight increase in the importance of C_{BTrepl} is noticed. It is worth to mention that with a t_{day} reduction both the diesel use and the BT degradation are reduced.

(15) When reducing c_f, a compromise between C_f and C_{BTrepl} is required to obtain a low LCC, as the reduction of diesel use losses influence. On the contrary, when increasing c_f, the reduction of the fuel use gains even more importance (except in the case of LFP).

(16) Only some minor changes are noticed in the case of LFP: when reducing much c_{BT}, minimizing C_f turns to be more important that minimizing C_{BTrepl}.

3.6 Results of Sensitivity Analysis to Driving Cycle

This section presents and evaluates the results obtained in the sensitivity analysis to the driving cycle. As it was specified in the methodology presented in Chapter 2, this last sensitivity analysis focuses on evaluating how do the results and conclusions of the powertrain design (Section 3.4) differ when varying the characteristics of the route that

the H-DEMU completes (i.e., the driving cycle). Figure 3.41 shows where it is located the current sensitivity analysis in the holistic design methodology proposed in this Ph.D. Thesis. Specifically, 16 driving cycles of different lengths and average demands have been used in this analysis, as it was detailed in Section 3.2.4. The results have been obtained for the nominal parametrization of the economic model.

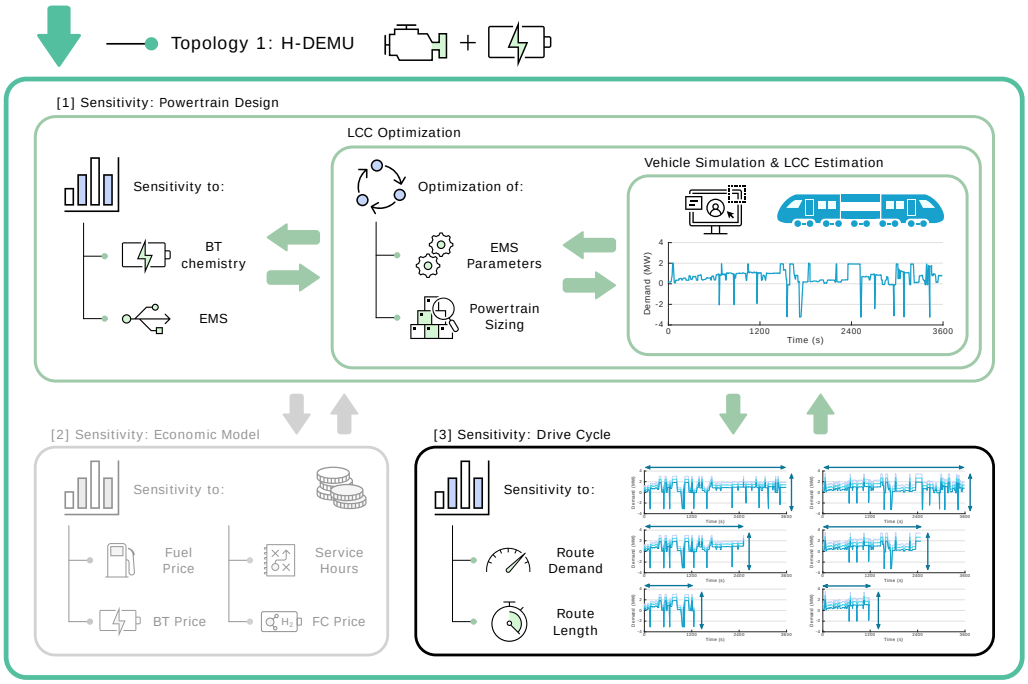

Figure 3.41: Current step of holistic design methodology.

Considering the conclusions obtained in the previous sensitivity analyses, and with the aim of reducing the number of cases to be simulated and evaluated, the number of considered EMSs and BT chemistries has been reduced. Regarding the control strategies, RB1 and GA-FL are not evaluated. Indeed, in the contexts analysed so far it has been demonstrated that RB1 and GA-FL do not outperform RB2 and GA-SM, respectively. Therefore, they are excluded from the analysis of this section, as it is expected that they will not improve their performance in the new scenarios. Regarding the BT chemistries, the same decision has been made with LFP: as it has been demonstrated that in the contexts analysed so far it is not a competitive option compared to NMC or LTO, it is excluded from the current analysis.

In order to improve the evaluation of the obtained results, the analysis is divided into different sections. First, in Section 3.6.1 the variation of the LCC results when simulating different driving cycles is analysed. Then, Section 3.6.2 focuses on how do the optimal values of the optimization variables (n_{GS}, n_{BT} and SOC_0) vary at the different proposed scenarios. A similar analysis is developed in Section 3.6.3, but in this case the analysis focuses on the key cost terms of the LCC model (C_{GS}, C_{BT}, C_f and C_{BTrepl}). Finally, the main conclusions are reviewed in Section 3.6.4.

3.6.1 Analysis of LCC Values

In order to analyse the variation of the LCC values in the different scenarios, the graph depicted in Figure 3.42 is proposed. For each of the 16 driving cycles, the results of NMC and LTO chemistries and RB2, GA-SM and DP strategies are given. The results are grouped in rows by each chemistry, and the markers represent the different EMSs. For the results of each driving cycle, the LCC is normalized in relation to the result of DP with LTO, as it was found to be the optimal case in the first analysis (Section 3.4). The number inside the square in the right of the graph represents the ID of the driving cycle, which will be useful afterwards in Sections 3.6.2 and 3.6.3. Besides, the numbers depicted in the left define the approximate characteristics of each driving cycle: the length of the non-electrified section (h) and the average demand power (kW), respectively. In order to better differentiate the cases, a different background colour is used for each section length.

As it can be noticed, in some driving cycles the BEMU is the optimal option (i.e., the option with no gensets, only powered by BTs). Therefore, in these cases only a single EMS is depicted, as the comparison of the control strategies does not make sense. When this happens, the LCC is normalized in relation to the result of the BEMU with LTO. Specifically, the BEMU is the optimal option in the scenarios with the lowest demands, what demonstrates that this topology is only valid for scenarios where the demand of the non-electrified sections is lower than 150-200 kWh (energy demand of scenario 2).

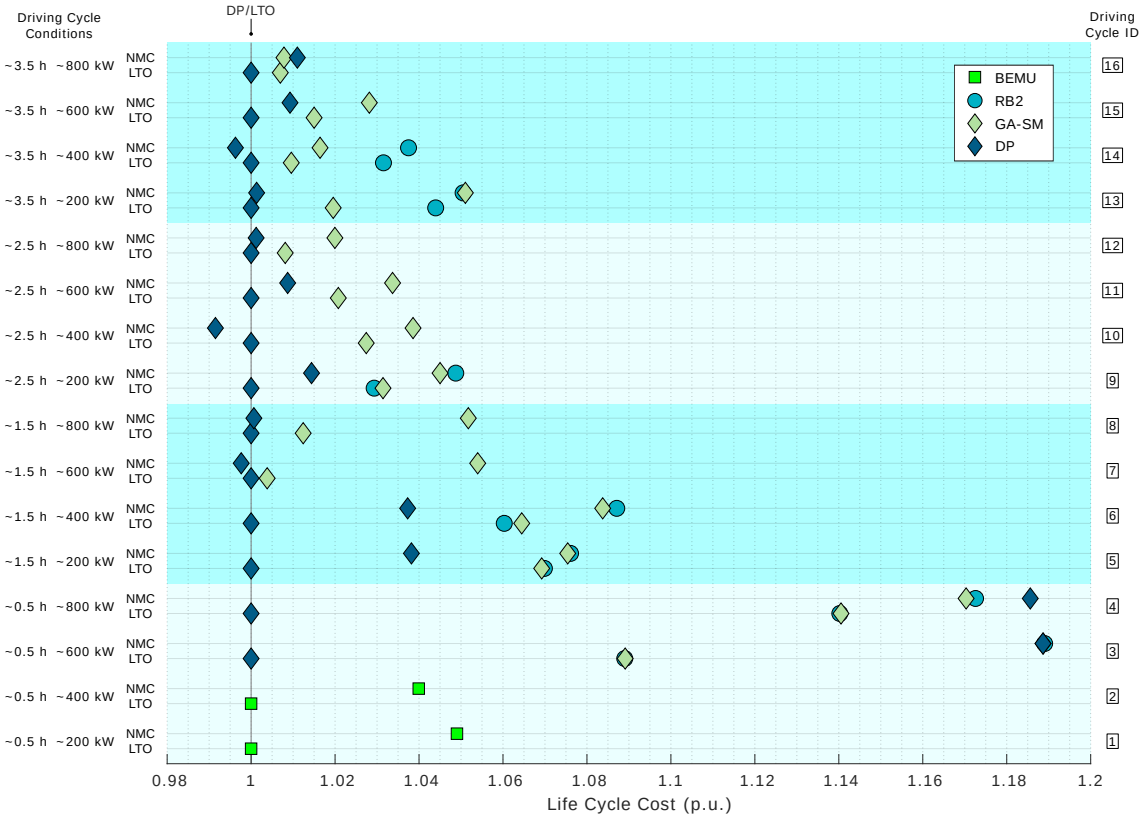

Figure 3.42: Sensitivity of LCC values to different driving cycles.

The results are evaluated from two points of view: focusing on the comparison of the different chemistries, and focusing on the comparison of the different EMSs.

Regarding the different chemistries, the results show that in general LTO continues being the chemistry with the lowest LCC. In the case of GA-SM and RB2, LTO obtains always better results, and in the case of DP only in three driving cycles (IDs 7, 10 and 14) is NMC the chemistry with the best result. Besides, in the cases when NMC obtains a better result, the LCC difference between both chemistries is never higher than the 0.8%. Therefore, these results demonstrate that the conclusions obtained in the nominal scenario do not differ much from the ones obtained in the new driving cycles.

The distance between LTO and NMC seems to be higher in the driving cycles with lowest demand: in driving cycles 1 to 6, the LCC difference between the best result of both chemistries is always higher than the 3.7%. On the contrary, in the scenarios with a higher demand that distance is reduced. For instance, in the scenarios with a non-electrified section of 3.5 h, the distances between LTO and NMC are generally around 1%. This trend suggests that NMC obtains better results in the scenarios with a higher demand, due to the fact that it can integrate higher BT sizes compared with LTO. In shorter and less demanding scenarios, however, there is no need to integrate big BT systems, what brings no benefit for NMC.

Regarding the comparison of the different strategies, a first look to the results demonstrates that DP continues being the best option also when varying the driving cycle. Excluding the scenarios where the optimal option is the BEMU, there are only two cases where GA-SM obtains a better result compared to DP: ID 16 and ID 4, in both cases with NMC chemistry. Moreover, in ID 16 the LCC difference is just 0.4%. Therefore, this enforces the idea that under any new scenario, probably DP will obtain the lowest LCC.

The results also show that the LCC difference between DP and the other two EMSs is increased in the scenarios with a lower demand, and that it is reduced in the scenarios with a higher demand. The reason behind this trend may be that in the shorter or less demanding driving cycles (e.g., IDs 3, 4, 5 and 6) DP forces the battery to be more discharged, what inevitably saves more diesel and improves the LCC. On the contrary, GA-SM and RB2 cannot provide that operation in the scenarios with a lower demand, as in the case of these strategies, the BT discharge speed depends on the difference between the demand and the genset operation point (which is fixed regardless the demand level of the route, see Section 3.2.1). That is to say, they do not force the BT to be discharged.

Comparing the results of the other two strategies, it can be noticed that GA-SM obtains better results than RB2, specially in the most demanding scenarios. In the scenarios with a low demand (e.g., IDs 3, 4, 5 and 6) there are some cases where both strategies obtain nearly the same result. The reason is that in the scenarios with a low demand, the BT is not discharged much. Therefore, in the case of GA-SM the strategy always works in the high SOC state, which indeed replicates the operation of RB2. However, in most of the

scenarios with a high demand, GA-SM improves the LCC of RB2, what demonstrates that it is better designed. Moreover, there are several scenarios (IDs 7, 8, 10, 11, 12, 15 and 16) where RB2 cannot provide a feasible solution, what proves also its lower robustness.

3.6.2 Analysis of Optimization Variables

This subsection analyses the variation of the optimization variables in the proposed driving cycles. The analysed optimization variables are the genset size, BT size and initial SOC. Figure 3.43 depicts a series of graphs that relate the demand level of each scenario (in the x-axis, measured by the traction energy required during the non-electrified section) and the values of the optimization variables (in the y-axis). The upper graphs show the optimal genset sizes, the middle graphs the optimal BT sizes, and the lower graphs the optimal SOC_0 values. Besides, the left-side graphs present the results of LTO chemistry, and the right-side graphs the results of NMC.

At each graph, different marker shapes are used for the EMSs. In addition, two different background colours are used for the markers: the darker colours refer to the best solution of each scenario, and the lighter colours are used for the remainder strategies. The objective of this differentiation in the colour is to highlight at each driving cycle which is the value proposed by the case with the best LCC.

Focusing on the results of the optimal sizing, logical results are obtained. It has been already demonstrated that in nominal conditions integrating big BT systems and small gensets becomes the optimal option, as it allows reducing more the diesel use. However, the demand level of the route constraints this conclusion, as the biggest possible BT system would not be enough for providing traction energy during all the route. In this cases, it is necessary to increase the size of the genset. This is what Figures 3.43a and 3.43b show: as higher is the overall energy required for traction, bigger gensets are required, as this is the only option for obtaining a feasible solution.

In the case of LTO, the BEMU (n_{GS}=0) is the optimal option in the scenarios with demands lower than 250 kWh, the genset of 500 kW is the optimal option with demands between 250 kWh and 80 kWh, and the genset of 1000 kW is the optimal option with demands higher than 800 kWh (at least until nearly 3000 kWh).

Besides, in the case of NMC similar conclusions are obtained, but with different ranges: the BEMU is the optimal option in scenarios with demands lower than 250 kWh, the genset of 500 kW is the optimal option with demands between 250 kWh and 1400 kWh, and the genset of 1000 kW is the optimal option with demands between 1400 kWh and 2000 kWh. The scenario with the highest demand (2851 kWh) proposes the genset of 1500 kW, what demonstrates that in scenarios with high demands the option of that genset may become the optimal option. There are also two scenarios (IDs 3 and 4) which do not follow the mentioned trend: even if they have a low overall demand, the optimal genset size is 1000 kW. The reason is that these driving cycles have short sections with high peak demands,

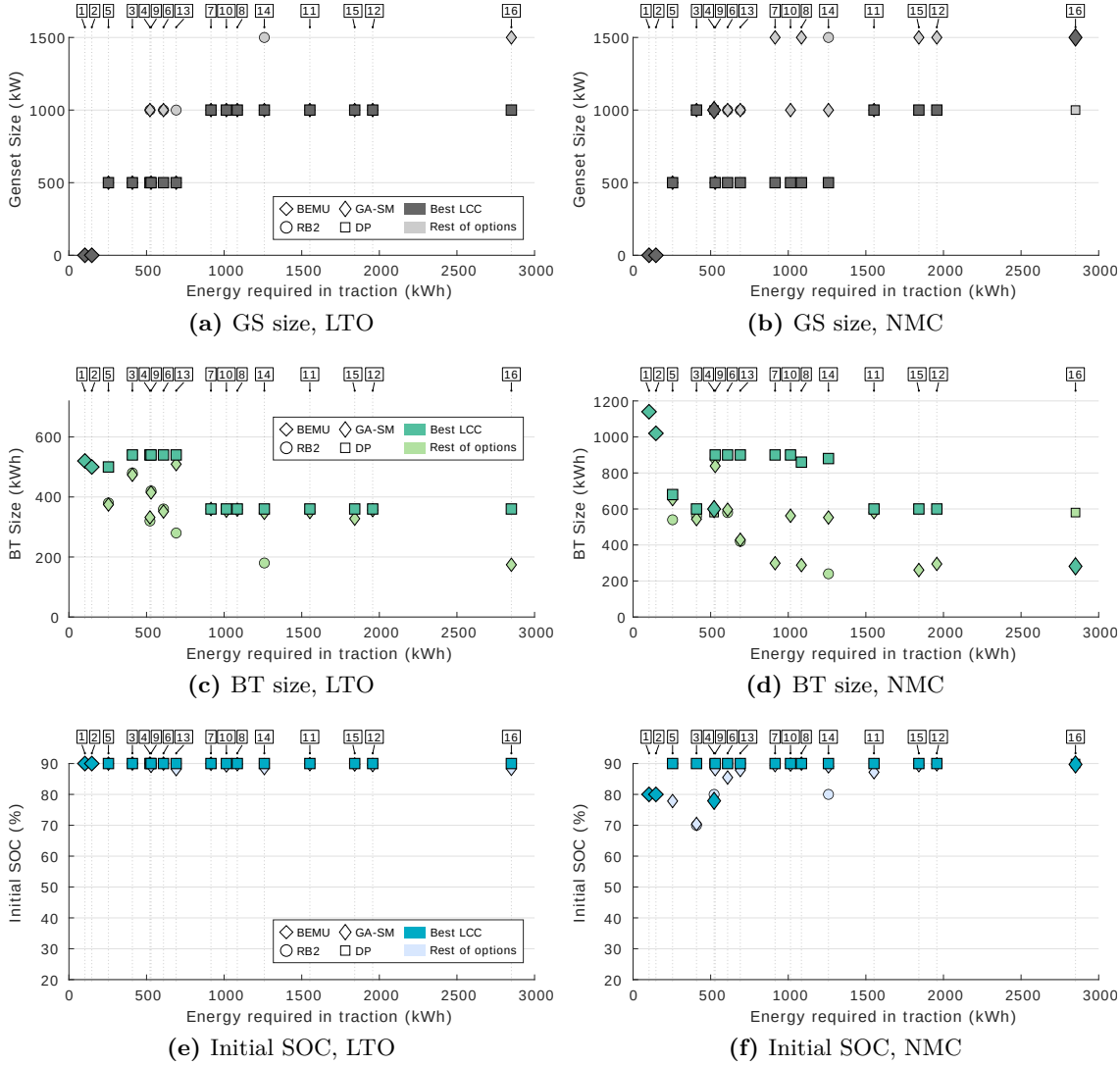

(a) GS size, LTO **(b)** GS size, NMC

(c) BT size, LTO **(d)** BT size, NMC

(e) Initial SOC, LTO **(f)** Initial SOC, NMC

Figure 3.43: Sensitivity of optimization variables to different driving cycles.

which cannot be provided by the combination of a 500 kW genset and the maximum allowable NMC size. This proves that the conclusions enumerated before may not be transversal for all the cases. The specific characteristics (e.g., maximum peaks) of the driving cycles may also be checked in some cases.

Regarding the results of the optimal BT sizing, it can be noticed that in general the best option is to integrate the maximum size that the optimal genset allows. This conclusion is transversal to both chemistries. The exceptions are the scenarios with lowest demand: IDs 1, 2 and 5. Figures 3.43c and 3.43d show that in these scenarios lower sizings are proposed, which are found to be near the lowest sizing that provides a feasible solution.

Different reasons are found for these lower sizings. ID 1 and ID 2 are the cases where the BEMU is the optimal option. In the case of the BEMU, bigger BTs tend to increase

the BT lifetime, because for the same energy demand they made a lower DOD. However, bigger sizes will only be cost-efficient if the reduction of the BT replacements compensates the higher cost that bigger BT systems require. For the analysed case, it has been found that it does not compensate, and consequently lower BT sizes become the optimal option.

In the case of scenario ID 3, another reason is found. In a H-DEMU with bigger BT sizes, typically the diesel use is reduced, as the contribution of the genset can be minimized. In most of the cases analysed so far, the saved diesel compensates the higher cost of a bigger BT. However, in the case of ID 3, as the demand is lower, less diesel can be saved when deploying a bigger BT. Consequently, the cost of the bigger BT is not compensated, and the optimal option is a smaller size.

Finally, the results of the optimal initial SOC demonstrate that in general the conclusions obtained in previous analyses are maintained. In the case of LTO, the option of the 90% is the optimal one in all the proposed driving cycles. Therefore, it is demonstrated that when integrating LTO, starting the non-electrified section in the highest possible SOC is always the optimal option. In the case of NMC, the option of 90% is also the optimal one in most of the scenarios. However, in the driving cycles with lower demand (e.g., IDs 1, 2 and 4) the optional option is to start the non-electrified section with a charge around the 80%. The reason may be that in the case of NMC, when a low DOD is made, a lower middle SOC increases notably the BT lifetime.

3.6.3 Influence of Key Cost Terms on Overall LCC

After analysing the LCC values and the results of the optimization variables, this subsection focuses on how does the influence of the key cost terms of the economic model (C_{GS}, C_{BT}, C_f and C_{BTrepl}) vary when modifying the driving scenario.

For this analysis, Figure 3.44 depicts a series of graphs that relate each of the cost terms (in the y-axis) and the demand level of each scenario (in the x-axis, measured by the traction energy required during the non-electrified section). Subfigures a-b depict the values of C_{GS}, subfigures c-d the values of C_{BT}, subfigures e-f the values of C_f, and subfigures g-h the values of C_{BTrepl}. At each row, the left side graph shows the results for LTO, and the right side graph the results for NMC. The graphs follow a similar format as the previously presented Figure 3.43: the values are normalized in relation to the best case of each driving cycle and chemistry, different marker shapes are used to represent each EMS, and the EMS with the best result at each case is represented by a darker colour. Besides, all the graphs respect the same scale for the y-axis (from 0 to 0.4), as in this way it is easier to find correlations between the depicted variables.

First of all, it can be checked that the contribution of C_{GS} and C_{BT} on the overall LCC remains low even if the driving cycle is varied. There is no case where C_{GS} contributes more than the 3% or where C_{BT} contributes more than the 5% of the referential LCC. C_{GS} tends to be increased and C_{BT} tends to be decreased when the traction energy of the

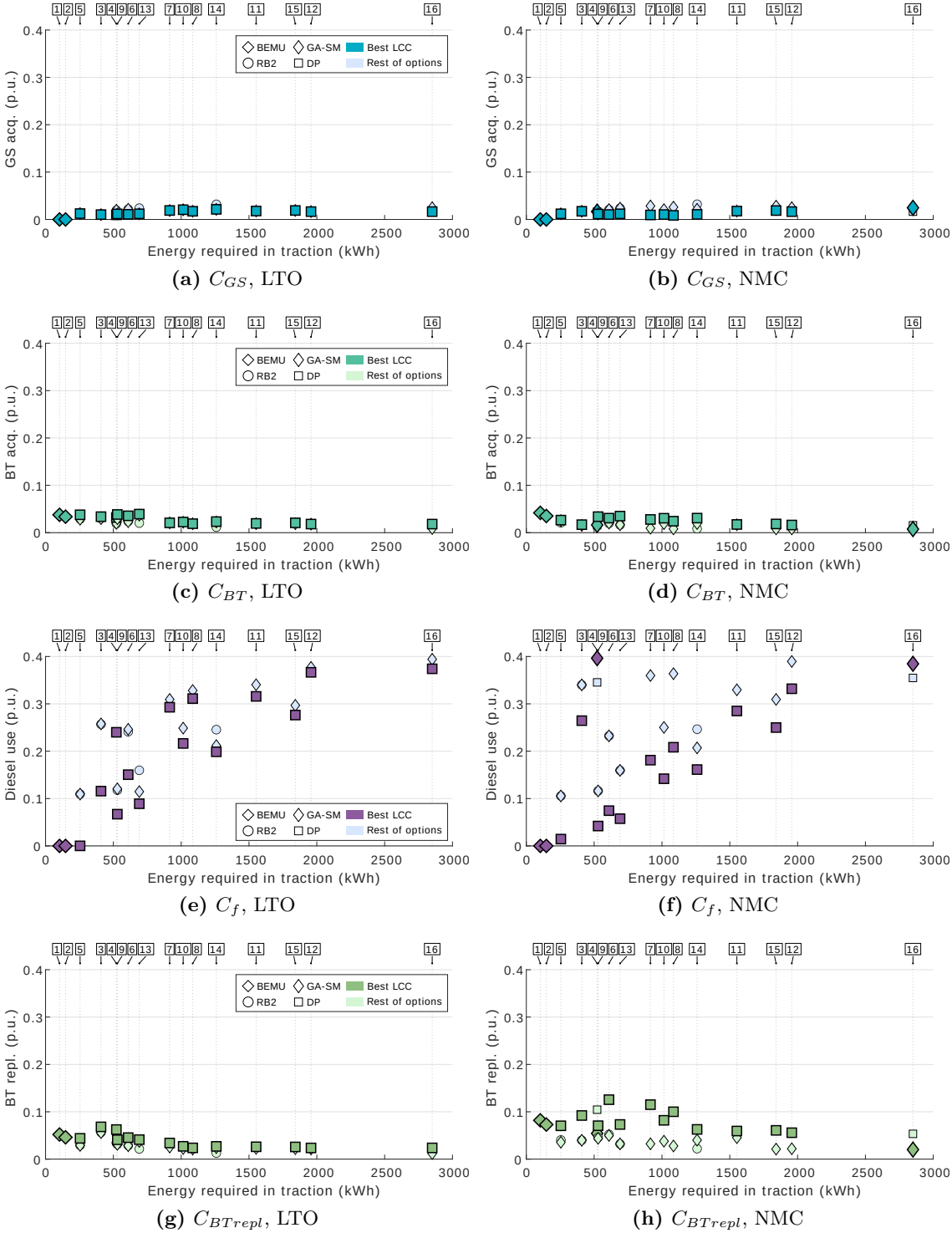

(a) C_{GS}, LTO **(b)** C_{GS}, NMC

(c) C_{BT}, LTO **(d)** C_{BT}, NMC

(e) C_f, LTO **(f)** C_f, NMC

(g) C_{BTrepl}, LTO **(h)** C_{BTrepl}, NMC

Figure 3.44: Sensitivity of key cost terms to different driving cycles.

driving cycle is increased. This is a logical trend, as the acquisition cost of both traction sources is affected by its optimal size (this was analysed in the previous subsection). In

short, it is noticed that neither C_{GS} or C_{BT} have an important influence on the LCC even when varying the driving cycle.

Regarding C_f, it can be checked that it is the variable whose value varies more from one scenario to another. In driving cycles with a higher demand, the genset has to be used more, as the energy that the BT can provide is limited due to the restrictions on its size. Therefore, in scenarios with a higher energy demand, the diesel use is inevitably increased. However, the importance of reducing the diesel use is maintained practically unchanged, as in most of the scenarios the best strategy continues being the one that reduces more the fuel use (i.e., DP), as seen in Figures 3.44e and 3.44f.

The reason to this fact is that even if the value of C_f varies notably from the scenarios with lower demand to the ones with higher demand, the rest of cost terms do not vary their values in the same range. The value of C_{BTrepl} is increased in the scenarios with lower demand, but it is never higher than the 8% in the case of LTO or higher than the 12% in the case of NMC. This makes the influence of C_f unchanged. Moreover, Figures 3.44g and 3.44h show that in most of the cases the strategies that propose a higher C_{BTrepl} value are the ones with a better LCC. Therefore, it can be concluded that C_{BTrepl} has not much influence even when changing the driving scenario.

Logically, the only exceptions are the cases where the optimal option is the BEMU. In these cases, a compromise between C_{BT} and C_{BTrepl} has to be reached. As it was already highlighted in the previous subsection, bigger BT sizes tend to increase the BT lifetime, but it may not be enough to reduce the replacement costs.

3.6.4 Review of Sensitivity Analysis to Driving Cycle

In this section the effect of varying the driving cycle has been analysed. The analysis has been focused on how the optimal powertrain design is affected when varying the driving cycle. Specifically, the variations in the LCC value of the different EMSs and BT chemistries, the variations in the returned optimization variables (n_{GS}, n_{BT} and SOC_0), and the variations in the influence of the cost terms (C_{GS}, C_{BT}, C_f and C_{BTrepl}) have been evaluated. Table 3.13 reviews the main conclusions obtained in this sensitivity analysis. In short, the table defines how much does the variation of the driving cycle affect in the main points analysed through this section. The superscript numbers refer to the comment at which each conclusion is further discussed. The comments and conclusions are listed below.

(1) The order of the different control strategies is kept unchanged, except in some minor exceptions. That is to say, DP continues being the optimal option even when varying the driving cycle. The distances between the EMSs are reduced in the scenarios where the overall traction energy demand is higher.

(2) The same conclusion is obtained regarding the optimality of the different BT

Table 3.13: How much does the variation of the scenario influence the optimal design of the H-DEMU powertrain.

	Variation of Driving Cycle
Optimality of EMSs	●○○(1)
Optimality of BT chemistries	●○○(2)
Optimal genset size	●●●(3)
Optimal BT size	●●○(4)
Optimal SOC_0	◐○○(5)
Influence of cost terms	◐○○(6)

chemistries: except in some minor exceptions, LTO obtains always a LCC lower than NMC. The distances between both chemistries are reduced in scenarios with a higher demand, and they are increased in scenarios with a lower demand.

(3) The optimal genset size is affected by the characteristics of the driving cycle: as higher is the traction energy demand, a higher genset size is required. The reason is that even if bigger BT sizes tend to reduce the LCC, in scenarios with high demand they cannot provide a feasible solution. Therefore, bigger genset sizes and lower BT sizes are required.

(4) The optimal BT size is constrained by the optimal genset size. Anyway, generally the optimal option is the maximum BT size that the optimal genset size allows. The exceptions are the scenarios with low demand (traction energy requirement bellow 250 kWh), where the optimal size is near the lowest one that provides a feasible solution.

(5) The optimal initial SOC remains being 90% regardless the driving scenario. The exceptions are the cases that integrate NMC and have a low demand (energy requirement bellow 200-250 kWh). In these cases, the optimal SOC_0 value is reduced to nearly 80%.

(6) Even if its contribution to the overall LCC can widely vary from one scenario to another, C_f continues being the variable with the major influence. Logically, the only exception are the cases where the optimal option is the BEMU. In these cases, a compromise between C_{BT} and C_{BTrepl} has to be reached.

3.7 Conclusions

This chapter has presented the first case study of the current Ph.D. Thesis, which is focused on the implementation of the holistic design methodology with the rail vehicle topology denoted as the Bi-mode H-DEMU. The Bi-mode H-DEMU can drive powered by the genset, BT or catenary.

In the first sections of this chapter (Sections 3.1, 3.2 and 3.3), the methodology previously introduced in Chapter 2 has been particularized to the vehicle being analysed in the current case study. Section 3.1 has detailed the general characteristics of the H-DEMU vehicle considered for the development of the analysis, which is based on the CIVITY

vehicle manufactured by CAF.

Section 3.2 has introduced all the cases of the different sensitivity analyses, including the different control strategies, BT chemistries, parametrizations of the economic model, and driving cycles. Regarding the EMSs, rule-based (RB1, RB2, RB3, RB-SM and RB-FL), optimization-based (GA-SM, GA-FL and DP) and learning-based (ANFIS) strategies have been considered. For the BT chemistries, LTO, NMC and LFP technologies have been modelled. Regarding the economic model, first a nominal parametrization has been set. Then, the parameters with the highest probability to suffer variations have been selected (t_{day}, c_f and c_{BT}), and three scenarios have been defined for each of them: low, medium and high (LS, MS and HS, respectively). Finally, different driving scenarios have been introduced. As in the case of the economic model, first a nominal case has been set, which is based on the real railway line "A Coruña - A Coruña". Then, additional 16 synthetic driving cycles have been created. These driving cycles have been designed with the aim of representing scenarios with different mean traction demands and route lengths.

In Section 3.3, the LCC optimization problems have been particularized for each EMS. Indeed, depending on the control strategy being optimized, the optimization variables and optimization methodology have been varied. In the case of RB strategies, a simple exhaustive search has been defined. In the case of DP, the same exhaustive search method has been defined, but with an additional optimization variable (SOC_K). Finally, in the case of GA-SM and GA-FL, two different GA-based optimization approaches have been set, as in this case the internal parameters of both strategies are also optimized.

The results obtained when deploying the holistic design methodology have been presented in Sections 3.4, 3.5 and 3.6. First, in Section 3.4 the analysis has focused on evaluating the performance of the different control strategies and BT chemistries with the nominal economic scenario and driving cycle. Specifically, the following points have been analysed: the LCC values of the different EMSs and BT chemistries, the optimal values of the optimization variables (genset size, BT size and initial SOC), and the influence that the key cost terms of the economic model (C_{GS}, C_{BT}, C_f and C_{BTrepl}) have on the overall LCC. The obtained main conclusions are listed below:

- *Comparison of EMSs.* DP is overally the strategy with the best result when appropriate BT chemistries are integrated (i.e., LTO or NMC). However, its real time implementation is barely possible. GA-SM has been found to be close to DP results, as it is just a 0.7% behind in terms of LCC. The replication of DP results has been explored with the implementation of ANFIS. The results are promising (1-1.9% behind of DP), but further development of the LB strategy is required in order to improve the results of GA-SM.

- *Comparison of BT chemistries.* In all the analysed cases, LTO is the chemistry with the lowest LCC. NMC is close to LTO, as in most of the cases the LCC difference is lower than 1%. LFP is found to be far from the results of the other chemistries.

- *Optimal genset size.* The genset of 1000 kW has been found to be the optimal option.
- *Optimal BT size.* The solutions with a lower LCC propose to integrate the maximum allowable energy with the genset of 1000 kW: 600 kWh in the case of NMC and 360 kWh in the case of LTO.
- *Optimal initial SOC.* Starting the non-electrified section with the BT totally charged is found to be the optimal option.
- *Influence of cost terms.* When an EMS successes in limiting the BT degradation (as in NMC and LTO), the potential reduction of C_f (diesel use) becomes the most important parameter of the LCC model. In these cases, if an EMS is able to reduce the diesel use, it will success in obtaining a competitive LCC.

Then, the analysis of Sections 3.5 and 3.6 has been focused on evaluating how do these conclusions vary when modifying the parametrization of the economic model and the driving cycle, respectively. These analyses have unveiled in which conditions the conclusions obtained in the first sensitivity analysis may not be completely true. In the following lines these conditions are listed:

- *Comparison of EMSs.* DP is the optimal option in all the proposed scenarios, even if the distance between the different EMSs tends to be reduced. Specifically, DP tends to worsen its result in the following conditions: (1) when reducing t_{day}, (2) when reducing c_f, (3) when increasing c_{BT}, and (4) in driving cycles with low energy demands.
- *Comparison of BT chemistries.* NMC can improve the results of LTO when the price of NMC is reduced, or when the price of LTO is increased. Anyway, in these conditions LTO stays close to NMC. NMC can also get closer to LTO, but without improving it, when c_f is increased or in driving cycles with a high energy demand.
- *Optimal genset size.* The optimal n_{GS} value is mostly affected by the characteristics of the driving cycle: as higher is the energy demand, a higher genset is required.
- *Optimal BT size.* In the following conditions becomes cost-efficient to integrate lower BT sizes than the ones proposed in the nominal analysis (i.e., lower than the maximum allowable size): (1) when reducing t_{day}, (2) when reducing c_f, (3) in the case of NMC, when reducing its price c_{BT}, and (4) in driving cycles with low energy demand (below 250 kWh). In the rest of cases the optimal BT size only changes when the optimal genset size also does.
- *Optimal initial SOC.* The optimal SOC_0 value is also reduced from the 90% in the case of driving scenarios with low energy demands (below 200-250 kWh) and when NMC batteries are integrated.
- *Influence of cost terms.* When reducing t_{day} or c_f, the influence of C_{BTrepl} is increased, and normally a compromise between C_f and C_{BTrepl} has to be reached to

obtain an optimal LCC. Additionally, in scenarios with very low demand, C_f losses its influence since the BEMU becomes the optimal option. In that case a compromise between C_{BT} and C_{BTrepl} has to be also reached.

4

Case Study B: Hydrogen Electric Multiple Unit

Summary

In this fourth chapter the second case study of this Ph.D. Thesis is developed. The holistic design methodology described in Chapter 2 is implemented with the vehicle topology denoted as the Hydrogen Electric Multiple Unit. As a first step, the methodology is particularized for the current case study: the different cases of the sensitivity analysis are presented, and the details of the deployed optimization problems are given. Then, the results of the different sensitivity analyses are explained successively: the sensitivity analysis to the powertrain design, the sensitivity analysis to the economic parameters, and the sensitivity analysis to the driving cycle.

4.1 Introduction

This fourth chapter introduces the second case study of the current Ph.D. Thesis. In this case, the holistic design methodology proposed in Chapter 2 is implemented with the vehicle topology denoted as the H_2EMU, which drives powered by a FC as primary source and a BT as secondary source. Contrary to the vehicle analysed in Chapter 3, the proposed H_2EMU only drives through non-electrified sections, what becomes important for the design and analysis of the control strategies.

The architecture of the vehicle analysed in the current chapter is depicted in Figure 4.1. The models of the main powertrain elements were introduced in Chapter 2. As it was specified, the FC and BT characteristics are proportionally scaled when analysing different sizings, and the BT parameters are defined depending on the chemistry being analysed (this will be further detailed in Section 4.2.2).

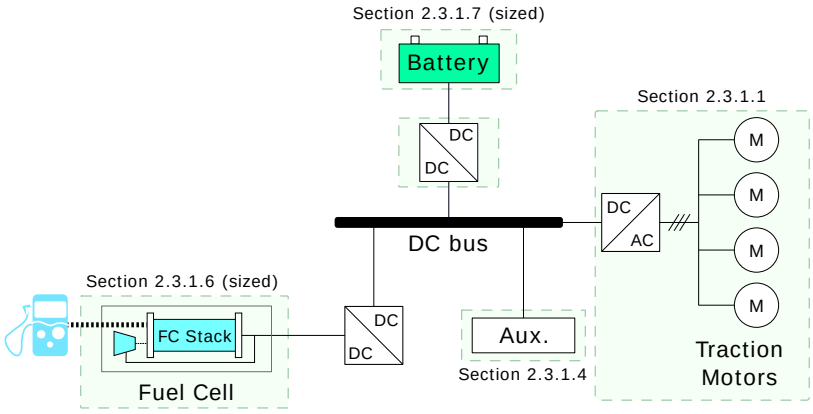

Figure 4.1: Considered H_2EMU vehicle architecture.

Additionally, Table 4.1 shows the general characteristics of the simulated vehicle, which is based on the CIVIA vehicle family manufactured by CAF [197].

Table 4.1: General information of modelled H_2EMU vehicle.

Parameter	Value
Length	62 m
Weight	120 t
Number of traction motors	4
Maximum speed	120 km/h
Maximum traction power at wheel	4.4 MW
DC Bus voltage	3,000 V
Auxiliaries consumption	100 kW

The remainder of the chapter is organized as follows. Section 4.2 introduces all the cases of the sensitivity analyses to be developed as part of the holistic design methodology. That is to say, in this section all the EMSs, BT chemistries, parameters of the economic model, and driving cycles analysed in this chapter are introduced. Then, Section 4.3 particularises the generic optimization problems presented in Section 2.4 to the specific

case study analysed in the current chapter. The results obtained when deploying the holistic design methodology are presented step by step in Sections 4.4 to 4.6. In a first stage, the sensitivity analysis focuses on the powertrain design (different BT chemistries and EMSs are compared, Section 4.4), then on the parameters of the economic model (Section 4.5), and eventually on the driving cycle (Section 4.6). At each section, the obtained results are evaluated in order to obtain the main conclusions related to the design of H_2EMU vehicles.

4.2 Overview of Sensitivity Analyses

Once this chapter has been introduced and the main aspects of the considered vehicle have been described, this section presents all the cases of the sensitivity analyses that are considered in the development of the current case study. The proposed control strategies, BT chemistries, parameters of the economic model and driving cycles are described in the following subsections.

4.2.1 Energy Management Strategies

The analysis of the State of the Art in Chapter 1 concluded that in this Ph.D. Thesis Rule-Based (RB), Optimization-Based (OB) and Learning-Based (LB) strategies would be developed and evaluated. In the current case study concerning the H_2EMU, 4 strategies will be based on rules, 3 strategies will be based on an off-line optimization, and an additional strategy will be based on a learning approach.

In all the cases, the EMS is in charge of defining the operation point of the FC (P_{FC-ref}) for each time step. Therefore, the description of each EMS will be focused on how the strategy defines P_{FC-ref}. Due to the response time of the FC, P_{FC-ref} and the real operation point (P_{FC}) may not match in all time steps. For further detail see Equations (2.11) and (2.12). Anyway, at any time step the BT will give or absorb the power difference between P_{FC} and the power demand (P_{Dem}). If the BT cannot absorb all the defined power, the braking resistors will be activated.

In contrast to the case study related to the Bi-mode H-DEMU, in this case there are some particularities that affect the way the EMSs have been designed:

(1) The control strategy should ensure a relatively low degradation of the FC, for instance avoiding fast transients and keeping P_{FC} in a steady value as long as possible.

(2) As it has been already highlighted, the H_2EMU will only drive on non-electrified tracks. Consequently, the EMS should also ensure that the SOC at the end of the trip stays near (or at least not much lower than) its initial value, so as not to run out of BT energy in the following trips.

In the following subsections, each of the proposed control strategies is described.

4.2.1.1 RB - Baseline Control (RB1-A and RB1-B)

The first strategy is called the Baseline Control, and as the strategy with the same name proposed for the H-DEMU case study, it consists on setting a constant operation point for the FC. The strategy will be denoted as RB1 in order to ease the classification of the different EMSs. In this case, the operation point is set at the nominal power of the FC, so it can provide the maximum possible energy for traction.

When working at a constant operation point, it may happen that the BT cannot be further charged, either because it is at its maximum SOC or because it exceeds the maximum charging C-rate. In the case of the genset, it was proposed to reduce its operation point under these circumstances, so as not to waste fuel unnecessarily. However, in the case of the FC this solution may accelerate its degradation. In order to overcome this issue, in the current case study two variations of RB1 are analysed: RB1-A and RB1-B.

Figure 4.2 shows an example of the difference in the working principle of both variations, which are further explained below.

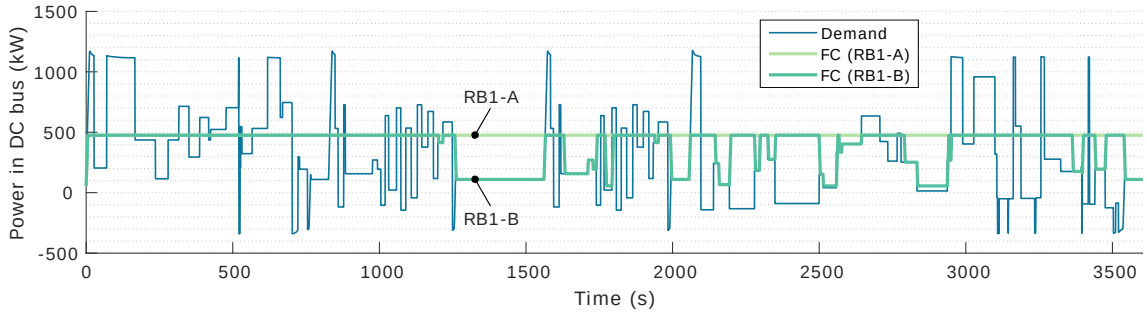

(a) Power in DC bus

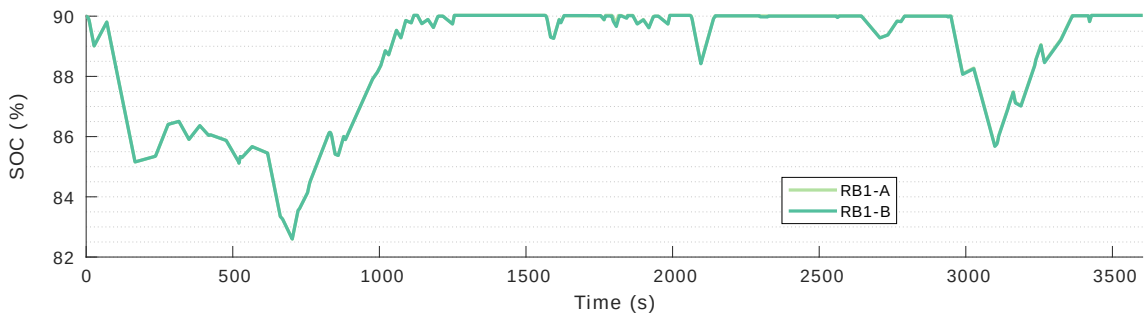

(b) Battery State of Charge

Figure 4.2: Example of RB1-A and RB1-B operation differences.

- In the case of RB1-A, the FC operation point is not varied if the BT cannot be charged. Therefore, there will be an exceed of generated power in the powertrain, which will be burned in the braking resistors.
- In the case of RB1-B, the FC operation point is reduced if the BT cannot be charged. P_{FC-ref} is defined as P_{Dem}, that is to say, the FC tries to follow the demand.

As it can be seen in the figure, the SOC profile is nearly the same with both variations, since the difference happens just in the FC operation when the BT is totally charged. RB1-A is supposed to consume more hydrogen but save the FC lifetime, while RB1-B is supposed to consume less hydrogen but enhance the FC degradation. The analysis of this chapter will unveil which is the best approach.

4.2.1.2 RB - SOC Adaptive Controller (RB2) and OB - Optimized SOC Adaptive Controller (GA-RB2)

The second EMS is aimed to overcome the disadvantages of the two RB1 variants. In this case, the FC reference P_{FC-ref} is reduced at high SOC values in order to avoid an overcharging of the BT, for instance in route sections with a low demand.

Figure 4.3 shows the working principle of this strategy, which is called the SOC Adaptive Controller and will be denoted as RB2 in order to ease the classification of the EMSs. The figure also highlights the difference between RB2 and RB1, in which the FC works constantly at the same operation point. As it can be seen, the controller curve is defined by 3 points: y_1 $[kW]$, y_2 $[kW]$ and x_1 [%]. From SOC_{min} until x_1, the FC works constantly at y_2. Then, from x_1 on, the FC reference point is reduced linearly until y_1, which is defined as the FC reference when the SOC is at SOC_{max}. This linear decrease in the operation point allows a soft operation for the FC, what may help reduce its degradation.

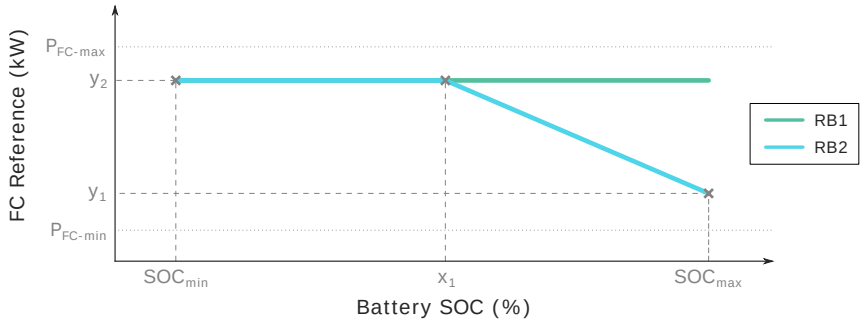

Figure 4.3: Working principle of RB2.

A challenging step of RB strategies consists on tuning the internal parameters of the EMS. From Figure 4.3 it can be deduced that values y_1, y_2 and x_1 may influence the performance of this EMS. In a first approach, the three points of the curve have been defined following a reasonable parametrization: y_1 is defined as the FC idle power ($y_1 = P_{FC-min}$), y_2 as the FC maximum power ($y_2 = P_{FC-max}$), and x_1 as the initial SOC ($x_1 = SOC_0$). However, this parametrization does not ensure an optimal operation of the controller. Therefore, in a second approach these values are optimized by means of a GA-based optimization method. Further information regarding how is this optimization coupled with the powertrain design optimization is given in Section 4.3.

In order to differentiate between both parametrizations, the strategy with the straight-

forward parametrization will be denoted just as the SOC Adaptive Controller (RB2), and the strategy with the optimized values will be denoted as the Optimized SOC Adaptive Controller (GA-RB2).

4.2.1.3 RB - Demand Adaptive Controller (RB3) and OB - Optimized Demand Adaptive Controller (GA-RB3)

The last RB strategy proposed in this case study is called the Demand Adaptive Controller, and will be denoted as RB3. The objective of this EMS is to reduce the BT DOD, so as its lifetime can be improved. For this approach, the FC operation point is adjusted to the average demand of each route section. Each section is defined as s, and the average demand in that section as $P_{Dem-avg}(s)$ $[kW]$. As longer the section is, the DOD that the BT completes might probably be higher (in case there are segments inside the section with a demand much lower/higher than the average). However, as shorter the section is, more changes in the FC operation point will be set during the same round trip. Therefore, with the aim of reaching a compromise, in the approach of the current Ph.D. Thesis the sections are defined as station-to-station route segments. Figure 4.4 shows an example of the route division for the same P_{Dem} profile used in Figure 4.2.

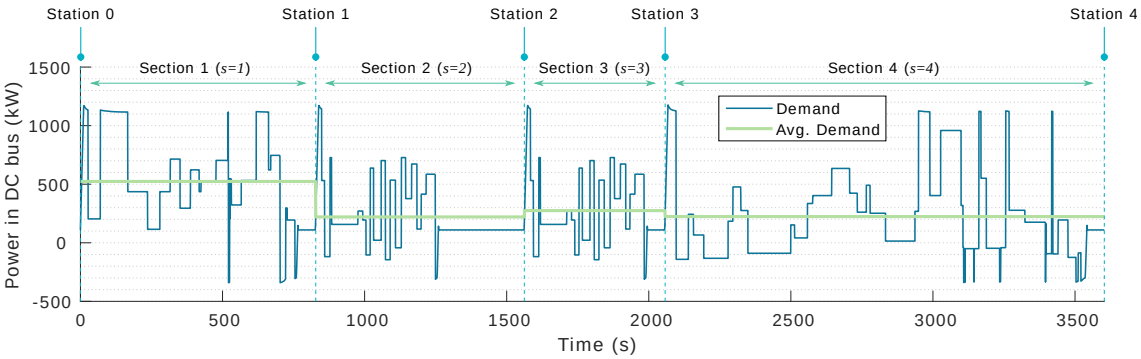

Figure 4.4: Example of route division by station inter-sections with different $P_{Dem-avg}$.

The main problem of this strategy may come at its real-time implementation, as the real P_{Dem} profile may not coincide with the profile used in the EMS design step. Therefore, in order to prevent issues related to an underestimation or overestimation of the required P_{FC} values, the use of a controller to adjust P_{FC-ref} is proposed. If the BT SOC is lower than the initial value when reaching the end of a specific section, it means that the P_{FC-ref} value has not been properly adjusted to the real mean demand of the route. Therefore, the value has to be increased in the next section in order to recover the original SOC. The opposite should be made in case the SOC value is higher than the expected one. Therefore, the controller depicted in Figure 4.5 is proposed for the implementation of RB3: depending on the SOC error (e_{SOC} [%]) the controller adjusts the K_{RB3} [−] gain, which is used to vary the original FC reference point set at $P_{Dem-avg}(s)$.

The controller acts just at the beginning of each section. Therefore, it is assumed

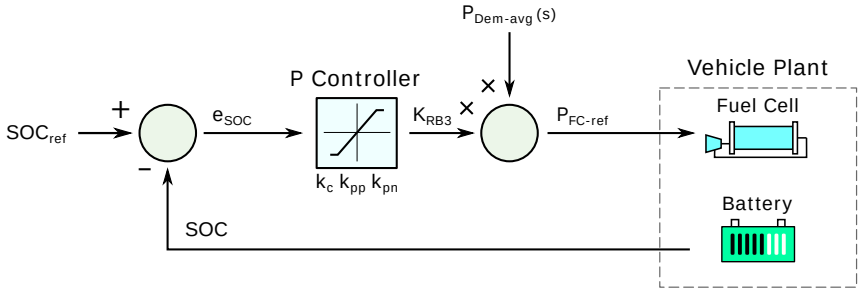

Figure 4.5: Working principle of the controller proposed for RB3.

that a simple proportional controller is enough to obtain an appropriate system response. In order to improve the effectiveness of the EMS, the use of two different proportional gains is proposed, one for a positive error (k_{pp} [−]) and one for a negative error (k_{pn} [−]). Besides, a constant gain is also used (k_c [−]), so as the value K_{RB3} is always positive. Consequently, K_{RB3} is calculated as follows:

$$K_{RB3} = \begin{cases} k_c + k_{pp} \cdot e_{SOC} & \text{for } e_{SOC} \geq 0 \\ k_c + k_{pn} \cdot e_{SOC} & \text{for } e_{SOC} < 0 \end{cases} \tag{4.1}$$

As it can be deduced, the proportional controller gains k_{pp} and k_{pn} and k_c may affect the EMS effectiveness. In a first approach, these values have been defined based on the conclusions obtained after some first tests. Specifically, values 0.0625, 0.05 and 1 have been defined for k_{pp}, k_{pn} and k_c, respectively. Besides, the SOC_{ref} value used to calculate the SOC error is fixed at SOC_0. However, this parametrization does not ensure an optimal operation. Therefore, in a second approach these values are optimized by means of a GA-based optimization method. Section 4.3 will give further information regarding how is this optimization approach coupled with the powertrain design optimization.

In order to differentiate between both parametrizations, the strategy with the manually tuned values will be denoted just as the Demand Adaptive Controller (RB3), and the strategy with the optimized values will be denoted as the Optimized Demand Adaptive Controller (GA-RB3).

4.2.1.4 OB - Dynamic Programming (DP)

DP consists on an algorithm that, based on Bellman's optimality principle, returns the optimal control trajectory that minimizes a certain cost function. DP strategy was already introduced and evaluated in the H-DEMU case study (Section 3.2.1.6), therefore in this section just the differences compared to that case study will be highlighted.

In the case of the H_2EMU case study, the same state variable (ι) will be maintained: $\iota = SOC$. However, the control variable (Φ) and cost function (J) are varied. Logically, Φ is changed to the FC reference P_{FC-ref}, being this the primary power source. And

for the cost function, J includes an additional term apart from the reduction of fuel use. The objective of this addition is to reduce the changes in the FC working point, what may ensure a longer FC lifetime. The following equations review the definitions of these variables and functions:

$$\Phi(k) = P_{FC-ref}(k) \tag{4.2}$$

$$\iota(k) = SOC(k) \tag{4.3}$$

$$J = \sum_{k=0}^{K-1} \Big(\gamma \cdot \dot{m}_{H2}\big(\Phi(k)\big) + \lambda \cdot \Delta P_{FC}\big(\Phi(k)\big) \Big) \cdot \Delta t \tag{4.4}$$

where γ [−] and λ [−] are the weight factors that give more importance to the reduction of hydrogen use ($\dot{m}_{H2}$) or to the reduction of deviations in the FC operation point (ΔP_{FC}). γ [−] and λ [−] have been tuned so that the maximum allowable ΔP_{FC} is respected.

As in the previous case study, the optimization problem also requires the specification of some constraints, which are defined as in Equation 4.5. As in this case study there are not electrified sections, the state variable (SOC) in the end of the simulation is defined to be at the same value as in the beginning of the simulation. Besides, the SOC is also constrained by the maximum and minimum allowable values. Finally, the control variable (P_{FC-ref}) is allowed to vary between the idle load point and the full load point.

$$\begin{cases} \iota(0) = SOC_0 \\ \iota(K) = SOC_0 \\ 20 \leq \iota(k) \leq 90 \\ P_{FC-min} \leq \Phi(k) \leq P_{FC-max} \end{cases} \tag{4.5}$$

In short, DP returns the optimal sequence of Φ that minimizes the defined cost function. As already highlighted in previous chapters, this sequence is only valid for the specific context (i.e., the specific drive cycle) for which the optimization is deployed. This makes the on-line implementation of DP practically unfeasible. Due to this reason, DP results are commonly used just as baseline for benchmarking other strategies. It is worth to mention that the DP algorithm integrated in the current Ph.D. Thesis is based on the function and scripts developed in [188] and available in [189].

4.2.1.5 LB - Neuro-Fuzzy Learning Based Controller (ANFIS)

In order to overcome the main disadvantage of DP optimization, in this Ph.D. Thesis the use of a LB strategy is proposed. The selected LB approach is the ANFIS, which was already introduced for the H-DEMU case study. Therefore, in this section just a brief review of the development and implementation of this strategy is given. The reader is referred to Section 3.2.1.7 for further detail.

In short, the objective of the ANFIS approach is to train a FL-based controller with data obtained from DP optimizations, so the controller is able to replicate in real-time the operation proposed by DP. Figure 4.6 shows the general overview of the ANFIS based learning technique, which is reviewed in the following paragraphs:

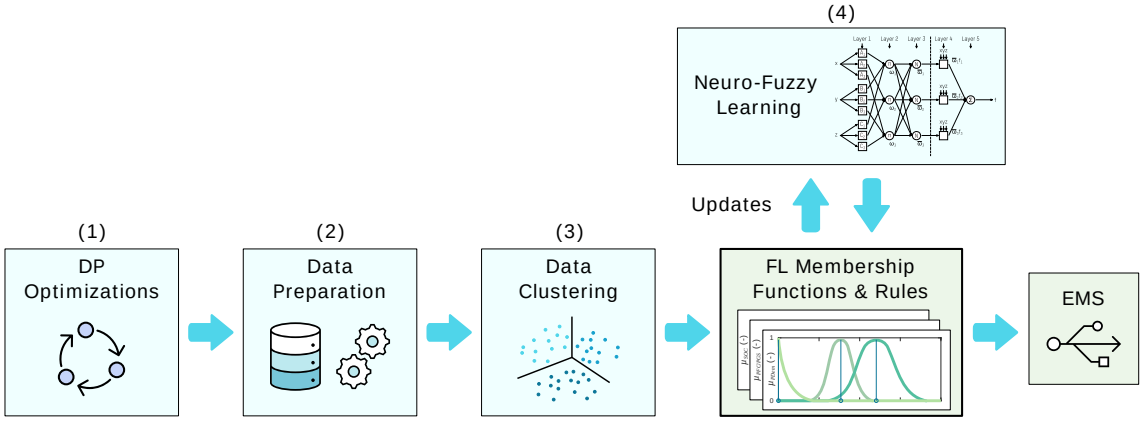

Figure 4.6: Overview of ANFIS based learning technique [27].

(1) In the first step, the data required for the training step is generated. The ANFIS controller should be robust to different contexts. Therefore, the DP data generated for the ANFIS training step is obtained optimizing the H_2EMU operation under different drive cycles. These drive cycles are generated varying the number of passengers (±7%) and the auxiliaries consumption (±30%) set in the nominal scenario, which will be presented in Section 4.2.4.

(2) Once the DP optimizations are completed, the data required by the ANFIS training is processed. The training requires a set of inputs and outputs, which will be the inputs and outputs required by the controller during real operation. Specifically, the BT SOC, length-ratio, and P_{Dem} profiles are set as the inputs, and the P_{FC-ref} profile as the output. The inputs and outputs are normalized within [0,1].

(3) The next step consists on the generation of the initial FL design, which is developed based on the subtractive-clustering technique of the datasets. This FL structure includes the initial designs for the membership functions and rules.

(4) Once the initial FL design is obtained, the next step consists on the ANFIS training. The training aims tuning the membership functions and refining the rules originally proposed by the data sub-clustering. For this approach, the 80% of the original DP data is used, as the other 20% is used to test the effectiveness of the learning process.

Eventually, once the training step is finalized, the FL-based controller is obtained, which can be implemented on-line in the H_2EMU.

4.2.2 Battery Chemistries

After explaining all the control strategies, this subsection focuses on the different BT chemistries that will be analysed in this case study. As it was defined in the H-DEMU case study, the following BT chemistries are analysed: LTO, NMC and LFP. The main characteristics and parameters of these chemistries were already detailed in Section 3.2.2, therefore the information given in the following tables is the same.

Table 4.2 shows the parameters related to the characterization of each BT chemistry. This information refers to the parametrization at cell level and at BOL. Moreover, Table 4.3 shows the characteristics of the proposed BT modules. Indeed, in the LCC optimization step the number of BT modules is optimized (variable n_{BT}). In order to obtain a fair comparison between the different BT capacities, modules with the same nominal energy (20 kWh) have been proposed for the 3 chemistries. Regarding the estimation of the degradation suffered by each BT chemistry, the degradation model introduced in Section 2.3.5 and the parametrizations given in Table 2.6 have been implemented.

Table 4.2: Characterization of BT cells.

Parameter	LFP	NMC	LTO
Q_{BT_0}	28 Ah	46 Ah	23 Ah
V_{BT_nom}	3.2 V	3.7 V	2.3 V
R_{nom}	1.8 mΩ	1.9 mΩ	1.2 mΩ
V_{BT_max}	3.6 V	4.2 V	2.7 V
V_{BT_min}	2.5 V	3 V	1.7 V
C_{max_ch}	4 C	3 C	4 C
C_{max_dch}	6.5 C	5 C	4.5 C
SOC_{max}	90 %	90 %	90 %
SOC_{min}	20 %	20 %	20 %

Table 4.3: Characterization of BT modules.

Parameter	LFP	NMC	LTO
E_{BT}	20 kWh	20 kWh	20 kWh
n_{cell}	112	118	189
m_{cell}	2	1	2
ρ_{BT_L}	81.1 Wh/L	112.2 Wh/L	52.8 Wh/L
ρ_{BT_E}	47.9 Wh/kg	86.9 Wh/kg	53.3 Wh/kg

4.2.3 Economic Model Parametrization

Once the EMSs and BT chemistries have been described, this subsection focuses on the parameters of the economic model that are used in the different sensitivity analyses. As in the previous case study, first a nominal parametrization is defined. This parametrization is used in the sensitivity to the powertrain design and in the sensitivity to the drive cycle. Secondly, based on the nominal parametrization, some parameters are selected and their sensitivity is analysed. This second parametrization is used in the sensitivity to the

parameters of the economic model (see Figure 2.2).

4.2.3.1 Nominal Parametrization

The nominal parametrization is depicted in Table 4.4. These values have been defined based on the parametrizations proposed in similar literature works [27, 48, 55, 195]. The parameters without a reference are own assumptions, which have been defined together with CAF Power & Automation.

Table 4.4: Nominal parameters for economic evaluation.

	Parameter	Value	Reference
General Parameters	Y	30 years	-
	I	2.5 %	-
	t_{op}	320 days/year	-
	t_{day}	15 h/day	-
Acquisition Costs	C_{train}	8,000,000 €	-
	c_{BT} - LTO	1500 €/kWh	[27, 195]
	c_{BT} - NMC	800 €/kWh	[27, 195]
	c_{BT} - LFP	1040 €/kWh	[48]
	c_{FC}	1000 €/kW	[48, 55]
Operation Costs	c_{H_2}	11 €/kg	[27]
Maintenance costs	c_{maint}	200,000 €/year	-

4.2.3.2 Scenarios for Sensitivity Analysis to Economic Model

Some of the parameters defined in the nominal scenario are understood to be unsteady, that is to say, they can easily vary from one context to another. This is the reason why these parameters are identified and their sensitivity is analysed. Specifically, the daily operation hours (t_{day}) may vary depending on the railway line or project, and the BT price (c_{BT}) may vary depending on the selected manufacturer. In addition, FC technology is regarded as an emerging technology, and therefore it is considered that both FC and hydrogen prices (c_{FC} and c_{H_2}) are subjected to big reductions in the near future [198].

For these parameters low, medium and high scenarios (LS, MS and HS, respectively) have been defined, as in the H-DEMU case study. Table 4.5 shows the values proposed for each variable. In the following lines the reasons behind these values are explained.

Table 4.5: Sensitivity to parameters of economic model.

Parameter	Low	Medium	High
t_{day}	5 h/day	10 h/day	15 h/day
c_{BT} - LTO	1200 €/kWh	1500 €/kWh	1800 €/kWh
c_{BT} - NMC	640 €/kWh	800 €/kWh	960 €/kWh
c_{BT} - LFP	520 €/kWh	1040 €/kWh	1560 €/kWh
c_{FC}	500 €/kW	800 €/kW	1000 €/kW
c_{H_2}	3 €/kg	7 €/kg	11 €/kg

- Regarding t_{day}, it is considered that it is more probable to have operation hours behind 15 h/day. Therefore, the nominal value is defined at the HS, and for the other scenarios reductions of the 33% and 66% are defined.
- The scenarios for the BT prices have been defined as in Chapter 3, following an analysis of the market prices. For further information, see Section 3.2.3.
- In the case of c_{FC}, it is not clear until which extend could its price go down in the future. Therefore, a high variability has been defined, in order to cover as many scenarios as possible. The nominal scenario is defined in the HS, and for the MS and LS a 20% and 50% reduction have been defined.
- Finally, in the case of c_{H_2}, the nominal value is also defined in the HS. For the MS and LS, the prices have been defined according to the scenarios given by the International Energy Agency (IEA) in [198]: 7€/kg refers to a scenario in which the hydrogen is generated from the grid electricity, and 3€/kg to a scenario in which the hydrogen is generated from electricity fully produced by renewable sources.

4.2.4 Driving Cycles

The last concept whose sensitivity will be analysed is the driving cycle. In this subsection all the driving cycles used in the different sensitivity analyses are explained. As in the case of the economic model, first a nominal case is defined. This case is used when analysing the sensitivity to the powertrain design and the sensitivity to the parameters of the economic model. Then, a series of driving profiles with different characteristics are proposed to develop the sensitivity to the driving cycle.

4.2.4.1 Nominal Driving Cycle

The nominal case is based on an existing railway line, which is denominated "Tardienta - Canfrac" line. Figure 4.7 shows the map of the line and Figure 4.8 depicts the corresponding speed profile, which corresponds to the round trip route. In both cases the locations of the stations are specified. The round trip route is composed of 313.2 km and 22 stations, and it is completed in 5 hours and 9 minutes.

The input required for the simulation model is the traction demand profile (P_{EM}), as it was explained in Section 2.3.1. Figure 4.9 depicts the demand profile provided by CAF Power and Automation. It is worth to mention that this profile already considers the demand from the auxiliaries, and therefore it refers to P_{Dem} ($P_{Dem} = P_{EM} + P_{Aux}$).

4.2.4.2 Scenarios for Sensitivity Analysis to Driving Cycle

For the development of the sensitivity analysis to the driving cycle, scenarios of different characteristics are required. As in the H-DEMU case study, synthetic driving cycles are

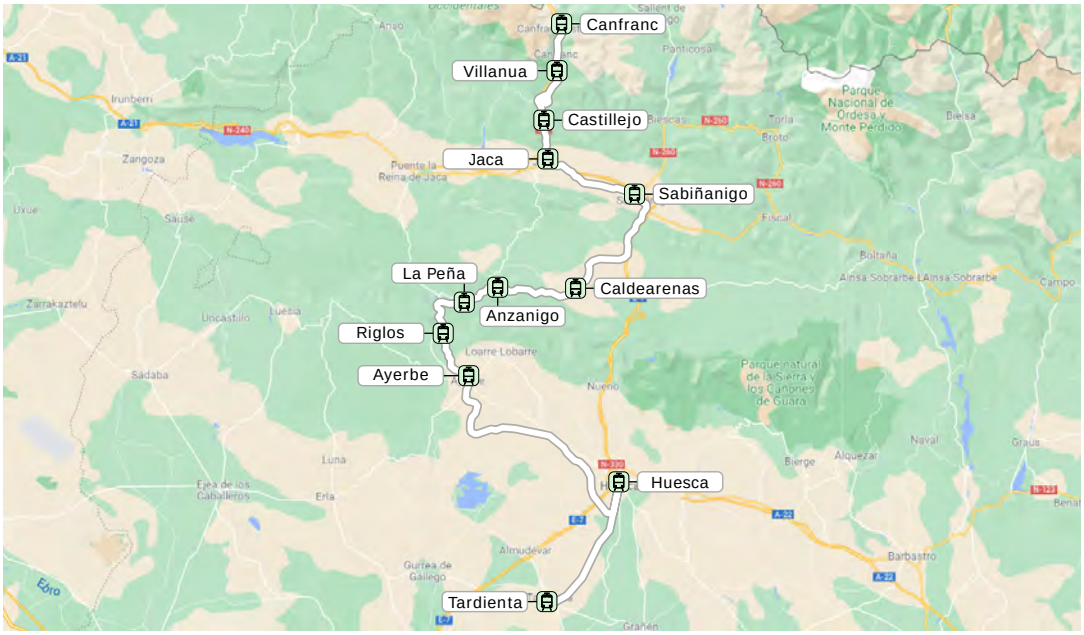

Figure 4.7: Journey of "Tardienta - Canfranc" railway line.

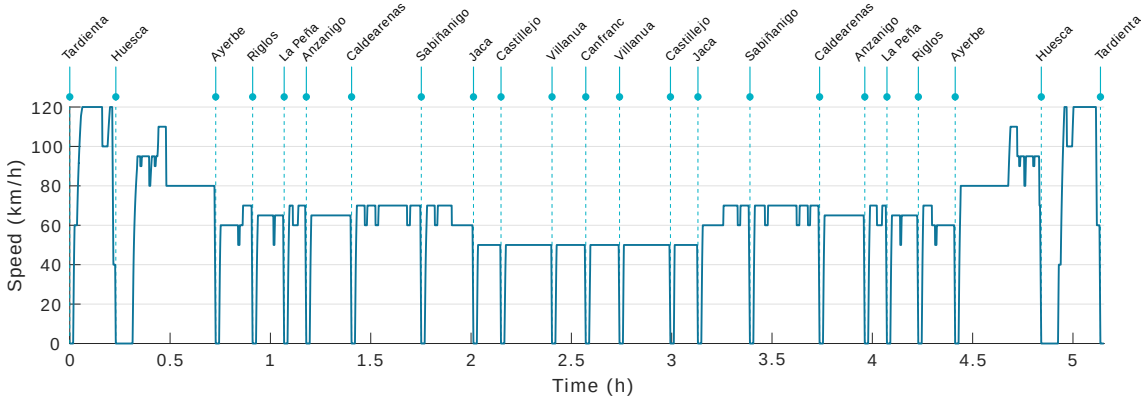

Figure 4.8: Speed profile of "Tardienta - Canfranc" railway line.

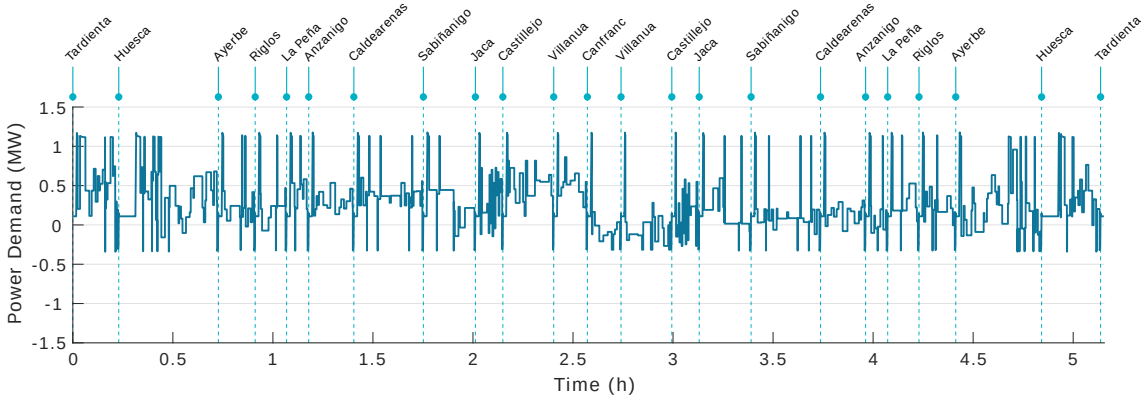

Figure 4.9: Power demand profile of "Tardienta - Canfranc" railway line.

used for this approach, as it is difficult to obtain information from many real railway lines. Two variables have been defined as the design criteria of the generated synthetic cycles, since they are representative of the characteristics of the driving cycles: the average power demand and the total energy demand. Anyway, as the average power demand and the total energy demand are correlated, the duration of the route has been used as design criteria instead of the total energy demand. These variables coincide with the ones used in the previous case study.

In order to generate the synthetic cycles, the "Tardienta - Canfranc" profile has been divided into station to station sub-profiles. Then, these sub-profiles have been combined to obtain driving cycles of diverse durations and average power demands. In order to obtain a sufficient dispare matrix of cases, 3 average power demands (100 kW, 300 kW, and 500 kW) and 4 running times (1 h, 3 h, 5 h and 7 h) have been proposed.

As the number of potential combinations of the sub-profiles is limited, the exact proposed values cannot be obtained. Figure 4.10 depicts the real matrix of the generated driving cycles. For each driving cycle, the total energy demand is also given. The obtained approximation is understood to be appropriate, as the aim of this approach is not to analyse the operation of the H_2EMU in drive cycles of exact characteristics. The graphs of the generated synthetic cycles can be found in Appendix A.

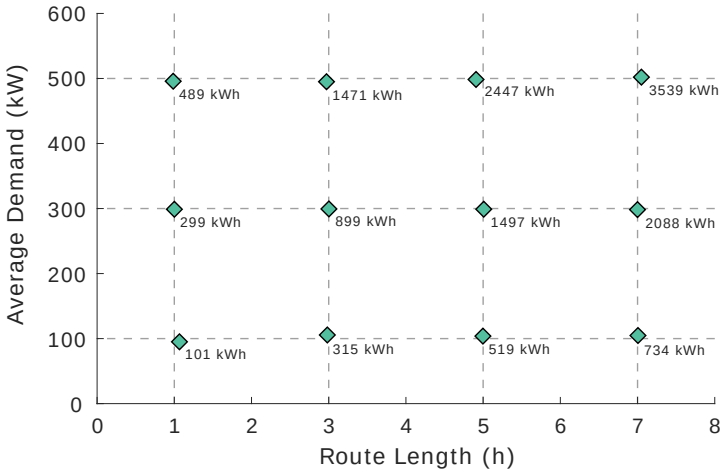

Figure 4.10: Matrix of generated synthetic driving cycles.

4.3 Definition of Optimization Problem

After presenting all the cases of the sensitivity analysis, this section focuses on the optimization problem. As it was explained in Chapter 2, the holistic design methodology proposed in the current Ph.D. Thesis includes the LCC optimization of each case of the sensitivity analysis. In the current case study related to the H_2EMU, this LCC optimization is focused on obtaining the cost-efficient powertrain sizing (n_{BT} and n_{FC}), initial BT SOC (SOC_0), and in some cases also the optimal EMS parameters.

In Section 2.4 generic methodologies to solve this optimization problem were introduced. As explained there, the optimization problem may differ depending of the strategy being analysed. Therefore, in this section these generic optimization methodologies are particularized for the EMSs introduced in this case study. Figure 4.11 shows the classification of optimization problems according to the EMS. The classification is further detailed below:

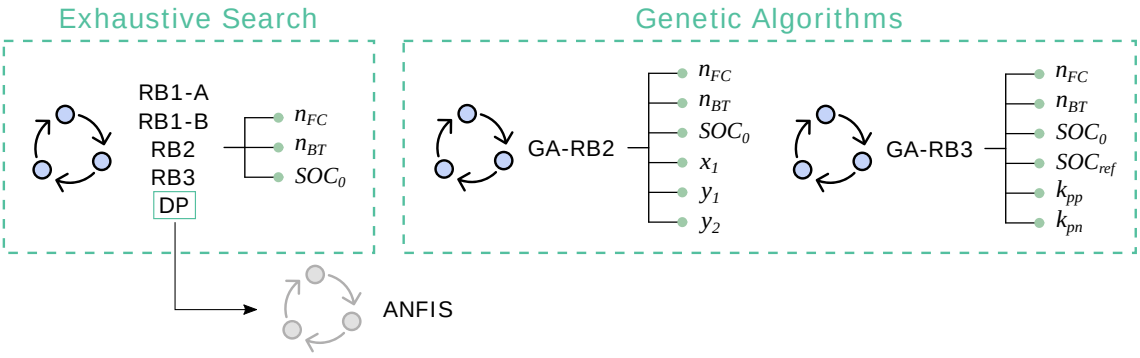

Figure 4.11: Distribution of Optimization approaches according to EMS.

(1) In the case of RB strategies (RB1-A, RB1-B, RB2 and RB3), the EMS is not optimized. Hence, as the number of optimization variables is low (n_{BT}, n_{FC} and SOC_0), the exhaustive search based optimization introduced in Section 2.4.1 is deployed. This generic optimization problem is particularized in Section 4.3.1.

(2) In the case of OB strategies, different design coordination concepts are deployed. On the one hand, in the case of DP the optimization is conducted in two levels. In the outer level, the powertrain sizing (n_{BT} and n_{FC}) and initial SOC value (SOC_0) are optimized (remember that in the case of the H_2EMU the initial and final SOC values coincide). Then, in the inner level the DP optimization is deployed for the specific n_{BT}, n_{FC} and SOC_0 values being evaluated in the outer level. That is to say, a nested optimization is deployed. The optimization variables of the outer level coincide with the ones of the RB strategies. Therefore, the same exhaustive search based optimization will be used for the outer level of DP.

(3) On the other hand, in the case of GA-RB2 and GA-RB3, the optimization is conducted in a single level, as all the variables are optimized together. That is to say, a simultaneous optimization approach is deployed. In this case, the GA-based approach introduced in Section 2.4.2 is deployed, as the number of optimization variables is higher. The generic problem introduced in that section is particularized in Section 4.3.2 for GA-RB2 and in Section 4.3.3 for GA-RB3.

(4) Finally, the ANFIS strategy is understood to be the real-time implementation of DP. Therefore, no optimization is deployed in this case, as the n_{BT}, n_{FC} and SOC_0 values obtained in the case of DP are used to calculate the LCC.

The fitness function is the same in all the mentioned optimization problems, as it consists on the minimization of the LCC. The fitness function is defined as follows:

$$minimize\ LCC(X)\ \mid\ X \in \Pi \tag{4.6}$$

where X represents the vector containing the optimization variables, and Π represents the space of feasible solutions. X and Π vary depending on the specific optimization problem, and therefore they are detailed in the following subsections.

It is worth to mention that in all the optimization problems, each n_{BT} refers to a 20 kWh BT module (as in the H-DEMU case study), and each n_{FC} to a 100 kW FC module. The definition of the remainder variables depends on the specific optimization problem, and therefore they are described in the following subsections.

4.3.1 Exhaustive Search Optimization

The exhaustive search optimization is deployed when analysing RB1-A, RB1-B, RB2, RB3, and DP strategies. The optimization variables vector X_{ES} and the space of feasible solutions Π_{ES} are defined in Equations 4.7 and 4.8. Π_{ES} has to be discretized into a feasible number of cases, so the optimization time is not extended too much. In the case of n_{FC} and n_{BT}, they are defined as natural numbers. n_{FC} ranges between 0 and the maximum number of FC modules (N_{FC} [−]). The case without FC modules refers to the BEMU. Besides, n_{BT} ranges between 1 and the maximum number of BT modules (N_{BT} [−]). The option of not deploying batteries is not considered, as the FC has to be always supported by a secondary power source. In the case of SOC_0, it has been discretized in steps of the 10%, and then just the minimum and maximum values (20% and 90%) are not considered, as they hardly lead to a feasible solution.

$$X_{ES} = \begin{bmatrix} n_{BT} \\ n_{FC} \\ SOC_0 \end{bmatrix} \tag{4.7}$$

$$\Pi_{ES} = \begin{cases} 1 \leq n_{BT} \leq N_{BT} \ \rightarrow n_{BT} \in \mathbb{Z} \\ 0 \leq n_{FC} \leq N_{FC} \ \rightarrow n_{FC} \in \mathbb{Z} \\ 30 \leq SOC_0 \leq 80 \ \rightarrow SOC_0 \in \{30, 40, ... 80\} \end{cases} \tag{4.8}$$

As it can be deduced, N_{FC} and N_{BT} are important constraints for the optimization problem. In order to obtain a realistic solution, it has been assumed that there is a maximum available space and weight in the vehicle for the integration of the FC and BT modules. This space is common for both traction sources. Therefore, this means that N_{BT} depends on n_{FC}, or that N_{FC} depends on n_{BT} (both dependencies rely on the same idea). In other words, depending on the number of FC modules that are being analysed, the maximum number of BT modules changes (and vice versa).

As in the case of the H-DEMU, the maximum allowable volume and weight values for the powertrain elements have been provided by CAF Power and Automation. This space is divided into 4 compartments, and it is considered that each space can be only filled by FC or BT modules, but not a combination of both. The volume and weight of each FC module has been estimated from the characteristics of commercial systems [128, 199]. From these values, it is calculated that the maximum number of FC modules at each compartment is 3 ($N_{FC} = 3$). Then, considering the density of each BT chemistry (see Table 4.3), the relation between N_{BT} and n_{FC} is obtained. Figure 4.12 depicts this relation. The same graph would be depicted to represent the relation between N_{FC} and n_{BT}.

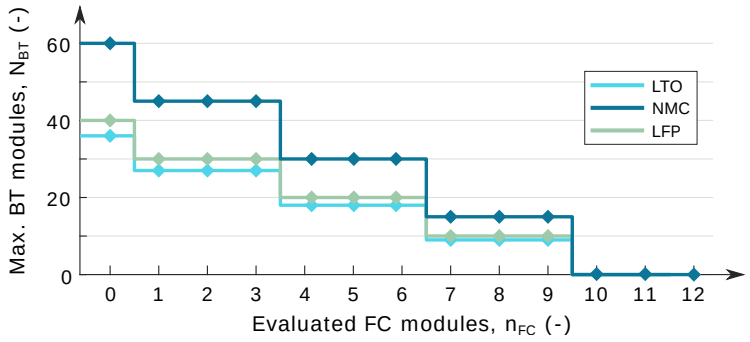

Figure 4.12: Relation of maximum number of FC and BT modules.

4.3.2 GA-RB2 Optimization

In this subsection, the generic Genetic Algorithm (GA) optimization presented in Section 2.4.2 is particularized for the case of GA-RB2. The optimization variables vector X_{GARB2} and the space of feasible solutions Π_{GARB2} are defined in Equations (4.9) and (4.10), respectively. In the case of the GA optimization, the defined space of feasible solutions does not exponentially increase the number of solutions to be evaluated. Therefore, a wider space is defined for the SOC, which ranges between SOC_{min} and SOC_{max}. The same space is defined for x_1. In the case of y_1 and y_2, they are constrained between the minimum and maximum FC operation points. Additionally, another constraint for these variables is defined in Equation (4.11). This makes y_2 be higher than y_1, what ensures that the FC operation point is reduced as the SOC goes higher (which is indeed the objective of RB2 strategy, see Figure 4.3).

$$X_{GARB2} = \begin{bmatrix} n_{BT} \\ n_{FC} \\ SOC_0 \\ x_1 \\ y_1 \\ y_2 \end{bmatrix} \tag{4.9}$$

$$\Pi_{GARB2} = \begin{cases} 1 \leq n_{BT} \leq N_{BT} \ \rightarrow n_{BT} \in \mathbb{Z} \\ 0 \leq n_{FC} \leq N_{FC} \ \rightarrow n_{FC} \in \mathbb{Z} \\ 20 \leq SOC_0 \leq 90 \ \rightarrow SOC_0 \in \mathbb{R} \\ 20 \leq x_1 \leq 90 \ \rightarrow x_1 \in \mathbb{R} \\ P_{FC-min} \leq y_1 \leq P_{FC-max} \ \rightarrow y_1 \in \mathbb{R} \\ P_{FC-min} \leq y_2 \leq P_{FC-max} \ \rightarrow y_2 \in \mathbb{R} \end{cases} \tag{4.10}$$

$$subject\ to: y_1 < y_2 \tag{4.11}$$

Moreover, Table 4.6 shows the relation of the parameters required by the GA. The population size is defined as 10 times the number of optimization variables. For the elite count and crossover fraction, the typically recommended values are defined [18]. In order to avoid a long running time, a maximum number of generations, a maximum number of stall generations and a maximum optimization time are defined, as in the H-DEMU case study. These values have been defined with the aim of obtaining a balance between the required running time and the optimality of the obtained solution.

Table 4.6: Parameters for the Genetic Algorithm in GA-RB2 optimization.

Parameter	Value	Parameter	Value
Population size	60	Max. generations	100
Elite count	5 %	Max. stall generation	50
Crossover fraction	80 %	Max. optimization time	24 h

4.3.3 GA-RB3 Optimization

As previously explained, in the case of GA-RB3 strategy another GA-based optimization is deployed. In this subsection, the details of this optimization are given. First, the equations below show the optimization variables vector X_{GARB3} and the space of feasible solutions Π_{GARB3}. These include the specific variables being optimized in the case of this strategy. SOC_0 and SOC_{ref} variables are constrained by the allowable SOC window (20-90%), as in the case of GA-RB2. For the positive and negative gains of the controller (k_{pp} and k_{pn}, respectively), the feasible space has been defined based on the conclusions obtained after same first tests.

$$X_{GARB3} = \begin{bmatrix} n_{BT} \\ n_{FC} \\ SOC_0 \\ SOC_{ref} \\ k_{pp} \\ k_{pn} \end{bmatrix} \tag{4.12}$$

$$\Pi_{GARB3} = \begin{cases} 1 \leq n_{BT} \leq N_{BT} \ \rightarrow n_{BT} \in \mathbb{Z} \\ 0 \leq n_{FC} \leq N_{FC} \ \rightarrow n_{FC} \in \mathbb{Z} \\ 20 \leq SOC_0 \leq 90 \ \rightarrow SOC_0 \in \mathbb{R} \\ 20 \leq SOC_{ref} \leq 90 \ \rightarrow SOC_{ref} \in \mathbb{R} \\ 1 \leq k_{pp} \leq 10 \ \rightarrow k_{pp} \in \mathbb{R} \\ -5 \leq k_{pn} \leq 1 \ \rightarrow k_{pn} \in \mathbb{R} \end{cases} \tag{4.13}$$

In addition, Table 4.7 shows the relation of the parameters required by the GA, which in this case coincide with the values proposed in the GA-RB2 optimization.

Table 4.7: Parameters for the Genetic Algorithm in GA-RB3 optimization.

Parameter	Value	Parameter	Value
Population size	60	Max. generations	100
Elite count	5 %	Max. stall generation	50
Crossover fraction	80 %	Max. optimization time	24 h

4.4 Results of Sensitivity Analysis to Powertrain Design

Once all the information required to launch the proposed design methodology has been provided, this section focuses on presenting the results of the sensitivity analysis to the powertrain design, which is indeed the first step of the mentioned methodology. As explained in Chapter 2, this first sensitivity analysis is focused on comparing the results of different EMSs and BT chemistries. Figure 4.13 depicts where is the current sensitivity analysis located in the overall design methodology. The nominal parametrization of the economic model and the nominal driving cycle have been used to obtain these results.

This section is divided into several subsections to ease the evaluation of the obtained results. In a first step, in Section 4.4.1 the raw results of the LCC optimization are presented. Then, the analysis of Section 4.4.2 focuses specifically on the LCC values obtained by the different EMSs and BT chemistries. Besides, in Section 4.4.3 the correlations between these LCC values and the variables returned by the optimization approach are highlighted. Section 4.4.4 focuses on the key cost terms of the economic model, and on how do they influence the overall LCC. Specifically, the cost terms that can vary between the different solutions are analysed: C_{FC}, C_{BT}, C_{H_2}, C_{FCrepl} and C_{BTrepl}.

When evaluating different EMSs it is important to consider more features than just the optimality in relation to the hydrogen use or the lifetime of the powertrain sources, which in the proposed approach are gathered in the LCC. As highlighted in Chapter 1, features such as the real time execution or the robustness to potential disturbances are also important. Therefore, in Section 4.4.5 the robustness and real time execution of the proposed control strategies are addressed. Finally, in Section 4.4.6 the main conclusions of the first sensitivity analysis are reviewed.

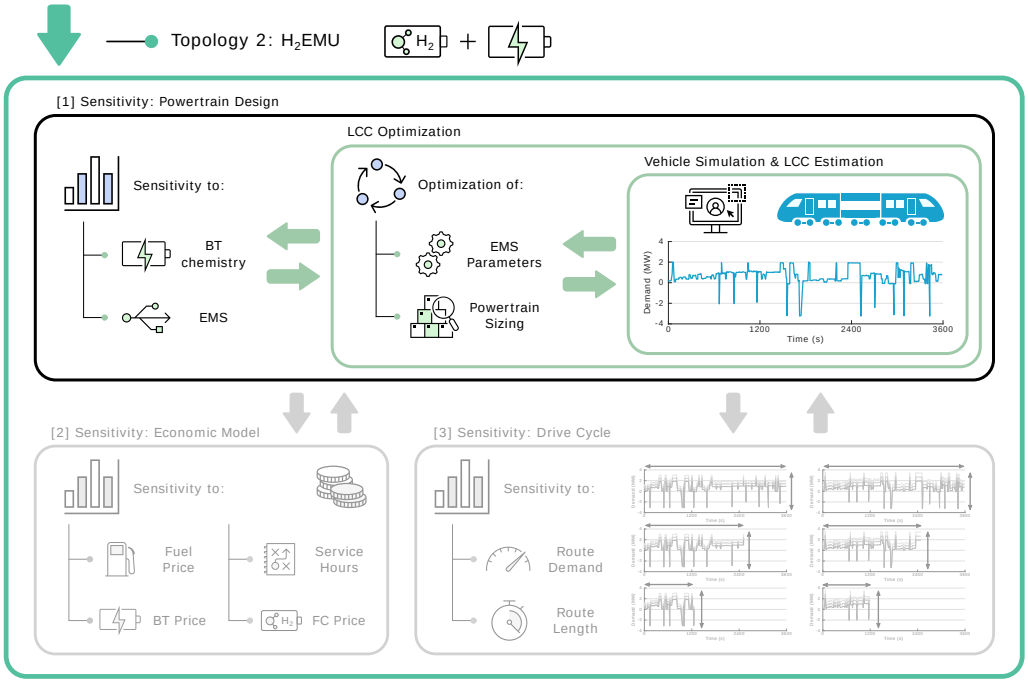

Figure 4.13: Current step of holistic design methodology.

4.4.1 Results of LCC Optimization

Table 4.8 presents a review of the results obtained when optimizing the LCC of each case of the sensitivity analysis. Each row introduces the results for a combination of BT chemistry and EMS, that is to say, the results for a case of the sensitivity analysis. In the first row the results of a conventional DEMU are also given. The DEMU is sized with a genset of 1500 kW (minimum value to provide the traction power peaks), and it is used as reference to compare the results of the sensitivity analysis. The reason to use the DEMU as a reference is that nowadays it is the most common vehicle for non-electrified lines.

In addition, at each column a representative parameter is given. First, the LCC value is depicted, that is to say, the optimization fitness function. This value is given in p.u. in relation to the LCC of the DEMU. In the following columns, the optimization variables returned by the optimization approach are given: n_{FC} (in kW), n_{BT} (in kWh) and SOC_0 (in %). After these values, a breakdown of the LCC into the key cost terms of the economic model is given: FC acquisition cost (C_{FC}), BT acquisition cost (C_{BT}), hydrogen use cost (C_{H_2}), FC replacement cost (C_{FCrepl}) and BT replacement cost (C_{BTrepl}). These values are also given in p.u. in relation to the LCC of the DEMU. C_{train} and C_{maint} are not given, as they are the same in all the cases. This is the reason why the sum of the cost terms given in the table does not coincide with the overall LCC. Eventually, the last columns depict the results returned by the FC and BT lifetime estimation models, respectively.

It is worth to mention that in Table 4.8 only the optimization variables shared in all the cases are shown, while the specific optimization variables of strategies GA-RB2 and GA-

Table 4.8: Sensitivity analysis to the powertrain design: representative results.

		LCC $(p.u.)$	n_{FC} (kW)	n_{BT} (kWh)	SOC_0 (%)	C_{FC} $(p.u.)$	C_{BT} $(p.u.)$	C_{H_2} $(p.u.)$	C_{FCrepl} $(p.u.)$	C_{BTrepl} $(p.u.)$	y_{FC} $(y.)$	y_{BT} $(y.)$
DEMU		1.000	1500[1]	-	-	0.034[1]	-	0.414[1]	-	-	-	-
LTO	**RB1-A**	1.918	400	220	80	0.018	0.015	1.211	0.101	0.021	3.4	10.2
	RB1-B	2.095	400	220	80	0.018	0.015	1.428	0.061	0.021	5.5	10.2
	RB2	1.681	600	280	70	0.027	0.019	0.964	0.095	0.025	5.1	10.9
	GA-RB2	1.629	600	280	63.5	0.027	0.019	0.912	0.092	0.026	5.5	10.3
	RB3	1.684	600	360	80	0.027	0.025	0.958	0.093	0.029	5.3	12.1
	GA-RB3	1.651	600	260	76.2	0.027	0.018	0.938	0.093	0.024	5.3	10.4
	DP	1.593	600	300	70	0.027	0.021	0.872	0.093	0.028	5.4	10.3
	ANFIS	1.656	600	300	70	0.027	0.021	0.934	0.095	0.028	5.0	10.5
NMC	**RB1-A**	1.943	400	360	80	0.018	0.013	1.225	0.099	0.036	3.6	6.3
	RB1-B	2.107	400	340	70	0.018	0.013	1.428	0.061	0.035	5.5	6.1
	RB2	1.699	600	340	70	0.027	0.013	0.979	0.094	0.035	5.2	6.0
	GA-RB2	1.641	600	440	65.4	0.027	0.016	0.922	0.092	0.032	5.5	8.0
	RB3	1.690	600	460	80	0.027	0.017	0.966	0.093	0.035	5.3	7.6
	GA-RB3	1.659	600	460	60.1	0.027	0.017	0.947	0.093	0.023	5.3	10.2
	DP	1.589	600	560	60	0.027	0.021	0.869	0.092	0.028	5.4	10.2
	ANFIS	1.647	600	560	60	0.027	0.021	0.926	0.094	0.028	5.2	10.4
LFP	**RB1-A**	1.962	400	280	80	0.018	0.013	1.212	0.101	0.066	3.4	3.8
	RB1-B	2.138	400	320	80	0.018	0.015	1.428	0.061	0.064	5.5	4.4
	RB2	1.725	600	360	70	0.027	0.017	0.963	0.094	0.072	5.2	4.4
	GA-RB2	1.686	600	380	75.3	0.027	0.018	0.909	0.092	0.087	5.4	3.9
	RB3	1.715	600	400	80	0.027	0.019	0.957	0.093	0.067	5.3	5.0
	GA-RB3	1.696	600	360	77.4	0.027	0.017	0.934	0.093	0.072	5.4	4.3
	DP	1.669	600	400	60	0.027	0.019	0.858	0.092	0.121	5.4	3.0
	ANFIS	1.724	600	400	60	0.027	0.019	0.914	0.093	0.119	5.3	3.1

[1] In the case of the DEMU, n_{FC} value refers to n_{GS}, C_{FC} value to C_{GS}, and C_{H_2} value to C_f

Table 4.9: Additional optimization variables of GA-RB2 and GA-RB3.

		Optimization variables
GA-RB2	**RB**[1]	x_1=70.0%, y_1=11.67%, y_2=100.0%
	LTO	x_1=57.2%, y_1=16.06%, y_2=61.95%
	NMC	x_1=57.3%, y_1=17.28%, y_2=62.30%
	LFP	x_1=70.3%, y_1=17.74%, y_2=65.72%
GA-RB3	**RB**[1]	SOC_{ref}=80.0%, k_{pp}=0.0625, k_{pn}=0.0500
	LTO	SOC_{ref}=79.5%, k_{pp}=0.0264, k_{pn}=0.0661
	NMC	SOC_{ref}=63.2%, k_{pp}=0.0355, k_{pn}=0.0896
	LFP	SOC_{ref}=82.8%, k_{pp}=0.0210, k_{pn}=0.0045

[1] Refers to the RB parametrization

RB3 are given in Table 4.9. In both cases, RB refers to the rule-based parametrizations (RB2 and RB3, specifically), which are the same for the different BT chemistries.

In short, in this subsection a qualitative analysis of the optimization results has been provided. In the following subsections, a quantitative analysis of the variables presented in this subsection is carried out.

4.4.2 Analysis of LCC Values

This subsection is focused on comparing the LCC values of the different cases of the sensitivity analysis. Figures 4.14 and 4.15 are depicted to ease this analysis. Figure 4.14 presents the LCC values clustered according to the BT chemistry. Besides, the varying shapes and colours represent the different control strategies. The LCC values are given in the x-axis, and hence the values located at the left refer to a better solution. Then, in Figure 4.14 the LCC value of each case of the sensitivity analysis is divided into the key cost terms of the economic model: C_{FC}, C_{BT}, C_{H_2}, C_{FCrepl} and C_{BTrepl}. In this way, the difference in the cost terms can be also highlighted.

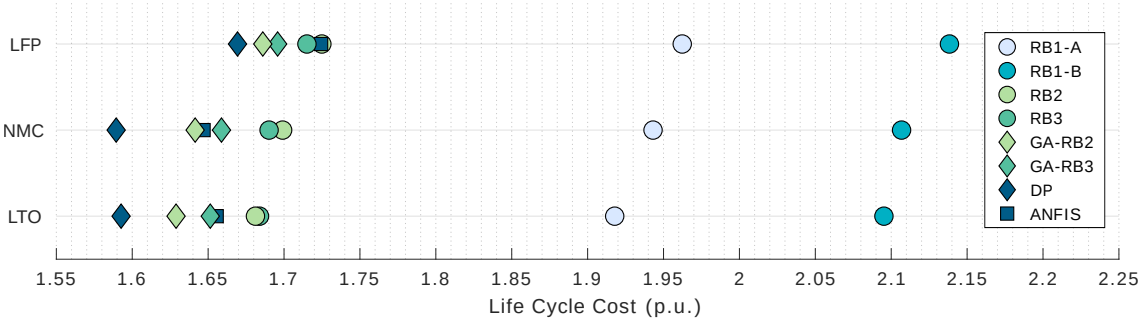

Figure 4.14: LCC results for different EMSs and BT chemistries.

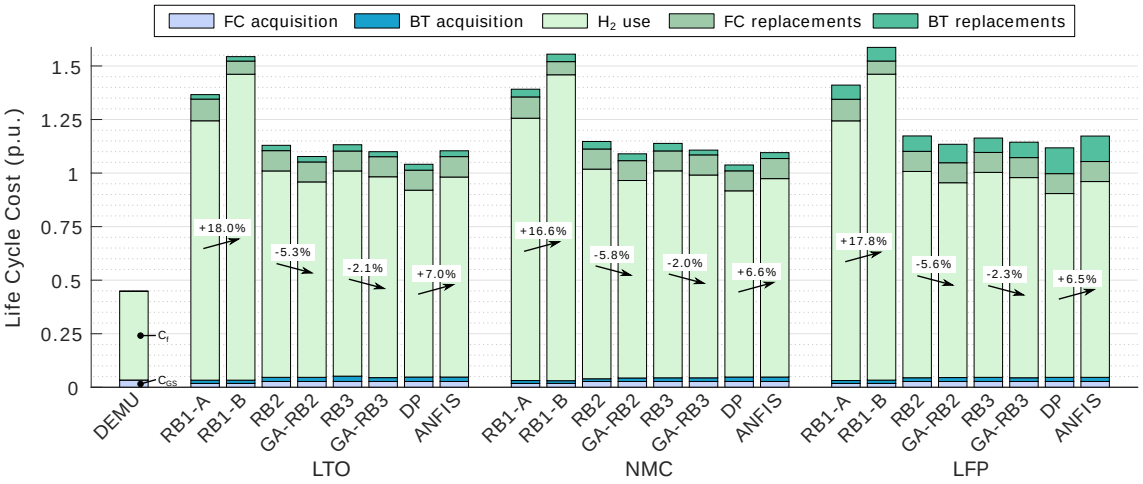

Figure 4.15: LCC breakdown into key cost terms.

A first evaluation of the LCC results unveils that in economic terms, the H_2EMU is far from the traditional DEMU. Even in the best cases of the H_2EMU, the LCC is nearly a 59% higher compared to the DEMU case (e.g., DP strategy with LTO or NMC chemistry). As it can be seen in Figure 4.15, the main reason comes due to the difference between the costs related to the use of hydrogen and diesel. Even in the cases that reduce most the C_{H_2} value (e.g., DP strategy), it doubles the C_f value of the DEMU. Therefore, a high reduction in the hydrogen price (c_{H_2}) is necessary for the H_2EMU to become a cost-effective solution compared to the DEMU. Indeed, in the best case of the sensitivity

analysis (DP strategy with NMC), c_{H_2} has to be reduced at least a 62%, what corresponds to a hydrogen price around 3.5€/kg. This issue is further discussed in Section 4.5.

4.4.2.1 Comparison of BT Chemistries

When comparing the results obtained by the different BT chemistries, it can be checked that LFP is behind the results obtained by the other two technologies. Comparing the results of the best strategy (DP in the three cases), the LCC of LFP is a 4.8% higher than LTO and a 5.0% higher than NMC. In the case of the remainder strategies, this difference is reduced. However, there is no case where the option of LFP is better than the other two chemistries. When looking to the more detailed results given in Figure 4.15, it can be concluded that the main difference between LFP and the remainder strategies is the higher cost related to the BT replacements. Indeed, LFP obtains similar results in the remainder cost terms (in some strategies it obtains even a lower hydrogen consumption than LTO), but the high C_{BTrepl} value inevitably penalises its results.

Regarding the results of LTO and NMC, it can be concluded that both chemistries are close in terms of LCC. LTO obtains a better result in the case of RB1-A (1.3% lower), RB1-B (0.6% lower), RB2 (1.1% lower), RB3 (0.4% lower), GA-RB1 (0.8% lower) and GA-RB2 (0.4% lower). On the contrary, NMC obtains a better result in the case of ANFIS (0.5% lower LCC) and DP (0.2% lower). Therefore, in most of the cases the difference is lower than the 1%. If the cost terms are compared, it can be concluded that the biggest difference is found in the BT acquisition and replacement costs: LTO requires a higher C_{BT} due to the higher price of the technology, but due to its much longer lifetime, it reduces C_{BTrepl} compared to NMC. In the two strategies where NMC improves the result of LTO, the improvement is obtained thanks to the hydrogen use reduction.

4.4.2.2 Comparison of Control Strategies

With the aim of adding further information to the comparison of the different EMSs, in the following pages the simulation results of all the cases of the sensitivity analysis are depicted in Figures 4.16 to 4.19. Each graph is composed of two subplots, which represent the FC power evolution and the SOC evolution, respectively. Both graphs help understanding the operation of the two H_2EMU power sources.

Starting with the results of the RB strategies, Figure 4.14 demonstrates that both variants RB1-A and RB1-B are far from the remainder strategies in terms of LCC. In the case of RB1-A, it obtains a LCC 20.4% higher than the best strategy (DP) and 13.9% higher than the closest strategy (RB3) when using LTO. In the case of the other two chemistries, similar values are also obtained: 22.3% and 14.4% higher in the case of NMC, and 17.6% and 13.7% higher in the case of LFP. Besides, the results of RB1-B are even worse than the results of RB1-A, as it obtains a LCC between 8.4-9.2% higher, depending on the chemistry.

Looking to the more detailed Figure 4.15, it can be checked that the main disadvantage of both strategies is their high hydrogen consumption. Compared to the strategy that most minimizes this consumption, RB1-A consumes between 38.9-41.3% more hydrogen, depending on the chemistry. In the case of RB1-B, these values are even higher: between 63.8-66.4% more hydrogen. Focusing on the differences between RB1-A and RB1-B, it is demonstrated that RB1-A obtains a lower hydrogen consumption, while RB1-B reduces the FC degradation (indeed, this was the objective when designing both strategies). The results of RB1-B show that the savings obtained by increasing the FC lifetime (between 38.4-39.6%, depending on the chemistry) do not payback the increase of the hydrogen consumption (between 16.6-18.0%). This demonstrates that in absolute numbers, reducing the hydrogen consumption is more important than increasing the FC lifetime. Consequently, RB1-A obtains by far a better result compared to RB1-B.

Focusing on the operation, the zoom into Figure 4.16a shows how in RB1-B the FC works always constantly, while in RB1-A there are frequent changes in the FC working point. This explains the differences in the hydrogen consumption and FC lifetime. Both graphs demonstrate that the operation of both powertrain sources is similar even when integrating different BT chemistries.

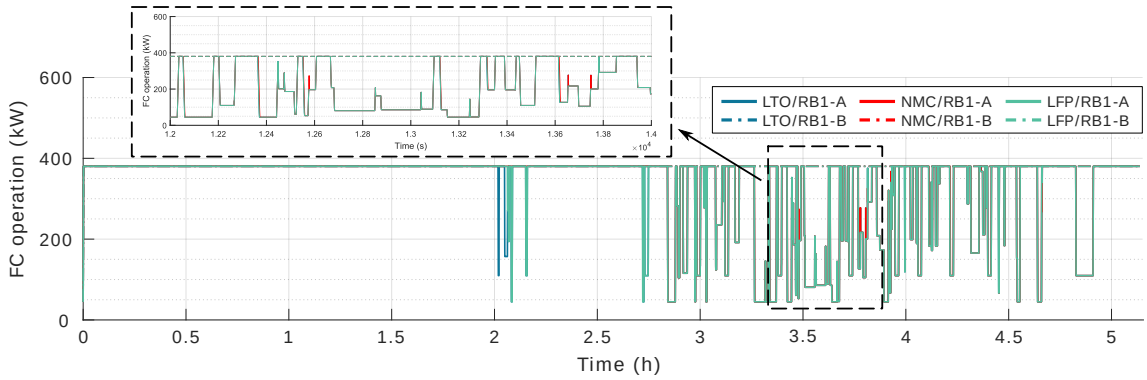

(a) FC Operation

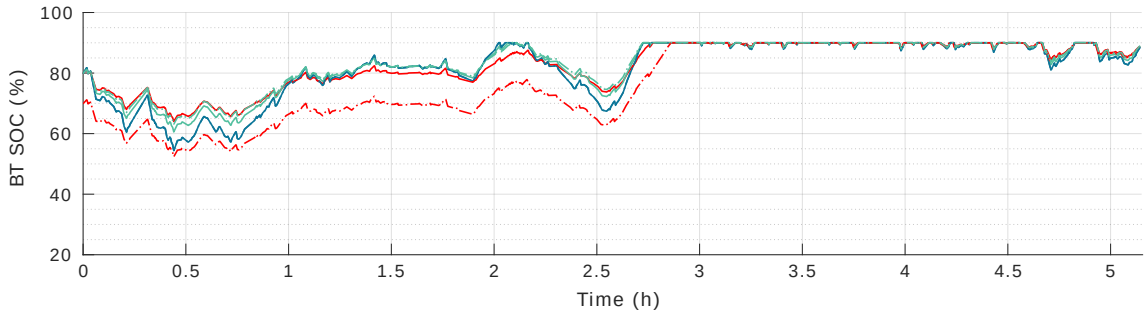

(b) BT SOC

Figure 4.16: Simulation results of RB1-A and RB1-B strategies.

Focusing on RB2, the results demonstrate that it improves the LCC of both RB1 variants. Therefore, it is concluded that reducing the FC operation point at high SOC values is an appropriate control approach, as it is the main difference between RB1 and

RB2. The main improvement compared to RB1 is obtained thanks to a reduction on the hydrogen use (between 20.1-20.5% compared to RB1-A and between 31.4-33.6% compared to RB1-B). Comparing the results of Figures 4.16 and 4.17, it can be checked that the SOC that the BT performs is similar in RB1-A, RB1-B and RB2. However, in RB2 the FC power, instead of being set at a constant value, fluctuates to avoid overcharging the BT, what eventually allows obtaining a lower hydrogen use. Anyway, the results of RB2 are yet far from the best strategy, as compared to DP the LCC is 5.5% higher in the case of LTO, 6.9% higher in the case of NMC, and 3.4% higher in the case of LFP.

The results also demonstrate that the LCC of RB2 can be improved by the proposed GA optimization. Indeed, compared to the RB version, GA-RB2 obtains a LCC reduction of the 3.1% (LTO), 3.4% (NMC), and 2.3% (LFP). With these results, GA-RB2 is found to be the second best strategy. Analysing the detailed results depicted in Figure 4.15, it can be stated that the main improvement is obtained thanks to the hydrogen use reduction, which ranges between 5.3-5.8% depending on the BT chemistry. The FC lifetime is also improved, but the difference is negligible compared to the hydrogen use reduction. Figure 4.17 shows how GA-RB2 proposes to reduce the y_2 value of the controller, which corresponds to the FC operation point in low-medium SOC values (see Figure 4.3). This allows maintaining the FC power at a constant value for half of the trip. When the SOC increases, the FC changes its working point, but these changes are softer than in RB2. The reason is that the difference between y_2 and y_1 is smaller in the cases of GA-RB2 compared to the case of RB2. Altogether, this operation turns to improve the fuel efficiency of the vehicle.

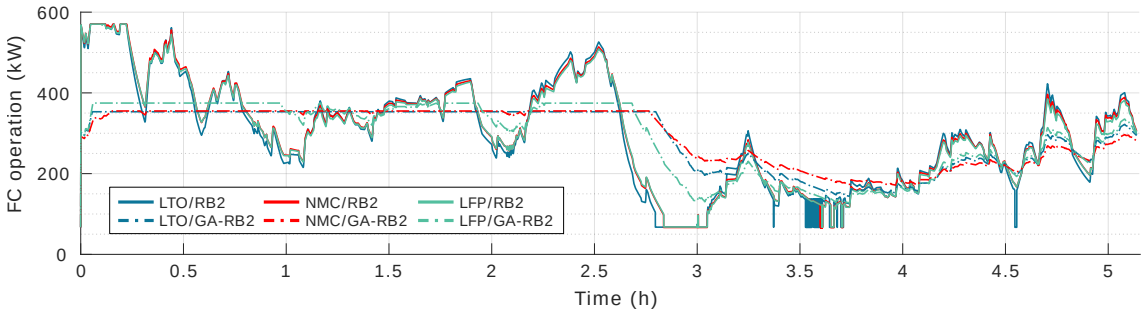

(a) FC Operation

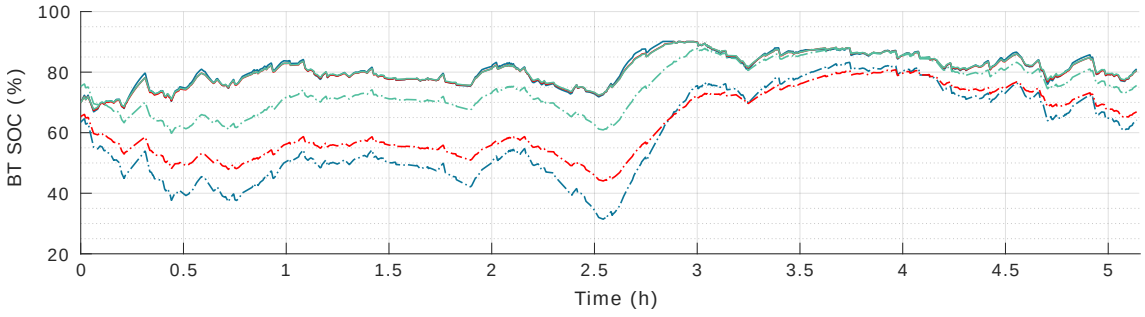

(b) BT SOC

Figure 4.17: Simulation results of RB2 and GA-RB2 strategies.

Regarding RB3, the results show that it is close to RB2 in terms of LCC: 0.2% higher with LTO, 0.5% lower with NMC, and 0.6% lower with LTO. However, the improvement obtained by the GA optimization is not as high as in the case of RB2. Consequently, GA-RB3 obtains a slightly worse result compared to GA-RB2 in terms of LCC: 1.4% higher with LTO, 1.1% higher with NMC, and 0.6% higher with LFP. Even if there are some minor changes in the remainder cost terms, the main reason to this higher LCC is again the hydrogen consumption, which is between 2.7-2.9% higher in GA-RB3 compared to GA-RB2. In short, it can be stated that in terms of cost-efficiency, the control approach proposed by RB2 is better than the one proposed by RB3.

Figure 4.18a shows that the operation of the FC does not differ much from RB3 to GA-RB3. Indeed, this control strategy is found to be more limited when trying to be optimized, as the controller cannot vary the FC operation point into a wide range. This is the reason why the improvement obtained by the GA approach is lower in RB3. Besides, Figure 4.18b shows how RB3 and GA-RB3 succeed in reducing the DOD performed by the BT. Even if this approach allows to reduce the BT degradation, the obtained improvement is not enough to overcome the slightly higher hydrogen consumption of GA-RB3 compared to GA-RB2, as it was already highlighted.

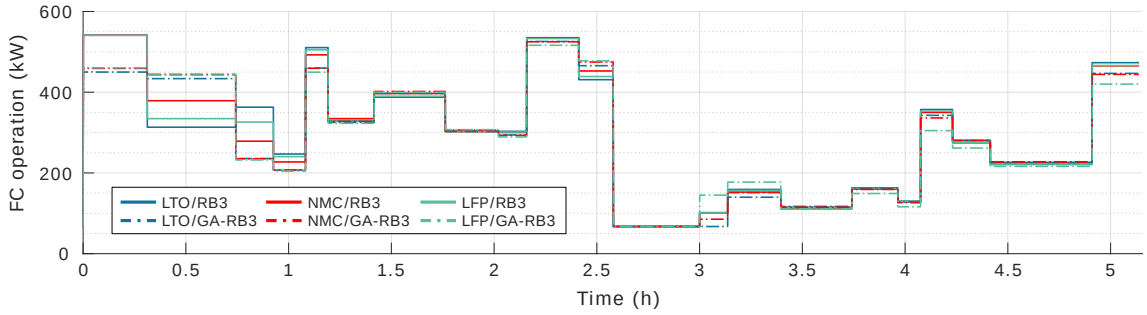

(a) FC Operation

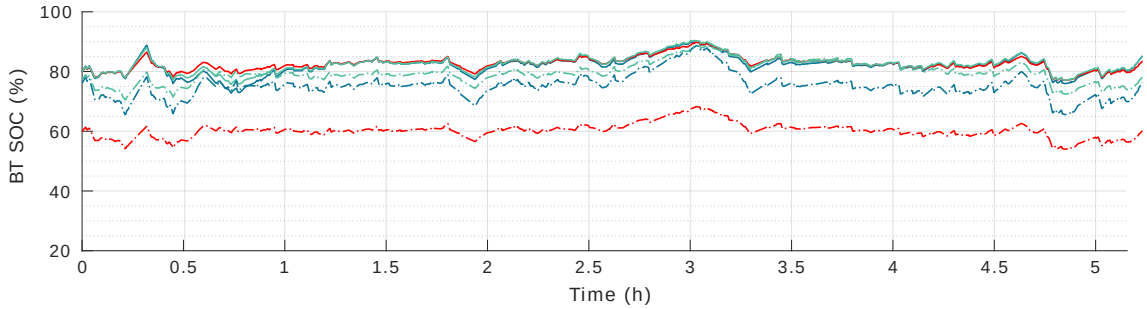

(b) BT SOC

Figure 4.18: Simulation results of RB3 and GA-RB3 strategies.

With any of the chemistries, the strategy with the best result is found to be DP. Indeed, it improves the LCC of GA-RB2 (the very next strategy) a 2.2% (LTO), 3.2% (NMC) and 1.0% (LFP). The main reason to these results is that DP is the strategy that obtains the lowest hydrogen consumption. Indeed, compared to GA-RB2, the hydrogen

use is reduced a 4.4% (LTO), 6.7% (NMC) and 6.6% (LFP). In the case of LFP, the overall LCC difference between DP and GA-RB2 is lower due to the fact that DP accelerates the BT degradation (the lifetime is reduced a 23%). The simulation results depicted in Figure 4.19a demonstrate that thanks to the proposed cost function (see Equation (4.4)), the FC achieves a soft operation, close to the one in previous strategies. Indeed, the strategy maintains the FC lifetime around the values of RB2, GA-RB2, RB3 and GA-RB3 while minimizing the hydrogen consumption, what it is translated into an optimal overall LCC.

As DP is hardly implementable in the real vehicle, ANFIS learning technique was proposed to replicate its operation. As seen in Figure 4.19, the replication obtained by ANFIS is not perfect. The main differences are found in the FC operation, which shows some spikes that were not proposed by DP. Due to these errors in the replication, the LCC of ANFIS is a 4.0% (LTO), 3.7% (NMC) and 3.3% (LFP) higher than DP. The main differences are found in the hydrogen consumption, which are 7.0%, 6.6% and 6.5% higher, respectively. Besides, due to the mentioned spikes in the FC operation, its lifetime tends to be reduced compared to DP, even if the impact of this issue in the overall LCC is low. Due to these results, it is found that ANFIS is not able to improve the LCC of GA-RB2. In the cases of LTO and LFP, GA-RB3 also obtains a lower LCC compared to ANFIS. Therefore, the obtained results evidence that a better replication of DP results is necessary, as the training errors are translated into an increased hydrogen use.

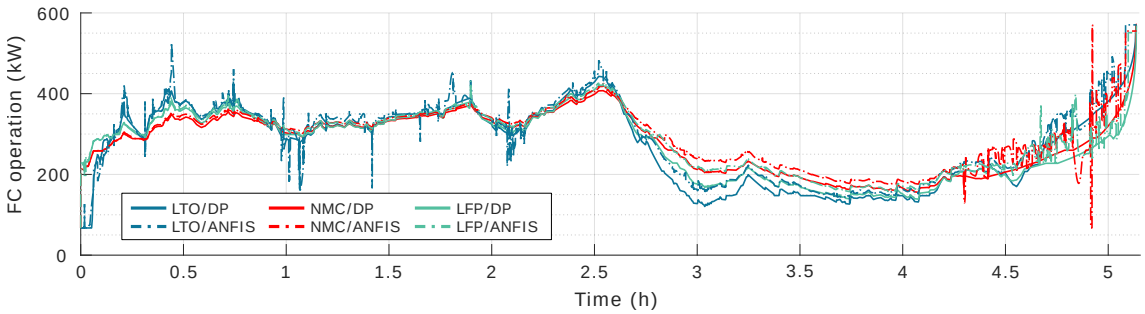

(a) FC Operation

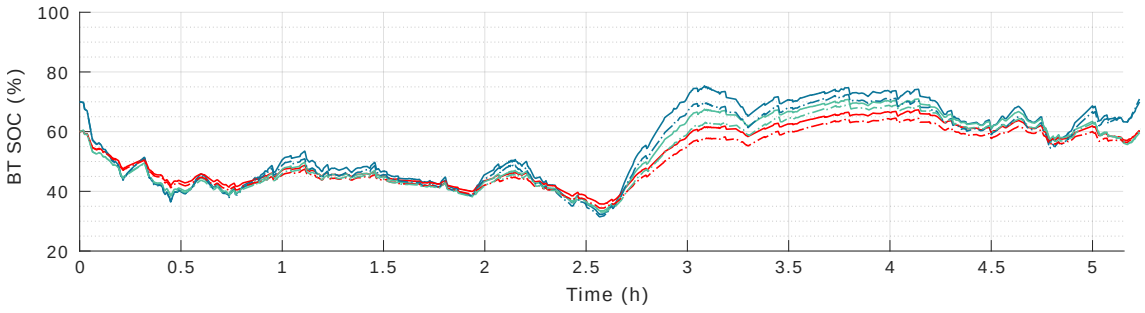

(b) BT SOC

Figure 4.19: Simulation results of DP and ANFIS strategies.

In short, the comparison of the different EMSs has proved that DP is the best option with all the chemistries. The replication of DP with the proposed ANFIS method has

obtained promising results, but it has been found that it is not enough to improve the LCC of other strategies, such as GA-RB2 or GA-RB3. Indeed, GA-RB2 has obtained the second best result with all the chemistries, with a LCC that is between 1.0-3.3% higher than the optimal DP solution. Therefore, it is concluded that GA-RB2 is also an appropriate strategy. The comparison of the different strategies will be further extended in Section 4.4.5 with the analysis of the robustness and real time execution.

4.4.3 Analysis of Optimization Variables

Once the LCC values have been analysed, this subsection focuses on the optimal values of the optimization variables. The objective of this analysis is to search for the correlations between these variables and a lower LCC value. To do so, Figure 4.20 depicts a series of graphs where the relation between the three optimization variables (n_{FC}, n_{BT} and SOC_0) and the LCC is shown for each case of the sensitivity analysis. The colours represent the values obtained by the different BT chemistries, as in the case of n_{BT} the constraints vary depending on the chemistry.

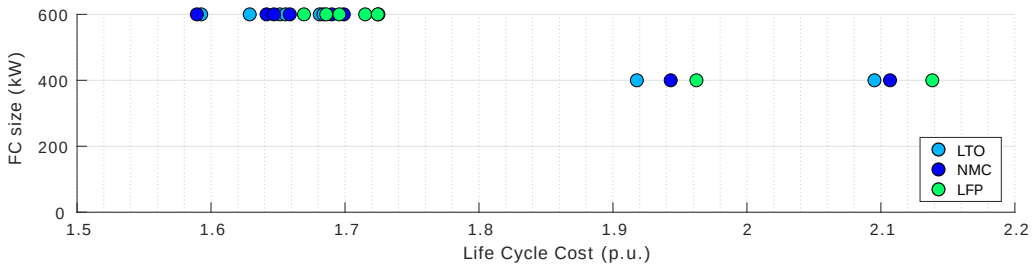

(a) Optimal FC size, n_{FC}

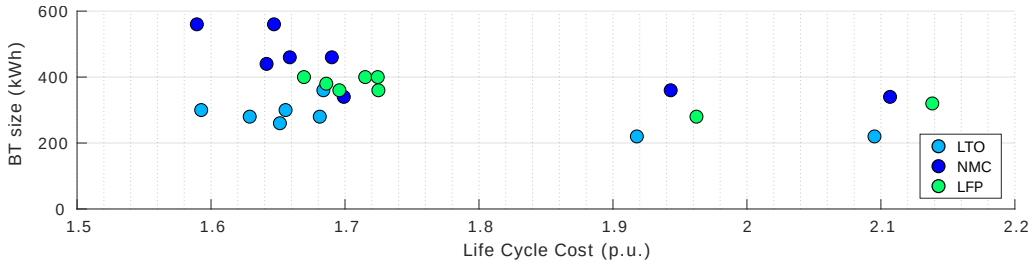

(b) Optimal BT size, n_{BT}

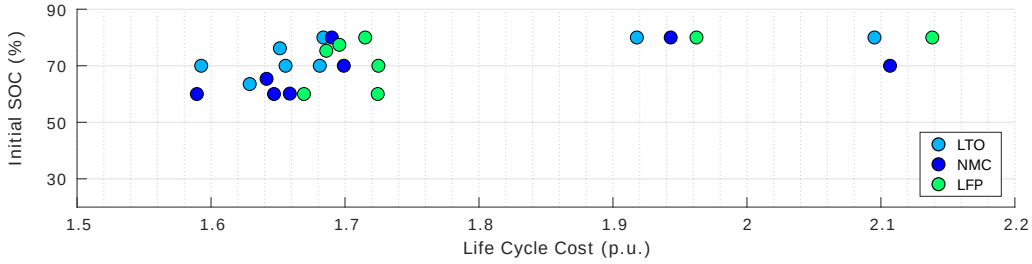

(c) Optimal initial SOC, SOC_0

Figure 4.20: Influence of optimization variables on LCC.

First of all, it can be concluded that in all the cases of the sensitivity analysis the optimal option for the sizing of the powertrain sources is to fill two compartments of the available space with the FC system, and the remainder two compartments with the BT system. The reasons are further discussed in the following paragraphs.

Regarding the FC size, Figure 4.20a shows that the strategies with a lower LCC propose to integrate a FC of 600 kW (specifically, all the strategies except RB1-A and RB1-B). Considering that in all the cases the average power that the FC provides through all the journey should be similar (it may be around the average demand, 260 kW, as in this way the BT maintains its energy through all the journey), bigger FCs tend to obtain lower consumptions, since the overall system efficiency is higher at lower operation points (see Figure 2.8). However, big FCs also increase the costs related to their acquisition and replacements. For the case of the current scenario, the best compromise is found to be the FC size of 600 kW. Anyway, it can be estimated that in scenarios where the importance of reducing the hydrogen consumption minimization is lower (e.g., due to a lower hydrogen cost), the optimal FC size may be reduced.

In the case of the BT size, the results of Figure 4.20b show that there is not a clear trend between n_{BT} and the obtained LCC. Excluding the non-optimal results of RB1-A and RB1-B, the following optimal values are proposed: in the case of LTO, sizes around 280-360 kWh; in the case of NMC, sizes around 340-560 kWh; and in the case of LFP, sizes around 360-400 kWh. Therefore, except in the case of LFP, the variation of the optimal n_{BT} value is considerable. It can be also noticed that the strategies with a lower LCC, specially DP, propose the higher value from the mentioned range. However, only in the case of LFP does this value coincide with the maximum allowable value (400 kWh with the FC of 600 kW). Therefore, contrary to the case of the H-DEMU, in this case the optimal BT sizes do not coincide with the maximum allowable values.

Finally, the graph in Figure 4.20c shows that there is not a clear trend regarding the optimal SOC_0. Regardless of the chemistry, the optimal values are around 60-80%. In the case of LTO, the values are found to be closer to 70-80%, while in the case of NMC they are closer to 60%. Contrary to the case of the H-DEMU, in this scenario the BT can not be discharged through the journey. Therefore, the SOC_0 value does not affect directly in the hydrogen consumption, and its impact in the final LCC is limited. The main effects of SOC_0 are on the BT degradation, even if this effect is low. SOC_0 can influence in the middle SOC and in the maximum DOD that the BT preforms: indeed, if the SOC starts in a high value, the BT cannot be much charged at the beginning of the journey, what limits the DOD that it performs.

4.4.4 Influence of Key Cost Terms on Overall LCC

After focusing on the LCC values and on the values of the optimization variables, in this subsection the variable terms of the LCC model are analysed in detail. The aim of this

approach is to identify the most influential terms of the cost model, that is to say, which are the cost terms that have to be reduced to minimize the overall LCC. For this approach, Figure 4.21 depicts for each case of the sensitivity analysis the relation between the overall LCC value and the cost terms that change from one possible solution to another: C_{FC}, C_{BT}, C_{H_2}, C_{FCrepl} and C_{BTrepl}. As in the previous figure, the different colours represent the analysed BT chemistries. All figures respect the same scale in the y-axis, since in this way it is easier to identify which is the cost term with the highest correlation with the LCC. In the case of C_{FC} and C_{BT}, a zoom is made to this axis in order to better identify the potential trends.

The results demonstrate that the most influential term of the LCC model is by far the hydrogen use, C_{H_2}. The difference with the remainder cost terms is notorious. As the dotted line highlighted in Figure 4.21c shows, there is a nearly linear relation between how much a combination of BT chemistry and EMS reduces the hydrogen use and how much it reduces the overall LCC. As it was already discussed when analysing Figure 4.15, C_{H2} is the cost term that contributes most to the overall LCC, as in the different cases of the sensitivity analysis it ranges between the 51-68% of the total cost (what corresponds to around 85-143% of the referential DEMU cost). Therefore, logically small variations of C_{H2} can lead to important variations in the overall LCC.

Regarding the remainder cost terms, it can be first concluded that the contribution of both acquisition costs C_{FC} and C_{BT} is very low. Indeed, C_{FC} represents less than the 3% of the referential DEMU cost, while C_{BT} represents around the 2%. Looking into the zooms made to Figure 4.21a and Figure 4.21b, it can be also noticed that there is no clear relation between these variables and the overall LCC, what demonstrates that they do not influence the optimality of an EMS and/or BT chemistry. In the case of the FC acquisition cost, its value is increased in the cases with a lower LCC. However, as it was previously highlighted, this is due to the fact that bigger FC systems can reduce the hydrogen consumption, and consequently the overall LCC.

Finally, the replacement costs of both traction sources have a bigger contribution to the overall LCC. In the case of C_{FCrepl}, it is close to the 10% of the referential cost. It can be noticed that all the strategies obtain similar FC replacement costs, what demonstrates that generally the objective of limiting the FC degradation is achieved. Regarding the case of C_{BTrepl}, its contribution depends on the BT chemistry: in the case of LTO it does not exceed the 3% of the referential cost, in the case of NMC it does not exceed the 4%, and in the case of LFP it reaches up to the 12%. This difference between LFP and the remainder chemistries is what makes this technology obtain higher LCC values. Indeed, this is also the cause to the fact that the trend of Figure 4.21c is not totally linear in the case of LFP. Indeed, the cases with a lower LCC also increase C_{BTrepl}, and therefore the high reduction of C_{H_2} is not enough to obtain a solution as competitive as in the best cases of NMC and LTO.

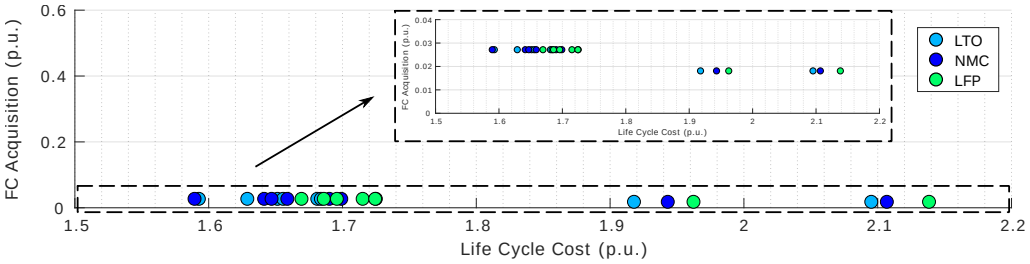

(a) Cost of FC acquisition, C_{FC}

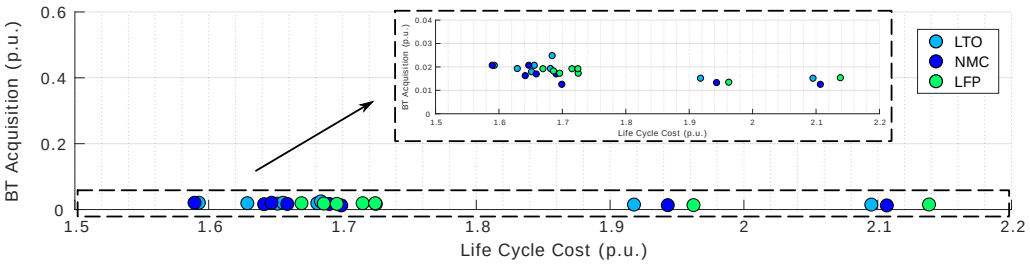

(b) Cost of BT acquisition, C_{BT}

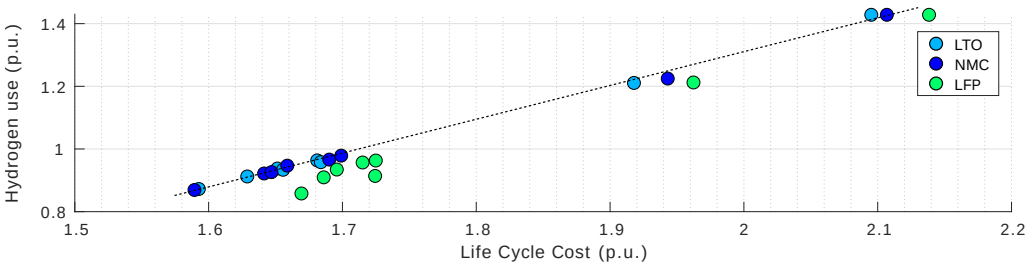

(c) Cost of hydrogen use, C_{H_2}

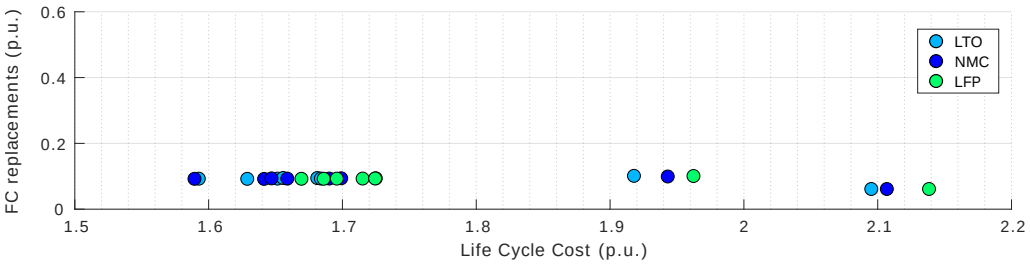

(d) Cost of FC replacements, C_{FCrepl}

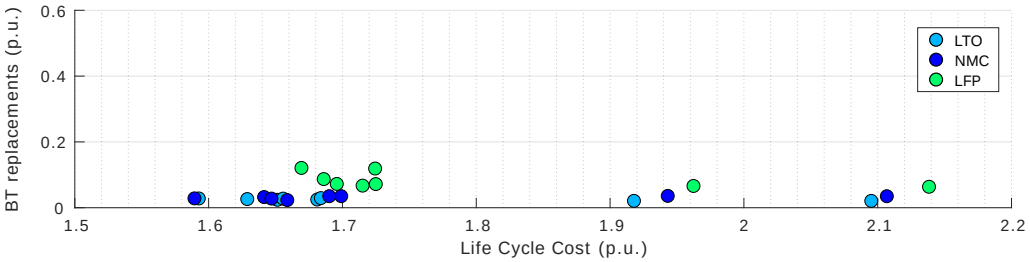

(e) Cost of BT replacements, C_{BTrepl}

Figure 4.21: Relation between LCC and LCC terms.

4.4.5 Analysis of EMS Robustness and Real Time Execution

In this subsection the evaluation of the different control strategies is extended. Indeed, this evaluation is focused on the robustness and real time execution capabilities of the proposed EMSs. Considering that these features could limit the efficiency of a control strategy when integrating in a real application, the evaluation of this subsection becomes also crucial in order to define which EMS turns to be the most appropriate

4.4.5.1 EMS Robustness

In a first step, the analysis is focused on evaluating if the proposed control strategies are robust. Indeed, each of the cases of the sensitivity analysis has been optimized for a specific driving cycle. But during real operation, this driving cycle is prone to suffer slight variations, and therefore the EMS must be able to give a feasible solution also under these circumstances.

This analysis is based on simulating again the optimal solution of each case of the sensitivity analysis, but varying the driving cycle. The new driving cycles are based on the nominal scenario, and they aim at representing potential disturbances that may occur while in real operation. Specifically, the variations are set in the number of passengers and the auxiliaries consumption, which have been altered a $\pm 7\%$ and $\pm 30\%$, respectively. This has lead to 8 new driving cycles, which coincide with the scenarios used to train the ANFIS controller (see Section 4.2.1.5).

It is worth to mention that for this analysis it is considered that DP is not robust. Indeed, even a slight variation in the driving cycle requires the deployment of a new DP optimization, as each optimization is only valid for a very specific driving cycle. Therefore, DP is kept out of the robustness analysis. Anyway, as it will be explained afterwards, DP results have been also obtained under the new scenarios. These results have been used as reference when evaluating the variation of the LCC values of the remainder strategies.

Not all the simulations have lead to a feasible solution. Figure 4.22 shows a bar graph where the relation of feasible and unfeasible solutions are given for each analysed strategy. It is worth to mention that for each strategy 27 simulations have been deployed, which correspond to the combination of 9 driving cycles (nominal case and the generated driving cycles) and 3 chemistries. The results show that most of the strategies provide a feasible solution even when the driving cycle is varied. Specifically, RB2, RB3, GA-RB3 and ANFIS have provided a feasible solution in all the proposed scenarios. However, both variations of RB1 and GA-RB2 are not able to provide always a feasible solution. Specifically, RB1-A becomes unfeasible in a 3.7% of the cases, RB1-B in a 7.4% of the cases, and GA-RB2 in a 33% of the cases.

In the case of both RB1 variants, the problem of the unfeasible solutions is that in the case of LTO the proposed BT sizing is not enough for the most demanding scenarios, as

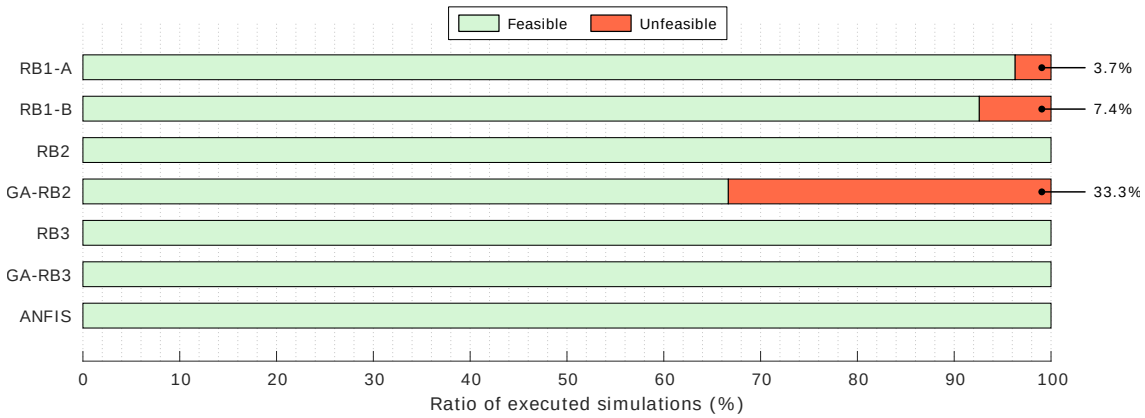

Figure 4.22: Analysis of EMS feasibility in different scenarios.

the BT is overdischarged during the most demanding sections of the route. Therefore, the problem comes from the proposed sizing, rather than from the strategy itself. Indeed, in the cases of RB1-A and RB1-B it is not possible to increase the FC reference to avoid a BT discharge, as it already works in the maximum operation point. An increase of the proposed BT sizing is necessary in order to overcome this issue.

In the case of GA-RB2, the problem of the unfeasible solutions also consist of an overdischarge of the BT during the most demanding route sections. As it was shown in Figure 4.17a, the optimized options of GA-RB2 propose to operate the FC at a constant fixed point for most of the route. This value, defined by parameter y_2, is lower than the maximum FC operation point, what compared to other control strategies allows obtaining a more efficient overall operation. However, for the most demanding scenarios, that FC operation point is not enough to prevent an overdischarge of the BT. Therefore, it is identified that GA-RB2 might be improved for its real time implementation, e.g., by modifying in real time the y_2 value depending on the deviation of the SOC value from the SOC profile obtained in simulation.

Besides analysing if the control strategies are able to give a feasible solution, it is interesting to analyse also if the LCC is altered excessively when varying the driving cycle. Indeed, if the strategy can provide a feasible solution, but increases overmuch the hydrogen use, it can be considered that it is not very robust. For each combination of BT chemistry and EMS (excluding DP), Figure 4.23 depicts the distribution of the LCC values under the new driving cycles. In order to make a reasonable comparison, the LCC under each new scenario has been normalized in relation to the best case of the sensitivity analysis (DP with NMC) under that same new scenario. In addition, the 'x' marks represent the LCC values of the nominal case (Table 4.8). In short, the figure allows evaluating if the majority of the cases stay close to the results obtained in the original optimization. When they do not, the figure also allows evaluating if the result is improved or worsened.

First of all, the results show that RB2, GA-RB2, RB3 and GA-RB3 are able to maintain similar performances when varying the driving cycle. This means that under different

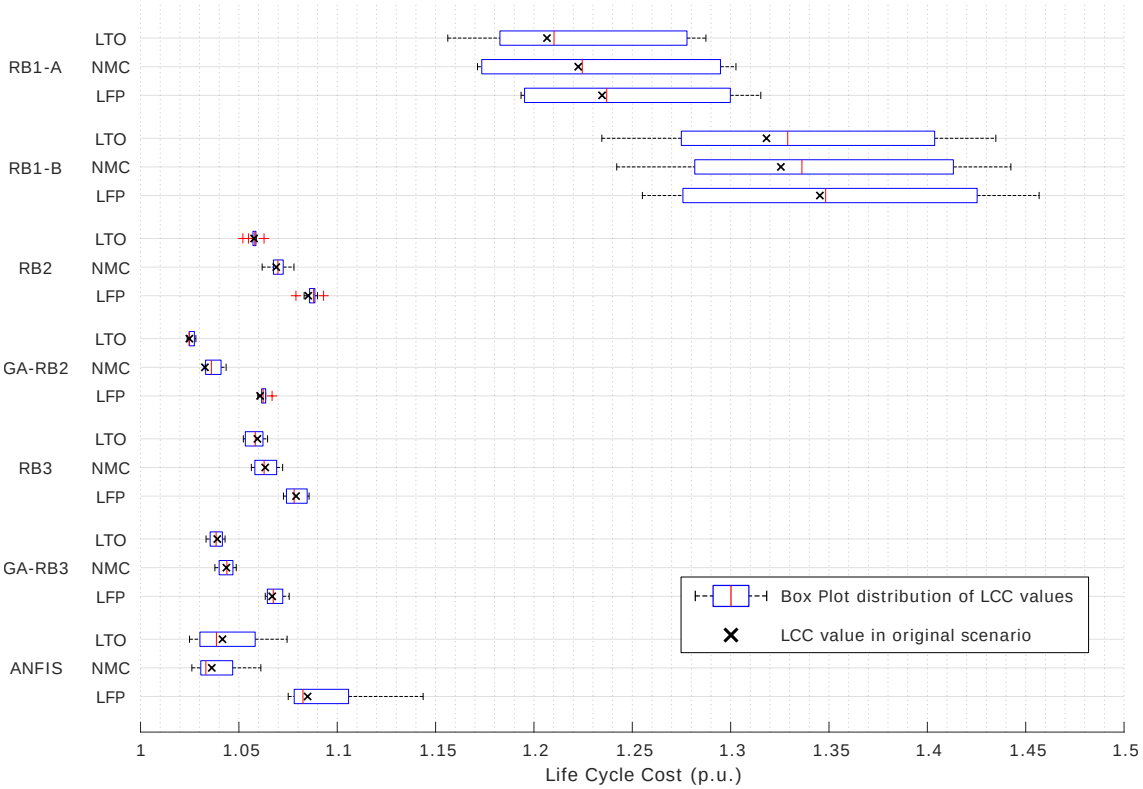

Figure 4.23: EMS robustness in different scenarios.

scenarios they are able to provide a FC and BT operation which does not lead to an increased hydrogen consumption or degradation of the power sources. Therefore, these strategies are robust from the LCC point of view, even if some of them are not able to provide always a feasible solution (e.g., GA-RB2).

On the contrary, some other strategies show more variability in the LCC when varying the scenario. In the case of ANFIS, there are some cases that increase overmuch the relative LCC compared to the original case. That is to say, the LCC is further away from the result of DP compared to the original scenario. Therefore, ANFIS can be considered to be less robust than the previously mentioned strategies. The main problem of this strategy comes in the most demanding scenarios, where the proposed operation leads to an increased hydrogen consumption in order to provide a feasible solution.

Finally, the results also show that RB1-A and RB1-B are the strategies with the highest LCC variability in the new scenarios. Actually, their operation does not differ depending on the scenario, as the FC always operates in the same point. This makes the operation be more appropriate for the more demanding scenarios, as the hydrogen consumption is closer to the optimal value of DP. On the contrary, in the less demanding scenarios, the hydrogen consumption is even further away from the optimal value, what makes the relative LCC be higher compared to the nominal scenario. Therefore, it can be concluded that RB1-A and RB1-B are not robust from the LCC point of view.

4.4.5.2 EMS Real Time Execution

In a second step, the analysis focuses on the time required for the execution of the simulations. The aim of this analysis is to evaluate the real time performance of the different control strategies. The simulation execution time cannot be considered to be an exact approximation of the real time performance. However, it can help understand which strategies will require higher or lower execution times, and therefore, their feasibility can be estimated. In any case, it has to be considered that the analysis of this section is just an approximation.

Figure 4.24 shows a box plot that represents the distribution of the execution times obtained by the simulations of each EMS. Specifically, the times required for executing the simulations of the EMS robustness analysis have been used (what means 27 simulations per strategy). These values are represented in p.u. in relation to the time required to execute the DEMU simulation, which does not have an EMS.

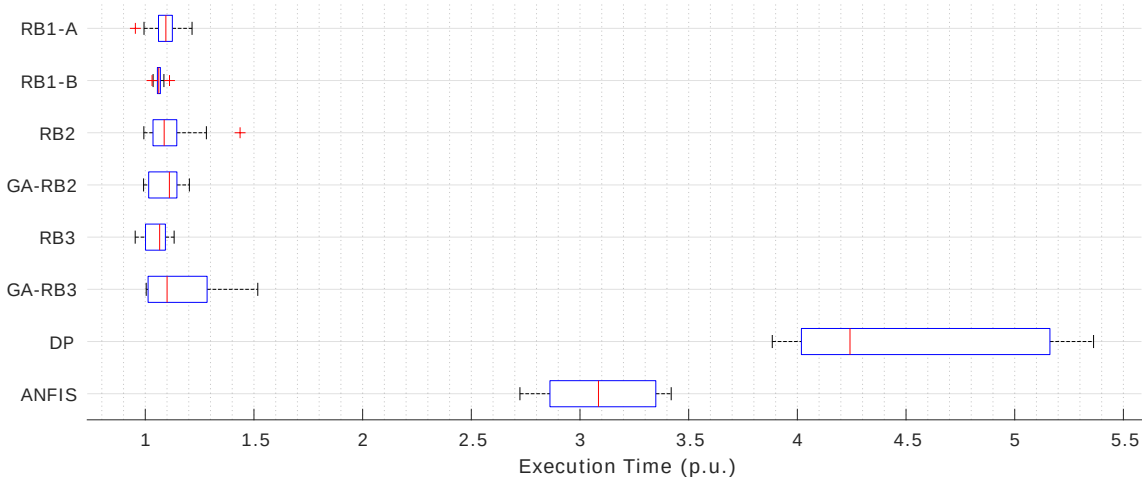

Figure 4.24: Box Plot representing the execution time of each EMS.

The results show that all the simulations of the RB strategies require similar times compared to the simulation of the DEMU. Specifically, the simulation time medians of these EMSs are between 6.2-11.1% higher than the DEMU. Therefore, it is demonstrated that the execution times of the control strategies proposed by RB1-A, RB1-B, RB2, RB3, GA-RB2 and GA-RB3 are low, and that their implementation in a real time application is feasible. In some cases there are some simulations that have required much more time that the median value (e.g., in GA-RB3). However, thay can be considered to be exceptions, as some external disturbances may have increased the computation time.

Regarding the ANFIS strategy, it is also based on a set of rules. However, as the FL-based structures are heavier and more complex, the execution time of this EMS is found to be more than three times higher than the referential value. This can question the real time implementation feasibility of the ANFIS strategy. A reduction of the complexity and weight of these structures is recommended in order to ease this implementation.

Finally, DP is the strategy that requires the highest simulation time (more than four times compared to the DEMU), due to the long time required for solving the optimization.

4.4.6 Review of Sensitivity Analysis to Powertrain Design

This subsection reviews the main conclusions obtained during the development of the sensitivity analysis to the powertrain design. This sensitivity analysis has been focused on evaluating and comparing the proposed EMSs and BT chemistries. In a first step, the LCC values obtained by each case of the sensitivity analysis have been compared, and the reasons behind these results have also been attained. In the case of the control strategies, their analysis has been extended by addressing their robustness and execution time. Then, the analysis has focused on the variables returned by the optimization of each case of the sensitivity analysis. Finally, the influence that the key cost terms of the economic model (C_{FC}, C_{BT}, C_{H_2}, C_{FCrepl} and C_{BTrepl}) have on the obtained LCC has also been analysed and discussed.

Regarding the comparison of the BT chemistries, Table 4.10 reviews the obtained conclusions. Specifically, the table shows the capabilities of LTO, NMC and LFP technologies to: (1) reduce the LCC, (2) minimize the hydrogen use, and (3) reduce the cost related to the BT replacements. More filled bullets refer to a better capability.

Table 4.10: Main capabilities of analysed BT chemistries.

	LCC	**H_2 use**	**BT lifetime**
LTO	●●●●●	●●●●◐	●●●●●
NMC	●●●●◐	●●●●◐	●●●●◐
LFP	●●●○○	●●●●◐	●●○○○

The main conclusions are reviewed bellow:

- LTO and NMC are close in terms of LCC (in most of the cases the difference is lower than the 1%), but generally LTO obtains a slightly lower LCC. The main improvement of LTO against NMC is the reduction of the BT replacement costs, what allows overcoming the higher acquisition cost of this technology.
- LFP obtains higher LCC values compared to LTO and NMC (4.8% and 5% in the case of DP, respectively). The main disadvantage of this chemistry is found to be its higher degradation.
- Contrary to the H-DEMU case study, all the chemistries lead to a similar hydrogen consumption. The reason is that as the BT energy should be maintained through all the journey, in this case study the size of the BT barely influences the fuel use.

In addition, Table 4.11 reviews the main capabilities of the proposed EMSs. The table follows the same format as Table 4.10, and in this case the capabilities related to

the robustness, execution time, and FC lifetime are also included. The values have been defined considering the average results of the three chemistries.

Table 4.11: Main capabilities of analysed EMSs.

	LCC	**H_2 use**	**FC lifetime**	**BT lifetime**	**Robustness**	**Execution time**
RB1-A	◐○○○○	●○○○○	●●●○○	●●●●○	●●○○○	●●●●◐
RB1-B	◐○○○○	◐○○○○	●●●●●	●●●●○	●●○○○	●●●●◐
RB2	●●◐○○	●●●○○	●●●●○	●●●●○	●●●●●	●●●●◐
GA-RB2	●●●●○	●●●●○	●●●●○	●●●●○	●●●○○	●●●●◐
RB3	●●◐○○	●●●○○	●●●●○	●●●●◐	●●●●●	●●●●◐
GA-RB3	●●●◐○	●●●◐○	●●●●○	●●●●●	●●●●●	●●●●◐
DP	●●●●●	●●●●●	●●●●○	●●●◐○	○○○○○	●○○○○
ANFIS	●●●◐○	●●●●○	●●●◐○	●●●◐○	●●●●○	●●○○○

The main conclusions are reviewed as follows:

- The best strategy in terms of LCC is DP. However, the long execution time and null robustness prevent its integration in a real application.
- The replication of DP by means of the proposed ANFIS learning technique does not obtain bad results in terms of LCC and hydrogen use, but there are some other OB strategies that obtain better results. In addition, the execution time should be reduced in order to improve its real time implementation possibilities.
- GA-RB2 stays just a 1.0-3.3% behind DP in terms of LCC, what means that it obtains better results than ANFIS. The optimization by means of the GA approach is found to be effective to improve the LCC. However, the robustness should be improved in order to avoid overdischarging the BT during real operation.
- GA-RB3 obtains slightly higher LCC values compared to GA-RB2, but it shows a better robustness. It is also the strategy that reduces most the BT degradation, even if this is not so crucial due to the high impact of the hydrogen use in this scenario. As in the GA-RB2 case, the GA optimization approach is also found to be effective to reduce the LCC.
- Finally, both variants of RB1 strategy obtain too high LCC and hydrogen use values, what demonstrates that they are not appropriate for the analysed scenario.

Once the analysis of the BT chemistries and strategies is finalized, some other conclusions can be highlighted regarding the analysis of the optimization results:

- The optimal FC size is found to be around 600 kW. With a lower size a feasible solution is also obtained, but the optimal option is found to be to oversize the FC. Indeed, even if higher acquisition and replacement costs are required, the FC can be operated more efficiently, what allows reducing the hydrogen consumption.

- No clear trend is found regarding the optimal BT size. In the case of LTO values around 280-360 kWh are proposed, in the case of NMC values around 340-560 kWh, and in the case of LFP values around 360-400 kWh. None of these values is in the maximum allowable sizes.

- There is neither a clear trend regarding the optimal initial SOC value. Regardless of the BT chemistry, the optimal values are found to be around 60-80%.

Finally, the analysis of the influence that the key cost terms of the economic model (C_{FC}, C_{BT}, C_{H_2}, C_{FCrepl} and C_{BTrepl}) have on the overall LCC has unveiled some additional conclusions:

- The most influential term is C_{H_2}, as there is a practically linear relation between a low hydrogen consumption and a low LCC. This is a logical conclusion considering that due to the high hydrogen cost, C_{H_2} is the term that contributes most to the overall LCC (in the analysed cases it ranges between the 51-68% of the LCC).

- The replacement costs have also some contribution to the overall cost. In the case of C_{FCrepl}, it is close to the 10% of the LCC, but as there is not much difference from one case to another, its influence is limited. Regarding C_{BTrepl}, it is an important cost term in the case of LFP, where it ranges up to the 12% of the LCC. Anyway, it is found that there is not a direct relation between C_{BTrepl} and the overall LCC.

- Finally, there is neither a noteworthy relation between C_{FC} and C_{BT} and the overall LCC, as their contribution to the LCC is low.

4.5 Results of Sensitivity Analysis to Economic Model

Once the results of the first sensitivity analysis have been presented, this section focuses on the results of the sensitivity analysis to the parameters of the economic model. The objective of this analysis is to evaluate how do the results and conclusions of the H_2EMU design (that is to say, of the previous sensitivity analysis) differ when varying the parameters of the economic model. Figure 4.25 shows where is this sensitivity analysis located in the methodology proposed in Chapter 2. In the current case study, the variability of the operation hours (t_{day}), hydrogen price (c_{H_2}), FC price (c_{FC}) and BT price (c_{BT}) is analysed. In c_{BT}, the price variation of the 3 chemistries is considered independently. The results are obtained for the same drive cycle used in the previous sensitivity analysis.

For an easier development of this sensitivity analysis, the number of considered control strategies has been reduced. On the one hand, RB2 and RB3 are kept out of the analysis of this section, as in the previous section the effectiveness of the GA-based strategies to improve the performance of the original rule-based strategies has been already demonstrated. Therefore, in this section just GA-RB2 and GA-RB3 are considered. On the other hand, ANFIS is also kept out of the analysis of this section. Indeed, this strategy

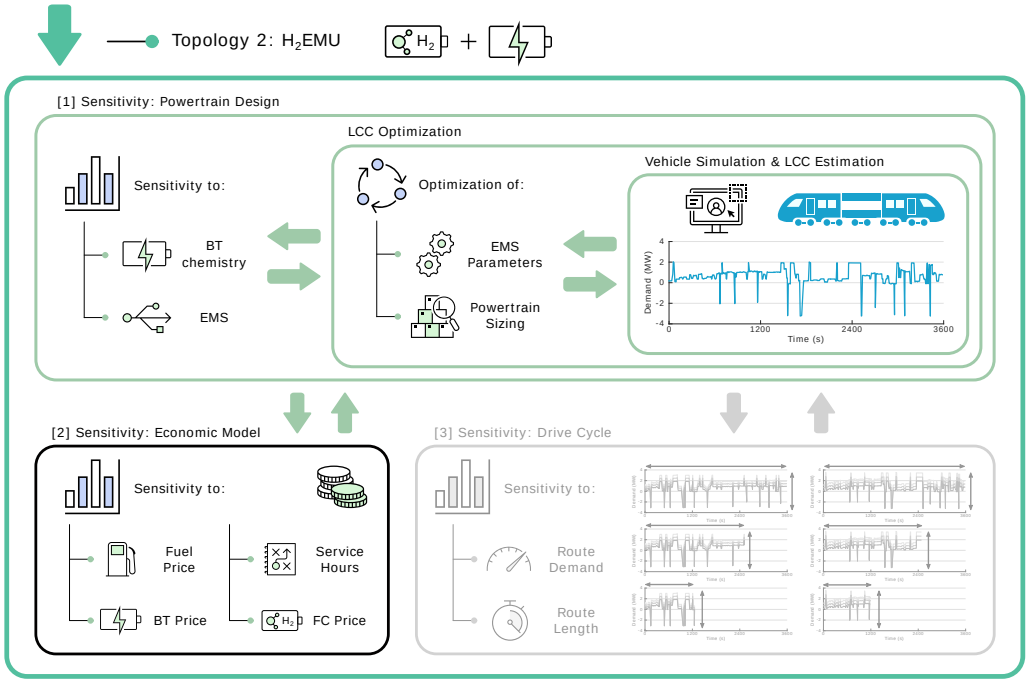

Figure 4.25: Current step of holistic design methodology.

requires long learning processes to be evaluated in many scenarios. In addition, as it consists on a replication of DP operation, it is considered that its potential performance can be fairly estimated from the results obtained by DP.

The analysis of this section is divided into different subsections, according to the parameter whose sensitivity is being analysed: sensitivity to the operation hours, sensitivity to the hydrogen price, sensitivity to the FC price, and sensitivity to the BT price.

4.5.1 Sensitivity to Operation Hours

In this first subsection, the sensitivity is focused on the operation hours that the H_2EMU drives per day (t_{day}). As it was defined in Section 4.2.3, three scenarios are proposed: in the Low Scenario (LS) the vehicle drives 5 h/day, in the Medium Scenario (MS) 10 h/day, and in the High Scenario (HS) 15 h/day. The nominal scenario analysed in the sensitivity analysis to the powertrain design corresponds to the HS. The analysis will be focused on evaluating how do the LCC values, optimal optimization variables and terms of the economic model vary within the different scenarios. For each analysis, an independent section is defined.

4.5.1.1 Analysis of LCC Values

Figure 4.26 depicts the LCC values obtained at each scenario. As the LCC may vary considerably from one scenario to another, the values of each scenario are normalized in

relation to the result of DP strategy with NMC chemistry (which in the nominal scenario of Section 4.4 was found to be the best option). The results are grouped by each chemistry, as in this way it is easier to analyse the effect of varying t_{day}. Each marker refers to a different EMS. The results will be analysed from two points of view: focusing on the comparison of the control strategies, and focusing on the comparison of the BT chemistries.

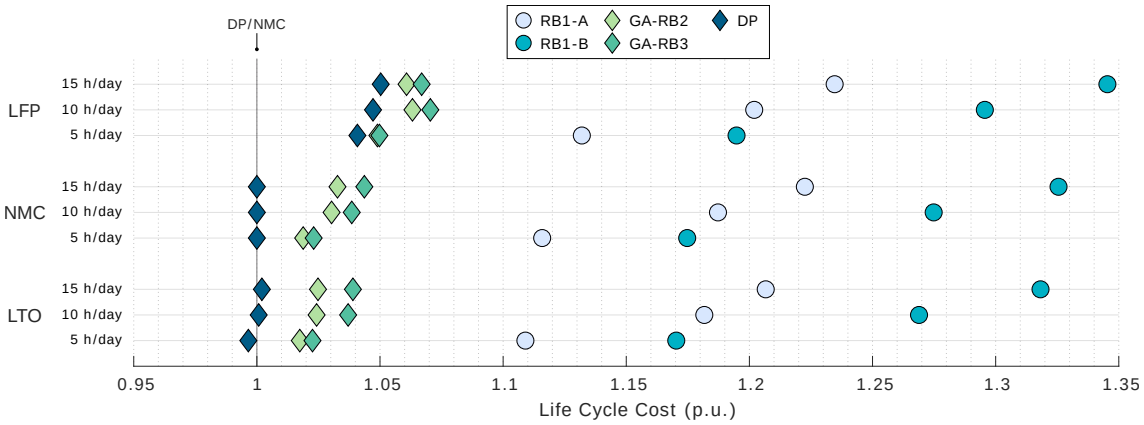

Figure 4.26: Sensitivity of LCC values to t_{day}.

Regarding the control strategies, the figure shows that as t_{day} is reduced, the LCC difference between the different EMSs is reduced. Anyway, in all the cases the same order as in the original scenario (HS) is respected: DP strategy continues being the best option, followed by GA-RB2, GA-RB3, RB1-A and RB1-B, respectively. In the cases of LTO and NMC, in the LS the difference between DP and GA-RB2 is reduced to the 2%. Therefore, the difference continues being remarkable. In the case of LFP, the difference is maintained around the 1%, close to the value in the original scenario. It is also worth to mention that the two variants of RB1 continue being far from the results of the remainder strategies (even in the best case, the difference with DP is higher than the 9%).

In the case of the BT chemistries, the figure unveils that few changes happen when varying t_{day}. LFP reduces slightly the LCC difference with the remainder strategies, but it stays far from LTO and NMC even in the LS (with DP strategy it obtains 4% and 4.4% higher LCC, respectively). The comparison of the results obtained by NMC and LTO unveils that they continue being close in the different scenarios, with LTO obtaining slightly better results (in the case of DP, GA-RB2 and GA-RB3 the difference between them tends to be lower than the 1%). As it will be analysed afterwards, t_{day} mainly affects in the hydrogen consumption. As the BT chemistry barely affects in the hydrogen use (see Table 4.10), this low variability between the different scenarios is reasonable.

4.5.1.2 Analysis of Optimization Variables

Apart from the LCC values, the optimization variables that the optimization returns may also vary when reducing the value of t_{day}. Figure 4.27 shows the relation between the optimization variables (n_{FC}, n_{BT} and SOC_0) and the LCC, following a similar format

as Figure 4.20. In this case, the LCC is normalized in relation to the best option of each scenario. Indeed, the objective is not analysing the exact LCC of each case, but focusing on the correlations between a lower LCC and the values of the optimization variables. At each column of graphs, a different optimization variable is presented, and each row of graphs corresponds to a different scenario (HS, MS and LS, respectively).

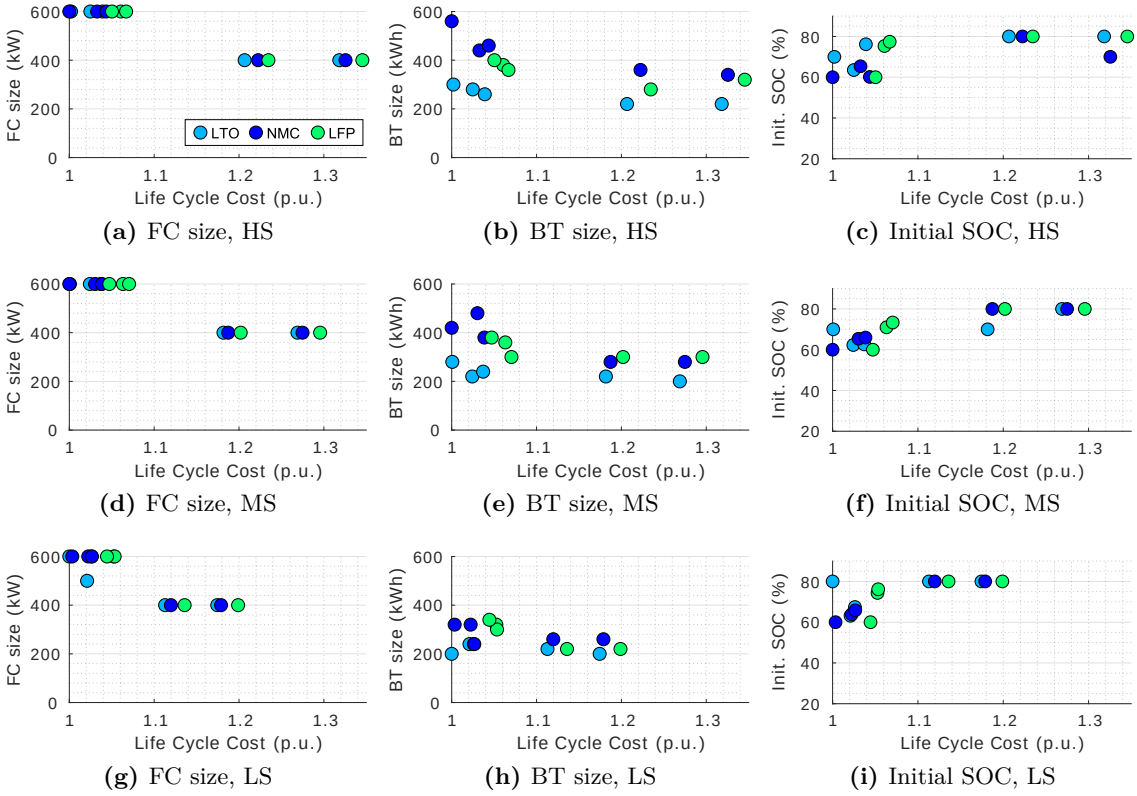

(a) FC size, HS **(b)** BT size, HS **(c)** Initial SOC, HS

(d) FC size, MS **(e)** BT size, MS **(f)** Initial SOC, MS

(g) FC size, LS **(h)** BT size, LS **(i)** Initial SOC, LS

Figure 4.27: Sensitivity of optimization variables to t_{day}.

Focusing on the optimal FC results, the figure shows that the best cases continue proposing to integrate a 600 kW FC. When reducing the operation hours, the overall hydrogen consumption is also reduced, what may diminish the advantage of bigger FC systems (i.e., to reduce the hydrogen consumption due to a more efficient operation). This is the reason why one of the options at LS proposes a FC of 500 kW. Anyway, the results demonstrate that t_{day} values lower than 5 h/day may be necessary to obtain optimal FC values much lower than 600 kW.

Regarding the optimal BT results, Figure 4.27 shows that when t_{day} is reduced, lower BT sizes are proposed. Indeed, in the HS the optimal BT sizes are found to be between 260-580 kWh, in the MS between 220-480 kWh, and in the LS between 200-340 kWh. As in the case of the FC, lower operation hours may diminish the advantage of big BT systems. Indeed, bigger BT systems require of higher acquisition costs, but they tend to improve their lifetime (as they reduce the FECs and the DODs), what compensates the initial cost. However, in the LS all the BT sizes tend to obtain longer lifetimes (less FECs

per day), and consequently, lower BT replacement costs. In this context, the advantage of big BT systems is reduced, and lower sizes become the cost-efficient option.

In the case of the optimal SOC_0, the results show that the general trend is not affected by t_{day}. Similarly to the original scenario, the optimal values are distributed between 60-80%, what demonstrates that there is no benefit from defining a higher or lower value.

4.5.1.3 Influence of Key Cost Terms on Overall LCC

As a last step, this subsection analyses how does the influence of the key cost terms (C_{FC}, C_{BT}, C_{H_2}, C_{FCrepl} and FC_{BTrepl}) change when varying the daily operation hours. The aim of this analysis is also to understand the LCC and optimization variables values obtained at each scenario, which were already analysed. Figure 4.28 shows the relation between the mentioned costs and the overall LCC at the different scenarios, following a similar format as Figure 4.21. At each column of graphs a different cost term is presented, and each row corresponds to a different scenario (HS, MS and LS, respectively). At each graph, both variables are normalized in relation to the LCC value of the best case. Besides, all the graphs use the same scale in the y-axis, as in this way is easier to identify the correlations between the cost terms and the overall LCC.

The results show that even when reducing the operation hours, C_{H_2} continues being the cost term that contributes most to the overall LCC. Its relative contribution is reduced, as the best solutions in the HS contribute to around the 55% of the overall LCC, while in the LS that value is reduced to the 30%. Anyway, the difference with the remainder cost terms is still high. Due to this reason, C_{H_2} continues being the cost term with the major importance, as even in the LS a linear relation between a lower LCC value and a lower C_{H_2} value is found.

The contributions of both replacement costs C_{BTrepl} and C_{FCrepl} are also slightly reduced in the lower scenarios, specially in the case of C_{FCrepl}. Indeed, with less operation hours the lifetimes of the powertrain components tend to be increased. In the case of C_{FCrepl}, its contribution is reduced from around the 5% in the HS to around the 3% in the LS (value for the cases with lower LCC). Regarding C_{BTrepl}, in the different scenarios its contribution is maintained around the 1-2% with LTO and NMC chemistries, and around the 4-8% in the case of LFP. The reason is that, as it was already highlighted, lower BT sizes are proposed in MS and LS, which tend to obtain lower lifetimes than the bigger systems proposed in the HS. Therefore, in the end the relative contribution is maintained around the original values. In short, the results demonstrate that C_{BTrepl} and C_{FCrepl} do not become important cost terms when reducing t_{day}, as they do not become crucial to define which EMS or BT chemistry obtains a better result.

In the case of the acquisition costs, similar conclusions are obtained. First, it can be checked that the contribution of C_{FC} tends to be increased when reducing t_{day}. Even if the optimal sizing values are maintained, as the overall LCC is reduced (due to the lower

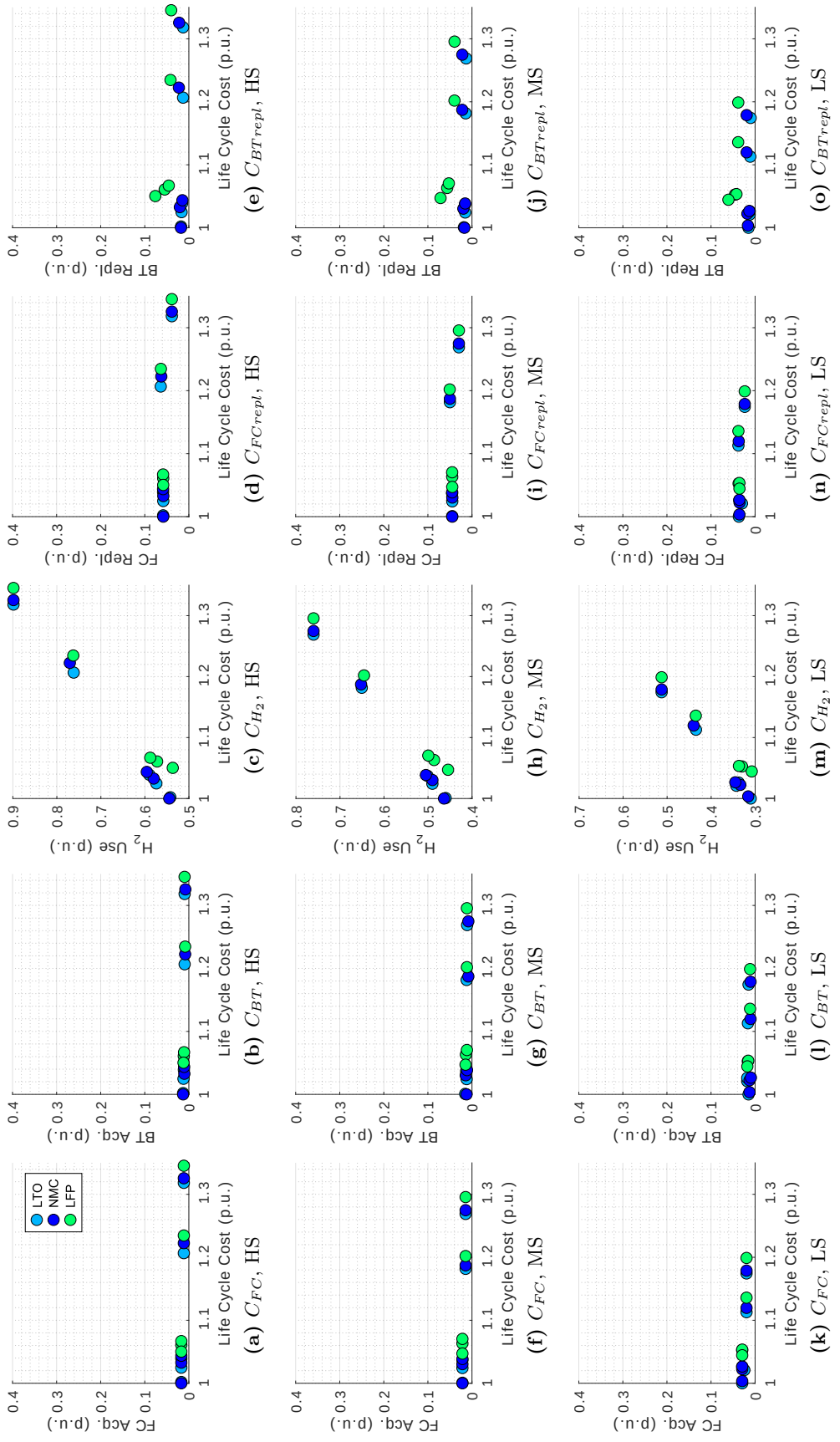

Figure 4.28: Sensitivity of key cost terms to t_{day}.

operation costs), its relative contribution is increased. Anyway, even in the LS, C_{FC} only contributes to around the 2-4% of the overall LCC. Besides, the contribution of C_{BT} is maintained around the 1% in all the scenarios. As it was already explained for the case of C_{BTrepl}, the main reason is that the BT sizes are reduced when reducing t_{day}. In short, it is concluded that neither C_{FC} or C_{BT} increase their importance when reducing t_{day}, mainly due to the fact that their contribution continues being residual.

4.5.2 Sensitivity to Hydrogen Price

In this subsection, the sensitivity focuses on varying the hydrogen price c_{H_2}. As it was specified in Section 4.2.3, the price is defined at 11€/kg in the HS (which corresponds to the nominal scenario), at 7€/kg in the MS, and at 3€/kg in the LS. The analysis will be focused on evaluating how do the LCC values, optimal optimization variables and terms of the economic model vary. Each analysis is developed in an independent section.

4.5.2.1 Analysis of LCC Values

Figure 4.29 shows how does the LCC vary from one scenario to another. The figure follows the same format as the previously introduced Figure 4.26: the LCC values are normalized in relation to DP/NMC, the results are grouped by each BT chemistry, and each marker refers to a different control strategy. The depicted results will be analysed focusing on the comparison of the control strategies and the comparison of the BT chemistries.

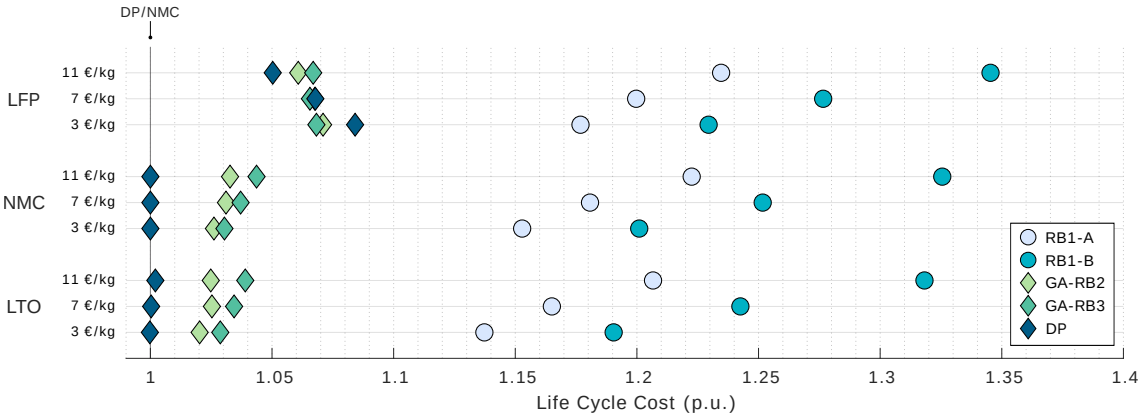

Figure 4.29: Sensitivity of LCC values to c_{H_2}.

The results suggest that when reducing c_{H_2}, the LCC difference between the different EMSs is slightly reduced. This reduction is similar for all the EMSs, except for DP, which tends to worsen its results more than the remainder strategies. Consequently, in the case of LFP chemistry, DP is not the best EMS in the MS and LS. In the cases of LTO and NMC, however, it continues being the best one, as the difference between DP and the remainder EMSs was high in the HS. As it will be explained afterwards, when reducing c_{H_2} the importance of minimizing the hydrogen consumption is also reduced. As

the main advantage of DP against the other EMSs is the hydrogen use minimization (see Table 4.11), this performance loss is reasonable. Regarding the remainder strategies, it is noticed that GA-RB2 obtains better results than GA-RB3 also in the MS and LS, and that both variants of RB1 continue being far from the best EMSs.

Focusing on the comparison of the BT chemistries, there is no notable change in the results of LTO and NMC. When reducing c_{H_2}, the LCC difference between both chemistries continues being lower than the 1% in the cases of the best strategies, with LTO obtaining a slightly lower LCC in most of the cases. In addition, both chemistries increase the difference with LFP when reducing the hydrogen price. The reason behind the performance decrease of LFP is that when reducing c_{H2}, the importance of C_{BTrepl} is increased (as it will be analysed afterwards). This becomes a disadvantage for LFP, as it degrades faster than the remainder chemistries.

4.5.2.2 Analysis of Optimization Variables

Besides analysing the variation of the LCC values, in this subsection the variation of the returned optimization variables is also analysed. For this approach, Figure 4.30 depicts the relation between these variables and the LCC values at the different scenarios. The figure follows the same format as the previously introduced Figure 4.27: the LCC is normalized in relation to the best option of each scenario, each column of graphs presents the results for one optimization variable, and each row of graphs corresponds to one scenario (HS, MS and LS, respectively).

Regarding the FC sizes, the results unveil that the optimal values tend to be reduced when reducing c_{H_2}. Indeed, excluding the results of the RB1 variants, in the HS all the cases propose the 600 kW FC, in the MS some cases propose the 500 kW FC, and in the LS all the cases propose the 500 kW FC. As mentioned before, reducing the hydrogen price reduces the importance of minimizing the hydrogen use. Consequently, the main advantage of big FC systems disappears, similarly to the case when t_{day} was reduced. However, compared to the previous sensitivity analysis, in this case the reduction of the optimal FC system is more notorious.

In the case of the optimal BT sizes, the results show that there are not important changes when varying the hydrogen price. In the different scenarios, the sizes of the best cases are maintained around 400-600 kWh for NMC, around 300-400 kWh for LFP, and around 200-300 kWh for LTO. Therefore, it can be concluded that varying c_{H_2} does not affect the result of the optimal BT size.

Regarding the optimization variable SOC_0, Figure 4.30 shows that some slight changes happen when reducing the hydrogen price. This is specially notorious in the case of NMC, as in some of the best cases the optimal SOC_0 is lower than the 60% in the MS and LS. Anyway, there is no clear trend between a specific SOC_0 value and a lower LCC.

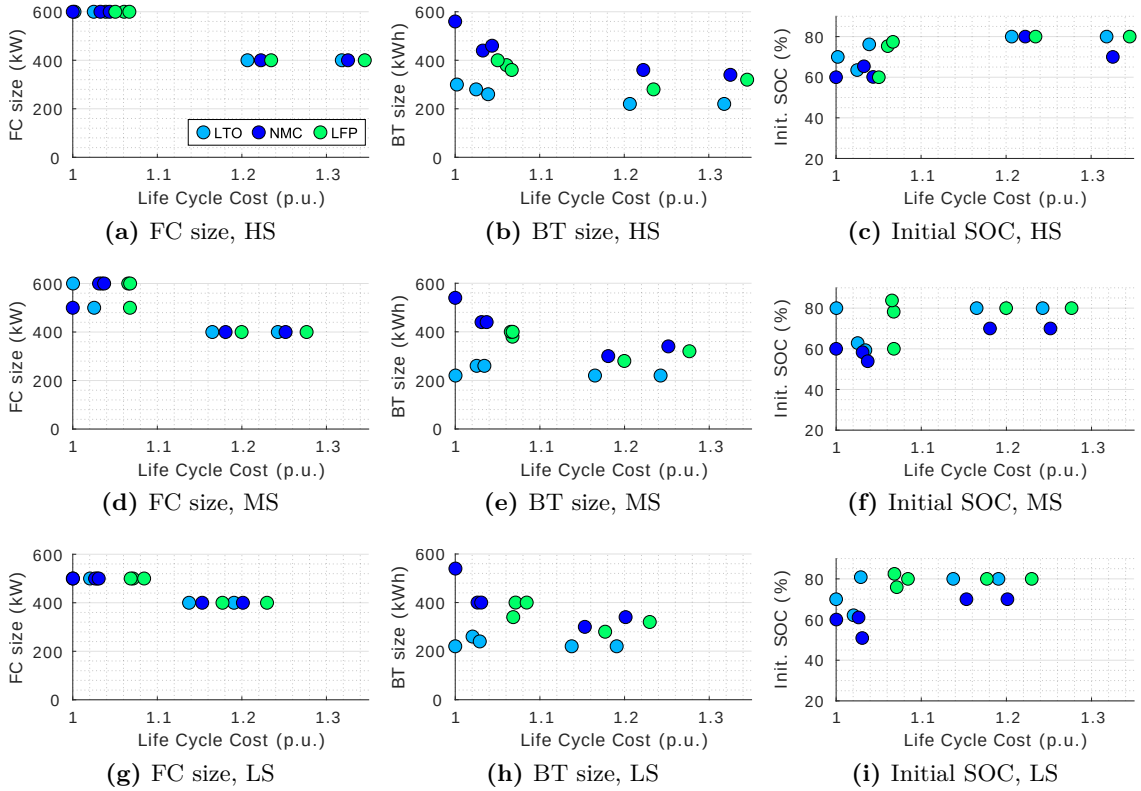

(a) FC size, HS **(b)** BT size, HS **(c)** Initial SOC, HS

(d) FC size, MS **(e)** BT size, MS **(f)** Initial SOC, MS

(g) FC size, LS **(h)** BT size, LS **(i)** Initial SOC, LS

Figure 4.30: Sensitivity of optimization variables to c_{H_2}.

4.5.2.3 Influence of Key Cost Terms on Overall LCC

Finally, the analysis of this subsection focuses on how does the influence of C_{FC}, C_{BT}, C_{H_2}, C_{FCrepl} and FC_{BTrepl} change when varying the hydrogen price. Figure 4.31 shows the relation between the mentioned costs and the overall LCC at the different scenarios. The figure follows the same format as the previously depicted Figure 4.28: both related variables are normalized in relation to the LCC of the best case, at each column of graphs a different cost term is introduced, and each row corresponds to a different scenario. Moreover, all the graphs share the same scale in the y-axis, as in this way it is easier to identify which are the strongest correlations.

The results show that even when reducing the hydrogen price, C_{H_2} continues being the cost term that contributes most to the overall LCC. The contribution of C_{H_2} in the best cases is reduced from around the 55% in the HS to around the 35% in the LS. Consequently, the importance of this term seems to be slightly reduced when reducing c_{H_2}. Indeed, in the HS the relation between the LCC and C_{H_2} is completely linear, but this linearity tends to be reduced in the lower scenarios. That is to say, the points in LS are more dispersed than in HS. The lost in the linearity is specially noticeable in the case of LFP, where the solutions with a lowest hydrogen consumption (DP and GA-RB2) are not the ones with the lowest LCC. Therefore, it can be concluded that when reducing

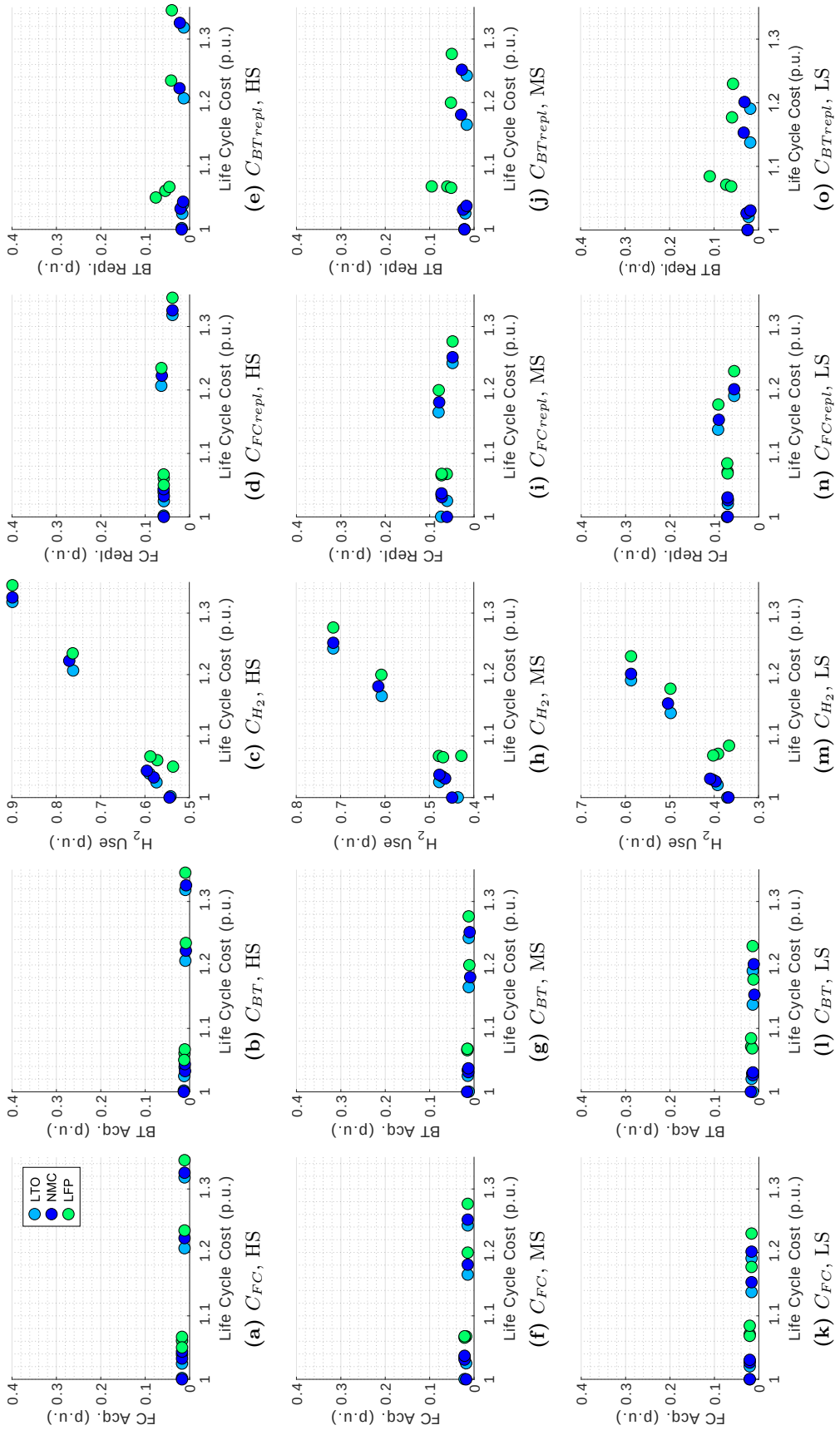

Figure 4.31: Sensitivity of key cost terms to c_{H_2}.

c_{H_2}, the importance of minimizing the hydrogen consumption is slightly reduced.

As the in the MS and LS the value of C_{H_2} is reduced, the contribution of the remainder cost terms may be slightly increased, even if they are not directly affected by the hydrogen cost reduction. This is specially notorious in the case of C_{BTrepl} when integrating LFP. In the worst case of the LS, the contribution of C_{BTrepl} to the overall LCC is around 11%, which is quite high compared to the values when integrating LTO or NMC. Due to this increase in the relative contribution of C_{BTrepl}, together with the reduction of C_{H_2}, reducing the BT degradation becomes important when integrating LFP chemistry. Indeed, as Figure 4.31o shows, the solutions with a lower C_{BTrepl} are the ones with a lower overall LCC.

In the case of C_{FCrepl}, its overall contribution is maintained around the 6-8% through the different scenarios, mainly due to the fact that when reducing the hydrogen price, slightly lower FC sizes are proposed. Anyway, it does not become an important cost term. A similar conclusion is obtained when analysing the values of C_{FC}, as its contribution is also maintained due to the reduction of the proposed FC sizes. In the case of the last acquisition cost C_{BT}, its contribution is slightly increased, but it is always maintained below the 4%. Therefore, it does neither become an important cost term.

4.5.3 Sensitivity to Fuel Cell Price

In this subsection, the sensitivity focuses on varying c_{FC}. As defined in Section 4.2.3, the following scenarios are proposed: in the HS the cost is 1000 €/kW (this corresponds to the nominal scenario), in the MS 800 €/kW, and in the LS 500 €/kW. The analysis will be focused on evaluating how do the LCC values, optimal optimization variables and terms of the economic model vary. For each analysis, an independent section is set.

4.5.3.1 Analysis of LCC Values

Figure 4.32 depicts the variation of the LCC values through the different scenarios. The figure follows the same format as the previously introduced Figures 4.26 and 4.29: the LCC values are normalized in relation to DP/NMC, the results are grouped by each BT chemistry, and each marker refers to a different EMS. The results are analysed focusing on the comparison of the control strategies and the comparison of the BT chemistries.

The comparison of the control strategies unveils that there are not important changes when varying c_{FC}. In general, the original order is maintained, as in the different scenarios DP continues being the best strategy, followed by GA-RB2, GA-RB3, RB1-A and RB1-B. The main changes are found in DP, which seems to slightly increase the LCC difference with the remainder strategies. The reason is that when reducing c_{FC}, the importance of the remainder cost terms (including C_{H2}) is slightly increased, as it will be analysed afterwards. Therefore, as it is the strategy that most minimizes this cost term, DP improves

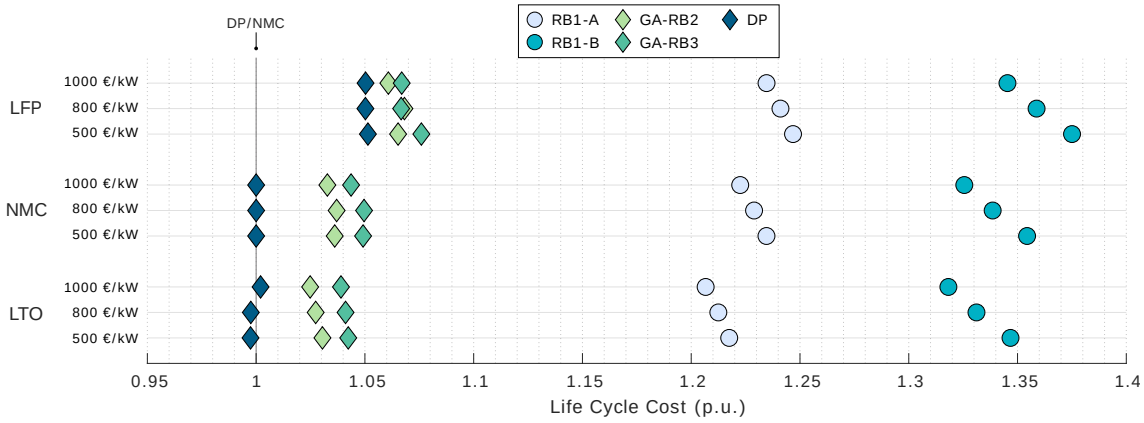

Figure 4.32: Sensitivity of LCC values to c_{FC}.

its performance. By contrast, RB1-B seems to worsen its performance when reducing c_{FC}. Indeed, the main benefit of this strategy is the lower FC degradation. Therefore, when c_{FC} is reduced, its main advantage is diminished.

In addition, the figure shows that there is not much difference between the results of the different BT chemistries when varying the FC cost. Even in the LS, the LCC difference between LTO and NMC is maintained bellow the 1% in the cases of the best strategies. In addition, the difference of these two chemistries with LFP is also maintained around the same values of the original scenario (HS) when reducing the FC price.

4.5.3.2 Analysis of Optimization Variables

After the analysis of the LCC variation, the following paragraphs focus on the variation of the optimization variables. For this approach, Figure 4.33 depicts the relation between these variables and the LCC values at the different scenarios. The figure follows the same format as the previously introduced Figures 4.27 and 4.30: the LCC is normalized in relation to the best option of each scenario, each column of graphs presents the results for one optimization variable, and each row of graphs corresponds to one scenario (HS, MS and LS, respectively).

Regarding the optimal FC size, the results show that there is no change when varying c_{FC}. In all the scenarios, the cases with a better LCC propose to integrate a 600 kW FC. When reducing c_{FC}, it would be possible that even bigger FC become the best option, as their higher acquisition and replacement costs may be compensated by their higher hydrogen use efficiency. However, a FC bigger than 600 kW requires a lower BT size, what may not be optimal from a technical (required power peaks) or cost-efficiency (BT degradation acceleration) perspective.

Focusing on the remainder optimization variables, the results unveil that there are neither big changes when varying c_{FC}. In the different scenarios, the optimal BT sizes

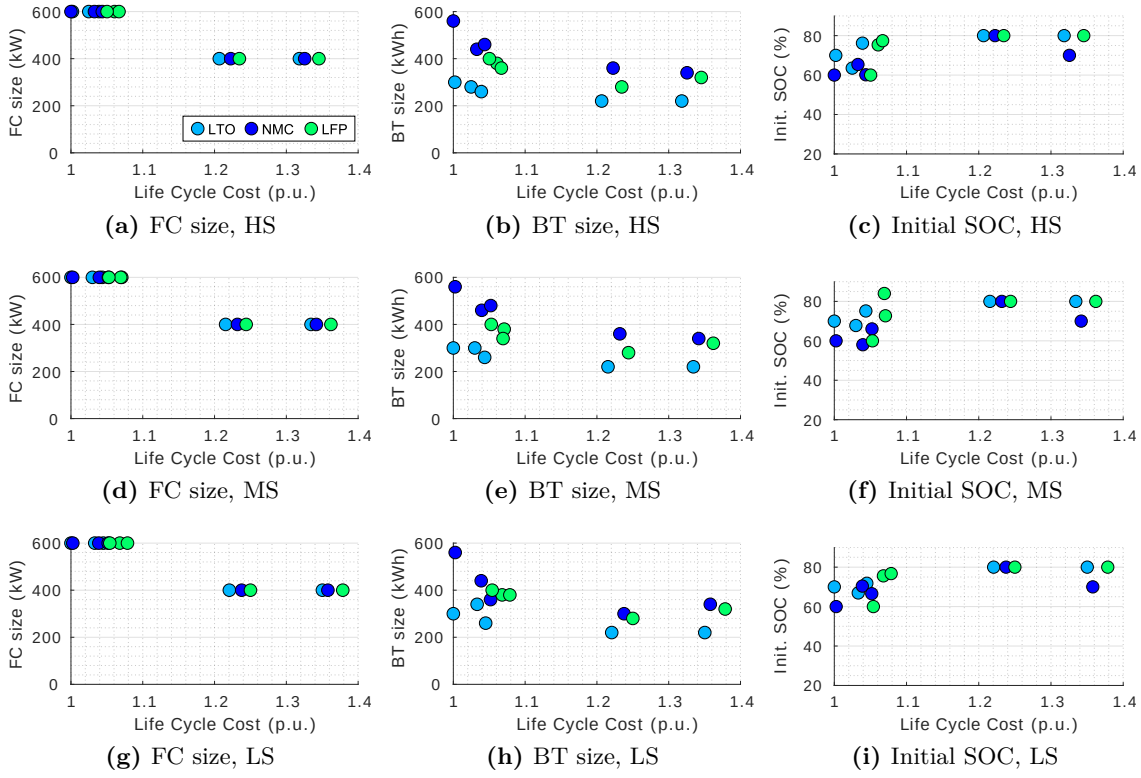

(a) FC size, HS **(b)** BT size, HS **(c)** Initial SOC, HS

(d) FC size, MS **(e)** BT size, MS **(f)** Initial SOC, MS

(g) FC size, LS **(h)** BT size, LS **(i)** Initial SOC, LS

Figure 4.33: Sensitivity of optimization variables to c_{FC}.

of the best cases are maintained between 260-340 kWh when integrating LTO, between 360-560 kWh with NMC, and between 340-400 kWh with LFP. Regarding SOC_0, the optimal values are also maintained between the 60-80% through the different scenarios.

4.5.3.3 Influence of Key Cost Terms on Overall LCC

Finally, this subsection focuses on how does the influence of each of the variable cost terms change when varying the FC price. Figure 4.31 shows the relation of the mentioned costs and the overall LCC at the different scenarios. The figure follows the same format as the previously depicted Figures 4.28 and 4.31: both related variables are normalized in relation to the LCC of the best case, at each column of graphs a different cost term is introduced, each row corresponds to a different scenario, and all the graphs share the same scale in the y-axis.

The analysis of the LCC and optimization variables has shown that little changes happen when varying c_{FC}. Logically, the analysis of Figure 4.34 also unveils that the importance of the different variable cost terms do not vary much when the FC cost is reduced. This clearly demonstrates that c_{FC} does not influence much the optimal design of the H_2EMU.

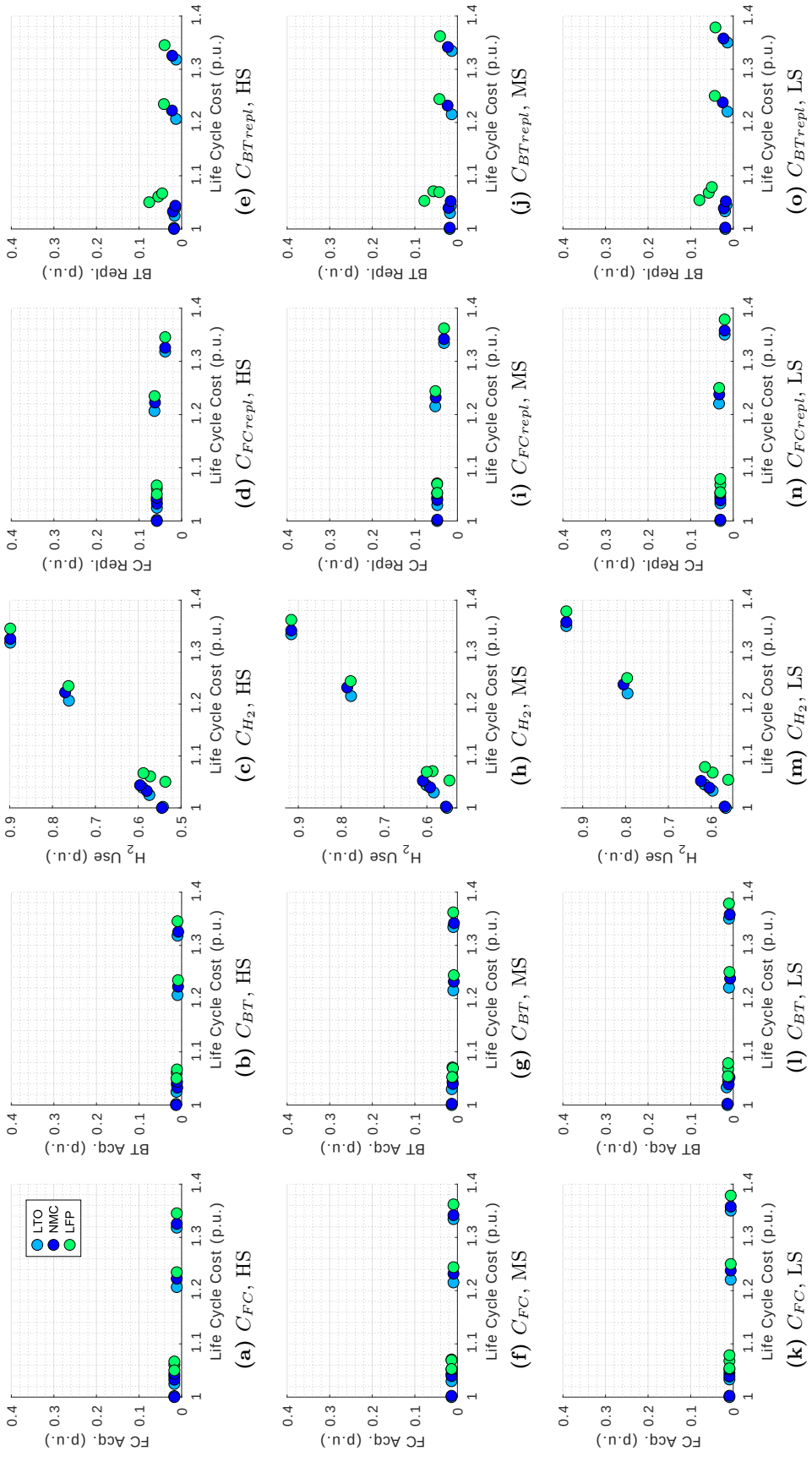

(a) C_{FC}, HS **(b)** C_{BT}, HS **(c)** C_{H_2}, HS **(d)** C_{FCrepl}, HS **(e)** C_{BTrepl}, HS

(f) C_{FC}, MS **(g)** C_{BT}, MS **(h)** C_{H_2}, MS **(i)** C_{FCrepl}, MS **(j)** C_{BTrepl}, MS

(k) C_{FC}, LS **(l)** C_{BT}, LS **(m)** C_{H_2}, LS **(n)** C_{FCrepl}, LS **(o)** C_{BTrepl}, LS

Figure 4.34: Sensitivity of key cost terms to c_{FC}.

The hydrogen use C_{H_2} continues being the cost term with the major contribution to the LCC. When reducing c_{FC}, this contribution slightly increases. Indeed, in the cases with a better LCC, the contribution of C_{H_2} stays around the 53-60% in the HS, around the 55-62% in the MS, and around the 56-63% in the HS. As it was already highlighted, this increase in the contribution influences the performance of DP: as the importance of C_{H_2} is increased, DP increases the LCC difference with the remainder strategies.

The contributions of the BT related cost terms (C_{BT} and C_{BTrepl}) are also slightly increased when reducing the FC price. However, as these values were already low in the HS, the increase is barely noticeable. In the case of C_{BT}, the values are maintained below the 1% also in the LS. Regarding C_{BTrepl}, the values are maintained below the 2% in the LS in the case of LTO and NMC, and below the 9% in the case of LFP. Therefore, it is concluded that C_{BT} and C_{BTrepl} do not increase their influence when varying c_{FC}.

The cause of the slightly increase in the contributions of C_{H_2}, C_{BT} and C_{BTrepl} is that the contributions of the FC related cost terms (C_{FC} and C_{FCrepl}) are logically reduced when reducing the FC price. In the case of the FC acquisition cost, this reduction is barely noticeable, as in the original scenario (HS) the contribution to the overall LCC was lower than the 1% in most of the cases. Regarding the FC replacement cost, the reduction is more evident: in the best cases, the contribution stays around the 6% in the HS, around the 5% in the MS, and around the 3% in the LS. Therefore, C_{FCrepl} is the cost term that reduces most its contribution to the overall LCC when reducing c_{FC}. Anyway, as it was already highlighted, this reduction in the contribution of both FC related cost terms barely affects the influence of the remainder cost terms.

4.5.4 Sensitivity to BT Price

Finally, the sensitivity analysis to the economic model focuses on varying the price the BT, c_{BT}. Considering that each BT chemistry has a different cost also in the nominal scenario, this analysis is developed individually for each chemistry. As previously defined, in the case of LTO 1200-1500-1800 €/kWh prices are proposed for each scenario (LS-MS-HS, respectively), in the case of NMC 640-800-960 €/kWh, and in the case of LFP 520-1040-1560 €/kWh. In all the cases, the MS corresponds to the nominal scenario already analysed in Section 4.4. The analysis of this subsection will be focused on evaluating how do the LCC values, optimization variables and terms of the economic model vary when varying c_{BT}. An independent section is defined for each analysis.

4.5.4.1 Analysis of LCC Values

Figure 4.35 depicts three graphs that represent the LCC variations at the different c_{BT} scenarios. When c_{BT} is varied for one chemistry, logically the results of the other chemistries are not affected. However, in order to better evaluate what happens when varying the price of a single chemistry, one independent graph is depicted for the variation

of each chemistry price: Figure 4.35a shows what happens when changing LTO price, Figure 4.35b when changing NMC price, and Figure 4.35c when changing LFP price. At each graph, the results of the three BT chemistries are depicted. In order to easily identify the chemistry that it is being analysed, the chemistries with no variation have a grey background. The figures respect the same format as the previously introduced Figures 4.26, 4.29 and 4.32, what means that NMC is the case used as a reference. This is why in Figure 4.35b the values of LFP and LTO change from one scenario to another. Indeed, even if their absolute values do not vary, as the reference values have changed, their relative values are not the same in the different scenarios.

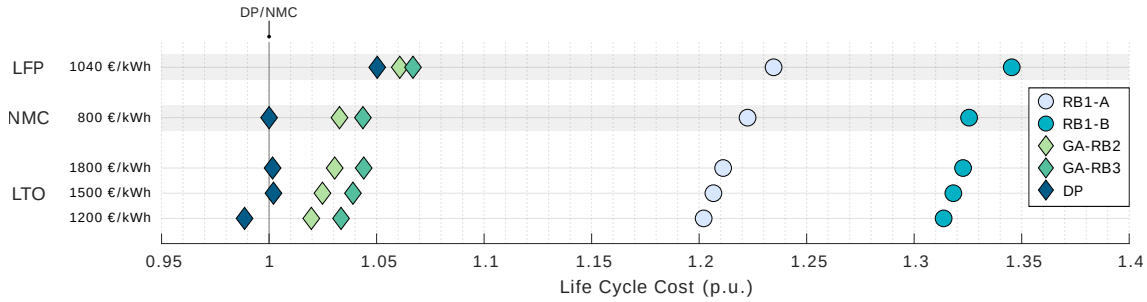

(a) Variation of LTO price

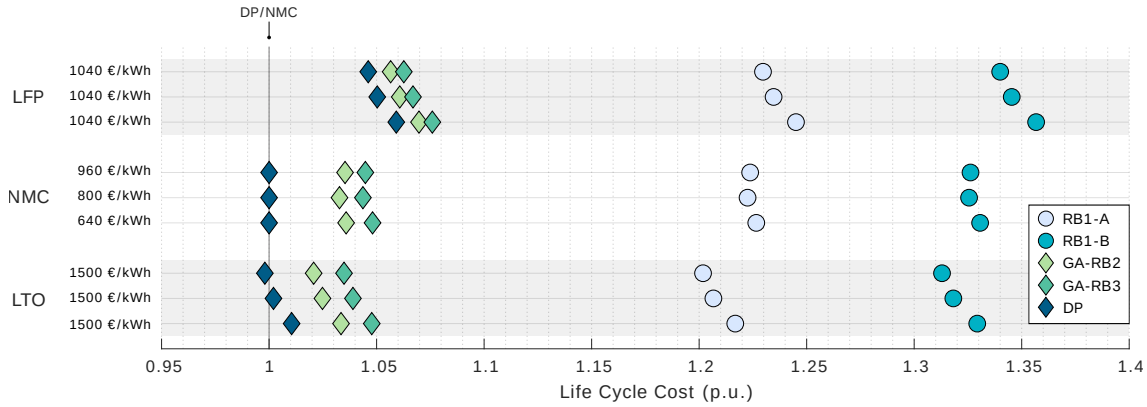

(b) Variation of NMC price

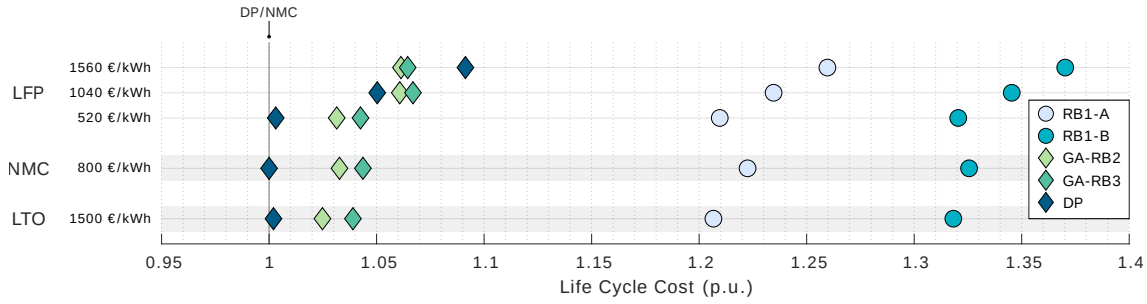

(c) Variation of LFP price

Figure 4.35: Sensitivity of LCC values to c_{BT}.

In a first step, the analysis is focused on comparing the performance of the control strategies in the different scenarios. LTO and NMC price variation seem to have small

effect on the performance of the different control strategies: when varying their price, DP continues being the best strategy, followed by GA-RB2, GA-RB3, RB1-A and RB1-B. Besides, there is no notable variation in the LCC difference between the different strategies.

However, in the case of LFP some changes in relation to the original case are identified, specially regarding the performance of DP. As it will be analysed afterwards, when the BT price is reduced, the importance of C_{BTrepl} is also reduced, what has a notorious impact in the case of LFP. When integrating this chemistry, DP is the strategy that degrades most the BT. Therefore, DP improves its performance when reducing c_{BT} (in the LS it increases the LCC difference with GA-RB2 and GA-RB3 to nearly the 3% and 4%, respectively), and it worsens its performance when increasing c_{BT} (in the HS it obtains higher LCC than GA-RB2 and GA-RB3). On the contrary, GA-RB3 is the strategy that reduces most the BT degradation. Therefore, it tends to improve its performance when increasing LFP price, but even in the HS this is not enough to improve GA-RB2 result.

In a second step, the analysis is focused on the comparison of the different chemistries. Regarding LTO, the results show that when increasing its price, the LCC values of LTO and NMC become closer: 0.2% difference with DP and GA-RB2, and 0.1% difference with GA-RB3 (RB1 results are excluded as they are not representative). On the contrary, when reducing its price, LTO clearly becomes the best option, as the LCC difference with NMC becomes notorious in the LS: 1.1% lower LCC in the case of DP, 1.3% lower in the case of GA-RB2, and 1% lower in the case of GA-RB3. When varying NMC price, similar conclusions are obtained. On the one hand, reducing NMC price has a similar impact as increasing LTO price: LTO and NMC obtain similar LCC values. And on the other hand, increasing NMC price has a similar impact as reducing LTO price: LTO becomes clearly the best option. Therefore, it can be concluded that a higher LTO price increase or NMC price decrease are necessary for NMC to become the best option against LTO.

Regarding LFP price variation, the results unveil that when reducing its price, it can become a competitive option. Indeed, it can be checked that in the LS the LCC values of this chemistry get close to the values of LTO and NMC: in the case of DP strategy, it is just 0.1% and 0.3% behind LTO and NMC; in the case of GA-RB2, 0.7% behind LTO and 0.1% ahead of NMC; and in the case of GA-RB3, 0.3% behind LTO and 0.1% ahead of NMC. On the contrary, when increasing its price, the difference with the remainder chemistries becomes even higher than in the original scenario (MS), what makes LFP be an unfeasible option from the economic scope.

4.5.4.2 Analysis of Optimization Variables

Besides the analysis of the LCC variation, in this subsection the variation of the optimization variables is also analysed. For this approach, Figure 4.36 depicts the relation between these variables and the LCC values at the different scenarios. The figure follows the same format as the previously introduced Figures 4.27, 4.30 and 4.33. As it was al-

ready mentioned, the aim of this figure is to evaluate the variations in the optimization variables, instead of comparing the exact LCC values. Due to this reason and in the sake of simplicity, at each cost scenario the results of each chemistry refer to the results when solely varying their price. As an example, in Figure 4.36a the results refer to the case when all the BT prices are in the HS: the results of LTO refer to the increase of its cost to 1800 €/kWh, the results of NMC to the increase of its cost to 960 €/kWh, and the results of LFP to the increase of its cost to 1560 €/kWh.

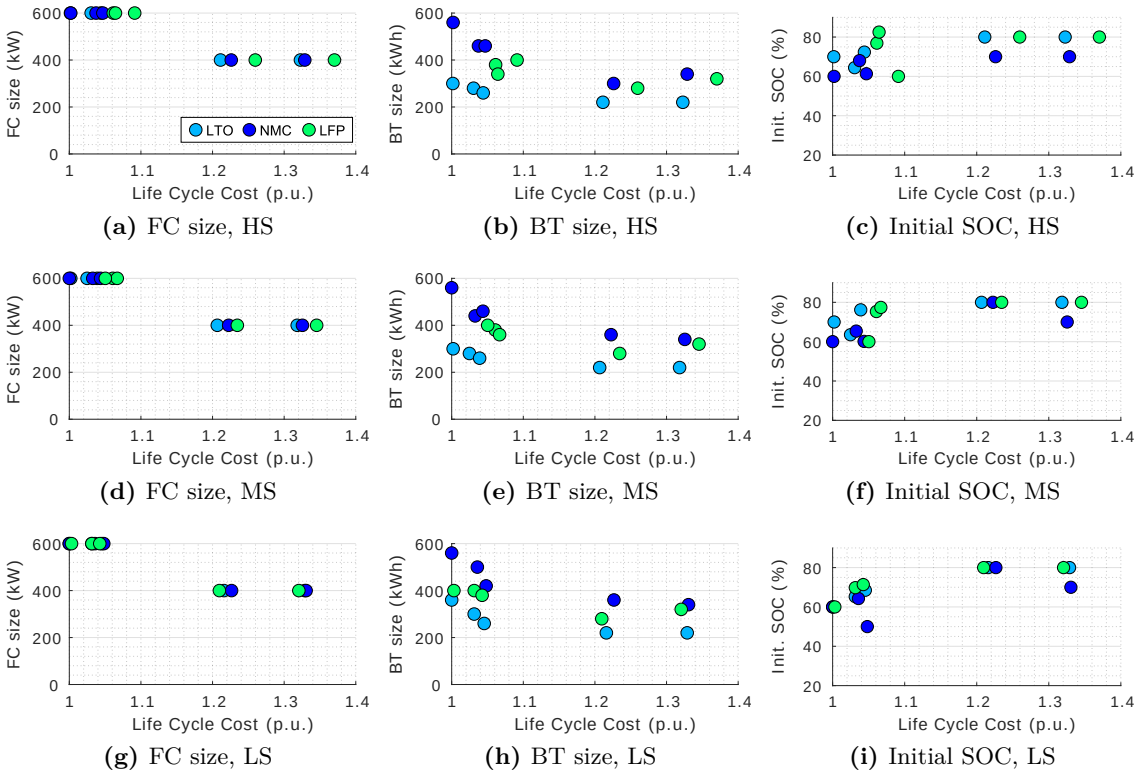

(a) FC size, HS **(b)** BT size, HS **(c)** Initial SOC, HS

(d) FC size, MS **(e)** BT size, MS **(f)** Initial SOC, MS

(g) FC size, LS **(h)** BT size, LS **(i)** Initial SOC, LS

Figure 4.36: Sensitivity of optimization variables to c_{BT}.

Regarding the optimal FC size (Figures 4.36a, 4.36d and 4.36g), the results show that no variation happens when reducing or increasing c_{BT}. Indeed, in all the scenarios the cases with a lower LCC propose to integrate the FC of 600 kW.

Focusing on the optimal BT size, some slight changes are identified, but in general the same tendencies as in the original scenario (MS) are maintained. In the case of LTO, when increasing its costs the optimal values of the best cases are maintained around 260-300 kWh, which are the same values as in the MS. When reducing its price, some of the best solutions propose higher sizes (up to 360 kWh), due to the fact that the influence of C_{BT} and C_{BTrepl} is reduced. In the case of NMC and LFP, no important changes are identified, as in the different scenarios the optimal values are maintained around 420-560 kWh (NMC) and around 340-400 kWh (LFP).

Regarding the optimal initial SOC values, some slight changes are also identified. In

the case of NMC, some values closer to the 50% are proposed when reducing its price. In the remainder cases, the values are concentrated around the 60-80%, as in the original scenario (MS). These results confirm that there is no remarkable SOC_0 value that reduces the LCC even when varying c_{BT}.

4.5.4.3 Influence of Key Cost Terms on Overall LCC

After having analysed the LCC values and the returned optimization variables, this last step focuses on the key cost terms of the economic model (C_{FC}, C_{BT}, C_{H_2}, C_{FCrepl} and FC_{BTrepl}). Figure 4.37 depicts a series of graphs that relate the obtained LCC values and these cost terms for the different BT cost scenarios. The figure and subplots follow the same arrangement as the previously introduced Figures 4.28, 4.31 and 4.34. All the graphs share the same scale in the y-axis in order to better identify the correlations. Moreover, as in Figure 4.36, the results of each chemistry refer only to the variation of their price. Therefore, these graphs are not convenient to compare the LCC values of the different BT chemistries or EMSs.

The results show that in the different scenarios C_{H_2} continues being the cost term with the highest contribution to the overall LCC. Indeed, its contribution is barely increased or decreased when varying c_{BT}, as the best values are always around the 52%. However, its influence is affected by the BT price variation: in the LS and MS the relation between the LCC and C_{H_2} is practically linear, but this linearity is slightly lost in the HS (specially in the case of LFP).

The reason of this linearity loss is that when increasing c_{BT}, the importance of the BT replacements increases, specially in the case of LFP (as this chemistry shows the shortest lifetimes). As it can be seen, the contribution of C_{BTrepl} is higher as the BT price increases, and it reaches the 11% in the worst case of LFP. This reverses the tendency between C_{BTrepl} and the LCC: in LS the solutions with a lower C_{BTrepl} obtain a worse LCC, but in the HS the solutions with a lower C_{BTrepl} are the ones that obtain a better LCC. This demonstrates that in the HS of LFP a compromise between the hydrogen use and the battery degradation has to be reached.

The BT acquisition costs are also increased when increasing c_{BT}. However, even in the HS, most of the cases do not contribute more than the 1%. Therefore, the influence of C_{BT} continues being residual. Finally, regarding the FC related costs, no important variations are found: in cases with a lowest LCC, the contribution of C_{FC} is maintained around the 1%, and the contribution of C_{FCrepl} around the 6%.

4.5.5 Review of Sensitivity Analysis to Economic Model

In this section the effects of varying the daily operation hours (t_{day}), the hydrogen price (c_{H_2}), the FC price (c_{FC}) and the BT price (c_{BT}) have been evaluated. The analysis

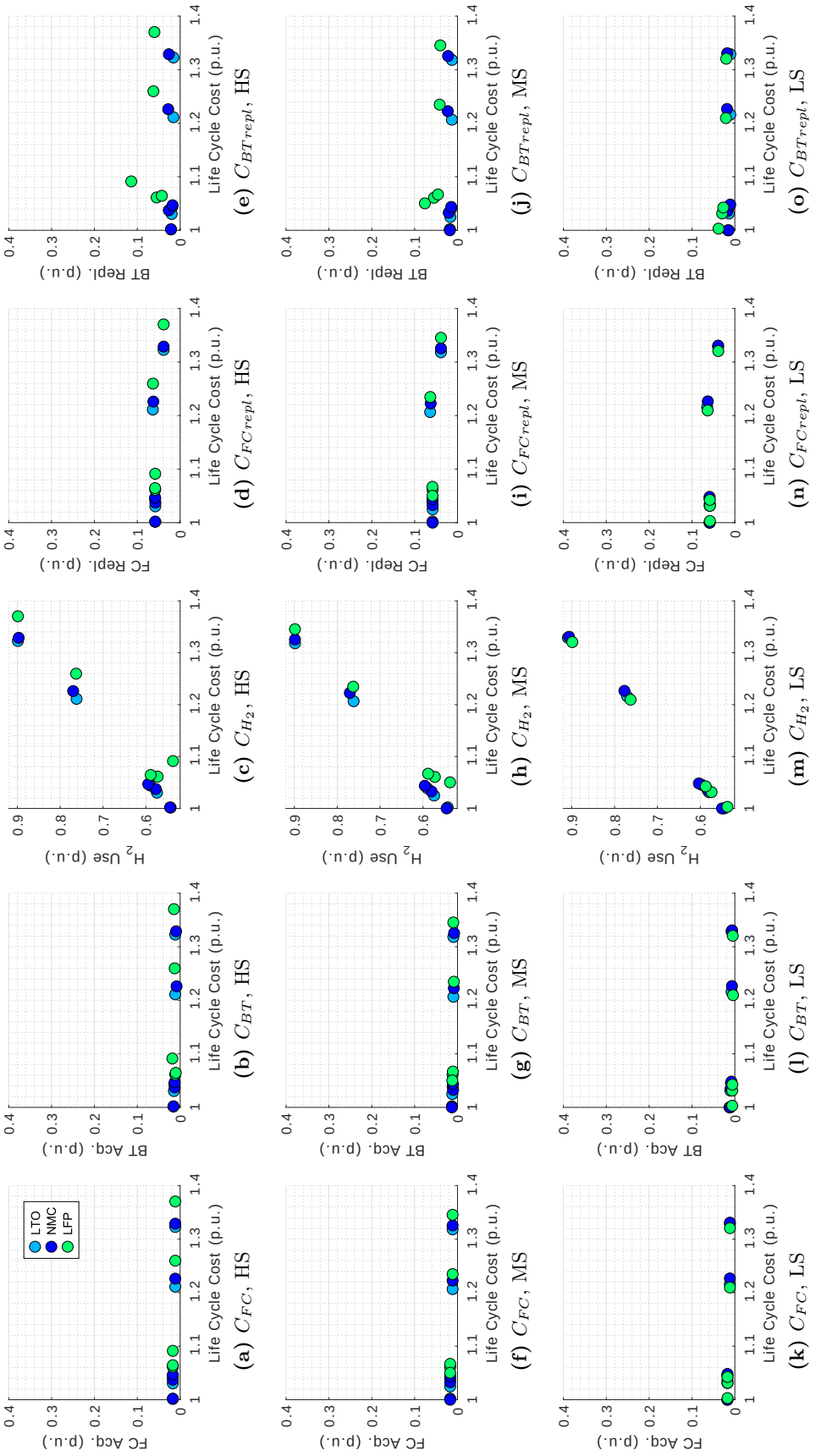

(a) C_{FC}, HS **(b)** C_{BT}, HS **(c)** C_{H_2}, HS **(d)** C_{FCrepl}, HS **(e)** C_{BTrepl}, HS
(f) C_{FC}, MS **(g)** C_{BT}, MS **(h)** C_{H_2}, MS **(i)** C_{FCrepl}, MS **(j)** C_{BTrepl}, MS
(k) C_{FC}, LS **(l)** C_{BT}, LS **(m)** C_{H_2}, LS **(n)** C_{FCrepl}, LS **(o)** C_{BTrepl}, LS

Figure 4.37: Sensitivity of key cost terms to c_{BT}.

has been focused on how is the H_2EMU optimal powertrain design affected when varying the mentioned parameters of the economic model. Specifically, the variations in the LCC values of the different control strategies and BT chemistries, the variations in the returned optimization variables, and the variations in the influence of the key cost terms of the economic model (C_{FC}, C_{BT}, C_{H_2}, C_{FCrepl} and FC_{BTrepl}) have been evaluated.

Table 4.12 reviews the main conclusions obtained in this section. At each column, the effect of the different parameters of the economic model are listed; and at each row, the analysed design decisions. In short, the value of each cell refers to how much the specific design decision has changed when varying the specific parameter of the economic model (e.g., how much have changed the results of the optimal BT size when varying the operation hours). At each cell, the superscript number refers to the comment at which each conclusion is further discussed. The corresponding comments are listed below:

Table 4.12: How much does the variation of each parameter influence the optimal design of the H_2EMU powertrain.

	Operation hours	**H_2 price**	**FC price**	**BT price**
Optimality of EMSs	●○○(01)	●●○(02)	◐○○(03)	◐○○(04)
Optimality of BT chemistries	◐○○(05)	●○○(06)	○○○(07)	●●●(08)
Optimal FC size	◐○○(09)	●◐○(10)	◐○○(11)	○○○(12)
Optimal BT size	●●○(13)	◐○○(14)	◐○○(15)	◐○○(16)
Optimal SOC_0	◐○○(17)	●○○(18)	◐○○(19)	●○○(20)
Influence of cost terms	●○○(21)	●●○(22)	○○○(23)	●○○(24)

(1) When reducing t_{day}, the LCC difference between the EMSs is reduced, but the reduction is proportional in all cases (no EMS improves/worsens its results).

(2) When reducing c_{H_2}, the LCC difference between the EMSs is reduced. Besides, the performance of DP goes down as the importance of minimizing C_{H_2} is reduced.

(3) When reducing c_{FC}, DP slightly increases the LCC difference with the remainder EMSs (the importance of minimizing C_{H_2} increases), but the overall picture is maintained.

(4) Only in the case of LFP, when its price is increased, DP performs worse and GA-RB3 obtains a slightly better result, as the importance of reducing C_{BTrepl} increases.

(5) When the operation hours are reduced, LFP reduces the LCC difference with the remainder chemistries (as the BT lifes are increased), but it is still far from LTO and NMC.

(6) When reducing c_{H_2}, LFP obtains even worse results compared to NMC and LTO, as the importance of C_{BTrepl} slightly increases.

(7) There are no notable changes when increasing or decreasing the FC price

(8) Several changes are found when varying c_{BT}. When NMC price is increased or

LTO price is reduced, the LCC difference between both chemistries is increased and LTO obtains clearly better results (difference higher than 1%). On the contrary, when NMC price is reduced or LTO price is increased, both chemistries obtain very similar LCC values (difference is residual). Finally, when LFP price is reduced, it becomes a competitive option, as it gets close to LTO and NMC in LCC terms (difference lower than 1%).

(9) When reducing t_{day} in the proposed terms, slight changes are found. If t_{day} is further reduced, lower FC sizes are expected to become the optimal option (the advantage of bigger sizes may be reduced).

(10) When reducing c_{H_2} in the proposed terms, the FC of 500 kW becomes the optimal option, as the advantage of bigger sizes is reduced.

(11) When reducing the FC price, even bigger FC sizes may become the optimal option, but the size restrictions impedes this. Consequently, no changes are found.

(12) There are no notable changes when increasing or decreasing the BT price.

(13) When reducing t_{day}, the optimal BT sizes are reduced, as the advantage of bigger sizes disappears.

(14) The trend of the original case is maintained when reducing the hydrogen price, even if slight changes are identified.

(15) Even if slight changes are identified, the trend of the original case is maintained when reducing the FC price.

(16) The trend of the original case is maintained when varying the BT price, even if slight changes are identified.

(17) When varying the operation hours, the optimal values are maintained around 60-80%, even if some changes are identified.

(18) When reducing c_{H_2}, some optimal values are found to be lower than 60%, but no different trend is found.

(19) When reducing the FC price, even if some changes are identified, the optimal values are maintained around 60-80%.

(20) When varying c_{BT}, in general the same trend is maintained, even if some optimal values are found to be lower than 60%.

(21) When reducing t_{day}, the contributions of C_{H_2} and C_{BTrepl} are reduced, and therefore C_{H_2} continues being the cost term with the major influence.

(22) When reducing c_{H2}, the contribution of C_{H_2} is logically reduced. Consequently, the contribution of the remainder cost term is increased, and in the case of LFP, C_{BTrepl}

becomes an important cost terms to reduce the overall LCC.

(23) No important changes are found when varying the FC price.

(24) When increasing the BT price, the contribution of C_{BTrepl} is increased, but the contribution of C_{H_2} is maintained. Consequently, C_{BTrepl} only becomes an important cost term in the case of LFP.

4.6 Results of Sensitivity Analysis to Driving Cycle

After presenting the results of the first two sensitivity analyses, this section focuses on the sensitivity analysis to the driving cycle. The objective of this section is to evaluate how do the results and conclusions of the powertrain design (Section 4.4) change when the H_2EMU drives through routes with different characteristics. For this approach, the sensitivity to the powertrain design is repeated in 12 routes of different lengths and average demands (which were presented in Section 4.2.4). The results have been obtained for the nominal parametrization of the economic model. Figure 4.38 shows the location of the current sensitivity analysis in the methodology proposed in this Ph.D. Thesis.

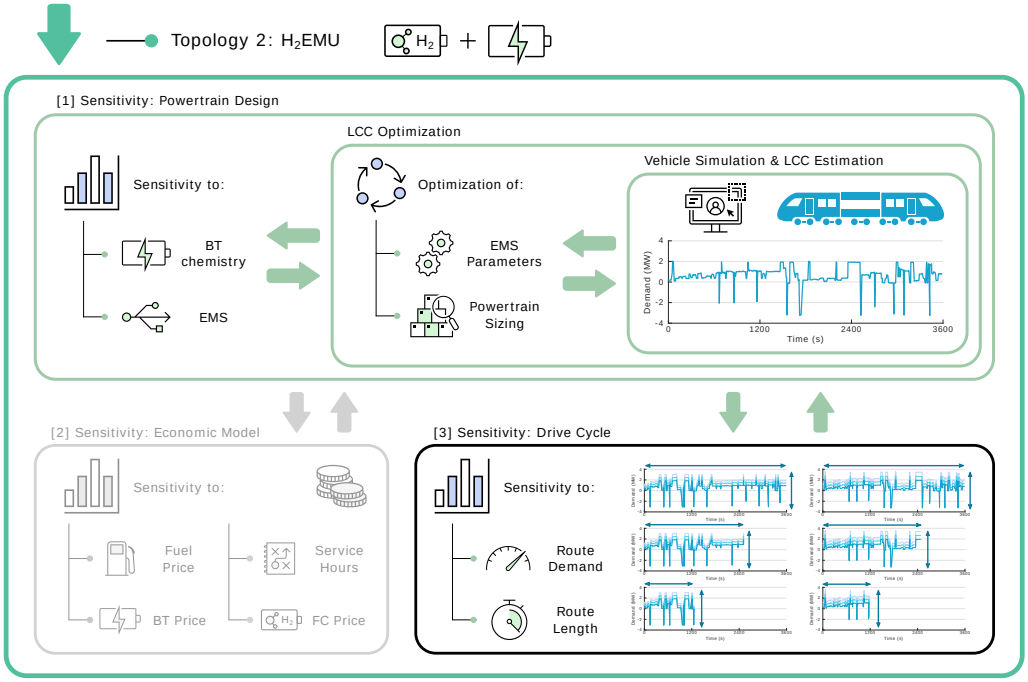

Figure 4.38: Current step of holistic design methodology.

As repeating the sensitivity analysis to the powertrain design in different scenarios is a time consuming process, some of the initially proposed EMSs and BT chemistries are kept out of the current analysis. This decision has been made considering the conclusions obtained in previous sections. Regarding the control strategies, the results have demonstrated that RB1-B is not able to outperform RB1-A. As it is estimated that due to its

characteristics, RB1-B will not improve the result of RB1-A even when varying the driving cycle, it is kept out of the current sensitivity analysis. In addition, a similar decision has been taken with LFP. The contexts analysed so far have demonstrated that LFP is behind NMC and LTO, and therefore it is excluded from the current sensitivity analysis.

The development of the sensitivity analysis is divided into different subsections, as it has been done in the previous two sensitivity analyses. First, Section 4.6.1 focuses on the LCC obtained by the different BT chemistries and control strategies when simulating different driving cycles. Then, in Section 4.6.2 the optimal values of the optimization variables are analysed. A similar analysis is developed in Section 4.6.3, but in this case the analysis focuses on the key cost terms of the LCC model (C_{FC}, C_{BT}, C_{H_2}, C_{FCrepl} and C_{BTrepl}). Finally, the main conclusions are reviewed in Section 4.6.4.

4.6.1 Analysis of LCC Values

Figure 4.39 helps in the analysis developed in this subsection, as it depicts the variation of the LCC values of the different cases through the modified scenarios. The results are grouped in rows by each BT chemistry, and the markers represent the different control strategies. For the results of each driving cycle, the LCC is normalized in relation to the result of DP with NMC, which corresponds to the optimal case of the first analysis (Section 4.4). The numbers in the left define the approximate characteristics of each driving cycle, i.e., the average demand power (kW) and the length of the route (h). To better differentiate the cases, a different background colour is used for each average power demand.

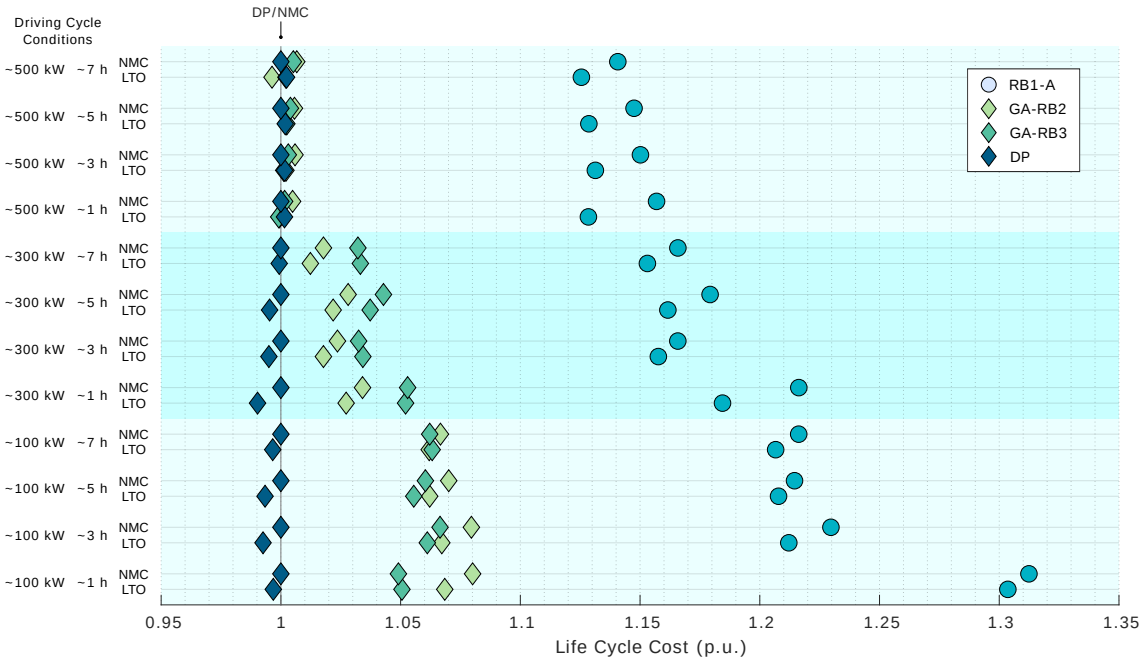

Figure 4.39: Sensitivity of LCC values to different driving cycles.

In the following paragraphs, the results will be analysed from two points of view: focusing on the comparison of the different BT chemistries, and focusing on the comparison of the different control strategies.

Regarding the BT chemistries, the results show that the conclusions obtained in the sensitivity analysis to the powertrain design are essentially maintained even when varying the driving cycle: the difference between both chemistries is low, but LTO tends to obtain better results. If we consider the 48 cases where the result of both chemistries can be fairly compared (12 driving cycles and 4 EMSs), LTO obtains a lower LCC in 40 cases, while there are just 8 cases where the LCC is favourable for NMC. Anyway, in most of the cases the difference between both chemistries is lower than the 1%: specifically, in 37 out of 48 cases. Moreover, most of the cases where the difference is higher than the 1% correspond to the results of RB1-A, which is not a representative EMS, as its results are far from the ones obtained by the other strategies. Therefore, it is demonstrated that the small LCC difference between LTO and NMC is maintained when both the mean power demand and the length of the route are varied.

Regarding the control strategies, the depicted results demonstrate that the performance of the different EMSs is affected by the characteristics of the driving cycle. The average demand of the route is found to affect this performance more than the length of the route, as it is analysed in detail in the following lines:

- With a mean demand around 100 kW, the LCC difference between DP and the remainder strategies is notorious: 5-7% difference with GA-RB3 and 6-8% difference with GA-RB2. In the majority of cases, GA-RB3 improves the results of GA-RB2, contrary to the conclusions obtained in previous sensitivity analyses. RB1-A stays far from the results of the remainder strategies: the LCC difference with DP is always higher than the 20%.
- When the mean demand is increased to 300 kW, the difference between the control strategies is reduced, but DP continues being always the best strategy. Specifically, it improves the LCC of GA-RB2 and GA-RB3 around 1-4% and around 3-6%, respectively. In this case, GA-RB2 obtains always a better result compared to GA-RB3, which coincides with the conclusions obtained in previous sensitivity analyses. Even if the difference is reduced, RB1-A continues being far from the remainder strategies.
- Finally, in the highest analysed mean demand (around 500 kW), the three best strategies obtain similar results. Indeed, the LCC difference between DP, GA-RB2 and GA-RB3 is always lower than the 2%, and in most of the cases lower than the 1%. Moreover, there is not a strategy that clearly obtains always the best result. The difference of these strategies with RB1-A is always higher than the 10%.

As previously mentioned, no big differences in the obtained results are found when varying the length of the route. As this variable is increased, GA-RB2 and RB1-A tend to improve their results, while there is no notable effect in the results of DP or GA-RB3.

Anyway, the effect of varying the route length is low, and never bigger than the effect of varying the mean demand.

4.6.2 Analysis of Optimization Variables

In the next step, this subsection focuses on the values of the optimization variables returned by the optimization approach in the different scenarios. As in previous cases, the analysed variables are the FC size (n_{FC}), the BT size (n_{BT}) and the initial SOC (SOC_0).

In order to ease the development of this analysis, Figure 4.40 shows a series of graphs that represent the variation of these variables (in the y-axis) with respect to the characteristics of the route (in the x-axis). The upper graphs show the results for n_{FC}, the graphs in the middle the results for n_{BT}, and the lower graphs the results for SOC_0. Then, the left side graphs present the results of LTO, and the right side graphs the results of NMC. Each control strategy has a different marker shape, as defined in the legend. In addition, different background colours are used: the darker colours refer to the best solution of each scenario, and the lighter colours are used for the remainder strategies. The objective of this differentiation in the colour is to highlight which is the value proposed by the case with the best LCC at each driving cycle.

The results show that there is a linear relation between the mean demand of the route and the optimal FC size. Indeed, in order to maintain the energy of the BT, the FC should give approximately that average power. Therefore, a bigger FC will be required in driving cycles with a higher mean power demand. With an average demand around 100 kW, the optimal FC sizes are found to be around 200-300 kW; with an average demand around 300 kW, the optimal FC sizes are increased to 600 kW; and with an average demand around 500 kW, the optimal FC sizes are further increased to 900 kW (these values correspond to the FC sizes obtained with the strategies that obtain the best results). Therefore, it is found that the optimal option continues being to oversize the FC, as in the sensitivity analysis to the powertrain design.

Regarding the route length, the graphs show that it roughly affects the definition of the optimal FC size. Indeed, there are just few cases where this value changes when varying the route length, and in some of this cases there is not even a linear relation between both variables (i.e., the optimal FC size is not increased when increasing the length). The optimal FC size is neither affected by the BT chemistry, as in both Figures 4.40a and 4.40b similar results are obtained.

Focusing on the optimal BT sizes, the results also show that this optimization variable is more correlated with the average route demand than to the route length. Regarding LTO chemistry, the strategies with the lowest LCC propose the following sizes: around 260 kWh when the average demand is nearly 100 kW; around 200 kWh when the average demand is nearly 300 kW; and around 160-180 kWh when the average demand is nearly 500 kW. Regarding NMC, a higher variation is found when changing the route length,

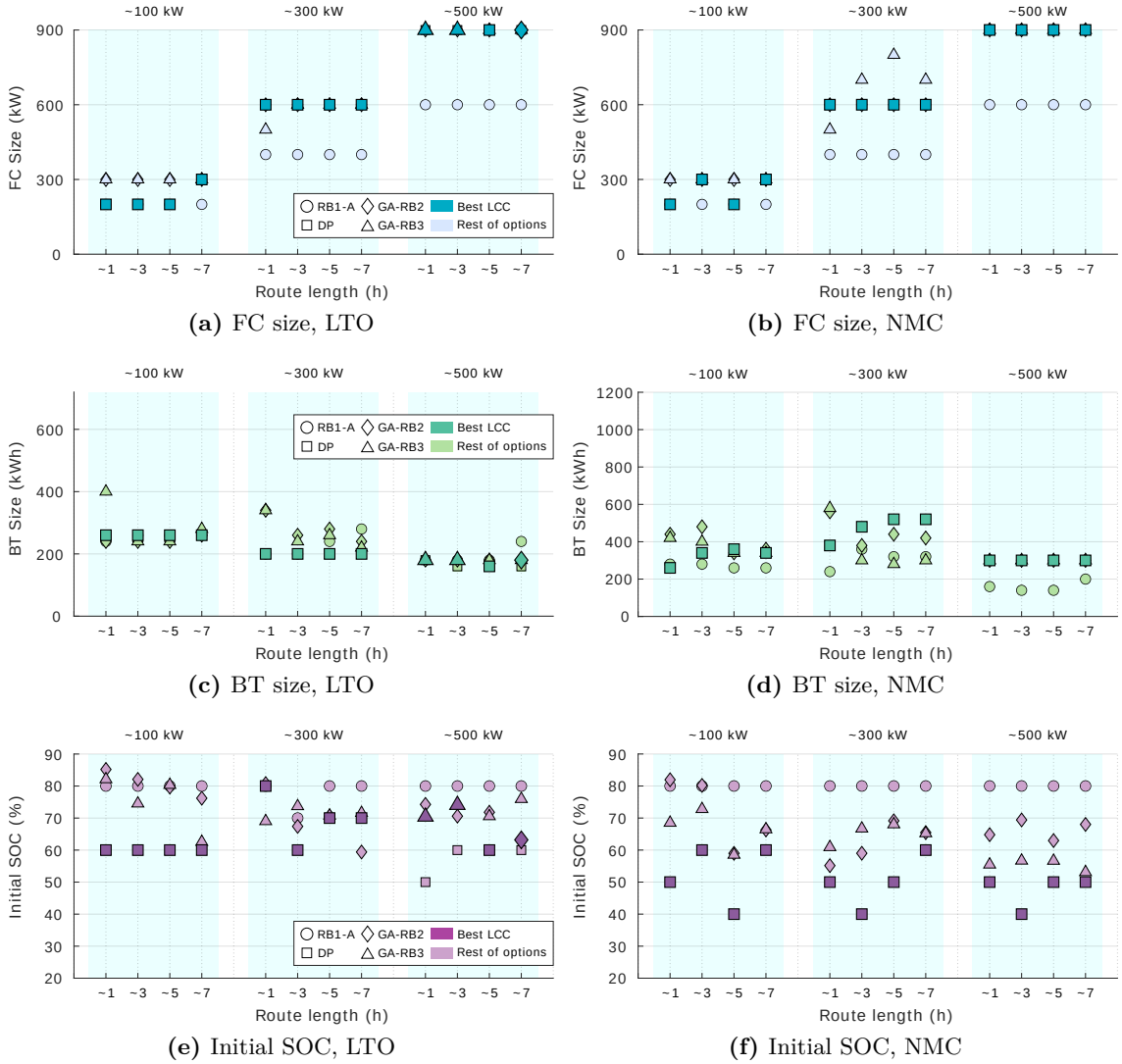

(a) FC size, LTO

(b) FC size, NMC

(c) BT size, LTO

(d) BT size, NMC

(e) Initial SOC, LTO

(f) Initial SOC, NMC

Figure 4.40: Sensitivity of optimization variables to different driving cycles.

but no clear correlation with this variable is obtained. The following optimal values are obtained: around 260-360 kWh when the average demand is nearly 100 kW; around 380-520 kWh when the average demand is nearly 300 kW; and around 300 kWh when the average demand is nearly 500 kW.

These results are affected by the limitations in the amount of energy that can be integrated in the vehicles (see Figure 4.12). As mentioned, the average demand limits the optimal FC size: as higher is the demand, bigger FC sizes are required, what leaves less available space for the BT system. In this context, different conclusions are obtained at each of the analysed average mean demands:

- In the case of an average demand around 100 kW, the maximum allowable BT energy is 540 kWh for LTO and 900 kWh for NMC. Therefore, the optimal BT sizes are far

from these maximum values.

- In the case of an average demand around 300 kW, the maximum allowable BT energy is 360 kWh for LTO and 600 kWh for NMC. Hence, the optimal BT sizes are closer to these values, even if they do not exactly match.
- Finally, in the case of an average demand around 500 kW, the maximum allowable BT energy is 180 kWh for LTO and 300 kWh for NMC. In this case, the optimal BT sizes coincide with the maximum allowable values. This indicates that without the specified space limitation, the optimal sizes may be bigger.

In short, it is demonstrated that as higher is the average route demand, the optimal BT sizes get closer to the maximum allowable values. It is also found that the optimal BT size is not affected by the route length.

The last analysed optimization variable is the initial SOC. As in previous sensitivity analyses, there is no clear correlation between this variable and the characteristics that are being analysed (in this case, the average demand and the route length). This may be due to two reasons. On the one hand, due to the fact that there is a small LCC difference when defining a different initial SOC. And on the other hand, due to the fact that there may be other route characteristics that define which is the best initial SOC: for instance, if the route starts with a downhill, it would be better to start the route at a low SOC; but if the route starts in an uphill, it would be better to start the route at a high SOC.

4.6.3 Influence of Key Cost Terms on Overall LCC

The last step of this sensitivity analysis consists on analysing how does the influence of the key cost terms of the economic model (C_{FC}, C_{BT}, C_{H_2}, C_{FCrepl} and C_{BTrepl}) vary when varying the characteristics of the driving scenario.

For this approach, in Figure 4.41 a series of graphs are depicted, which relate the mentioned cost terms and the route characteristics. As in Figure 4.40, in the x-axis of each graph the different driving cycles are presented, grouped according to the mean average demand. The values of the cost terms are presented in the y-axis, and they have been normalized in relation to the best case of each driving cycle. At each graph, each EMS is represented by a different shape. Besides, the markers that represent the cases with the lowest LCC are depicted with a darker colour, while the rest of cases have a lighter colour. In this way, it is easier to identify which is the best case of each driving cycle. All the graphs respect the same scale in the y-axis (from 0 to 0.6), so it is easier to find correlations between the depicted variables. Subfigures a-b depict the values of C_{FC}, subfigures c-d the values of C_{BT}, subfigures e-f the values of C_{H_2}, subfigures g-h the values of C_{FCrepl}, and subfigures i-j the values of C_{BTrepl}. The left side graphs corresponds to the results of LTO, and the right side graphs to NMC.

As in previous subsections, the graphs demonstrate that the results suffer more vari-

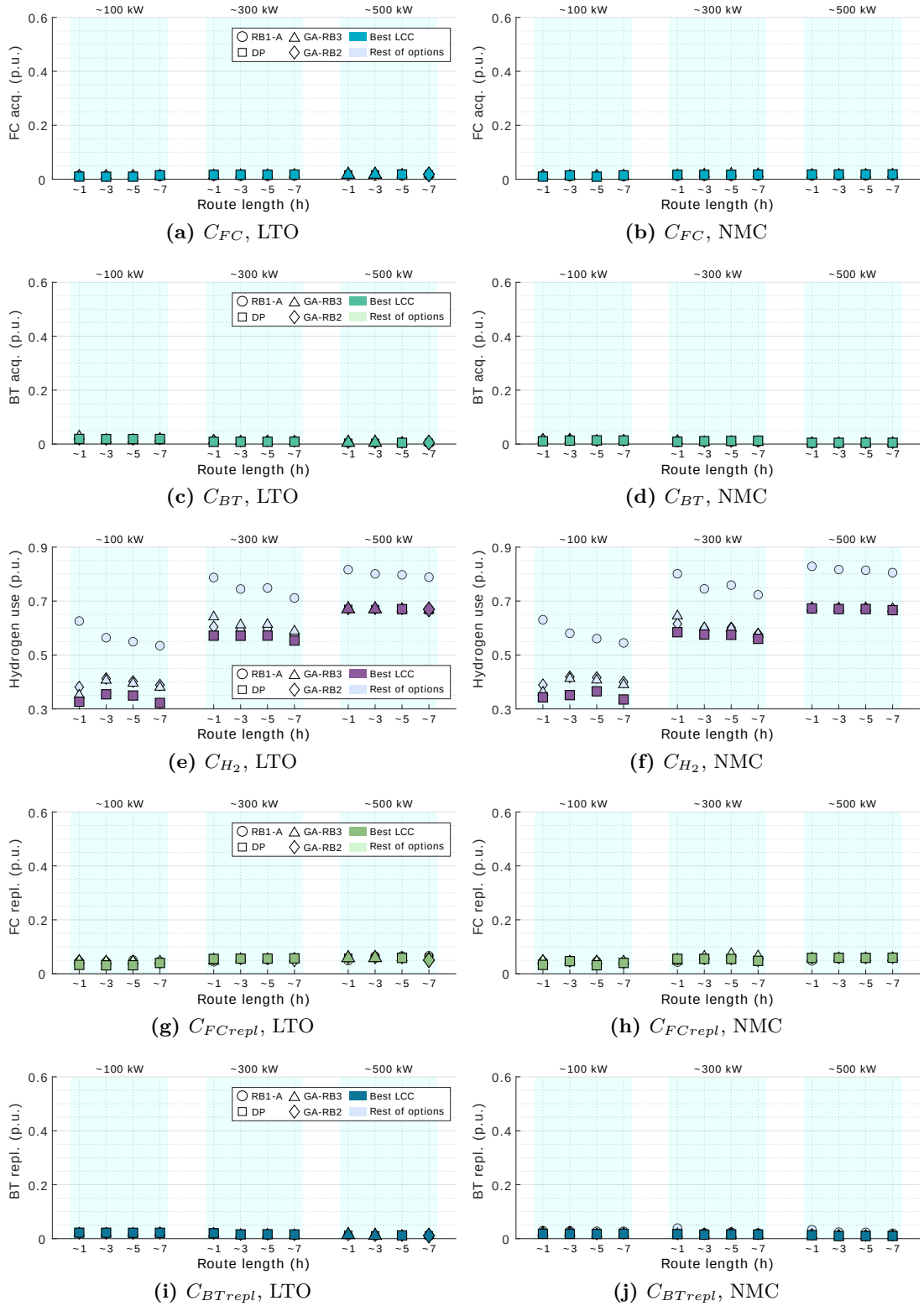

(a) C_{FC}, LTO **(b)** C_{FC}, NMC

(c) C_{BT}, LTO **(d)** C_{BT}, NMC

(e) C_{H_2}, LTO **(f)** C_{H_2}, NMC

(g) C_{FCrepl}, LTO **(h)** C_{FCrepl}, NMC

(i) C_{BTrepl}, LTO **(j)** C_{BTrepl}, NMC

Figure 4.41: Sensitivity of key cost terms to different driving cycles.

ation when increasing the average route demand than when increasing the route length. Therefore, it can be concluded that the route length barely affects in the powertrain design of the analysed H_2EMU.

The variable cost that it is most affected by the average route demand is the hydrogen use, C_{H_2}. Logically, as higher is the demand, the FC is required to work on a higher power, what is translated into a higher hydrogen consumption. Even in the scenarios with the lowest average demand, C_{H_2} is the cost term that contributes most to the LCC. Specifically, Figures 4.41e and 4.41f show that C_{H_2} corresponds to around the 30-35% of the overall cost when the average demand is close to 100 kW, to around the 55-60% when the average demand is close to 300 kW, and to around the 65-70% when the average demand is close to 500 kW. Therefore, the relation between C_{H_2} and the average demand is not completely linear.

These figures also show that C_{H_2} influences the final LCC obtained by each strategy. Indeed, it can be seen that when the strategies have a big difference in the hydrogen consumption, they also have a big difference in the LCC. This can be checked focusing on the results of RB1-A: in the majority of cases the difference in C_{H_2} between RB1-A and DP (Figures 4.41e and 4.41f) is similar to the difference in the LCC between both strategies (Figure 4.39). The same happens when comparing the results of GA-RB2 and GA-RB3 with DP: when the C_{H_2} difference between them is high, the LCC difference between them is high (e.g., the case when the average demand is around 100 kW); and when the C_{H_2} difference between them is low, the LCC difference between them is also low (e.g., the case when the average demand is around 500 kW). Therefore, it can be concluded that C_{H_2} is both the cost term that contributes most to the overall LCC and the cost term that influences most in the definition of the best control strategy.

Regarding the remainder cost terms, C_{FC} and C_{FCrepl} are slightly increased when the average route demand is increased. This is due to the fact that higher optimal FC sizes are proposed in these scenarios. Anyway, the contributions of C_{FC} and C_{FCrepl} to the overall LCC are never higher than the 3% and the 10%, respectively. Besides, both values barely differ with different control stategies or BT chemistries, what demonstrates that they do not influence the definition of the best case at each scenario.

Finally, similar conclusions are obtained with C_{BT} and C_{BTrepl}. The contribution of both cost terms is affected by the optimal BT size, but the difference is very low. In general terms, their contribution to the overall LCC is low, as their values barely exceed the 3%. Consequently, their influence in the performance of the different control strategies or BT chemistries is found to be low.

4.6.4 Review of Sensitivity Analysis to Driving Cycle

In this section the last sensitivity analysis of this chapter has been developed. The analysis has been focused on how is the optimal H_2EMU powertrain design affected when

varying the characteristics of the driving cycle. The driving cycles have been modelled so as to represent different route lengths and average demands. Specifically, the variations in the LCC value of the different control strategies and BT chemistries, the variations in the returned optimization variables, and the variations in the influence of the key cost terms of the economic model (C_{FC}, C_{BT}, C_{H_2}, C_{FCrepl} and C_{BTrepl}) have been evaluated.

Table 4.13 reviews the main conclusions obtained in this section. In short, the table defines how much does the variation of the route demand and length affect in the main points analysed through this section. The superscript numbers refer to the comment at which each conclusion is further discussed. The comments are listed below.

Table 4.13: How much does the variation of the scenario influence the optimal design of the H_2EMU powertrain.

	Route demand	**Route length**
Optimality of EMSs	●●○ (01)	◐○○ (02)
Optimality of BT chemistries	○○○ (03)	○○○ (03)
Optimal FC size	●●● (04)	○○○ (05)
Optimal BT size	●●○ (06)	◐○○ (07)
Optimal SOC_0	◐○○ (08)	●○○ (08)
Influence of cost terms	●◐○ (09)	○○○ (10)

(1) As the average demand of the route increases, the difference between DP and the remainder strategies is reduced. In the highest mean demand (around 500 kW) DP, GA-RB2 and GA-RB3 obtain nearly the same LCC.

(2) No important changes are identified when varying the route length. GA-RB2 tends to improve its result when increasing the route length, but the variation is low.

(3) There are no notable changes in the optimality of the BT chemistries when varying the characteristics of the driving cycle (both the demand and the length): in most of the cases LTO is found to be the best option, but the difference with NMC tends to be lower than the 1%.

(4) As higher is the average demand of the route, the optimal FC size is increased, as this is the primary traction source of the H_2EMU. The relation is nearly linear.

(5) No variation in the optimal FC size has been identified when increasing/decreasing the route length.

(6) The optimal BT size varies when increasing/decreasing the average demand mainly due to the variation of the optimal FC size, which restricts the available space for the secondary power source. Besides, as the average demand is increased, the optimal BT size gets closer to the maximum allowable energy.

(7) Some changes in the optimal BT size have been identified when varying the route length, specially in the case of NMC. However, there is no clear correlation between both

variables.

(8) Different SOC_0 values are obtained when varying both the route demand and the route length, but no clear correlation between these variables has been found. This indicates that other reasons may be behind these variations.

(9) Varying the route demand specially affects in the contribution of C_{H_2} (as higher is the demand, higher is the contribution). However, in all the analysed scenarios the hydrogen consumption continues being the cost term that influences most the definition of the optimal control strategy. In the remainder cost terms just slight variations are found.

(10) No notable changes in the influence of the key cost terms of the economic model have been found when increasing/decreasing the route length.

4.7 Conclusions

The fourth chapter of this Ph.D. Thesis has presented the second implementation of the holistic design methodology proposed in Chapter 2. Specifically, the methodology has been implemented with the rail vehicle topology denoted as the H_2EMU. As it has been explained, the H_2EMU traction unit is composed of a FC as primary power source and a BT as secondary power source.

In the first sections of this chapter (Sections 4.1, 4.2 and 4.3), the methodology previously introduced in Chapter 2 has been particularized to the vehicle being analysed in the current case study. First, Section 4.1 has detailed the general characteristics of the H_2EMU vehicle considered during the development of this chapter. This vehicle is based on the CIVIA vehicle family manufactured by CAF.

Then, in Section 4.2 a detailed description of the different sensitivity analyses has been given. Specifically, all the cases considered in these analyses have been presented, including the different control strategies, BT chemistries, parametrizations of the economic model, and driving cycles. Regarding the EMSs, rule-based (RB1-A, RB1-B, RB2 and RB3), optimization-based (GA-RB2, GA-RB3 and DP) and learning-based (ANFIS) strategies have been proposed. For the BT chemistries, three technologies have been modelled: LTO, NMC and LFP. Regarding the economic model, first a nominal parametrization has been set. Then, the parameters with the highest probability to suffer variations have been selected (t_{day}, c_{H_2}, c_{FC} and c_{BT}), and three scenarios have been defined for each of them: Low Scenario (LS), Medium Scenario (MS) and High Scenario (HS). Finally, different driving scenarios have been introduced. As in the case of the economic model, first a nominal case has been set, which is based on the real railway line "Tardienta - Canfranc". Then, additional 12 synthetic driving cycles have been created, which have been designed with the aim of representing scenarios with different mean traction demands and route lengths.

In Section 4.3, the LCC optimization problems have been particularized for each EMS. Indeed, depending on the control strategy being optimized, the optimization variables and optimization methodology are varied. In the case of RB strategies, a simple exhaustive search has been set to solve the optimization. The same methodology has been defined for DP strategy. Besides, in the case of GA-RB2 and GA-RB2, two different GA-based optimization approaches have been set, as in this case some of the internal parameters of the strategies are also optimized.

After particularizing the holistic design methodology for the current case study, in the next sections the results obtained when deploying the methodology have been presented. First, in Section 4.4 the performance of the different EMSs and BT chemistries with the nominal economic scenario and driving cycle has been evaluated. Specifically, the analysis has focused on the following features: the LCC values obtained by each case of the sensitivity analysis, the optimal values of the optimization variables proposed by each case (FC size, BT size and initial SOC), and the evolution of the key cost terms influence (C_{FC}, C_{BT}, C_{H_2}, C_{FCrepl} and C_{BTrepl}). The obtained main conclusions ar listed below:

- *Comparison of EMSs.* DP is the strategy that obtains the lowest LCC, but its real time implementation is barely possible. GA-RB2 has been found to be the closest strategy to DP in terms of LCC (1.0-3.3% higher LCC), but its robustness should be improved (what may not be difficult). ANFIS has been tested to replicate the results of DP, but as the replication is not perfect, it does not reduce the LCC of GA-RB2. Besides, its execution time should be improved. Finally, GA-RB3 has obtained slightly higher LCC values compared to GA-RB2 (0.6-1.3% higher), but it shows a better robustness.

- *Comparison of BT chemistries.* LTO and NMC obtain similar results, as the LCC difference between both chemistries tends to be lower than 1%. Anyway, in the majority of cases LTO obtains a lower LCC. LFP is found to be far from the results of the other chemistries.

- *Optimal FC size.* The optimal FC size is found to be around 600 kW. A smaller size would also be a feasible solution, but oversizing the FC allows improving the efficiency. Consequently, the higher acquisition and replacement costs are compensated by a reduced hydrogen consumption.

- *Optimal BT size.* No clear trend is found regarding the optimal BT size. In the case of LTO values around 280-360 kWh are proposed, in the case of NMC values around 340-560 kWh, and in the case of LFP values around 360-400 kWh. This means that the benefit of higher or lower BT systems is limited.

- *Optimal initial SOC.* There is neither a clear trend regarding the optimal SOC_0 value. Regardless the BT chemistry, the optimal values are found to be around 60-80%. That is to say, values in the middle-high feasible SOC window are preferred.

- *Influence of cost terms.* The cost term with the major influence is found to be C_{H_2}. Being the term with the highest contribution to the LCC (around the 51-68% of the overall cost), this is a logical conclusion. C_{FCrepl} has also a noteworthy contribution (around 10%), but the difference from case to case is low. C_{BTrepl} has some minor influence in the case of LFP chemistry. Finally, it is found that reducing the acquisition costs (C_{FC} and C_{BT}) is not directly related to a lower LCC value.

After this first sensitivity analysis, Sections 4.5 and 4.6 have focused on evaluating how do the conclusions obtained in Section 4.4 vary when varying the parametrization of the economic model and the characteristics of the driving cycle, respectively. These analyses have unveiled in which conditions the conclusions obtained in the first sensitivity analysis may not be completely true. These conditions are listed in the following lines:

- *Comparison of EMSs.* In the following circumstances, the distance between DP and the remainder strategies is reduced: (1) when reducing the hydrogen price, (2) in the case of LFP chemistry, when increasing its price, and (3) in routes with high average demands. In the case of the high LFP price, and in some of the high demand scenarios, GA-RB2 and GA-RB3 become the best strategies, but the difference with DP is always low. Besides, when the FC price is decreased, the distance between DP and the remainder strategies is increased.

- *Comparison of BT chemistries.* When NMC price is increased or LTO price is reduced, LTO becomes clearly the best option. When LFP price is reduced, it can become a competitive option, but the price reduction has to be high. Finally, when the operation hours are reduced, LFP reduces the LCC difference with the other chemistries, but it is still far from them.

- *Optimal FC size.* The optimal FC size is varied in the following circumstances: (1) when reducing the hydrogen cost lower sizes are proposed, and (2) when increasing or decreasing the average route demand, the FC size is also increased or decreased. In the case of the operation hours and the FC price, higher variations than the ones proposed in this analysis may be necessary to obtain a different optimal FC size.

- *Optimal BT size.* The optimal BT size is clearly varied in the following circumstances: (1) when reducing the operation hours lower sizes are proposed, and (2) when the route demand is increased, the optimal BT size is affected by the change in the optimal FC size, as this leaves less available space for the battery.

- *Optimal initial SOC.* In some cases, SOC_0 values lower than the 60% have been obtained (when reducing c_{H_2} and c_{BT}, or when varying the characteristics of the driving cycle). However, no special correlation between the variations in these values and the variations in the initial SOC values have been found.

- *Influence of cost terms.* Some changes are found in the case of LFP, as it is the chemistry with the highest degradation: (1) C_{BTrepl} becomes an important cost

term when reducing the hydrogen cost, as C_{H_2} losses some importance, and (2) C_{BTrepl} gains some importance also when incresing the LFP price. For the remainder chemistries, no remarkable changes are found.

5

Conclusions and Future Lines

Summary

In this final chapter the conclusions, main findings and key contributions of this Ph.D. Thesis are reviewed. Besides, the main research lines to continue the topics developed in the present work are also identified.

5.1 Conclusions of Ph.D. Thesis

This Ph.D. Thesis has addressed the topic of the optimal powertrain design for innovative railway vehicle topologies, which include the Hybrid Diesel-Electric Multiple Unit (H-DEMU) and the Hydrogen Electric Multiple Unit (H_2EMU). These topologies integrate BT and FC systems, which have not been yet widely adapted in commercial railway vehicles, but provide efficient solutions for the necessary transport decarbonization path. In order to be competitive in the market, the integration of these power sources has to be cost-competitive compared to traditional options. This is why this Ph.D. Thesis has proposed and implemented **a novel holistic design methodology to obtain cost-efficient solutions when integrating BT and FC systems in H-DEMU and H_2EMU** vehicle topologies.

The review of the state of the art developed in Chapter 1 unveiled that the design methodology should focus on defining the following features: (i) the size of the power sources, (ii) the BT technology, and (iii) the EMS or control strategy. In the case of the BT technology, the analysis should focus on comparing different chemistries, which were defined at LTO, NMC and LFP. Regarding the EMS, it was defined that different approaches should be compared, including rule-based, optimization-based and learning-based strategies. Typically, the mentioned features are defined *ad-hoc* for a specific context, that is to say, for a specific driving cycle or economic context. However, this requires to repeat the design analysis each time the context changes. Therefore, it was decided that the methodology should also focus on finding the interrelations between the cost-optimal powertrain design and the characteristics of the driving cycle and economic model.

In order to handle together all the mentioned features, it was decided to base the holistic design methodology on an integral LCC analysis. Therefore, Chapter 2 presented the different steps that compose the LCC analysis, together with all the methods and models required to develop this analysis. As developing a sensitivity analysis that considers together all the features identified above is an unviable approach, it was decided to divide the LCC analysis into three steps:

(1) First, a sensitivity analysis focused on the powertrain design is set. In this step, the cost-optimal EMS, BT chemistry and size of the powertrain sources are solved for a specific context.

(2) In the second step, another sentivitiy analysis is developed, which is focused on varying the parameters of the economic model. In this way, it is checked if the conclusions obtained in the previous analysis are replicated in different scenarios.

(3) Finally, the characteristics of the driving cycle are modified in a last sensitivity analysis. As in the previous case, the aim of these variations is to check if the conclusions obtained in the first analysis are replicated.

For the development of the mentioned holistic design methodology, a vehicle simulation model was set, which has been based on the ITINER tool previously developed by

CAF I+D. The model was fed with data provided by CAF Power & Automation, what has allowed deploying simulations based on real vehicle and routes data. Moreover, an additional feature of the methodology is that it includes the use of FC and BT degradation models to evaluate the amount of replacements required during the vehicle useful lifetime. In the case of the BT, **a novel chemistry-dependent empirical degradation model was proposed** as part of the Ph.D. Thesis developments. The model was defined and parametrized based on a batch of 500 degradation tests collected from the literature, and has already been published in a journal paper [36].

Once the holistic design methodology was set, it was implemented in two case studies. The first case study, presented in Chapter 3, was focused on the bi-mode H-DEMU vehicle topology. The second case study, presented in Chapter 4, was focused on the H_2EMU. One significant difference between both case studies is that the H-DEMU drives in partially electrified lines, while the H_2EMU drives all the time through non-electrified lines. This fact affected in the conclusions related to the optimal design of the powertrain, as the use of the BT differs depending on the availability of catenary sections. For each case study, first all the cases of the different sensitivity analyses were presented, including the control strategies, BT chemistries, parameters of the economic model and driving cycles. Among the EMSs, **the implementation of the learning-based ANFIS strategy was defined as an additional contribution of the Ph.D. Thesis**, as it had not been previously proposed for rail applications.

Focusing on the outcomes of the case studies, several conclusions related to the H-DEMU powertrain design were obtained when implementing the holistic design methodology. It is worth to mention that some of these conclusions have also been published in a journal paper [200]. The conclusions are classified according to the different features that were analysed:

- *Comparison of EMSs.* In all the analysed scenarios, Dynamic Programming (DP) is the best performing strategy in terms of LCC, at least when appropriate BT chemistries are integrated (i.e., LTO or NMC). However, its real time implementation is barely possible, what forces to find other alternatives. The next strategy with the best LCC result is found to be GA-SM, which is an optimization-based EMS. In the nominal scenario, GA-SM stays just a 0.7% behind DP. It is also found that this distance can be reduced when the train drives few hours per day, with low diesel prices, with high battery prices, or when driving in routes with a low energy demand. ANFIS strategy has also obtained promising results, as in the nominal scenario it stays 1-2% behind DP. However, further developments of the ANFIS or other learning-based strategy are required to improve the results of GA-SM.
- *Comparison of BT chemistries.* In most of the analysed scenarios, LTO is the best performing chemistry, but with NMC close in terms of LCC (the difference between them is lower than 1%). The only cases where NMC overcomes LTO are the ones in which NMC price is reduced or LTO price is increased. Besides, when the fuel price is increased or when driving in routes with a high demand, the difference between

both chemistries is almost residual. Finally, LFP is found to be far from the results of LTO and NMC in all the analysed cases, as generally the difference is higher than the 4%. The main drawback of LFP is found to be the degradation that it suffers.

- *Optimal size of power sources.* This feature is found to be the least transversal to a change in the scenario. The genset size is mainly affected by the characteristics of the driving cycle. Besides, the BT size is constrained by the optimal genset size, due to the limitations in the available space for both components. In routes with an energy demand below 250 kWh, the optimal option consists of not deploying any genset (i.e., the BEMU); in routes with a medium demand between 250-800 kWh (LTO) or 250-1400 kWh (NMC), the optimal option is the genset of 500 kW; and in routes with a high demand, the optimal option is the genset of 1000 kW. Generally, the optimal BT size is found to be close to the maximum allowable value (considering the optimal genset size). That is to say, once the genset size is defined, the optimal option is to integrate as much BT energy as possible. The only cases when the optimal BT size is lower than the maximum allowable value are listed as follows: (1) when the train drives few hours per day, (2) with a low fuel price, (3) in the case of the BEMU, and (4) in the case of NMC, when its price is reduced.

The conclusions obtained in this extended analysis have allowed defining which are the features most dependent and most transversal to the context or scenario characteristics. Figure 5.1 reviews this context dependency for the H-DEMU case. The most transversal features are the strategy (GA-SM) and the BT chemistry (LTO), while the powertrain sizing and the optimal parameters of the strategy are more dependent to the context or the scenario. These context-dependent solutions are influenced by the economic parameters and the route energy demand.

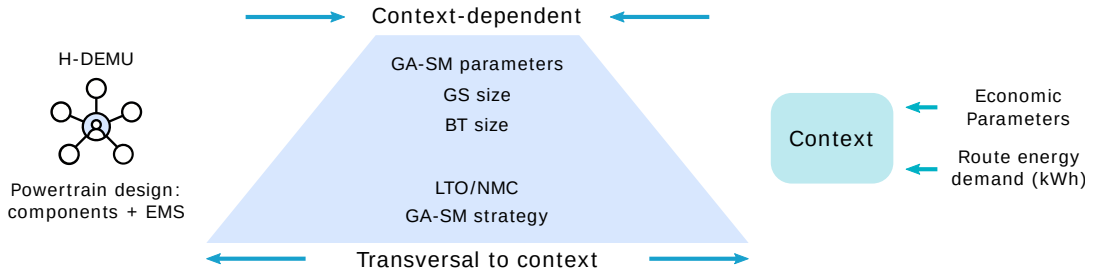

Figure 5.1: Context dependency of analysed concepts (H-DEMU case).

Regarding the second case study, some other conclusions were obtained. It is worth to mention that some of these conclusions have also been published in a paper [201]. Specifically, the following conclusions were obtained when implementing the holistic design methodology with the H_2EMU topology:

- *Comparison of EMSs.* As in the case of the H-DEMU, the best performing strategy is DP, but its real-time implementation is barely possible. The next best strategy is found to be GA-RB2, which is an optimization-based EMS. In the nominal scenario, its LCC is found to be between 1-3.3% higher compared to DP. There are some

cases where GA-RB2 outperforms DP: when LFP price goes up, and in some of the scenarios with a high demand. Besides, when reducing the hydrogen price, the performance of GA-RB2 is also improved, but without overcoming DP. In this case study, the result of ANFIS is neither enough to improve the result of the best GA-based strategy. In the nominal scenario its LCC is 3.3-4% higher than in DP.

- *Comparison of BT chemistries.* In most of the scenarios the LCC difference between LTO and NMC is lower than the 1%, but with LTO obtaining generally a better result. NMC can outperform LTO when NMC price is reduced or when LTO price is increased. In the case of LFP, it is far from the results of the other two chemistries in most of the cases, but it can become a competitive option when its price is reduced. As in the other case study, the main drawback of LFP is its degradation.

- *Optimal size of power sources.* As in the case of the H-DEMU, this feature is also found to be the least transversal to the scenario. However, some differences are found compared to the previous case study. These differences happen due to the fact that in this case no catenary sections are available, and therefore the BT charge has to be maintained through all the route. Regarding the FC, its optimal size is linked to the route average power demand: with an average demand around 100 kW, the optimal FC size is found to be around 300 kW, and with an average demand around 500 kW, the optimal size is found to be around 900 kW. These values show that the tendency is to deploy a FC size higher than the average demand, as in this way it can be operated more efficiently. This tendency is respected in all the analysed scenarios, except when reducing the hydrogen price. In that case, lower sizes than the mentioned ones become the optimal option. Besides, regarding the optimal BT size, no clear trend is found, as during the development of the case study different values were found depending on the scenario being analysed.

The obtained conclusions have allowed defining the features that are most dependent and most transversal to the context or scenario characteristics. Figure 5.2 reviews this context dependency for the H_2EMU case. As in the previous case study, the strategy (GA-RB2) and the BT chemistry (LTO) are the most transversal features, while the powertrain sizing and the optimal parameters of the EMS are more dependent to the context. These context-dependent solutions are influenced by the economic parameters and the route average power demand.

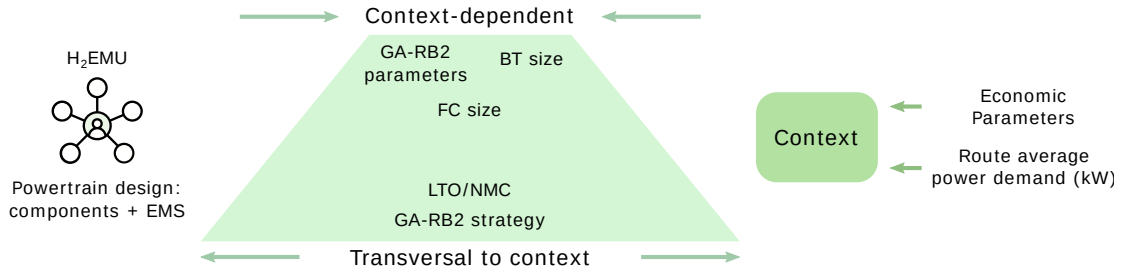

Figure 5.2: Context dependency of analysed concepts (H_2EMU case).

As general conclusion, this Ph.D. Thesis has made an important contribution in the field of railway transportation, specially in the one concerning the integration of BT and FC systems. The **implementation of the proposed holistic design methodology has provided valuable conclusions for the design of powertrain systems** that integrate BT and FC systems and combine them with traditional technologies. These conclusions may specially help railway manufacturers to take faster decisions regarding the powertrain design when preparing the tenders for new projects dealing with H-DEMU and H_2EMU vehicles.

5.2 Future Research Lines

After the development of the Ph.D. Thesis, some potential future research lines have been identified. These research lines could not be addressed in this Ph.D. Thesis and may help push the state of the art forward:

- To develop **a tool for the optimal design of the powertrain** of H-DEMU and H_2EMU vehicles. The aim of this tool would be to help with the features that were found to be the least transversal in the conclusions of the Ph.D. Thesis: the size of the traction sources and the parameters of the EMS. For this approach, the tool would first learn from the results of all the simulations launched for the development of the case studies of this Ph.D. Thesis. After this learning phase, the tool may be able to provide an advice for the cost-optimal design of the powertrain based on the characteristics of a route that was not used during the mentioned learning process. The tool may be useful for railway manufacturers to speed up the powertrain design of H-DEMU or H_2EMU vehicles, specially when preparing the tender of a new project.
- To couple the development and analysis of H_2EMU control strategies with **more detailed FC simulation and degradation models**. Indeed, models that represent in a more reliable way the performance limitations and the causes of the degradation of FC systems may help understand the potential limitations of the proposed EMSs when integrating them in a real vehicle. For this aim, the first step consists on setting FC characterization and degradation tests in a laboratory environment. The data obtained in these tests may be then post-processed to build more realistic simulation and degradation models. These models could also be integrated in the methodology proposed in this Ph.D. Thesis.
- To continue exploring the **capacities, advantages and limitations of learning-based control strategies** with the aim of getting closer to the results obtained by the global optimization (DP). The LCC results obtained by the learning-based EMS proposed in this Ph.D. Thesis (ANFIS) are still far from DP, and even in some cases there are optimization- and rule-based strategies that obtain better results. Besides, the real-time performance of ANFIS was also found to be poor compared to typical RB strategies. This demonstrates that there is still room to improve the

overall performance of ANFIS. For this aim, the use of different learning approaches is proposed, including reinforcement learning, deep learning or neural networks.

- **To update the methodology** proposed in this Ph.D. Thesis **with the latest advances in energy storage systems**. Future generations of storage systems such as solid-state and post-lithium batteries are not expected to be commercially ready in the near future, but they may bring important advances in terms of specific energy and energy density by the time they are ready. These improvements may increase the BT sizing limits set in the optimization problems of the Ph.D. methodology, enabling an increase in the hybridization level in favour of the BT.

A

Supplementary Material for Case Studies

A.1 Introduction

This appendix presents additional information for the two case studies of this Ph.D. Thesis. Specifically, the synthetic driving cycles generated for the sensitivity analysis to the driving cycle are depicted in the following pages.

A.2 Synthetic Cycles for H-DEMU

Section 3.2.4 has presented the methodology followed for the generation of the H-DEMU synthetic driving cycles. In this appendix these driving cycles are given. Figures A.1 to A.4 present these profiles, with the average power demand and running time values highlighted.

A.3 Synthetic Cycles for H_2EMU

Section 4.2.4 has presented the methodology followed for the generation of the H_2EMU synthetic driving cycles. In this appendix these driving cycles are given. Figures A.5 to A.7 present these profiles, with the average power demand and running time values highlighted.

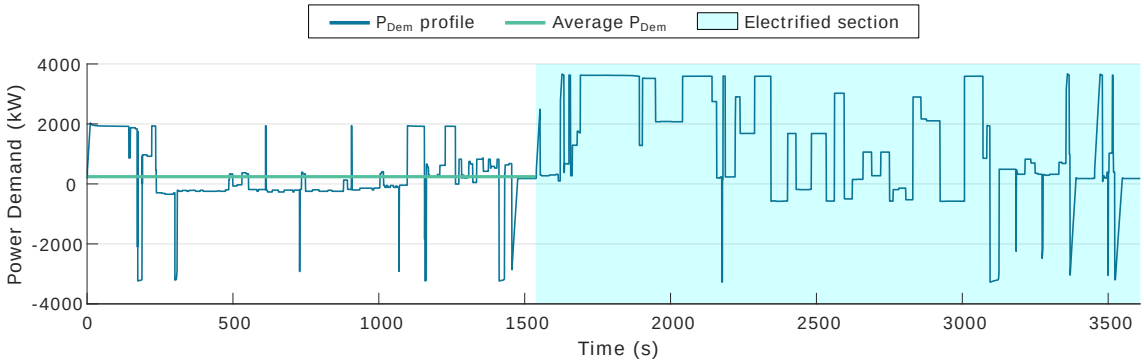

(a) Average demand around 200 kW

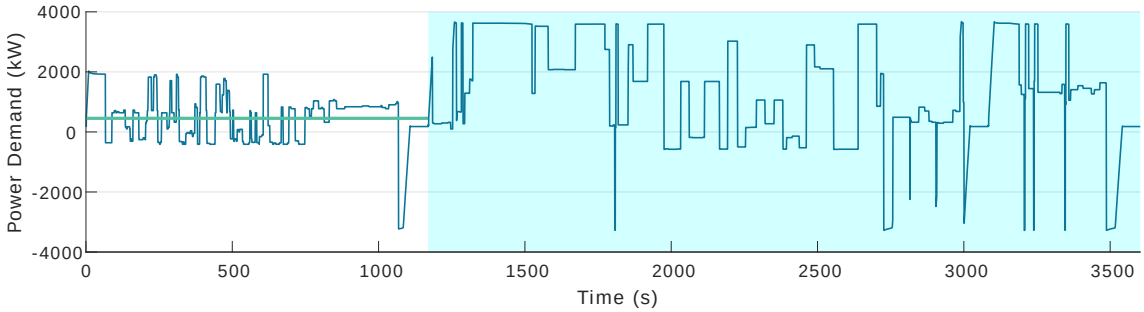

(b) Average demand around 400 kW

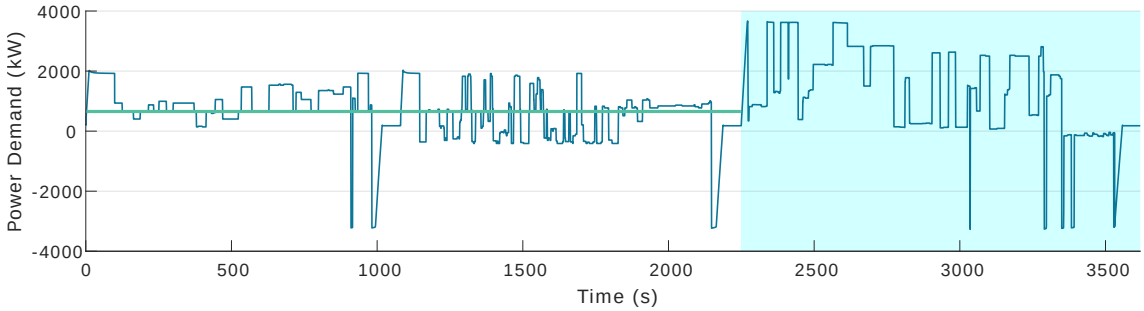

(c) Average demand around 600 kW

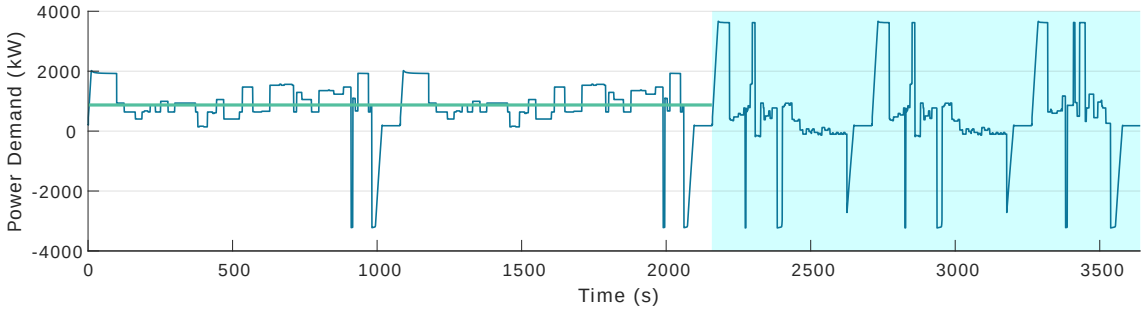

(d) Average demand around 800 kW

Figure A.1: H-DEMU synthetic drive cycles, non-electrified section around 0.5 h.

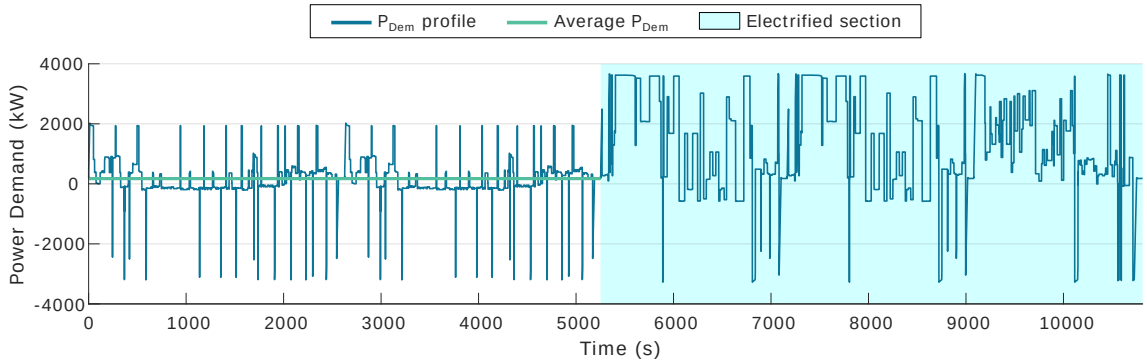

(a) Average demand around 200 kW

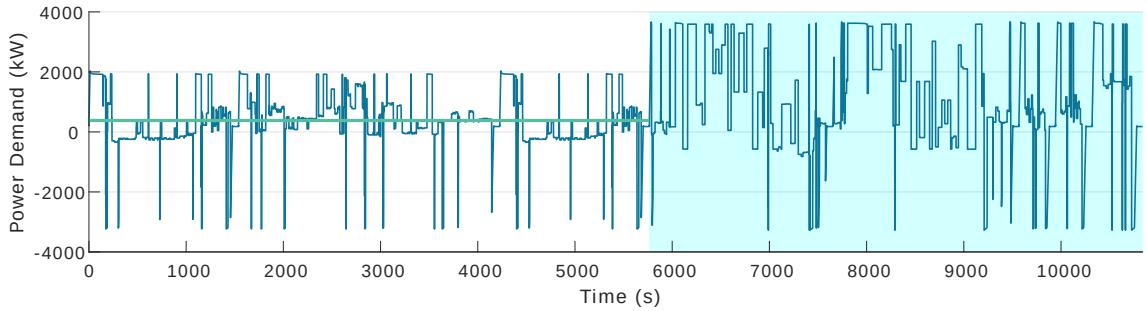

(b) Average demand around 400 kW

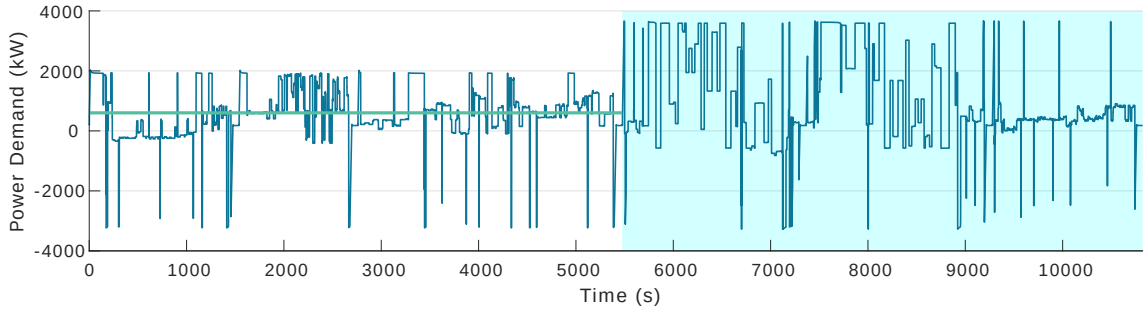

(c) Average demand around 600 kW

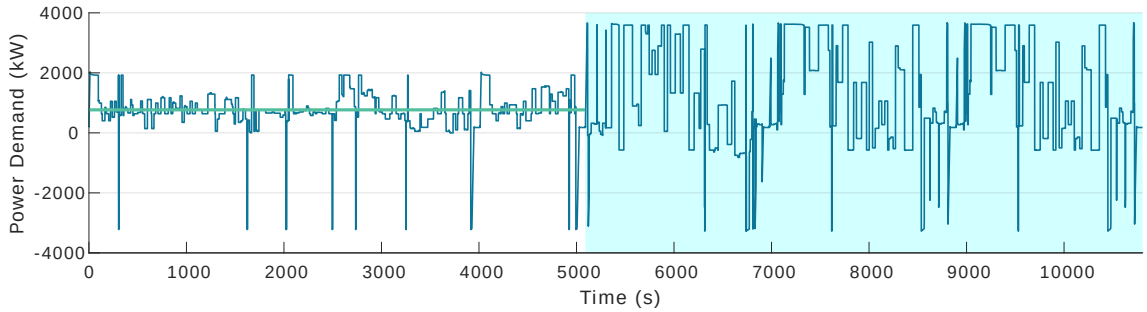

(d) Average demand around 800 kW

Figure A.2: H-DEMU synthetic drive cycles, non-electrified section around 1.5 h.

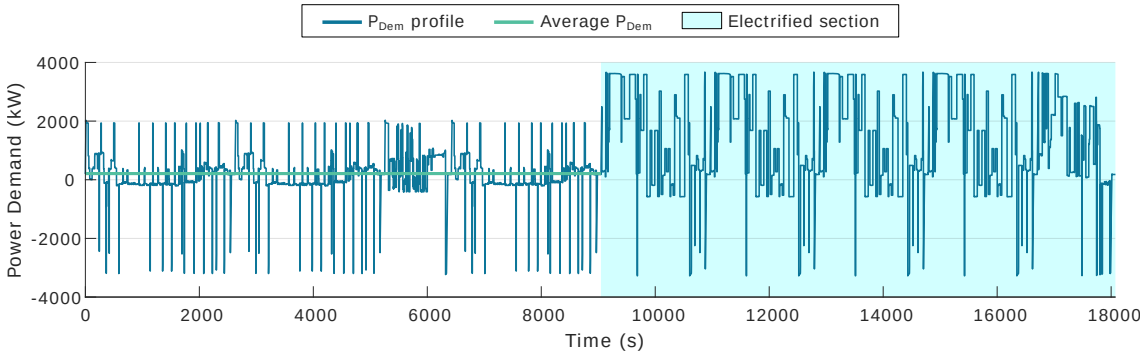

(a) Average demand around 200 kW

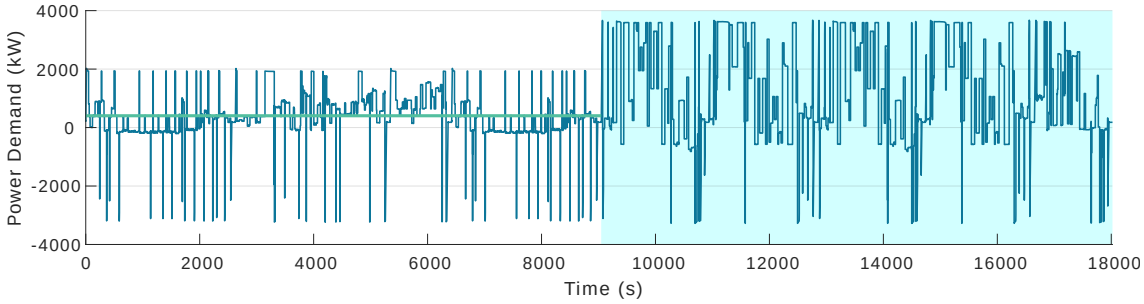

(b) Average demand around 400 kW

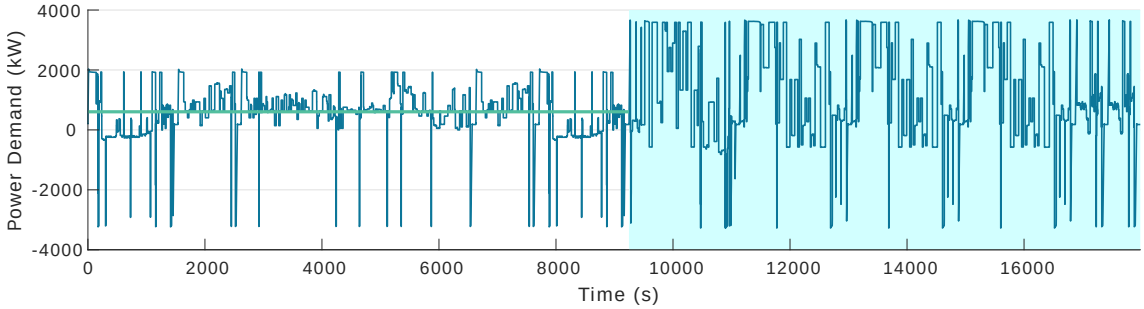

(c) Average demand around 600 kW

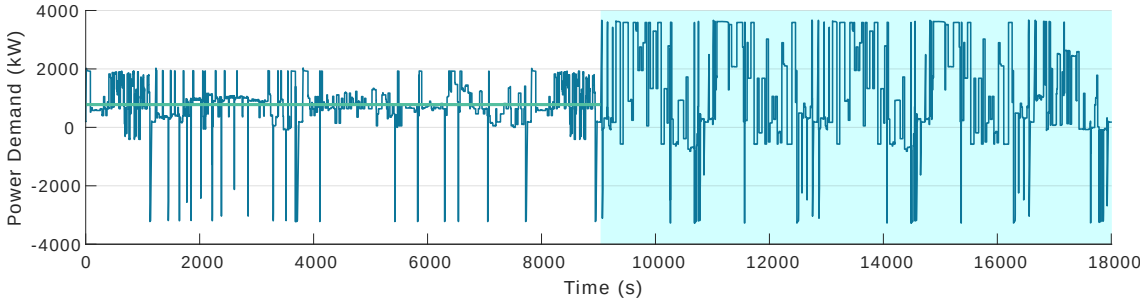

(d) Average demand around 800 kW

Figure A.3: H-DEMU synthetic drive cycles, non-electrified section around 2.5 h.

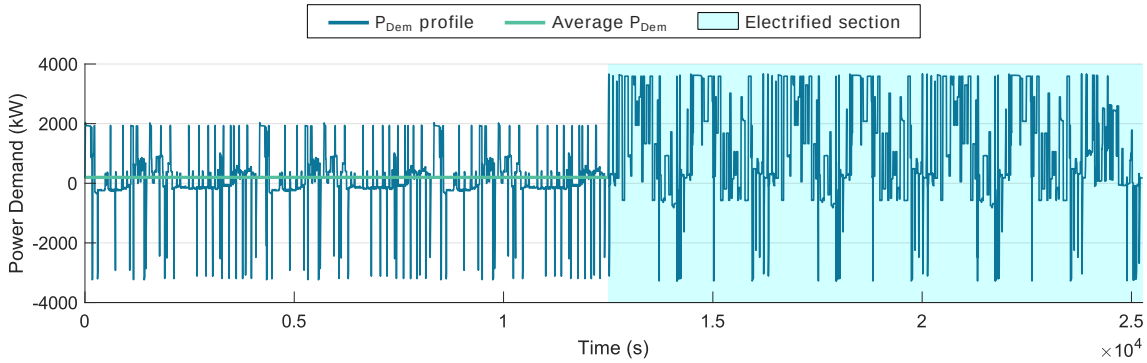

(a) Average demand around 200 kW

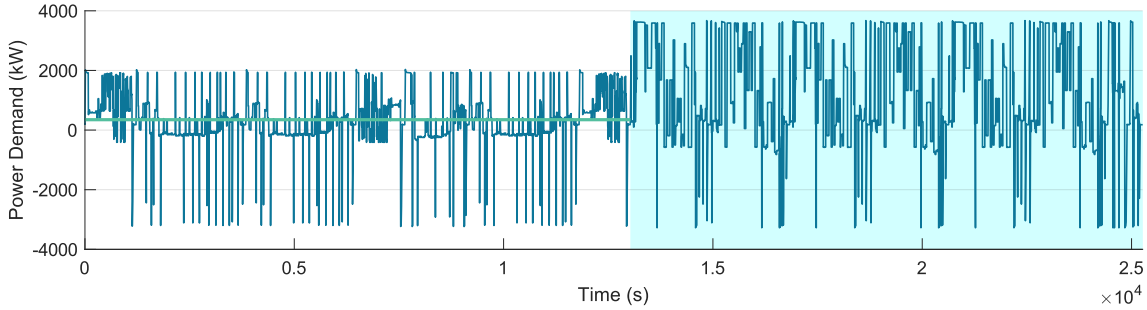

(b) Average demand around 400 kW

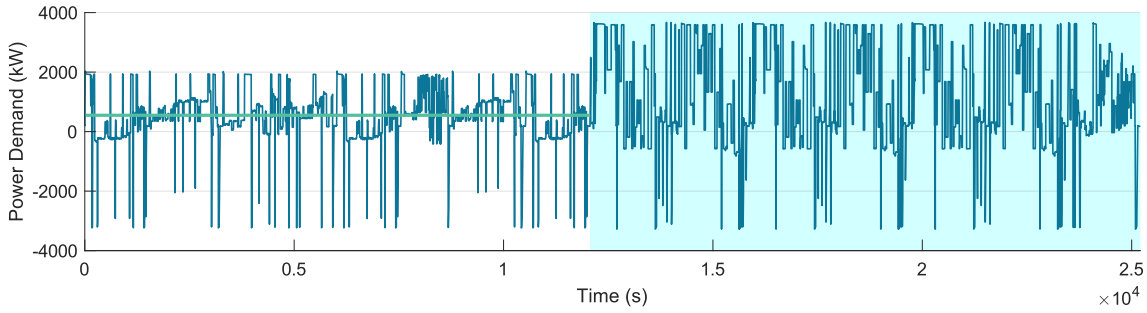

(c) Average demand around 600 kW

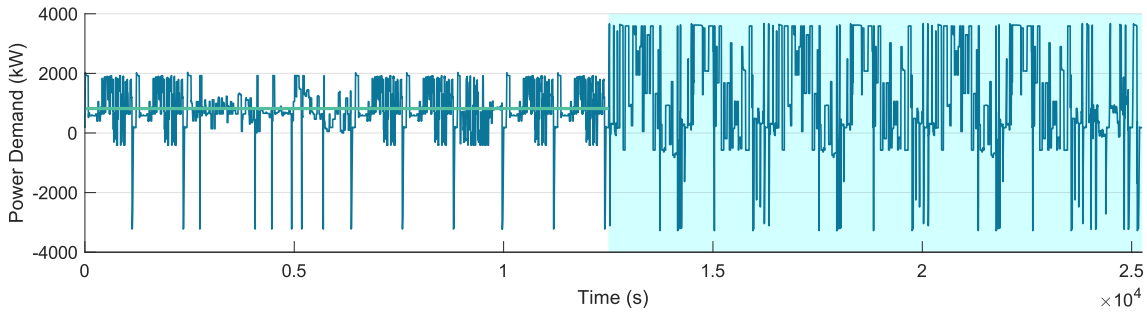

(d) Average demand around 800 kW

Figure A.4: H-DEMU synthetic drive cycles, non-electrified section around 3.5 h.

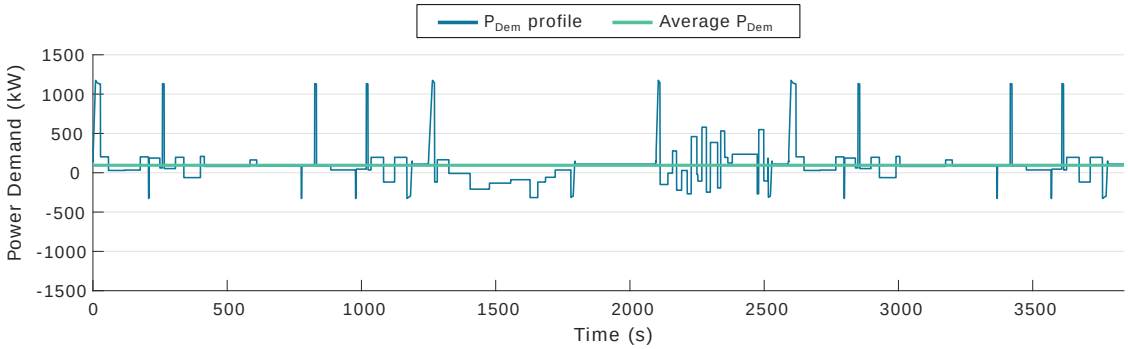

(a) Route length around 1 h

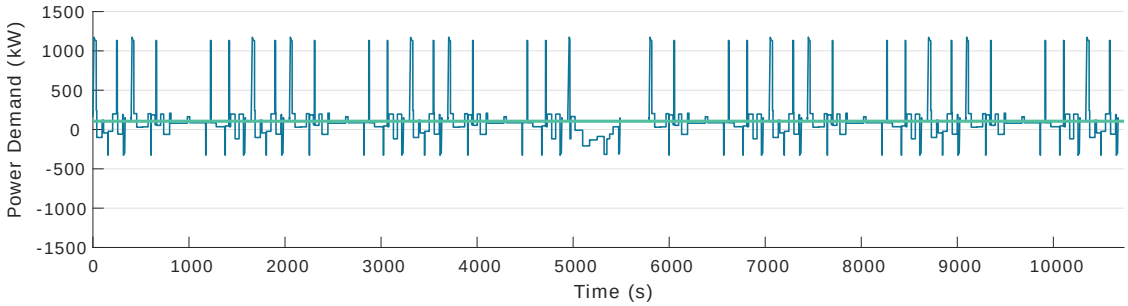

(b) Route length around 3 h

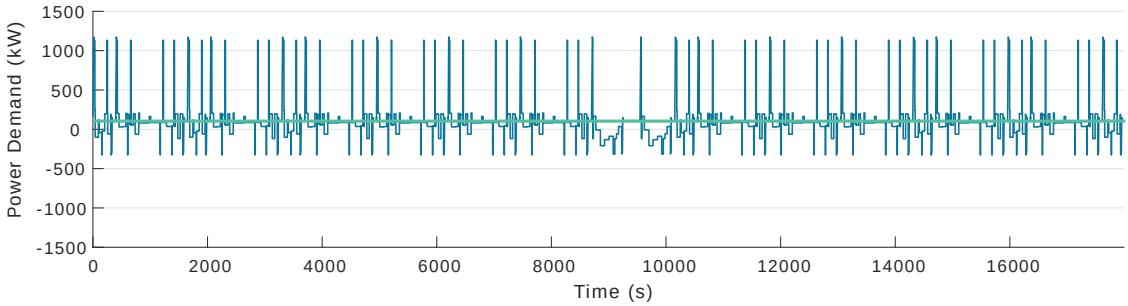

(c) Route length around 5 h

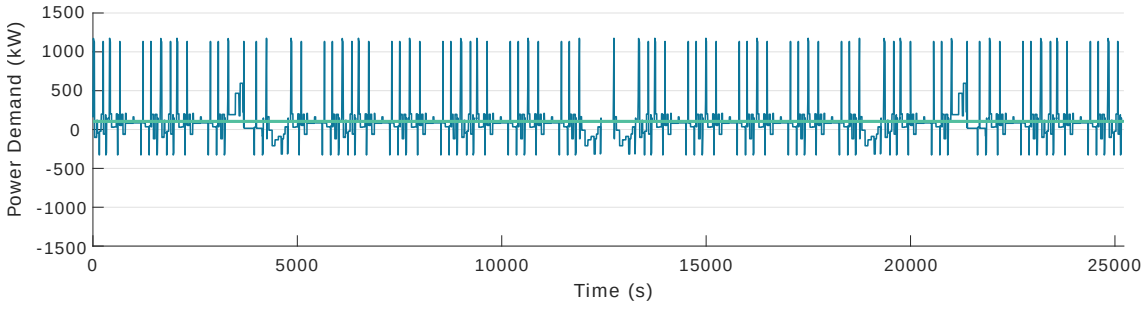

(d) Route length around 7 h

Figure A.5: H_2EMU synthetic drive cycles, average demand around 100 kW.

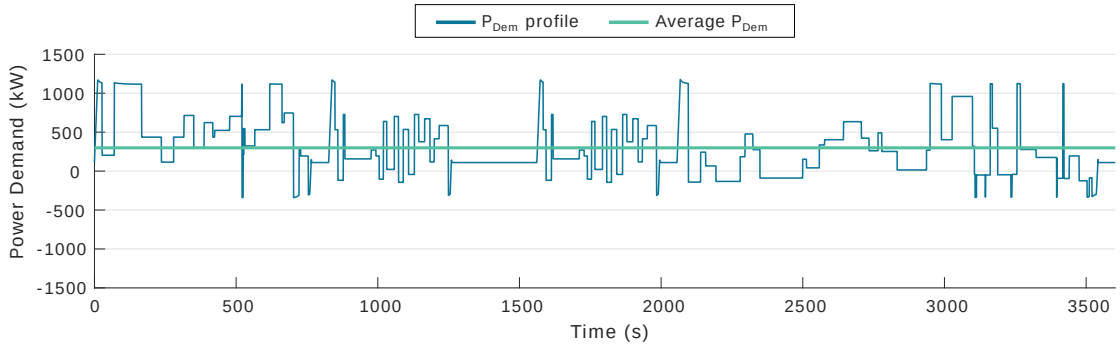

(a) Route length around 1 h

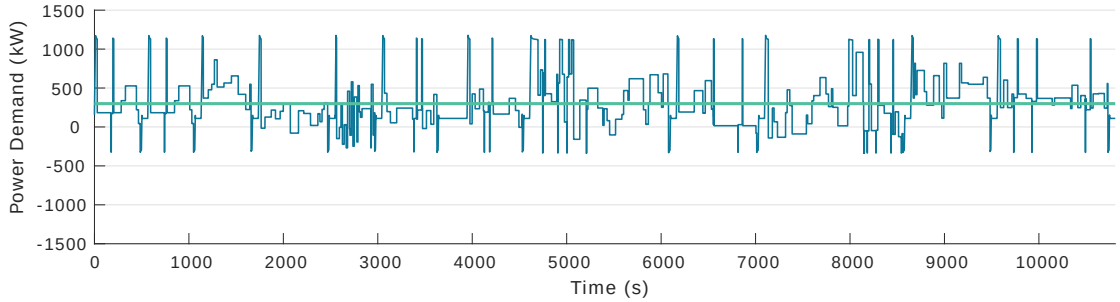

(b) Route length around 3 h

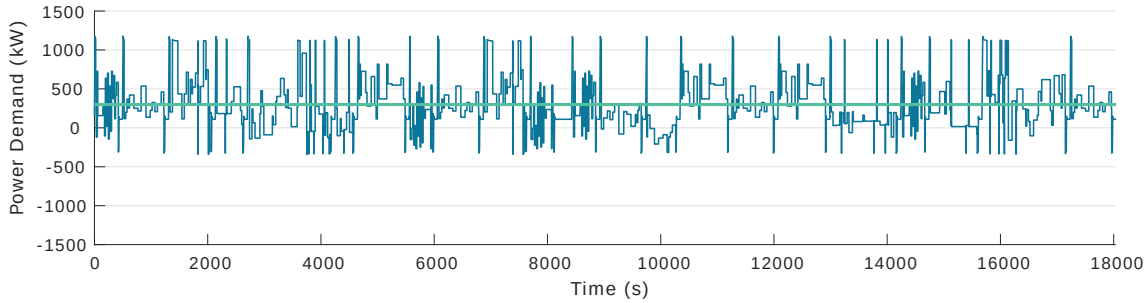

(c) Route length around 5 h

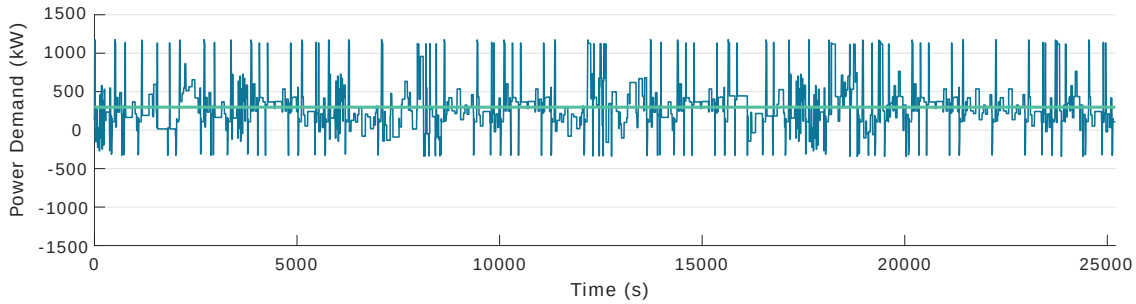

(d) Route length around 7 h

Figure A.6: H_2EMU synthetic drive cycles, average demand around 300 kW.

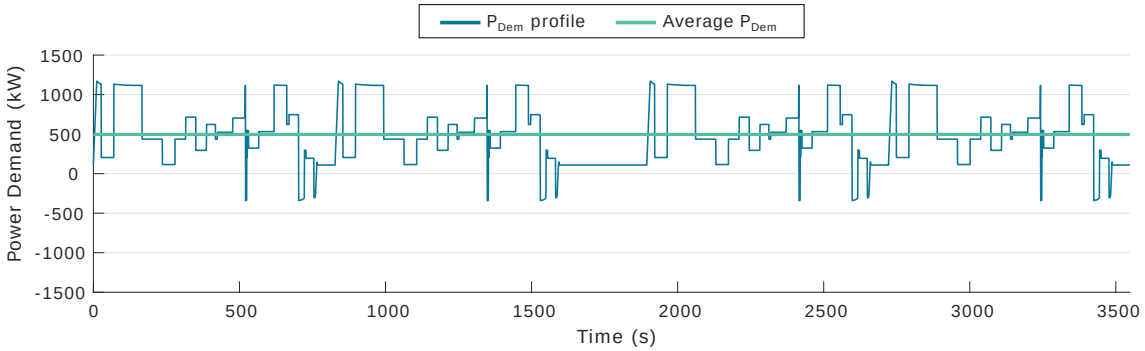

(a) Route length around 1 h

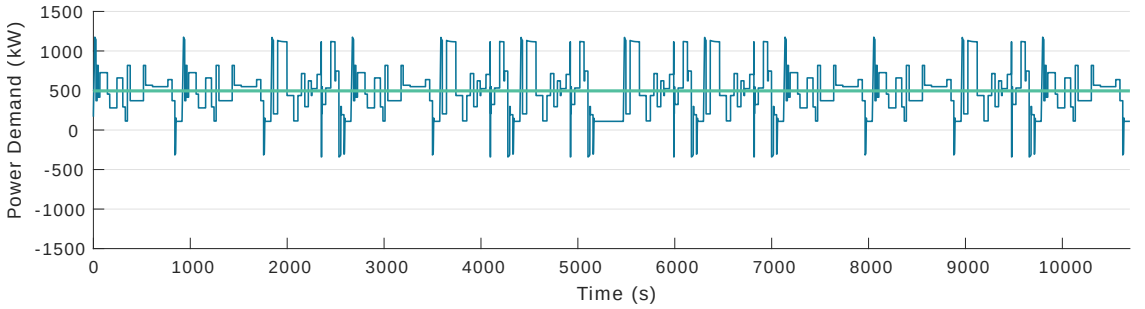

(b) Route length around 3 h

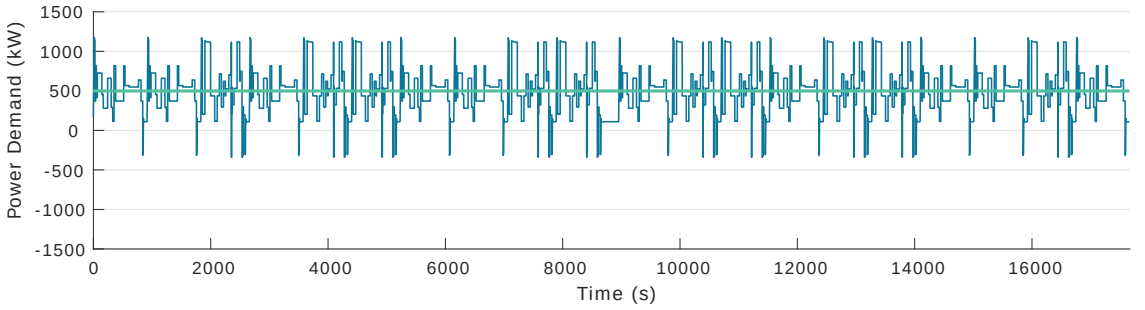

(c) Route length around 5 h

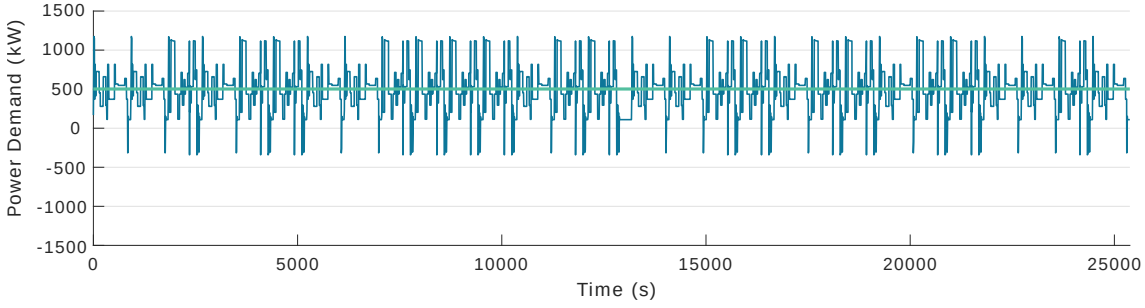

(d) Route length around 7 h

Figure A.7: H_2EMU synthetic drive cycles, average demand around 500 kW.

Bibliography

[1] International Energy Agency (IEA). Net Zero by 2050: A Roadmap for the Global Energy Sector. Technical report, IEA, Paris, 2021. URL https://www.iea.org/reports/net-zero-by-2050.

[2] International Energy Agency (IEA). Tracking Transport 2020. Technical report, IEA, Paris, 2020. URL https://www.iea.org/reports/tracking-transport-2020.

[3] International Energy Agency (IEA). Global Energy Review: CO2 Emissions in 2020. Technical report, IEA, Paris, 2021. URL https://www.iea.org/articles/global-energy-review-co2-emissions-in-2020.

[4] European Comission. Sustainable and Smart Mobility Strategy: Putting European transport on track for the future. Technical report, European Comission, Brussels, 2020. URL https://ec.europa.eu/transport/sites/default/files/2021-mobility-strategy-and-action-plan.pdf.

[5] International Energy Agency (IEA). Energy Technology Perspectives 2020. Technical report, IEA, Paris, 2020. URL https://www.iea.org/reports/energy-technology-perspectives-2020.

[6] Sjoerd Bakker and Rob Konings. The transition to zero-emission buses in public transport – The need for institutional innovation. *Transportation Research Part D: Transport and Environment*, 64(August):204–215, oct 2018. ISSN 13619209. doi: 10.1016/j.trd.2017.08.023.

[7] International Energy Agency (IEA). The Future of Rail. Technical report, IEA, Paris, 2019. URL https://www.iea.org/reports/the-future-of-rail.

[8] European Commission. Electrification of the Transport System: Studies and Reports. Technical report, Brussels, 2017. URL https://ec.europa.eu/programmes/horizon2020/en/news/electrification-transport-system-expert-group-report.

[9] Antonio García-Olivares, Jordi Solé, Roger Samsó, and Joaquim Ballabrera-Poy. Sustainable European Transport System in a 100% Renewable Economy. *Sustainability*, 12(12):5091, jun 2020. ISSN 2071-1050. doi: 10.3390/su12125091.

[10] Amine Jaafar, C.R. Akli, Bruno Sareni, Xavier Roboam, and A. Jeunesse. Sizing and Energy Management of a Hybrid Locomotive Based on Flywheel and Accumulators. *IEEE Transactions on Vehicular Technology*, 58(8):3947–3958, oct 2009. ISSN 0018-9545. doi: 10.1109/TVT.2009.2027328.

[11] Federico Zenith, Raphael Isaac, Andreas Hoffrichter, Magnus Skinlo Thomassen, and Steffen Møller-Holst. Techno-economic analysis of freight railway electrification by overhead line, hydrogen and batteries: Case studies in Norway and USA. *Proceedings of the Institution of Mechanical Engineers, Part F: Journal of Rail and Rapid Transit*, 234(7):791–802, aug 2020. ISSN 0954-4097. doi: 10.1177/0954409719867495.

[12] Yvonne Ruf, Thomas Zorn, Pinar Akcayoz De Neve, Patrick Andrae, Svetlana Erofeeva, Frank Garrison, and Andreas Schwilling. Study on the use of fuel cells and hydrogen in the railway environment. Technical report, Shift2Rail Joint Undertaking and Fuel Cells and Hydrogen Joint Undertakin, 2019.

[13] Chaoxian Wu, Shaofeng Lu, Fei Xue, Lin Jiang, and Minwu Chen. Optimal Sizing of Onboard Energy Storage Devices for Electrified Railway Systems. *IEEE Transactions on Transportation Electrification*, 6(3):1301–1311, sep 2020. ISSN 2332-7782. doi: 10.1109/TTE.2020.2996362.

[14] Zhihong Zhong, Zhongping Yang, Xiaochun Fang, Fei Lin, and Zhongbei Tian. Hierarchical Optimization of an On-Board Supercapacitor Energy Storage System Considering Train Electric Braking Characteristics and System Loss. *IEEE Transactions on Vehicular Technology*, 69(3):2576–2587, mar 2020. ISSN 0018-9545. doi: 10.1109/TVT.2020.2967467.

[15] Arturo González-Gil, Roberto Palacin, and Paul Batty. Sustainable urban rail systems: Strategies and technologies for optimal management of regenerative braking energy. *Energy Conversion and Management*, 75(75):374–388, nov 2013. ISSN 01968904. doi: 10.1016/j.enconman.2013.06.039.

[16] Dai-Duong Tran, Majid Vafaeipour, Mohamed El Baghdadi, Ricardo Barrero, Joeri Van Mierlo, and Omar Hegazy. Thorough state-of-the-art analysis of electric and hybrid vehicle powertrains: Topologies and integrated energy management strategies. *Renewable and Sustainable Energy Reviews*, 119:109596, mar 2020. ISSN 13640321. doi: 10.1016/j.rser.2019.109596.

[17] Emilia Silvas, Theo Hofman, Nikolce Murgovski, Pascal Etman, and Maarten Steinbuch. Review of Optimization Strategies for System-Level Design in Hybrid Electric Vehicles. *IEEE Transactions on Vehicular Technology*, 66(1):1–1, 2016. ISSN 0018-9545. doi: 10.1109/TVT.2016.2547897.

[18] Victor Isaac Herrera. *Optimized Energy Management Strategies and Sizing of Hybrid Storage Systems for Transport Applications*. PhD thesis, UPV/EHU, 2017.

[19] V. Fernão Pires, Enrique Romero-Cadaval, D. Vinnikov, I. Roasto, and J.F. Martins. Power converter interfaces for electrochemical energy storage systems – A review. *Energy Conversion and Management*, 86:453–475, oct 2014. ISSN 01968904. doi: 10.1016/j.enconman.2014.05.003.

[20] Yasaman Balali and Sascha Stegen. Review of energy storage systems for vehicles based on technology, environmental impacts, and costs. *Renewable and Sustainable Energy Reviews*, 135(July 2020):110185, jan 2021. ISSN 13640321. doi: 10.1016/j.rser.2020.110185.

[21] M.A. Hannan, M.M. Hoque, A. Mohamed, and A. Ayob. Review of energy storage systems for electric vehicle applications: Issues and challenges. *Renewable and Sustainable Energy Reviews*, 69(November 2016):771–789, mar 2017. ISSN 13640321. doi: 10.1016/j.rser.2016.11.171.

[22] Siang Fui Tie and Chee Wei Tan. A review of energy sources and energy management system in electric vehicles. *Renewable and Sustainable Energy Reviews*, 20:82–102, apr 2013. ISSN 13640321. doi: 10.1016/j.rser.2012.11.077.

[23] Christophe Pillot. The Rechargeable Battery Market and Main Trends 2018-2030. In *Battery Experts Forum 2019*, 2019.

[24] Heide Budde-Meiwes, Julia Drillkens, Benedikt Lunz, Jens Muennix, Susanne Rothgang, Julia Kowal, and Dirk Uwe Sauer. A review of current automotive battery technology and future prospects. *Proceedings of the Institution of Mechanical Engineers, Part D: Journal of Automobile Engineering*, 227(5):761–776, 2013. ISSN 09544070. doi: 10.1177/0954407013485567.

[25] C. C. Chan. The State of the Art of Electric, Hybrid, and Fuel Cell Vehicles. *Proceedings of the IEEE*, 95(4):704–718, apr 2007. ISSN 0018-9219. doi: 10.1109/JPROC.2007.892489.

[26] Xing Luo, Jihong Wang, Mark Dooner, and Jonathan Clarke. Overview of current development in electrical energy storage technologies and the application potential in power system operation. *Applied Energy*, 137:511–536, 2015. ISSN 03062619. doi: 10.1016/j.apenergy.2014.09.081.

[27] Jon Ander Lopez-Ibarra. *Intelligent and Self-adaptive strategies for improved energy management in fleets of vehicles*. PhD thesis, UPV/EHU, 2021.

[28] Wenjie Chen, Alf Kare Adnanses, Jan Fredrik Hansen, John Olav Lindtjorn, and Tianhao Tang. Super-capacitors based hybrid converter in marine electric propulsion system. In *The XIX International Conference on Electrical Machines - ICEM 2010*, pages 1–6. IEEE, sep 2010. ISBN 978-1-4244-4174-7. doi: 10.1109/ICELMACH.2010.5607967.

[29] Aqib Muzaffar, M. Basheer Ahamed, Kalim Deshmukh, and Jagannathan Thirumalai. A review on recent advances in hybrid supercapacitors: Design, fabrication

and applications. *Renewable and Sustainable Energy Reviews*, 101(October 2018): 123–145, mar 2019. ISSN 13640321. doi: 10.1016/j.rser.2018.10.026.

[30] Guizhou Ren, Guoqing Ma, and Ning Cong. Review of electrical energy storage system for vehicular applications. *Renewable and Sustainable Energy Reviews*, 41: 225–236, 2015. ISSN 13640321. doi: 10.1016/j.rser.2014.08.003.

[31] Thomas B. Reddy and David Linden, editors. *Linden's Handbook of Batteries*. McGraw-Hill, 4th edition, 2011. ISBN 9780071624190.

[32] Elixabet Sarasketa-Zabala. *A novel approach for Li-ion battery selection and lifetime prediction*. PhD thesis, Mondragon Unibertsitatea, 2014.

[33] Jia Ying Yong, Vigna K. Ramachandaramurthy, Kang Miao Tan, and N. Mithulananthan. A review on the state-of-the-art technologies of electric vehicle, its impacts and prospects. *Renewable and Sustainable Energy Reviews*, 49:365–385, sep 2015. ISSN 13640321. doi: 10.1016/j.rser.2015.04.130.

[34] Tatiana L. Kulova. A Brief Review of Post-Lithium-Ion Batteries. *International Journal of Electrochemical Science*, pages 7242–7259, aug 2020. ISSN 14523981. doi: 10.20964/2020.08.22.

[35] Yu Miao, Patrick Hynan, Annette von Jouanne, and Alexandre Yokochi. Current Li-Ion Battery Technologies in Electric Vehicles and Opportunities for Advancements. *Energies*, 12(6):1074, mar . ISSN 1996-1073. doi: 10.3390/en12061074.

[36] Josu Olmos, Iñigo Gandiaga, Andoni Saez-de Ibarra, Xabier Larrea, Txomin Nieva, and Iosu Aizpuru. Modelling the cycling degradation of Li-ion batteries: Chemistry influenced stress factors. *Journal of Energy Storage*, 40(June):102765, aug 2021. ISSN 2352152X. doi: 10.1016/j.est.2021.102765.

[37] Mahammad A. Hannan, Md Murshadul Hoque, Aini Hussain, Yushaizad Yusof, and Pin Jern Ker. State-of-the-Art and Energy Management System of Lithium-Ion Batteries in Electric Vehicle Applications: Issues and Recommendations. *IEEE Access*, 6:19362–19378, 2018. ISSN 2169-3536. doi: 10.1109/ACCESS.2018.2817655.

[38] Aakash Kumar and Mayank Sehgal. Hydrogen Fuel Cell Technology for a Sustainable Future: A Review. In *SAE Technical Papers*, volume 2018-April, pages 1–11, apr 2018. doi: 10.4271/2018-01-1307.

[39] Rosalin Rath, Piyush Kumar, Smita Mohanty, and Sanjay Kumar Nayak. Recent advances, unsolved deficiencies, and future perspectives of hydrogen fuel cells in transportation and portable sectors. *International Journal of Energy Research*, (May):er.4795, aug 2019. ISSN 0363-907X. doi: 10.1002/er.4795.

[40] Omer Berkehan Inal and Cengiz Deniz. Assessment of fuel cell types for ships: Based on multi-criteria decision analysis. *Journal of Cleaner Production*, 265:121734, aug 2020. ISSN 09596526. doi: 10.1016/j.jclepro.2020.121734.

[41] Kaushik Rajashekara and Akshay K Rathore. Power Conversion and Control for Fuel Cell Systems in Transportation and Stationary Power Generation. *Electric Power Components and Systems*, 43(12):1376–1387, jul 2015. ISSN 1532-5008. doi: 10.1080/15325008.2015.1034383.

[42] Gonzalo Abad. *Power Electronics and Electric Drives for Traction Applications*. John Wiley & Sons, Ltd, Chichester, UK, oct 2016. ISBN 9781118954454. doi: 10.1002/9781118954454. URL http://doi.wiley.com/10.1002/9781118954454.

[43] Mihael Cipek, Danijel Pavković, Zdenko Kljaić, and Tomislav Josip Mlinarić. Assessment of battery-hybrid diesel-electric locomotive fuel savings and emission reduction potentials based on a realistic mountainous rail route. *Energy*, 173:1154–1171, apr 2019. ISSN 03605442. doi: 10.1016/j.energy.2019.02.144.

[44] Sebastian Schmid, Kambiz Ebrahimi, Antonios Pezouvanis, and Walter Commerell. Model-based comparison of hybrid propulsion systems for railway diesel multiple units. *International Journal of Rail Transportation*, 6(1):16–37, jan 2018. ISSN 2324-8378. doi: 10.1080/23248378.2017.1390790.

[45] Marko Kapetanović, Alfredo Núñez, Niels van Oort, and Rob M.P. Goverde. Reducing fuel consumption and related emissions through optimal sizing of energy storage systems for diesel-electric trains. *Applied Energy*, 294(April):117018, jul 2021. ISSN 03062619. doi: 10.1016/j.apenergy.2021.117018.

[46] Joachim J. Mwambeleko and Thanatchai Kulworawanichpong. Battery electric multiple units to replace diesel commuter trains serving short and idle routes. *Journal of Energy Storage*, 11(November 2015):7–15, jun 2017. ISSN 2352152X. doi: 10.1016/j.est.2017.01.004.

[47] Simon J. Royston, Daniel T. Gladwin, David A. Stone, Richard Ollerenshaw, and Patrick Clark. Development and Validation of a Battery Model for Battery Electric Multiple Unit Trains. In *IECON 2019 - 45th Annual Conference of the IEEE Industrial Electronics Society*, volume 2019-Octob, pages 4563–4568. IEEE, oct 2019. ISBN 978-1-7281-4878-6. doi: 10.1109/IECON.2019.8927299.

[48] Johannes Pagenkopf and Stefan Kaimer. Potentials of alternative propulsion systems for railway vehicles — A techno-economic evaluation. In *2014 Ninth International Conference on Ecological Vehicles and Renewable Energies (EVER)*, pages 1–8. IEEE, mar 2014. ISBN 978-1-4799-3787-5. doi: 10.1109/EVER.2014.6843995.

[49] Andrea Mazzone, Mathias Schönbacher, and Xabier Larrea. Future Freight Locomotives in Shift2Rail – Development of Full Electric Last Mile Propulsion System. In *7th Transport Research Arena*, Vienna, 2018.

[50] Jean Francois Reynaud, Maitane Garmendia, and Txomin Nieva. Comprehensive integration of Onboard Energy Storage systems in tramways: Birmingham tram

case study. In *2018 IEEE International Conference on Electrical Systems for Aircraft, Railway, Ship Propulsion and Road Vehicles & International Transportation Electrification Conference (ESARS-ITEC)*, pages 1–6. IEEE, nov 2018. ISBN 978-1-5386-4192-7. doi: 10.1109/ESARS-ITEC.2018.8607554.

[51] Dongdong Zhao, Liangcai Xu, Yigeng Huangfu, Manfeng Dou, and Jianxing Liu. Semi-physical modeling and control of a centrifugal compressor for the air feeding of a PEM fuel cell. *Energy Conversion and Management*, 154(August):380–386, dec 2017. ISSN 01968904. doi: 10.1016/j.enconman.2017.11.030.

[52] Hujun Peng, Jianxiang Li, Andreas Thul, Kai Deng, Cem Ünlübayir, Lars Löwenstein, and Kay Hameyer. A scalable, causal, adaptive rule-based energy management for fuel cell hybrid railway vehicles learned from results of dynamic programming. *eTransportation*, 4(September 2016):100057, may 2020. ISSN 25901168. doi: 10.1016/j.etran.2020.100057.

[53] Guorui Zhang, Qi Li, Weirong Chen, Xiang Meng, and Huiwen Deng. A coupled power-voltage equilibrium strategy based on droop control for fuel cell/battery/supercapacitor hybrid tramway. *International Journal of Hydrogen Energy*, 44(35): 19370–19383, jul 2019. ISSN 03603199. doi: 10.1016/j.ijhydene.2018.09.070.

[54] Upasana Sarma and Sanjib Ganguly. Determination of the component sizing for the PEM fuel cell-battery hybrid energy system for locomotive application using particle swarm optimization. *Journal of Energy Storage*, 19(February):247–259, 2018. ISSN 2352152X. doi: 10.1016/j.est.2018.08.008.

[55] Wenbin Zhang, Jianqiu Li, Liangfei Xu, Minggao Ouyang, Yuwen Liu, Qingjun Han, and Kelei Li. Comparison study on life-cycle costs of different trams powered by fuel cell systems and others. *International Journal of Hydrogen Energy*, 41(38): 16577–16591, 2016. ISSN 03603199. doi: 10.1016/j.ijhydene.2016.03.032.

[56] Han Zhang, Jibin Yang, Jiye Zhang, Pengyun Song, and Xiaohui Xu. A Firefly Algorithm Optimization-Based Equivalent Consumption Minimization Strategy for Fuel Cell Hybrid Light Rail Vehicle. *Energies*, 12(14):2665, jul 2019. ISSN 1996-1073. doi: 10.3390/en12142665.

[57] Maksym Spiryagin, Colin Cole, Yan Quan Sun, Mitchell McClanachan, Valentyn Spiryagin, and Tim McSweeney. *Design and Simulation of Rail Vehicles*. CRC Press, may 2014. ISBN 9781466575677. doi: 10.1201/b17029.

[58] Mustafa İnci, Mehmet Büyük, Mehmet Hakan Demir, and Göktürk İlbey. A review and research on fuel cell electric vehicles: Topologies, power electronic converters, energy management methods, technical challenges, marketing and future aspects. *Renewable and Sustainable Energy Reviews*, 137(December 2020):110648, mar 2021. ISSN 13640321. doi: 10.1016/j.rser.2020.110648.

[59] Nan Xu, Yan Kong, Liang Chu, Hao Ju, Zhihua Yang, Zhe Xu, and Zhuoqi Xu. Towards a Smarter Energy Management System for Hybrid Vehicles: A Comprehensive Review of Control Strategies. *Applied Sciences*, 9(10):2026, may 2019. ISSN 2076-3417. doi: 10.3390/app9102026.

[60] Chao Yang, Mingjun Zha, Weida Wang, Kaijia Liu, and Changle Xiang. Efficient energy management strategy for hybrid electric vehicles/plug-in hybrid electric vehicles: Review and recent advances under intelligent transportation system. *IET Intelligent Transport Systems*, 14(7):702–711, 2020. ISSN 1751956X. doi: 10.1049/iet-its.2019.0606.

[61] Qicheng Xue, Xin Zhang, Teng Teng, Jibao Zhang, Zhiyuan Feng, and Qinyang Lv. A Comprehensive Review on Classification, Energy Management Strategy, and Control Algorithm for Hybrid Electric Vehicles. *Energies*, 13(20):5355, oct 2020. ISSN 1996-1073. doi: 10.3390/en13205355.

[62] Meiling Yue, Samir Jemei, Rafael Gouriveau, and Noureddine Zerhouni. Review on health-conscious energy management strategies for fuel cell hybrid electric vehicles: Degradation models and strategies. *International Journal of Hydrogen Energy*, 44 (13):6844–6861, mar 2019. ISSN 03603199. doi: 10.1016/j.ijhydene.2019.01.190.

[63] Ahmed Ali and Dirk Söffker. Towards Optimal Power Management of Hybrid Electric Vehicles in Real-Time: A Review on Methods, Challenges, and State-Of-The-Art Solutions. *Energies*, 11(3):476, feb 2018. ISSN 1996-1073. doi: 10.3390/en11030476.

[64] Ioan-Sorin Sorlei, Nicu Bizon, Phatiphat Thounthong, Mihai Varlam, Elena Carcadea, Mihai Culcer, Mariana Iliescu, and Mircea Raceanu. Fuel Cell Electric Vehicles—A Brief Review of Current Topologies and Energy Management Strategies. *Energies*, 14(1):252, jan 2021. ISSN 1996-1073. doi: 10.3390/en14010252.

[65] Juan P. Torreglosa, Pablo Garcia-Triviño, David Vera, and Diego A. López-García. Analyzing the Improvements of Energy Management Systems for Hybrid Electric Vehicles Using a Systematic Literature Review: How Far Are These Controls from Rule-Based Controls Used in Commercial Vehicles? *Applied Sciences*, 10(23):8744, dec 2020. ISSN 2076-3417. doi: 10.3390/app10238744.

[66] Atriya Biswas and Ali Emadi. Energy Management Systems for Electrified Powertrains: State-of-the-Art Review and Future Trends. *IEEE Transactions on Vehicular Technology*, 68(7):6453–6467, jul 2019. ISSN 0018-9545. doi: 10.1109/TVT.2019.2914457.

[67] He Tian, Shengbo Eben Li, Xu Wang, Yong Huang, and Guangyu Tian. Data-driven hierarchical control for online energy management of plug-in hybrid electric city bus. *Energy*, 142:55–67, jan 2018. ISSN 03605442. doi: 10.1016/j.energy.2017.09.061.

[68] Zhang Xin and Tian Yi. Research of hybrid electric locomotive control strategy. In *2011 International Conference on System science, Engineering design and Manu-*

facturing informatization, volume 1, pages 118–122. IEEE, oct 2011. ISBN 978-1-4577-0246-4. doi: 10.1109/ICSSEM.2011.6081159.

[69] Clement Mayet, Julien Pouget, Alain Bouscayrol, and Walter Lhomme. Influence of an Energy Storage System on the Energy Consumption of a Diesel-Electric Locomotive. *IEEE Transactions on Vehicular Technology*, 63(3):1032–1040, mar 2014. ISSN 0018-9545. doi: 10.1109/TVT.2013.2284634.

[70] Upasana Sarma and Sanjib Ganguly. Design optimisation for component sizing using multi-objective particle swarm optimisation and control of PEM fuel cellbattery hybrid energy system for locomotive application. *IET Electrical Systems in Transportation*, 10(1):52–61, 2020. ISSN 20429746. doi: 10.1049/iet-est.2018.5053.

[71] Mazhar Abbas, Inho Cho, and Jonghoon Kim. Reliability-constrained optimal sizing and rechargeable battery selection for improved load distribution in a fuel-cell hybrid railway propulsion system. *Energy Conversion and Management*, 196(April):1167–1179, 2019. ISSN 01968904. doi: 10.1016/j.enconman.2019.06.061.

[72] Guorui Zhang, Weirong Chen, and Qi Li. Modeling, optimization and control of a FC/battery hybrid locomotive based on ADVISOR. *International Journal of Hydrogen Energy*, 42(29):18568–18583, 2017. ISSN 03603199. doi: 10.1016/j.ijhydene.2017.04.172.

[73] C. R. Akli, X. Roboam, B. Sareni, and A. Jeunesse. Energy management and sizing of a hybrid locomotive. In *2007 European Conference on Power Electronics and Applications*, volume c, pages 1–10. IEEE, 2007. ISBN 9075815115. doi: 10.1109/EPE.2007.4417333.

[74] Shota Okano and Keiichiro Kondo. Study on a method by energy management the engine for controlling output power of hybrid powered railway vehicles with Electric Double Layer Capacitors. In *IECON 2011 - 37th Annual Conference of the IEEE Industrial Electronics Society*, pages 1608–1613. IEEE, nov 2011. ISBN 978-1-61284-972-0. doi: 10.1109/IECON.2011.6119547.

[75] Hiroyuki Shibuya and Keiichiro Kondo. Designing Methods of Capacitance and Control System for a Diesel Engine and EDLC Hybrid Powered Railway Traction System. *IEEE Transactions on Industrial Electronics*, 58(9):4232–4240, sep 2011. ISSN 0278-0046. doi: 10.1109/TIE.2010.2100332.

[76] Kenta Tsukahara and Keiichiro Kondo. A study on energy management system for hybrid powered railway vehicles with fuel cells and Electric Double Layer Capacitors. In *ICEMS 2012 - Proceedings: 15th International Conference on Electrical Machines and Systems*, pages 1–6. IEEE, 2012. ISBN 9784886860774.

[77] Cem Unlubayir, Thomas Nemeth, Fabian Meishner, Hujun Peng, Kai Deng, and DIrk Uwe Sauer. Simulation Model with an Optimal Operation Strategy for a Hybrid Train Powered by a Battery and a Fuel Cell. In *2019 IEEE Vehicle Power*

and Propulsion Conference (VPPC), pages 1–5. IEEE, oct 2019. ISBN 978-1-7281-1249-7. doi: 10.1109/VPPC46532.2019.8952422.

[78] Pablo García, Luis M. Fernández, Juan P. Torreglosa, and Francisco Jurado. Operation mode control of a hybrid power system based on fuel cell/battery/ultracapacitor for an electric tramway. *Computers & Electrical Engineering*, 39(7):1993–2004, oct 2013. ISSN 00457906. doi: 10.1016/j.compeleceng.2013.04.022.

[79] Pablo Garcia, Juan P. Torreglosa, Luis M. Fernandez, and Francisco Jurado. Control strategies for high-power electric vehicles powered by hydrogen fuel cell, battery and supercapacitor. *Expert Systems with Applications*, 40(12):4791–4804, 2013. ISSN 09574174. doi: 10.1016/j.eswa.2013.02.028.

[80] Ying Han, Xiang Meng, Guorui Zhang, Qi Li, and Weirong Chen. An energy management system based on hierarchical control and state machine for the PEMFC-battery hybrid tramway. In *2017 IEEE Transportation Electrification Conference and Expo, Asia-Pacific (ITEC Asia-Pacific)*, pages 1–5. IEEE, aug 2017. ISBN 978-1-5386-2894-2. doi: 10.1109/ITEC-AP.2017.8080856.

[81] Ying Han, Qi Li, Tianhong Wang, Weirong Chen, and Lei Ma. Multisource Coordination Energy Management Strategy Based on SOC Consensus for a PEMFC–Battery–Supercapacitor Hybrid Tramway. *IEEE Transactions on Vehicular Technology*, 67(1):296–305, jan 2018. ISSN 0018-9545. doi: 10.1109/TVT.2017.2747135.

[82] Qi Li, Hanqing Yang, Ying Han, Ming Li, and Weirong Chen. A state machine strategy based on droop control for an energy management system of PEMFC-battery-supercapacitor hybrid tramway. *International Journal of Hydrogen Energy*, 41(36):16148–16159, sep 2016. ISSN 03603199. doi: 10.1016/j.ijhydene.2016.04.254.

[83] Ayoub Aroua, Amadou Ball, Sabrina Messal, Walter Lhomme, and Clement Depature. Fuel Cell Dual-mode Train: Impact of Charge Depleting Strategy on Hydrogen Consumption. In *2020 IEEE Vehicle Power and Propulsion Conference (VPPC)*, pages 1–6, Gijón, nov 2020. IEEE. ISBN 978-1-7281-8959-8. doi: 10.1109/VPPC49601.2020.9330965.

[84] Mihael Cipek, Danijel Pavković, Matija Krznar, Zdenko Kljaić, and Tomislav Josip Mlinarić. Comparative Analysis of Conventional Diesel-Electric and Hypothetical Battery-Electric Heavy Haul Locomotive Operation in terms of Fuel Savings and Emissions Reduction Potentials. *Energy*, 232:121097, 2021. ISSN 03605442. doi: 10.1016/j.energy.2021.121097.

[85] Clement Depature and Tony Letrouve. Innovative Train Technologies Energy Comparison on One Non Electrified Railway. In *2020 IEEE Vehicle Power and Propulsion Conference (VPPC)*, pages 1–6, Gijón, nov 2020. IEEE. ISBN 978-1-7281-8959-8. doi: 10.1109/VPPC49601.2020.9330938.

[86] Ivan Krastevm, Nilanjan Mukherjee, Pietro Tricoli, and Stuart Hillmansen. New modular hybrid energy storage system and its control strategy for a fuel cell locomotive. In *2015 17th European Conference on Power Electronics and Applications (EPE'15 ECCE-Europe)*, pages 1–10. IEEE, sep 2015. ISBN 978-9-0758-1522-1. doi: 10.1109/EPE.2015.7309371.

[87] Guorui Zhang, Qi Li, Weirong Chen, and Xiang Meng. Synthetic Strategy Combining Speed Self-Adjusting Operation Control and Adaptive Power Allocation for Fuel Cell Hybrid Tramway. *IEEE Transactions on Industrial Electronics*, 68(2): 1454–1465, feb 2021. ISSN 0278-0046. doi: 10.1109/TIE.2020.2967735.

[88] Qi Li, Weirong Chen, Zhixiang Liu, Ming Li, and Lei Ma. Development of energy management system based on a power sharing strategy for a fuel cell-battery-supercapacitor hybrid tramway. *Journal of Power Sources*, 279:267–280, apr 2015. ISSN 03787753. doi: 10.1016/j.jpowsour.2014.12.042.

[89] R. Bellman. Dynamic Programming. *Science*, 153(3731):34–37, jul 1966. ISSN 0036-8075. doi: 10.1126/science.153.3731.34.

[90] Marco Sorrentino, Kréhi Serge Agbli, Daniel Hissel, Frédéric Chauvet, and Tony Letrouve. Application of dynamic programming to optimal energy management of grid-independent hybrid railcars. *Proceedings of the Institution of Mechanical Engineers, Part F: Journal of Rail and Rapid Transit*, 0(0):095440972092008, apr 2020. ISSN 0954-4097. doi: 10.1177/0954409720920080.

[91] Maik Leska and Harald Aschemann. Fuel-optimal combined driving strategy and energy management for a parallel hybrid electric railway vehicle. In *2015 20th International Conference on Methods and Models in Automation and Robotics (MMAR)*, pages 1127–1132. IEEE, aug 2015. ISBN 978-1-4799-8701-6. doi: 10.1109/MMAR.2015.7284037.

[92] Charley Lanneluc, Julien Pouget, Marie Poline, Frederic Chauvet, and Laurent Gerbaud. Optimal Energy Management of a Hybrid Train: Focus on Saving Braking Energy. In *2017 IEEE Vehicle Power and Propulsion Conference (VPPC)*, volume 2018-Janua, pages 1–6. IEEE, dec 2017. ISBN 978-1-5386-1317-7. doi: 10.1109/VPPC.2017.8330927.

[93] Yu Yan, Qi Li, Wenqiang Huang, and Weirong Chen. Operation Optimization and Control Method Based on Optimal Energy and Hydrogen Consumption for the Fuel Cell/Supercapacitor Hybrid Tram. *IEEE Transactions on Industrial Electronics*, 68 (2):1342–1352, feb 2021. ISSN 0278-0046. doi: 10.1109/TIE.2020.2967720.

[94] Maik Leska, Tobias Gruning, Harald Aschemann, and Andreas Rauh. Optimization of the longitudinal dynamics of parallel hybrid railway vehicles. In *2012 IEEE International Conference on Control Applications*, number Mode 4, pages 202–207. IEEE, oct 2012. ISBN 978-1-4673-4505-7. doi: 10.1109/CCA.2012.6402436.

[95] Han Zhang, Jibin Yang, Jiye Zhang, Pengyun Song, and Ming Li. Optimal energy management of a fuel cell-battery-supercapacitor-powered hybrid tramway using a multi-objective approach. *Proceedings of the Institution of Mechanical Engineers, Part F: Journal of Rail and Rapid Transit*, 234(5):511–523, may 2020. ISSN 0954-4097. doi: 10.1177/0954409719849804.

[96] Jerome Baert, S. Jemei, Didier Chamagne, Daniel Hissel, Samuel Hibon, and D. Hegy. Energetic Macroscopic Representation and Optimal Fuzzy Logic Energy Management Strategy of a Hybrid Electric Locomotive with experimental characterization of Nickel-Cadmium battery cells. *EPE Journal*, 24(4):56–67, dec 2014. ISSN 0939-8368. doi: 10.1080/09398368.2014.11755459.

[97] Marie Poline, Laurent Gerbaud, Julien Pouget, and Frédéric Chauvet. Simultaneous optimization of sizing and energy management—Application to hybrid train. *Mathematics and Computers in Simulation*, 158:355–374, apr 2019. ISSN 03784754. doi: 10.1016/j.matcom.2018.09.021.

[98] Qi Li, Tianhong Wang, Chaohua Dai, Weirong Chen, and Lei Ma. Power Management Strategy Based on Adaptive Droop Control for a Fuel Cell-Battery-Supercapacitor Hybrid Tramway. *IEEE Transactions on Vehicular Technology*, 67 (7):5658–5670, jul 2018. ISSN 0018-9545. doi: 10.1109/TVT.2017.2715178.

[99] Yu Yan, Qi Li, Weirong Chen, Bo Su, Jiawei Liu, and Lei Ma. Optimal Energy Management and Control in Multimode Equivalent Energy Consumption of Fuel Cell/Supercapacitor of Hybrid Electric Tram. *IEEE Transactions on Industrial Electronics*, 66(8):6065–6076, aug 2019. ISSN 0278-0046. doi: 10.1109/TIE.2018.2871792.

[100] Pei Zhang, Fuwu Yan, and Changqing Du. A comprehensive analysis of energy management strategies for hybrid electric vehicles based on bibliometrics. *Renewable and Sustainable Energy Reviews*, 48:88–104, aug 2015. ISSN 13640321. doi: 10.1016/j.rser.2015.03.093.

[101] Kai Deng, Hujun Peng, Steffen Dirkes, Jonas Gottschalk, Cem Ünlübayir, Andreas Thul, Lars Löwenstein, Stefan Pischinger, and Kay Hameyer. An adaptive PMP-based model predictive energy management strategy for fuel cell hybrid railway vehicles. *eTransportation*, 7:100094, feb 2021. ISSN 25901168. doi: 10.1016/j.etran.2020.100094.

[102] Hujun Peng, Jianxiang Li, Lars Löwenstein, and Kay Hameyer. A scalable, causal, adaptive energy management strategy based on optimal control theory for a fuel cell hybrid railway vehicle. *Applied Energy*, 267(April):114987, 2020. ISSN 03062619. doi: 10.1016/j.apenergy.2020.114987.

[103] Hujun Peng, Hanqing Cao, Steffen Dirkes, Zhu Chen, Kai Deng, Jonas Gottschalk, Cem Ünlübayir, Andreas Thul, Lars Löwenstein, Dirk Uwe Sauer, Stefan Pischinger, and Kay Hameyer. Validation of robustness and fuel efficiency of a universal

model-based energy management strategy for fuel cell hybrid trains: From analytical derivation via simulation to measurement on test bench. *Energy Conversion and Management*, 229(November 2020):1–22, 2021. ISSN 01968904. doi: 10.1016/j.enconman.2020.113734.

[104] C.C. Chan, Alain Bouscayrol, and Keyu Chen. Electric, Hybrid, and Fuel-Cell Vehicles: Architectures and Modeling. *IEEE Transactions on Vehicular Technology*, 59(2):589–598, feb 2010. ISSN 0018-9545. doi: 10.1109/TVT.2009.2033605.

[105] Andres F Obando, Victor I Herrera, Haizea Gaztanaga, Begona Gallardo, Txomin Nieva, and Maider Varela. Optimization Methodology of Infrastructure and Onboard Energy Storage System for Cost-Reduction in Tramway Lines Design. In *2017 IEEE Vehicle Power and Propulsion Conference (VPPC)*, pages 1–7. IEEE, dec 2017. ISBN 978-1-5386-1317-7. doi: 10.1109/VPPC.2017.8331051.

[106] Victor Isaac Herrera, Aitor Milo, Haizea Gaztanaga, Javier Ramos, and Haritza Camblong. Adaptive and Non-Adaptive Strategies for Optimal Energy Management and Sizing of a Dual Storage System in a Hybrid Electric Bus. *IEEE Transactions on Intelligent Transportation Systems*, 20(9):3435–3447, sep 2019. ISSN 1524-9050. doi: 10.1109/TITS.2018.2874092.

[107] Li Sun, Jiong Shen, Qingsong Hua, and Kwang Y. Lee. Data-driven oxygen excess ratio control for proton exchange membrane fuel cell. *Applied Energy*, 231(August): 866–875, 2018. ISSN 03062619. doi: 10.1016/j.apenergy.2018.09.036.

[108] Olle Sundstrom and Anna Stefanopoulou. Optimal power split in fuel cell hybrid electric vehicle with different battery sizes, drive cycles, and objectives. In *2006 IEEE Conference on Computer Aided Control System Design, 2006 IEEE International Conference on Control Applications, 2006 IEEE International Symposium on Intelligent Control*, pages 1681–1688. IEEE, oct 2006. ISBN 0780397967. doi: 10.1109/CACSD-CCA-ISIC.2006.4776894.

[109] Pucheng Pei, Dongfang Chen, Ziyao Wu, and Peng Ren. Nonlinear methods for evaluating and online predicting the lifetime of fuel cells. *Applied Energy*, 254(August): 113730, nov 2019. ISSN 03062619. doi: 10.1016/j.apenergy.2019.113730.

[110] P. Pei, Q. Chang, and T. Tang. A quick evaluating method for automotive fuel cell lifetime. *International Journal of Hydrogen Energy*, 33(14):3829–3836, jul 2008. ISSN 03603199. doi: 10.1016/j.ijhydene.2008.04.048.

[111] Huicui Chen, Pucheng Pei, and Mancun Song. Lifetime prediction and the economic lifetime of proton exchange membrane fuel cells. *Applied Energy*, 142:154–163, 2015. ISSN 03062619. doi: 10.1016/j.apenergy.2014.12.062.

[112] Wenlu Zhou, Yanping Zheng, Zhengjun Pan, and Qiang Lu. Review on the Battery Model and SOC Estimation Method. *Processes*, 9(9):1685, sep 2021. ISSN 2227-9717. doi: 10.3390/pr9091685.

[113] Gaizka Saldaña, José Ignacio San Martín, Inmaculada Zamora, Francisco Javier Asensio, and Oier Oñederra. Analysis of the Current Electric Battery Models for Electric Vehicle Simulation. *Energies*, 12(14):2750, jul 2019. ISSN 1996-1073. doi: 10.3390/en12142750.

[114] M.A. Hannan, M.S.H. Lipu, A. Hussain, and A. Mohamed. A review of lithium-ion battery state of charge estimation and management system in electric vehicle applications: Challenges and recommendations. *Renewable and Sustainable Energy Reviews*, 78(August 2016):834–854, oct 2017. ISSN 13640321. doi: 10.1016/j.rser.2017.05.001.

[115] Jinfeng Wu, Xiao Zi Yuan, Jonathan J. Martin, Haijiang Wang, Jiujun Zhang, Jun Shen, Shaohong Wu, and Walter Merida. A review of PEM fuel cell durability: Degradation mechanisms and mitigation strategies. *Journal of Power Sources*, 184 (1):104–119, sep 2008. ISSN 03787753. doi: 10.1016/j.jpowsour.2008.06.006.

[116] Jian Zhao and Xianguo Li. A review of polymer electrolyte membrane fuel cell durability for vehicular applications: Degradation modes and experimental techniques. *Energy Conversion and Management*, 199(June 2019):112022, nov 2019. ISSN 01968904. doi: 10.1016/j.enconman.2019.112022.

[117] Peng Ren, Pucheng Pei, Yuehua Li, Ziyao Wu, Dongfang Chen, and Shangwei Huang. Degradation mechanisms of proton exchange membrane fuel cell under typical automotive operating conditions. *Progress in Energy and Combustion Science*, 80:100859, sep 2020. ISSN 03601285. doi: 10.1016/j.pecs.2020.100859.

[118] Xinfeng Zhang, Daijun Yang, Minghui Luo, and Zuomin Dong. Load profile based empirical model for the lifetime prediction of an automotive PEM fuel cell. *International Journal of Hydrogen Energy*, 42(16):11868–11878, apr 2017. ISSN 03603199. doi: 10.1016/j.ijhydene.2017.02.146.

[119] Tom Fletcher, Rob Thring, and Martin Watkinson. An Energy Management Strategy to concurrently optimise fuel consumption & PEM fuel cell lifetime in a hybrid vehicle. *International Journal of Hydrogen Energy*, 41(46):21503–21515, dec 2016. ISSN 03603199. doi: 10.1016/j.ijhydene.2016.08.157.

[120] Patrick Urchaga, Thomas Kadyk, Steven G. Rinaldo, Antonio O. Pistono, Jingwei Hu, Wendy Lee, Chris Richards, Michael H. Eikerling, and Cynthia A. Rice. Catalyst Degradation in Fuel Cell Electrodes: Accelerated Stress Tests and Model-based Analysis. *Electrochimica Acta*, 176:1500–1510, sep 2015. ISSN 00134686. doi: 10.1016/j.electacta.2015.03.152.

[121] Wu Bi and Thomas F. Fuller. Modeling of PEM fuel cell Pt/C catalyst degradation. *Journal of Power Sources*, 178(1):188–196, mar 2008. ISSN 03787753. doi: 10.1016/j.jpowsour.2007.12.007.

[122] Thomas Jahnke, Georg A. Futter, Andrea Baricci, Claudio Rabissi, and Andrea Casalegno. Physical Modeling of Catalyst Degradation in Low Temperature Fuel Cells: Platinum Oxidation, Dissolution, Particle Growth and Platinum Band Formation. *Journal of The Electrochemical Society*, 167(1):013523, nov 2020. ISSN 0013-4651. doi: 10.1149/2.0232001JES.

[123] M. Chandesris, V. Médeau, N. Guillet, S. Chelghoum, D. Thoby, and F. Fouda-Onana. Membrane degradation in PEM water electrolyzer: Numerical modeling and experimental evidence of the influence of temperature and current density. *International Journal of Hydrogen Energy*, 40(3):1353–1366, jan 2015. ISSN 03603199. doi: 10.1016/j.ijhydene.2014.11.111.

[124] Georg A. Futter, Arnulf Latz, and Thomas Jahnke. Physical modeling of chemical membrane degradation in polymer electrolyte membrane fuel cells: Influence of pressure, relative humidity and cell voltage. *Journal of Power Sources*, 410-411(October 2018):78–90, jan 2019. ISSN 03787753. doi: 10.1016/j.jpowsour.2018.10.085.

[125] Manik Mayur, Stephan Strahl, Attila Husar, and Wolfgang G. Bessler. A multi-timescale modeling methodology for PEMFC performance and durability in a virtual fuel cell car. *International Journal of Hydrogen Energy*, 40(46):16466–16476, dec 2015. ISSN 03603199. doi: 10.1016/j.ijhydene.2015.09.152.

[126] Zunyan Hu, Jianqiu Li, Liangfei Xu, Ziyou Song, Chuan Fang, Minggao Ouyang, Guowei Dou, and Gaihong Kou. Multi-objective energy management optimization and parameter sizing for proton exchange membrane hybrid fuel cell vehicles. *Energy Conversion and Management*, 129:108–121, dec 2016. ISSN 01968904. doi: 10.1016/j.enconman.2016.09.082.

[127] Languang Lu, Minggao Ouyang, Haiyan Huang, Pucheng Pei, and Fuyuan Yang. A semi-empirical voltage degradation model for a low-pressure proton exchange membrane fuel cell stack under bus city driving cycles. *Journal of Power Sources*, 164 (1):306–314, jan 2007. ISSN 03787753. doi: 10.1016/j.jpowsour.2006.10.061.

[128] Ballard. Fuel Cell Power Module for Heavy Duty Motive Applications. https://www.ballard.com/docs/default-source/motive-modules-documents/fcmovetm.pdf?sfvrsn=6a83c380_6, . [Last accessed: 2022-02-15].

[129] Ballard's commitment to fuel cell technology innovation — for 40 years and counting. https://blog.ballard.com/ballard-fuel-cell-technology-innovation?utm_campaign=FuelCell-Product&utm_content=150939191&utm_medium=social&utm_source=linkedin&hss_channel=lcp-10026. [Last accessed: 2021-10-18].

[130] Xuebing Han, Languang Lu, Yuejiu Zheng, Xuning Feng, Zhe Li, Jianqiu Li, and Minggao Ouyang. A review on the key issues of the lithium ion battery degradation among the whole life cycle. *eTransportation*, 1:100005, aug 2019. ISSN 25901168. doi: 10.1016/j.etran.2019.100005.

[131] Christoph R. Birkl, Matthew R. Roberts, Euan McTurk, Peter G. Bruce, and David A. Howey. Degradation diagnostics for lithium ion cells. *Journal of Power Sources*, 341:373–386, feb 2017. ISSN 03787753. doi: 10.1016/j.jpowsour.2016.12.011.

[132] Xuanchen Zhu, Ying Chen, Haofeng Chen, and Weiling Luan. The diffusion induced stress and cracking behaviour of primary particle for Li-ion battery electrode. *International Journal of Mechanical Sciences*, 178(February):105608, jul 2020. ISSN 00207403. doi: 10.1016/j.ijmecsci.2020.105608.

[133] Xiao-Guang Yang, Yongjun Leng, Guangsheng Zhang, Shanhai Ge, and Chao-Yang Wang. Modeling of lithium plating induced aging of lithium-ion batteries: Transition from linear to nonlinear aging. *Journal of Power Sources*, 360:28–40, aug 2017. ISSN 03787753. doi: 10.1016/j.jpowsour.2017.05.110.

[134] Aiping Wang, Sanket Kadam, Hong Li, Siqi Shi, and Yue Qi. Review on modeling of the anode solid electrolyte interphase (SEI) for lithium-ion batteries. *npj Computational Materials*, 4(1):15, dec 2018. ISSN 2057-3960. doi: 10.1038/s41524-018-0064-0.

[135] Thomas Waldmann, Björn-Ingo Hogg, and Margret Wohlfahrt-Mehrens. Li plating as unwanted side reaction in commercial Li-ion cells – A review. *Journal of Power Sources*, 384(March):107–124, apr 2018. ISSN 03787753. doi: 10.1016/j.jpowsour.2018.02.063.

[136] Satu Kristiina Heiskanen, Jongjung Kim, and Brett L. Lucht. Generation and Evolution of the Solid Electrolyte Interphase of Lithium-Ion Batteries. *Joule*, 3(10):2322–2333, oct 2019. ISSN 25424351. doi: 10.1016/j.joule.2019.08.018.

[137] Jorn M. Reniers, Grietus Mulder, and David A. Howey. Review and Performance Comparison of Mechanical-Chemical Degradation Models for Lithium-Ion Batteries. *Journal of The Electrochemical Society*, 166(14):A3189–A3200, sep 2019. ISSN 0013-4651. doi: 10.1149/2.0281914jes.

[138] Tanja Gewald, Adrian Candussio, Leo Wildfeuer, Dirk Lehmkuhl, Alexander Hahn, and Markus Lienkamp. Accelerated Aging Characterization of Lithium-ion Cells: Using Sensitivity Analysis to Identify the Stress Factors Relevant to Cyclic Aging. *Batteries*, 6(1):6, jan 2020. ISSN 2313-0105. doi: 10.3390/batteries6010006.

[139] Madeleine Ecker, Nerea Nieto, Stefan Käbitz, Johannes Schmalstieg, Holger Blanke, Alexander Warnecke, and Dirk Uwe Sauer. Calendar and cycle life study of Li(NiMnCo)O2-based 18650 lithium-ion batteries. *Journal of Power Sources*, 248:839–851, feb 2014. ISSN 03787753. doi: 10.1016/j.jpowsour.2013.09.143.

[140] Yuanyuan Li, Daniel-Ioan Stroe, Yuhua Cheng, Hanmin Sheng, Xin Sui, and Remus Teodorescu. On the feature selection for battery state of health estimation based on charging–discharging profiles. *Journal of Energy Storage*, 33(September 2020):102122, jan 2021. ISSN 2352152X. doi: 10.1016/j.est.2020.102122.

[141] Weiping Diao, Ijaz Haider Naqvi, and Michael Pecht. Early detection of anomalous degradation behavior in lithium-ion batteries. *Journal of Energy Storage*, 32(June): 101710, dec 2020. ISSN 2352152X. doi: 10.1016/j.est.2020.101710.

[142] Sébastien Grolleau, Arnaud Delaille, Hamid Gualous, Philippe Gyan, Renaud Revel, Julien Bernard, Eduardo Redondo-Iglesias, and Jérémy Peter. Calendar aging of commercial graphite/LiFePO4 cell – Predicting capacity fade under time dependent storage conditions. *Journal of Power Sources*, 255:450–458, jun 2014. ISSN 03787753. doi: 10.1016/j.jpowsour.2013.11.098.

[143] John Wang, Ping Liu, Jocelyn Hicks-Garner, Elena Sherman, Souren Soukiazian, Mark Verbrugge, Harshad Tataria, James Musser, and Peter Finamore. Cycle-life model for graphite-LiFePO4 cells. *Journal of Power Sources*, 196(8):3942–3948, apr 2011. ISSN 03787753. doi: 10.1016/j.jpowsour.2010.11.134.

[144] Matthieu Dubarry, Nan Qin, and Paul Brooker. Calendar aging of commercial Li-ion cells of different chemistries – A review. *Current Opinion in Electrochemistry*, 9:106–113, jun 2018. ISSN 24519103. doi: 10.1016/j.coelec.2018.05.023.

[145] M. Lucu, E. Martinez-Laserna, I. Gandiaga, K. Liu, H. Camblong, W.D. Widanage, and J. Marco. Data-driven nonparametric Li-ion battery ageing model aiming at learning from real operation data - Part B: Cycling operation. *Journal of Energy Storage*, 30(March):101410, aug 2020. ISSN 2352152X. doi: 10.1016/j.est.2020.101410.

[146] Anthony Barré, Benjamin Deguilhem, Sébastien Grolleau, Mathias Gérard, Frédéric Suard, and Delphine Riu. A review on lithium-ion battery ageing mechanisms and estimations for automotive applications. *Journal of Power Sources*, 241:680–689, nov 2013. ISSN 03787753. doi: 10.1016/j.jpowsour.2013.05.040.

[147] M. Lucu, E. Martinez-Laserna, I. Gandiaga, and H. Camblong. A critical review on self-adaptive Li-ion battery ageing models. *Journal of Power Sources*, 401(May): 85–101, oct 2018. ISSN 03787753. doi: 10.1016/j.jpowsour.2018.08.064.

[148] Samuel Pelletier, Ola Jabali, Gilbert Laporte, and Marco Veneroni. Battery degradation and behaviour for electric vehicles: Review and numerical analyses of several models. *Transportation Research Part B: Methodological*, 103:158–187, sep 2017. ISSN 01912615. doi: 10.1016/j.trb.2017.01.020.

[149] Martin Petit, Eric Prada, and Valérie Sauvant-Moynot. Development of an empirical aging model for Li-ion batteries and application to assess the impact of Vehicle-to-Grid strategies on battery lifetime. *Applied Energy*, 172:398–407, 2016. ISSN 03062619. doi: 10.1016/j.apenergy.2016.03.119.

[150] Johannes Schmalstieg, Stefan Käbitz, Madeleine Ecker, and Dirk Uwe Sauer. A holistic aging model for Li(NiMnCo)O2 based 18650 lithium-ion batteries. *Journal of Power Sources*, 257:325–334, jul 2014. ISSN 03787753. doi: 10.1016/j.jpowsour.2014.02.012.

[151] Joris de Hoog, Jean-Marc Timmermans, Daniel Ioan-Stroe, Maciej Swierczynski, Joris Jaguemont, Shovon Goutam, Noshin Omar, Joeri Van Mierlo, and Peter Van Den Bossche. Combined cycling and calendar capacity fade modeling of a Nickel-Manganese-Cobalt Oxide Cell with real-life profile validation. *Applied Energy*, 200: 47–61, aug 2017. ISSN 03062619. doi: 10.1016/j.apenergy.2017.05.018.

[152] Daniel-Ioan Stroe, Maciej Swierczynski, Ana-Irina Stan, Remus Teodorescu, and Soren Juhl Andreasen. Accelerated Lifetime Testing Methodology for Lifetime Estimation of Lithium-Ion Batteries Used in Augmented Wind Power Plants. *IEEE Transactions on Industry Applications*, 50(6):4006–4017, nov 2014. ISSN 0093-9994. doi: 10.1109/TIA.2014.2321028.

[153] Maik Naumann, Franz B. Spingler, and Andreas Jossen. Analysis and modeling of cycle aging of a commercial LiFePO4/graphite cell. *Journal of Power Sources*, 451 (September 2019):227666, mar 2020. ISSN 03787753. doi: 10.1016/j.jpowsour.2019.227666.

[154] Chang Liu, Yujie Wang, and Zonghai Chen. Degradation model and cycle life prediction for lithium-ion battery used in hybrid energy storage system. *Energy*, 166: 796–806, jan 2019. ISSN 03605442. doi: 10.1016/j.energy.2018.10.131.

[155] M. Schimpe, M. E. von Kuepach, M. Naumann, H. C. Hesse, K. Smith, and A. Jossen. Comprehensive Modeling of Temperature-Dependent Degradation Mechanisms in Lithium Iron Phosphate Batteries. *Journal of The Electrochemical Society*, 165(2):A181–A193, jan 2018. ISSN 0013-4651. doi: 10.1149/2.1181714jes.

[156] E. Sarasketa-Zabala, I. Gandiaga, E. Martinez-Laserna, L.M. Rodriguez-Martinez, and I. Villarreal. Cycle ageing analysis of a LiFePO4/graphite cell with dynamic model validations: Towards realistic lifetime predictions. *Journal of Power Sources*, 275:573–587, feb 2015. ISSN 03787753. doi: 10.1016/j.jpowsour.2014.10.153.

[157] Md Sazzad Hosen, Danial Karimi, Theodoros Kalogiannis, Ashkan Pirooz, Joris Jaguemont, Maitane Berecibar, and Joeri Van Mierlo. Electro-aging model development of nickel-manganese-cobalt lithium-ion technology validated with light and heavy-duty real-life profiles. *Journal of Energy Storage*, 28(November 2019):101265, apr 2020. ISSN 2352152X. doi: 10.1016/j.est.2020.101265.

[158] Meinert Lewerenz and Dirk Uwe Sauer. Evaluation of cyclic aging tests of prismatic automotive LiNiMnCoO2-Graphite cells considering influence of homogeneity and anode overhang. *Journal of Energy Storage*, 18(June):421–434, aug 2018. ISSN 2352152X. doi: 10.1016/j.est.2018.06.003.

[159] Quan Xia, Zili Wang, Yi Ren, Laifa Tao, Chen Lu, Jun Tian, Daozhong Hu, Yituo Wang, Yuzhuan Su, Jin Chong, Haizu Jin, and Yongshou Lin. A modified reliability model for lithium-ion battery packs based on the stochastic capacity degradation and dynamic response impedance. *Journal of Power Sources*, 423(December 2018): 40–51, may 2019. ISSN 03787753. doi: 10.1016/j.jpowsour.2019.03.042.

[160] Simon F. Schuster, Tobias Bach, Elena Fleder, Jana Müller, Martin Brand, Gerhard Sextl, and Andreas Jossen. Nonlinear aging characteristics of lithium-ion cells under different operational conditions. *Journal of Energy Storage*, 1(1):44–53, 2015. ISSN 2352152X. doi: 10.1016/j.est.2015.05.003.

[161] Yiduo Zhu, Fuwu Yan, Jianqiang Kang, Changqing Du, Chi Zhang, and Richard Fifi Turkson. Fading analysis of the Li(NiCoMn)O2 battery under different SOC cycle intervals. *Ionics*, 23(6):1383–1390, jun 2017. ISSN 0947-7047. doi: 10.1007/s11581-016-1968-7.

[162] M J Smith, D T Gladwin, and D A Stone. A comparison of the effects of charging strategies on lithium-ion cell performance in high temperature environments. In *Proceedings of the IEEE International Conference on Industrial Technology*, volume 2019-Febru, pages 1107–1112. IEEE, feb 2019. ISBN 9781538663769. doi: 10.1109/ICIT.2019.8755246.

[163] Taedong Goh, Minjun Park, Minhwan Seo, Jun Gu Kim, and Sang Woo Kim. Capacity estimation algorithm with a second-order differential voltage curve for Li-ion batteries with NMC cathodes. *Energy*, 135:257–268, sep 2017. ISSN 03605442. doi: 10.1016/j.energy.2017.06.141.

[164] K. Jalkanen, J. Karppinen, L. Skogström, T. Laurila, M. Nisula, and K. Vuorilehto. Cycle aging of commercial NMC/graphite pouch cells at different temperatures. *Applied Energy*, 154:160–172, sep 2015. ISSN 03062619. doi: 10.1016/j.apenergy.2015.04.110.

[165] Rujian Fu, Song-Yul Choe, Victor Agubra, and Jeffrey Fergus. Modeling of degradation effects considering side reactions for a pouch type Li-ion polymer battery with carbon anode. *Journal of Power Sources*, 261:120–135, sep 2014. ISSN 03787753. doi: 10.1016/j.jpowsour.2014.03.045.

[166] Thorsten Baumhöfer, Manuel Brühl, Susanne Rothgang, and Dirk Uwe Sauer. Production caused variation in capacity aging trend and correlation to initial cell performance. *Journal of Power Sources*, 247:332–338, feb 2014. ISSN 03787753. doi: 10.1016/j.jpowsour.2013.08.108.

[167] Johannes Philipp Fath, Daniel Dragicevic, Laura Bittel, Adnan Nuhic, Johannes Sieg, Severin Hahn, Lennart Alsheimer, Bernd Spier, and Thomas Wetzel. Quantification of aging mechanisms and inhomogeneity in cycled lithium-ion cells by differential voltage analysis. *Journal of Energy Storage*, 25(May):100813, oct 2019. ISSN 2352152X. doi: 10.1016/j.est.2019.100813.

[168] Dane Sotta. MAT4BAT: Project Final Report. Technical report, Advanced Materials for Batteries, 2017. URL https://cordis.europa.eu/project/id/608931/reporting.

[169] Kristen A. Severson, Peter M. Attia, Norman Jin, Nicholas Perkins, Benben Jiang, Zi Yang, Michael H. Chen, Muratahan Aykol, Patrick K. Herring, Dimitrios Fraggedakis, Martin Z. Bazant, Stephen J. Harris, William C. Chueh, and

Richard D. Braatz. Data-driven prediction of battery cycle life before capacity degradation. *Nature Energy*, 4(5):383–391, may 2019. ISSN 2058-7546. doi: 10.1038/s41560-019-0356-8.

[170] Jens Groot, Maciej Swierczynski, Ana Irina Stan, and Søren Knudsen Kær. On the complex ageing characteristics of high-power LiFePO4/graphite battery cells cycled with high charge and discharge currents. *Journal of Power Sources*, 286:475–487, jul 2015. ISSN 03787753. doi: 10.1016/j.jpowsour.2015.04.001.

[171] Meinert Lewerenz, Jens Münnix, Johannes Schmalstieg, Stefan Käbitz, Marcus Knips, and Dirk Uwe Sauer. Systematic aging of commercial LiFePO 4 |Graphite cylindrical cells including a theory explaining rise of capacity during aging. *Journal of Power Sources*, 345:254–263, mar 2017. ISSN 03787753. doi: 10.1016/j.jpowsour.2017.01.133.

[172] Andrea Marongiu, Marco Roscher, and Dirk Uwe Sauer. Influence of the vehicle-to-grid strategy on the aging behavior of lithium battery electric vehicles. *Applied Energy*, 137:899–912, 2015. ISSN 03062619. doi: 10.1016/j.apenergy.2014.06.063.

[173] Yong Zheng, Yan-Bing He, Kun Qian, Dongqing Liu, Qingwen Lu, Baohua Li, Xindong Wang, Jianling Li, and Feiyu Kang. Influence of charge rate on the cycling degradation of LiFePO4/mesocarbon microbead batteries under low temperature. *Ionics*, 23(8):1967–1978, aug 2017. ISSN 0947-7047. doi: 10.1007/s11581-017-2032-y.

[174] Haining Liu, Ijaz Haider Naqvi, Fajia Li, Chengliang Liu, Neda Shafiei, Yulong Li, and Michael Pecht. An analytical model for the CC-CV charge of Li-ion batteries with application to degradation analysis. *Journal of Energy Storage*, 29(March):101342, jun 2020. ISSN 2352152X. doi: 10.1016/j.est.2020.101342.

[175] Dongxu Ouyang, Jingwen Weng, Mingyi Chen, and Jian Wang. Impact of high-temperature environment on the optimal cycle rate of lithium-ion battery. *Journal of Energy Storage*, 28(November 2019):101242, apr 2020. ISSN 2352152X. doi: 10.1016/j.est.2020.101242.

[176] Chao Lyu, Yankong Song, Jun Zheng, Weilin Luo, Gareth Hinds, Junfu Li, and Lixin Wang. In situ monitoring of lithium-ion battery degradation using an electrochemical model. *Applied Energy*, 250(May):685–696, sep 2019. ISSN 03062619. doi: 10.1016/j.apenergy.2019.05.038.

[177] S Barcellona and L Piegari. Effect of current on cycle aging of lithium ion batteries. *Journal of Energy Storage*, 29(November 2019):101310, jun 2020. ISSN 2352152X. doi: 10.1016/j.est.2020.101310.

[178] Simone Barcellona, Morris Brenna, Federica Foiadelli, Michela Longo, and Luigi Piegari. Analysis of Ageing Effect on Li-Polymer Batteries. *The Scientific World Journal*, 2015:1–8, 2015. ISSN 2356-6140. doi: 10.1155/2015/979321.

[179] John Wang, Justin Purewal, Ping Liu, Jocelyn Hicks-Garner, Souren Soukazian, Elena Sherman, Adam Sorenson, Luan Vu, Harshad Tataria, and Mark W. Verbrugge. Degradation of lithium ion batteries employing graphite negatives and nickel–cobalt–manganese oxide + spinel manganese oxide positives: Part 1, aging mechanisms and life estimation. *Journal of Power Sources*, 269:937–948, dec 2014. ISSN 03787753. doi: 10.1016/j.jpowsour.2014.07.030.

[180] Matthieu Dubarry and Arnaud Devie. Battery durability and reliability under electric utility grid operations: Representative usage aging and calendar aging. *Journal of Energy Storage*, 18:185–195, aug 2018. ISSN 2352152X. doi: 10.1016/j.est.2018.04.004.

[181] Yongzhi Zhang, Rui Xiong, Hongwen He, and Michael G. Pecht. Lithium-Ion Battery Remaining Useful Life Prediction With Box–Cox Transformation and Monte Carlo Simulation. *IEEE Transactions on Industrial Electronics*, 66(2):1585–1597, feb 2019. ISSN 0278-0046. doi: 10.1109/TIE.2018.2808918.

[182] Rui Xiong, Yongzhi Zhang, Ju Wang, Hongwen He, Simin Peng, and Michael Pecht. Lithium-Ion Battery Health Prognosis Based on a Real Battery Management System Used in Electric Vehicles. *IEEE Transactions on Vehicular Technology*, 68(5):4110–4121, may 2019. ISSN 0018-9545. doi: 10.1109/TVT.2018.2864688.

[183] Josu Olmos, Andoni Saez-de ibarra, Dimas Lopez, Txomin Nieva, and Iosu Aizpuru. Hidrogeno tren baten diseinu eta operazioaren optimizazioa. In *Ikergazte 2021: Nazioarteko Ikerketa Euskeraz*, pages 1–8, Gasteiz, 2021. doi: https://dx.doi.org/10.26876/ikergazte.iv.03.18. URL http://www.inguma.eus/fso/fitxategia/79-ikergazte.iv.03.145-152.hidrogeno-tren.pdf.

[184] Lincun Fang, Shiyin Qin, Gang Xu, Tianli Li, and Kemin Zhu. Simultaneous Optimization for Hybrid Electric Vehicle Parameters Based on Multi-Objective Genetic Algorithms. *Energies*, 4(3):532–544, mar 2011. ISSN 1996-1073. doi: 10.3390/en4030532.

[185] CAF. CIVITY train family, . URL https://www.caf.net/en/productos-servicios/familia/civity/index.php.

[186] Jon Ander López-Ibarra, Nerea Goitia-Zabaleta, Victor Isaac Herrera, Haizea Gazta ñaga, and Haritza Camblong. Battery aging conscious intelligent energy management strategy and sensitivity analysis of the critical factors for plug-in hybrid electric buses. *eTransportation*, 5:100061, aug 2020. ISSN 25901168. doi: 10.1016/j.etran.2020.100061. URL https://doi.org/10.1016/j.etran.2020.100061https://linkinghub.elsevier.com/retrieve/pii/S2590116820300187.

[187] Fausto Cavallaro. A Takagi-Sugeno Fuzzy Inference System for Developing a Sustainability Index of Biomass. *Sustainability*, 7(9):12359–12371, sep 2015. ISSN 2071-1050. doi: 10.3390/su70912359.

[188] Olle Sundstrom and Lino Guzzella. A generic dynamic programming Matlab function. In *2009 IEEE International Conference on Control Applications*, number 7, pages 1625–1630. IEEE, jul 2009. ISBN 978-1-4244-4601-8. doi: 10.1109/CCA.2009.5281131.

[189] ETH Zürich Institute for Dynamic Systems and Control. Downloads. URL https://idsc.ethz.ch/research-guzzella-onder/downloads.html.

[190] Xiang Tian, Ren He, and Yiqiang Xu. Design of an Energy Management Strategy for a Parallel Hybrid Electric Bus Based on an IDP-ANFIS Scheme. *IEEE Access*, 6:23806–23819, 2018. ISSN 2169-3536. doi: 10.1109/ACCESS.2018.2829701.

[191] Xiang Tian, Ren He, Xiaodong Sun, Yingfeng Cai, and Yiqiang Xu. An ANFIS-Based ECMS for Energy Optimization of Parallel Hybrid Electric Bus. *IEEE Transactions on Vehicular Technology*, 69(2):1473–1483, feb 2020. ISSN 0018-9545. doi: 10.1109/TVT.2019.2960593.

[192] Saft. Modul'ion range. URL https://www.saftbatteries.com/products-solutions/products/modulion%C2%AE.

[193] Akasol. Akasystem 15 akm 53 poc. URL https://www.akasol.com/library/Downloads/Datenbl%C3%A4tter/02-05-2019/Data%20sheet-AKASOL-AKASystem-15AKM53POC-WEB.pdf.

[194] Impact Clear Power Technology. Uves lto standard battery pack. URL https://icpt.pl/wp-content/uploads/2021/05/Leaflet_LTO_STANDARD-3_color_bW.pdf.

[195] Jon Ander López-Ibarra, Haizea Gaztañaga, Andoni Saez-de Ibarra, and Haritza Camblong. Plug-in hybrid electric buses total cost of ownership optimization at fleet level based on battery aging. *Applied Energy*, 280(August):115887, dec 2020. ISSN 03062619. doi: 10.1016/j.apenergy.2020.115887.

[196] Antti Lajunen and Timothy Lipman. Lifecycle cost assessment and carbon dioxide emissions of diesel, natural gas, hybrid electric, fuel cell hybrid and electric transit buses. *Energy*, 106:329–342, jul 2016. ISSN 03605442. doi: 10.1016/j.energy.2016.03.075.

[197] CAF. CIVIA train family, . URL https://www.caf.net/en/soluciones/proyectos/proyecto-detalle.php?p=133.

[198] International Energy Agency (IEA). The Future of Hydrogen. Technical report, IEA, Paris, 2019. URL https://www.iea.org/reports/the-future-of-hydrogen.

[199] Ballard. Heavy Duty Modules. https://www.ballard.com/fuel-cell-solutions/fuel-cell-power-products/motive-modules, . [Last accessed: 2022-02-15].

[200] Josu Olmos, Inigo Gandiaga, Dimas Lopez, Xabier Larrea, Txomin Nieva, and Iosu Aizpuru. Li-ion Battery-based Hybrid Diesel-Electric Railway Vehicle: In-depth Life

Cycle Cost Analysis. *IEEE Transactions on Vehicular Technology*, pages 1–1, 2021. ISSN 0018-9545. doi: 10.1109/TVT.2021.3128754.

[201] Josu Olmos, Andoni Saez-de Ibarra, Haizea Gaztanaga, Dimas Lopez, Txomin Nieva, and Iosu Aizpuru. In-depth Life Cycle Cost Analysis of a Hydrogen Electric Multiple Unit. In *2021 IEEE Vehicle Power and Propulsion Conference (VPPC)*, pages 1–6. IEEE, oct 2021. ISBN 978-1-6654-0528-7. doi: 10.1109/VPPC53923.2021.9699227.

Abbreviations

ANFIS Adaptive Neuro Fuzzy Inference System

BT Battery

BEMU Battery Electric Multiple Unit

BOL Beginning of Life

DEMU Diesel-Electric Multiple Unit

DOD Depth of Discharge

DP Dynamic Programming

ECMS Equivalent Consumption Minimization Strategy

EECMS Equivalent Energy Consumption Minimization Strategy

EDLC Electric Double Layer Capacitor

EMU Electric Multiple Unit

EMS Energy Management Strategy

EOL End of Life

ESS Energy Storage System

FC Fuel Cell

FEC Full Equivalent Cycle

FIS Fuzzy Inference System

FL Fuzzy Logic

FW Flywheel

GA Genetic Algorithm

GA-FL Optimized Fuzzy Logic

GA-RB2 Optimized SOC Adaptive Controller

GA-RB3 Optimized Demand Adaptive Controller

GA-SM Optimized State Machine

H_2EMU Hydrogen Electric Multiple Unit

H-DEMU Battery Hybrid Diesel-Electric Multiple Unit

H-EMU Battery Hybrid Electric Multiple Unit

HS High Scenario

ICE Internal Combustion Engine

LAM Loss of Active Material

LB Learning-based

LCC Life Cycle Cost

LCO Lithium Cobalt Oxide

LFP Lithium Iron Phosphate

Li-ion Lithium-ion

LIB Lithium-ion Battery

LLI Loss of Lithium Inventory

LMO Lithium Manganese Oxide

LTO Lithium Titanate

LS Low Scenario

MPC Model Predictive Control

MS Medium Scenario

NCA Lithium Nickel Cobalt Aluminium Oxide

NMC Lithium Nickel Manganese Cobalt Oxide

OB Optimization-based

ORI Ohmic Resistance Increase

Pb Lead-acid

PEMFC Proton Exchange Membrane Fuel Cell

PMP Portryagin's Minimum Principle

PSO Particle Swarm Optimization

QP Quadratic Programming

RB Rule-based

RB1 Baseline Control

RB1-A Baseline Control Variation

RB1-B Baseline Control Variation

RB2 Improved Baseline Control for Charge Sustaining (H-DEMU Case)

RB2 SOC Adaptive Controller (H_2EMU Case)

RB3 Improved Baseline Control for Charge Depleting (H-DEMU Case)

RB3 Demand Adaptive Controller (H_2EMU Case)

RB-FL Rule Based Fuzzy Logic

RB-SM Rule Based State Machine

SEI Solid Electrolyte Interphase

SM State Machine

SOC State of Charge

SOH State of Health

SQP Sequential Quadratic Programming

T Temperature

List of Symbols

Symbol	Description	Unit
c_{BT}	Battery referential cost	[€/kWh]
c_f	Diesel referential cost	[€/L]
c_{FC}	Fuel cell referential cost	[€/kW]
c_{GS}	Genset referential cost	[€/kW]
c_{H_2}	Hydrogen referential cost	[€/kg]
c_{maint}	Maintenance cost per year	[€/$year$]
C	Battery C-rate	[h^{-1}]
C_{acq}	Acquisition costs	[€]
C_{BT}	Battery acquisition cost	[€]
C_{BTrepl}	Cost of battery replacements	[€]
C_{cat}	Cost of catenary consumption	[€]
C_{ch}	Battery charging C-rate	[h^{-1}]
C_{dch}	Battery discharging C-rate	[h^{-1}]
C_f	Cost of diesel consumption	[€]
C_{FC}	Fuel cell acquisition cost	[€]
C_{FCrepl}	Cost of fuel cell replacements	[€]
C_{GS}	Genset acquisition cost	[€]
C_{H_2}	Cost of hydrogen consumption	[€]
C_{maint}	Maintenance costs	[€]
C_{max_ch}	Maximum battery C-rate at charging	[h^{-1}]
C_{max_dch}	Maximum battery C-rate at discharging	[h^{-1}]
C_{op}	Operation costs	[€]

Symbol	Description	Unit
C_{train}	Train acquisition cost, excluding variable costs	[€]
DOD	Battery depth of discharge	[%]
e_{SOC}	SOC error in RB3 controller for H_2EMU	[%]
E	Rail electrification state	[−]
$E_{braking}$	Estimated energy recovered by the battery in braking	$[Wh]$
E_{BT}	Battery nominal energy	$[Wh]$
E_{BT-cat}	Required energy from catenary to BT to recover SOC_{ref}	$[Wh]$
E_{Cat}	Electricity consumption from catenary	$[Wh]$
E_{Cat_BOL}	Electricity consumption from catenary in BOL simulation	$[kWh]$
E_{Cat_day}	Daily electricity consumption from catenary	$[kWh]$
E_{Cat_EOL}	Electricity consumption from catenary in EOL simulation	$[kWh]$
E_{GS}	Energy generated by the genset	$[Wh]$
FEC	Battery full equivalent cycles	[−]
GS_i	Fuzzy logic possible P_{GS} output value	$[W]$
i	Individual in genetic algorithms optimization	[−]
I	Discount rate	[%]
I_{BT}	Battery current	$[A]$
$I_{BT\_max\_ch}$	Maximum battery charging current	$[A]$
$I_{BT\_max\_dch}$	Maximum battery discharging current	$[A]$
I_{FC}	Fuel cell stack current	$[A]$
j	Feasible solution in exhaustive search optimization	[−]
J	Dynamic programming cost function	[−]
k	Simulation time step	[−]
k_1	Battery degradation model coefficient	[−]
k_2	Battery degradation model coefficient	$[K]$
k_3	Battery degradation model coefficient	$[\%^{-1}]$
k_4	Battery degradation model coefficient	$[h]$
k_5	Battery degradation model coefficient	$[h]$
k_6	Battery degradation model coefficient	$[\%^{-1}]$
k_7	Battery degradation model coefficient	[%]
k_{FL1}	Fuzzy logic-based EMS parameter	[%]
k_{FL2}	Fuzzy logic-based EMS parameter	[%]

Symbol	Description	Unit
k_{FL3}	Fuzzy logic-based EMS parameter	[%]
k_{FL4}	Fuzzy logic-based EMS parameter	[%]
k_{FL5}	Fuzzy logic-based EMS parameter	[%]
k_c	Constant gain of RB3 controller for H_2EMU	[−]
k_{pn}	Positive proportional gain of RB3 controller for H_2EMU	[−]
k_{pp}	Negative proportional gain of RB3 controller for H_2EMU	[−]
k_{SM1}	State Machine EMS parameter	[%]
k_{SM2}	State Machine EMS parameter	[%]
k_{SM3}	State Machine EMS parameter	[%]
k_{SM4}	State Machine EMS parameter	[%]
K	Total number of simulation time steps	[−]
K_{RB3}	Gain of RB3 controller for H_2EMU	[−]
L_{f_BOL}	Diesel consumption in BOL simulation	$[L]$
L_{f_day}	Daily diesel consumption	$[L]$
L_{f_EOL}	Diesel consumption in EOL simulation	$[L]$
$L_{H_2\_BOL}$	Hydrogen consumption in BOL simulation	$[kg]$
$L_{H_2\_day}$	Daily hydrogen consumption	$[kg]$
$L_{H_2\_EOL}$	Hydrogen consumption in EOL simulation	$[kg]$
LCC	Life cycle cost	[€]
LHV	Hydrogen low heating value	$[J/g]$
m_{cell}	Number of battery cells connected in parallel	[−]
$\dot{m}_f$	Genset fuel mass consumption	$[g/s]$
$\dot{m}'_f$	Genset fuel mass consumption per generated energy unit	$[\frac{g}{kWh}]$
$\dot{m}_{H_2}$	Fuel cell hydrogen mass consumption	$[g/s]$
$mSOC$	Battery middle state of charge	[%]
n_{BT}	Number of battery modules integrated in vehicle	[−]
n_{cell}	Number of battery cells connected in series	[−]
n_{FC}	Number of fuel cell modules integrated in vehicle	[−]
n_{GS}	Number of gensets integrated in vehicle	[−]
n_{trips}	Number of trips per day	$[\frac{trips}{day}]$
N_{BT}	Maximum number of battery modules	[−]
N_{FC}	Maximum number of fuel cell modules	[−]

Symbol	Description	Unit
N_{GS}	Maximum number of gensets	$[-]$
N_i	Number of individuals per generation in GA	$[-]$
N_j	Number of feasible solutions in exhaustive search	$[-]$
N_x	Number of generations in GA	$[-]$
O_i^1	Layer 1 of ANFIS arquitecture	$[-]$
O_i^2	Layer 2 of ANFIS arquitecture	$[-]$
O_i^3	Layer 3 of ANFIS arquitecture	$[-]$
O_i^4	Layer 4 of ANFIS arquitecture	$[-]$
O^5	Layer 5 of ANFIS arquitecture	$[-]$
p_0	Fuel cell degradation accelerating coefficient	$[-]$
p_1	Fuel cell degradation rate due to load change cycling	$[\frac{V}{cycle}]$
p_2	Fuel cell degradation rate due to start-stop cycles	$[\frac{V}{cycle}]$
p_3	Fuel cell degradation rate due to idle operation	$[V/s]$
p_4	Fuel cell degradation rate due to high power load	$[V/s]$
p_{EMS}	Set of optimization variables related to EMS parameters	$[-]$
P_{Aux}	Power absorbed by auxiliary systems (@ DC bus)	$[W]$
P_{BT}	Power provided/absorbed by the battery (@ DC bus)	$[W]$
P'_{BT}	Power provided/absorbed by the battery	$[W]$
$P_{BT-max-ch}$	Maximum battery charging power	$[W]$
$P_{BT-max-dch}$	Maximum battery discharging power	$[W]$
P_{BT-cat}	Battery power target in EMS for electrified sections	$[W]$
P_{Cat}	Power provided/absorbed by the catenary (@ DC bus)	$[W]$
P'_{Cat}	Power provided/absorbed by the catenary	$[W]$
P_{Dem}	Power demand (@ DC bus)	$[W]$
$P_{Dem-avg}$	Average power demand (@ DC bus) in specific section s	$[W]$
P_{EM}	Power demanded by traction motors	$[W]$
P_{FC}	Power provided by the fuel cell (@ DC bus)	$[W]$
P'_{FC}	Power provided by the fuel cell	$[W]$
P'_{FC-max}	Fuel cell maximum operation point	$[W]$
P'_{FC-min}	Fuel cell idle operation point	$[W]$
P'_{FC-ref}	Fuel cell power reference defined by EMS	$[W]$
P_{GS}	Power provided by the genset (@ DC bus)	$[W]$

Symbol	Description	Unit
P'_{GS}	Power provided by the genset	$[W]$
P'_{GS_k}	Power provided by the genset in time step $k-1$	$[W]$
P_{GS-eff}	Genset maximum efficiency operation point	$[W]$
P_{GS-max}	Genset maximum power operation point	$[W]$
P_{GS1}	Threshold of low efficiency genset operation zone	$[W]$
P_{GS2}	Threshold of medium efficiency genset operation zone	$[W]$
P_{ICE}	Power generated by the ICE	$[W]$
P_{Peak}	Typical P_{Dem} power peak	$[W]$
P_{Res}	Power absorbed by the braking resistors (@ DC bus)	$[W]$
Q_{BT}	Current battery capacity	$[Ah]$
Q_{BT_0}	Battery capacity at BOL	$[Ah]$
r_{BT}	Current battery replacement	$[-]$
r_{FC}	Current fuel cell replacement	$[-]$
R_{BT}	Total number of battery replacements	$[-]$
R_{FC}	Total number of fuel cell replacements	$[-]$
R_{int_BT}	Battery internal resistance (@ module level)	$[\Omega]$
R_{int_cell}	Battery internal resistance (@ cell level)	$[\Omega]$
s	Specific section of a route	$[-]$
S_{BT}	Size of a battery module (integrated energy)	$[kWh]$
S_{FC}	Size of a fuel cell module (nominal power)	$[kW]$
S_{GS}	Size of a genset (nominal power)	$[kW]$
SOC	Battery state-of-charge	$[\%]$
SOC_0	Initial battery state of charge	$[\%]$
SOC_K	Final battery state of charge	$[\%]$
SOC_{max}	Maximum allowable battery state of charge	$[\%]$
SOC_{min}	Minimum allowable battery state of charge	$[\%]$
SOC_{ref}	Reference battery state of charge	$[\%]$
SOH_{BT}	Battery state of health	$[\%]$
t	Time	$[s]$
t_{day}	Operation hours per day	$[\frac{h}{day}]$
t_{op}	Operation days per year	$[\frac{days}{year}]$
t_{res}	Estimated time until end of trip	$[s]$

Symbol	Description	Unit
T	Battery Temperature	$[K]$
T_{ICE}	ICE torque	$[Nm]$
V_{BT}	Battery voltage	$[V]$
V_{BT_max}	Maximum allowable battery voltage	$[V]$
V_{BT_min}	Minimum allowable battery voltage	$[V]$
V_{OCV_BT}	Battery open circuit voltage (@ module level)	$[V]$
V_{OCV_cell}	Battery open circuit voltage (@ cell level)	$[V]$
w_1	Number of fuel cell load changing cycles	$[\frac{cycles}{year}]$
w_2	Number of fuel cell start-stop cycles	$[\frac{cycles}{year}]$
w_3	Fuel cell time in idle operation	$[\frac{s}{year}]$
w_4	Fuel cell time in high power load	$[\frac{s}{year}]$
w_{GS_i}	Weight defining the contribution of the FL rules to GS_i	$[-]$
w_{rule_n}	Weight of the fuzzy logic rule n	$[-]$
x	Generation in genetic algorithm optimization	$[-]$
x_1	Parameter of RB2 controller for H_2EMU	$[-]$
X	Vector of Optimization Variables	$[-]$
X_{ES}	Vector of Optimization Variables in Exhaustive Search	$[-]$
X_{DP}	Vector of Optimization Variables in DP case	$[-]$
X_{GAFL}	Vector of Optimization Variables in GA-FL case	$[-]$
X_{GARB2}	Vector of Optimization Variables in GA-RB2 case	$[-]$
X_{GARB3}	Vector of Optimization Variables in GA-RB3 case	$[-]$
X_{GASM}	Vector of Optimization Variables in GA-SM case	$[-]$
y	Current year	$[year]$
y_1	Parameter of RB2 controller for H_2EMU	$[-]$
y_2	Parameter of RB2 controller for H_2EMU	$[-]$
y_{BT}	Estimated battery lifetime	$[years]$
y_{FC}	Estimated fuel cell lifetime	$[years]$
Y	Service life of the vehicle	$[years]$
α	Battery degradation model coefficient	$[-]$
β	Battery degradation model coefficient	$[\%]$
γ	Weight factor in DP cost function (H_2EMU case)	$[-]$
γ_{cat}	Coefficient for catenary transmission loss	$[\%]$

Symbol	Description	Unit
δ_{FC}	Fuel cell degradation rate	$[\frac{V}{year}]$
δ_{BT_cal}	Battery degradation rate due to calendar ageing	$[\%/day]$
δ_{BT_cyc}	Battery degradation rate due to cycling ageing	$[\%/FEC]$
ΔP_{FC_max}	Saturation of fuel cell operation point	$[W/s]$
ΔSOH_{BT_cal}	Battery capacity decay due to calendar ageing	$[\%]$
ΔSOH_{BT_cyc}	Battery capacity decay due to cycling ageing	$[\%]$
ΔV_{FC}	Fuel cell voltage decrease at end of life	$[V]$
η_{conv_BT}	Battery converter efficiency	$[\%]$
η_{conv_FC}	Fuel cell converter efficiency	$[\%]$
η_{eff}	Coefficient for battery charging efficiency	$[\%]$
η_{FC}	Fuel cell efficiency	$[\%]$
η_{inv_cat}	Catenary inverter efficiency	$[\%]$
η_{inv_GS}	Genset inverter efficiency	$[\%]$
η_{tr_cat}	Catenary transformer efficiency	$[\%]$
λ	Weight factor in DP cost function (H_2EMU case)	$[-]$
μ_{PDem}	Degree of membership functions related to P_{Dem}	$[-]$
μ_{PGSk}	Degree of membership functions related to P_{GS_k}	$[-]$
μ_{SOC}	Degree of membership functions related to SOC	$[-]$
Π	Space of feasible solutions	$[-]$
Π_{ES}	Space of feasible solutions in Exhaustive Search	$[-]$
Π_{DP}	Space of feasible solutions in DP optimization case	$[-]$
Π_{GAFL}	Space of feasible solutions in GA-FL optimization case	$[-]$
Π_{GARB2}	Space of feasible solutions in GA-RB2 optimization case	$[-]$
Π_{GARB3}	Space of feasible solutions in GA-RB3 optimization case	$[-]$
Π_{GASM}	Space of feasible solutions in GA-SM optimization case	$[-]$
ρ_{BT_E}	Battery energetic density	$[Wh/kg]$
ρ_{BT_L}	Battery volumetric density	$[Wh/L]$
Φ	Dynamic programming control variable(s)	$[-]$
ω_{ICE}	ICE rotational speed	$[\frac{rad}{s}]$
ι	Dynamic programming state variable(s)	$[-]$

Glossary of Terms

Adaptive Neuro-Fuzzy Inference System (ANFIS)

A kind of artificial neural network that is based on Takagi-Sugeno fuzzy inference system. It integrates together both neural networks and fuzzy logic principles. In the scope of this Ph.D. Thesis, it is used as a learning-based energy management strategy. The neuro-fuzzy inference system is trained with results of optimal strategies, with the aim of replicating these performances in real time.

Ageing

Process which affect electrochemical cells over time, causing a reduction in their capacity to provide energy and power. This Ph.D. Thesis deals with the ageing of fuel cells and batteries.

Battery (BT)

A device that converts chemical energy into electrical energy, and vice versa. Batteries typically consist of several cells interconnected in modules, branches or racks to form a whole battery pack.

Battery Chemistry

The anode, cathode and electrolyte of battery cells can be made up of different materials. Depending on the combination of these materials, different battery chemistries exist. In the approach of the current Ph.D. Thesis, different lithium-ion based battery chemistries are analysed.

Beginning of Life (BOL)

The point in time at which battery or fuel cell use begins.

C-rate (C)

The discharge or charge battery current (in Amperes, A) expressed as a multiple of the

rated device capacity (in Ampere-hours, Ah). For example, for a device having a capacity of 1 Ah, when charging or discharging at 5 A, it would mean a 5 C rate. As the C-rate is a measure relative to the battery capacity, it also serves to compare the performance of devices with different nominal capacities.

Calendar Ageing

Degradation suffered by the battery when being at rest.

Capacity

The quantity of Ampere-hours (Ah) that can be withdrawn from a fully charged cell or battery under specified conditions of discharge.

Cycling Ageing

Degradation suffered by the battery caused by working cycles.

Depth of Discharge (DOD)

It refers to the State of Charge (SOC) window during each battery charge or discharge phase. That is to say, the DOD represents the absolute difference between the starting and ending SOC for each charge or discharge applied to a battery. If a battery is cycled between 60% and 80% SOC, this represents a 20% DOD.

Driving Cycle

A series of data points that represents the speed of a vehicle versus time. In the current Ph.D. Thesis, driving cycle is used to refer both to the speed and the traction demand profiles of a rail vehicle.

Dynamic Programming (DP)

An algorithmic technique for solving an optimization problem by breaking it down into simpler subproblems, utilizing the fact that the optimal solution to the overall problem depends upon the optimal solution to its subproblems. In the current Ph.D. Thesis, Dynamic Programming is used to solve the problem for the optimal energy management strategy.

End of Life (EOL)

A condition reached when a battery or fuel cell device is no longer capable of meeting the applicable goals. In the current Ph.D., battery end of life is defined as a 20% capacity loss, and fuel cell end of life as a 10% voltage loss, in both cases measured in relation to the initial rated values.

Energy Management Strategy (EMS)

The energy management is the control layer that organically coordinates the on-board energy sources in order to satisfy the power demand of the vehicle. This management is performed based on a strategy, which is denoted as the Energy Management Strategy. The energy management plays a critical role in hybrid powertrain configurations, as it directly affects in the fuel consumption of the vehicle, as well as on the lifetime of the different powertrain elements. The EMS can be based on rules (rule-based EMS), on an optimization approach (optimization-based EMS), or on a learning approach (learning-based EMS).

Exhaustive Search Based Optimization

A very general problem-solving technique that consists of systematically enumerating all possible candidates for the solution and checking whether each candidate satisfies the problem statement. Once all the candidates are checked, the one that better fits the fitness function is selected as the optimal solution.

Fuel Cell (FC)

An energy conversion device that converts chemical energy from a fuel and an oxidizing agent into electric energy without a combustion. It consists of two electrodes and an electrolyte separator. Different fuel cell types exist depending on the nature of the electrolyte and the used fuel. In the current Ph.D. Thesis, the generic fuel cell term refers to the Proton Exchange Membrane Fuel Cell (PEMFC), also known as hydrogen fuel cell. The hydrogen fuel cell produces electricity from a reaction in which hydrogen and oxygen are combined, with usable heat and water as the principal by-products.

Full Equivalent Cycle (FEC)

The number of complete cycles (100% DOD) that a battery has performed. One FEC corresponds to charging and discharging Q Ah, being Q the battery capacity.

Fuzzy Logic

A form of soft computing method that operates with the imprecision of the real world. In opposition to the traditional hard computing (or boolean logic), soft computing (or fuzzy logic) exploits the tolerance for imprecision, uncertainty, and partial truth. In short, the truth value of variables may be any real number between 0 and 1, instead of being integer values 0 or 1. Fuzzy logic is based on the observation that people make decisions based on imprecise and non-numerical information. In the approach of the current Ph.D. Thesis, fuzzy logic is applied to solve the energy management problem.

Genetic Algorithms (GA)

A search heuristic that is inspired in the theory of natural evolution. It belongs to the class of evolutionary algorithms. The algorithm reflects the process of natural selection where the fittest individuals are selected for reproduction to produce offspring of the next

generation. Genetic algorithms are commonly used to generate high-quality solutions to optimization and search problems by relying on the mutation, crossover and selection operators. In the current Ph.D. Thesis, Genetic Algorithms are applied to solve optimization problems that cannot be solved by brute force.

Holistic Design Methodology

The methodology proposed in the current Ph.D. Thesis to derive a cost-optimal design of the rail vehicle powertrain. The methodology considers holistically the effect of the powertrain elements technology and size, energy management strategy, economic context, and driving cycle.

Life Cycle Cost (LCC)

An approach that assesses the total cost of an asset over its life cycle, including initial capital costs, maintenance costs and operating costs.

Middle State of Charge (mSOC)

When a battery performs a certain DOD, the middle SOC value of that DOD is denoted as the Middle State of Charge. For instance, if a BT is cycled between 60% and 80% of SOC, it has performed a 20% DOD with a mSOC of the 70%.

Multiple Unit

A rail vehicle in which the traction elements are spread through the different carriages. Contrary to the locomotive, where all the traction elements are constituted in a single carriage. This Ph.D. Thesis is focused on two Multiple Unit topologies: the Hybrid Diesel-Electric Multiple Unit (powered by a genset and a battery) and the Hydrogen Electric Multiple Unit (powered by a fuel cell and a battery). When adding the term bi-mode, it means that the vehicle can also be powered by a catenary.

Nested Optimization

A special kind of optimization where one problem is embedded or nested within another. It is also known as bi-level optimization.

Optimization problem

The problem that consists of finding the best solution from a set of feasible solutions. An optimization problem is composed of a fitness function (the value or expression that has to be maximized/minimized), a set of optimization variables (the varibles that are varied to maximize/minimize the fitness function), a space of feasible solutions (the possible combinations of optimization variables) and a set of constraints (limits to the combinations of optimization variables).

Sensitivity Analysis

The study of how the uncertainty in the output of a mathematical model or system can be divided and allocated to different sources of uncertainty in its inputs. In short, it consists of recalculating outcomes under alternative assumptions to determine the impact of a variable. In the approach of this Ph.D. Thesis, a Life Cycle Cost Sensitivity Analysis is developed, as the impact of different features on the cost of railway vehicles is analysed.

State of Charge (SOC)

It defines the ratio between the amount of lithium ions remaining in the negative electrode and the total amount of active lithium ions in the battery cell. In practical applications, the SOC is used to represent the amount of available capacity in a battery. In this Ph.D. Thesis, the SOC is defined as the relation between the available capacity and the maximum capacity of a battery cell.

State of Health (SOH)

The State of Health reflects the loss of battery or fuel cell performance capability in relation to the initial conditions. In the case of the battery, and in the approach proposed in the current Ph.D. Thesis, the SOH is related to the loss of capacity. In the case of the fuel cell, the SOH is related to the loss of voltage.

List of Figures

List of Tables

Scientific contributions

Within this research project, several scientific contributions to the literature were published. These are listed below.

JOURNAL ARTICLES:

a. **Josu Olmos**, Iñigo Gandiaga, Andoni Saez-de-Ibarra, Xabier Larrea, Txomin Nieva and Iosu Aizpuru. Modelling the cycling degradation of Li-ion batteries: Chemistry influenced stress factors. *Journal of Energy Storage*, 40(June):102765, aug 2021. doi: 10.1016/j.est.2021.102765

b. **Josu Olmos**, Iñigo Gandiaga, Dimas Lopez, Xabier Larrea, Txomin Nieva, and Iosu Aizpuru. Li-ion battery-based hybrid diesel-electric railway vehicle: In-depth life cycle cost analysis. *IEEE Transactions on Vehicular Technology*, pages 1-1, 2021. doi: 10.1109/TVT.2021.3128754 (Article in press)

c. Mohammed Al-Saadi, **Josu Olmos**, Andoni Saez-de Ibarra, Joeri Van Mierlo, and Maitane Berecibar. Fast Charging Impact on the Lithium-Ion Batteries' Lifetime and Cost-Effective Battery Sizing in Heavy-Duty Electric Vehicles Applications. *Energies*, 15(4):1278, feb 2022. doi: 10.3390/en15041278.

CONFERENCE ARTICLES:

d. **Josu Olmos**, Iñigo Gandiaga, Jon Crego, Xabier Agirre, Txomin Nieva, and Iosu Aizpuru. Biziraupen estimazio modeloa garraio astuneko aplikazioetan erabiltzen diren superkondentsadoreentzako. In *Ikergazte 2019: Nazioarteko Ikerketa Euskeraz*, pages 1-7, Baiona, may 2019.

e. Iñigo Gandiaga, **Josu Olmos**, Xabier Agirre, Txomin Nieva. EDLC Lifetime Holistic Estimation for Heavy-Duty Applications. In *AABC Europe 2020*, Wiesbaden, jan 2020.

f. **Josu Olmos**, Iñigo Gandiaga, Dimas Lopez, Xabier Larrea, Txomin Nieva, and Iosu Aizpuru. Impact of Li-ion Battery Technology and Energy Management on the Life Cycle Costs of Hybrid Diesel-Electric Multiple Units. In *2020 Fifteenth International Conference on Ecological Vehicles and Renewable Energies (EVER)*, pages 1-8, Monaco, sep 2020. doi: 10.1109/EVER48776.2020.9242929

g. **Josu Olmos**, Iñigo Gandiaga, Dimas Lopez, Xabier Larrea, Txomin Nieva, and Iosu Aizpuru. In-depth Life Cycle Cost Analysis of a Li-ion Battery-based Hybrid Diesel-Electric Multiple Unit. In *2020 IEEE Vehicle Power and Propulsion Conference (VPPC)*, pages 1-5, Gijón, nov 2020. doi: 10.1109/VPPC49601.2020.9330908.

h. **Josu Olmos**, Andoni Saez-de-Ibarra, Dimas Lopez, Txomin Nieva, and Iosu Aizpuru. Hidrogeno tren baten diseinu eta operazioaren optimizazioa. In *Ikergazte 2021: Nazioarteko Ikerketa Euskeraz*, pages 1-8, Gasteiz, june 2021.

i. **Josu Olmos**, Andoni Saez-de-Ibarra, Haizea Gaztañaga, Dimas Lopez, Txomin Nieva, and Iosu Aizpuru. In-depth life cycle cost analysis of a hydrogen electric multiple unit. In *2021 IEEE Vehicle Power and Propulsion Conference (VPPC)*, pages 1-6. IEEE, oct 2021. doi: 10.1109/VPPC53923.2021.9699227

j. **Josu Olmos**, Andoni Saez-de-Ibarra, Haizea Gaztañaga, Dimas Lopez, Txomin Nieva, and Iosu Aizpuru. Cost-effectiveness of opportunity charging in non-electrified railway lines. In *2021 IEEE Vehicle Power and Propulsion Conference (VPPC)*, pages 1-6. IEEE, oct 2021. doi: 10.1109/VPPC53923.2021.9699314

BOOK CHAPTER:

k. Jon Ander López-Ibarra, Haizea Gaztañaga, **Josu Olmos**, Andoni Saez-de-Ibarra, and H. Camblong. Plug-in Hybrid Electric Buses with Different Battery Chemistries Total Cost of Ownership Planning and Optimization at Fleet Level Based on Battery Aging. In *Intelligent Control and Smart Energy Management*, pages 45-47. Springer Optimization and Its Applications, Springer Cham, 2022. doi: 10.1007/978-3-030-84474-5_2.

Vivió en un tren y lo llamó el Huracán,
Podía viajar sin tener que viajar,
Y cada día embarcaba su diario de sueños con él...

— La Raíz, «El Tren Huracán» (2012)

Mila esker! Muchas gracias! Thank you!